



HAL
open science

Observers for data assimilation - Applications to cardiac modeling

Philippe Moireau

► **To cite this version:**

Philippe Moireau. Observers for data assimilation - Applications to cardiac modeling. Modeling and Simulation. Université Paris Saclay; Université Paris Sud - Paris XI, 2016. tel-01404866

HAL Id: tel-01404866

<https://theses.hal.science/tel-01404866v1>

Submitted on 29 Nov 2016

HAL is a multi-disciplinary open access archive for the deposit and dissemination of scientific research documents, whether they are published or not. The documents may come from teaching and research institutions in France or abroad, or from public or private research centers.

L'archive ouverte pluridisciplinaire **HAL**, est destinée au dépôt et à la diffusion de documents scientifiques de niveau recherche, publiés ou non, émanant des établissements d'enseignement et de recherche français ou étrangers, des laboratoires publics ou privés.



FACULTÉ
DES SCIENCES
D'ORSAY



UNIVERSITÉ PARIS-SUD



Faculté des sciences d'Orsay

École doctorale de mathématiques Hadamard (ED 574)

Équipe-projet Inria M Ξ DISIM

(Mathematical and Mechanical Modeling with Data Interaction in SIMulation for Medecine)

Mémoire présenté pour l'obtention du

Diplôme d'habilitation à diriger les recherches

Discipline : Mathématiques

par

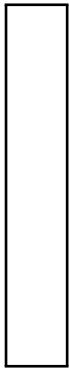
Philippe MOIREAU

Observateurs pour l'assimilation de données
Applications en cardiologie

Rapporteurs : K. KUNISCH University of Graz
B. MAURY Université Paris Sud
K. RAMDANI Inria

Date de soutenance : 28 Novembre 2016

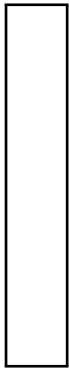
Composition du jury : F.-X. LE DIMET Université Grenoble-Alpes (Examineur)
J. LE ROUSSEAU Université Paris-Nord (Examineur)
Y. MADAY Université Pierre & Marie Curie (President)
B. MAURY Université Paris-Sud (Rapporteur)
E. TRELAT Université Pierre & Marie Curie (Examineur)
D. CHAPELLE Inria (Invité)



Contents

Preamble	1
I Summary of my research contribution & Research project	3
CHAPITRE 1 Summary of my research contribution	5
1.1 Introduction	6
1.2 What is data assimilation ?	6
1.3 The cardiovascular system playground	16
1.3.1 Electrophysiology	18
1.3.2 Cardiac Mechanics	19
1.3.3 The cardiovascular system	21
1.4 Past contributions	23
1.4.1 Data similarity measures and observer design	24
1.4.2 Observer analysis results	27
1.4.3 Parameter estimation results	28
1.4.4 Discretization Results	30
1.4.5 Modeling and application results	32
1.4.6 Other Results	34
1.5 Perspectives: Research Project	34
1.5.1 Challenge 1: From Data similarity measures to observer design	34
1.5.2 Challenge 2: Observer analysis	36
1.5.3 Challenge 3: Parameter estimation	37
1.5.4 Challenge 4: Discretization	37
1.5.5 Challenge 5: Applications	38

II Detailed presentation of my past contributions	41
CHAPITRE 2 Data assimilation contributions	43
2.1 Introduction	44
2.2 Toward a unified theory in optimal filtering of non-linear finite dimensional systems	44
2.2.1 Least square estimation and corresponding optimal estimator	44
2.2.2 Principle of the time-discretization and related time-discrete estimator . .	48
2.2.3 Approximated optimal filters in the light of the discrete-time Mortensen filter	51
2.3 Control-based sequential estimation strategies for PDEs	56
2.3.1 Optimal-control-based strategies	56
2.3.2 Luenberger observers formulations – The wave equation case	66
2.3.3 Luenberger observers: other models	81
2.3.4 Hybrid feedback design	92
2.4 Shape-based data assimilation	100
2.4.1 Motion extraction from images by sequential estimation based on a biomechanical model	101
2.4.2 A Luenberger observer for reaction-diffusion models with front position data	112
CHAPITRE 3 Cardiac modeling and model-data interaction	117
3.1 Introduction	118
3.2 Energy preserving models and coupling	118
3.2.1 An energy preserving micro-macro model of the heart contraction	118
3.2.2 An energy balanced coupling of porous flows and hyperelastic formulations	125
3.3 Reduced-order modeling	129
3.3.1 Dimensional reductions of a cardiac model for effective validation and calibration	129
3.3.2 Proper Orthogonal Decomposition for parameter-dependent problems – application to parameter estimation	133
3.4 Model-data interaction for the cardiovascular system	133
3.4.1 Estimation of tissue contractility from cardiac Cine-MRI – a pig experiment	133
3.4.2 Identification of boundary support parameters in a fluid-structure vascular model using patient image data	134
3.4.3 Estimation in electrophysiology	134
3.4.4 Applications within international collaborations	135
PERSONAL REFERENCES – ARTICLES	139
PERSONAL REFERENCES – PROCEEDINGS - PREPRINTS - THESIS	142
GENERAL REFERENCES	158



Preamble

*Les plans les plus méticuleux peuvent toujours être déjoués
par les événements, réduit à un magma confus.*

— Daniel Woodrell *Sous la lumière cruelle*

The philosophy of this document is to present a unified vision of my research started with my Master and PhD Thesis about data assimilation using observers with applications in cardiology...

The document is structured as follows. The first part is a presentation of my research contributions and my research project. My objective with this part is to clearly present my specific contributions and my research program for the next years. Then in a complementary second part, I present in more details my research results in an unified setting. In this respect, I have also included classical results of the literature and some new results that are only submitted or about to be submitted. This second part is separated in two chapters, a data assimilation chapter and a modeling and applications chapter.

I also want to emphasize that the bibliography is separated in two categories. My own papers are cited with numbers [N] in the rest of the document. I have also distinguished proceedings, preprint and thesis from articles in my bibliography. The rest of the literature is cited with the first author et al. convention [First Author et al., YEAR].

PART I

Summary of my research contribution &
Research project

Summary of my research contribution

*L'incertitude n'est pas dans les choses mais dans notre tête :
l'incertitude est une méconnaissance.*

— Jacques Bernoulli *Ars conjectandi*

Chapter contents

1.1	Introduction	6
1.2	What is data assimilation ?	6
1.3	The cardiovascular system playground	16
1.3.1	Electrophysiology	18
1.3.2	Cardiac Mechanics	19
1.3.3	The cardiovascular system	21
1.4	Past contributions	23
1.4.1	Data similarity measures and observer design	24
1.4.2	Observer analysis results	27
1.4.3	Parameter estimation results	28
1.4.4	Discretization Results	30
1.4.5	Modeling and application results	32
1.4.6	Other Results	34
1.5	Perspectives: Research Project	34
1.5.1	Challenge 1: From Data similarity measures to observer design	34
1.5.2	Challenge 2: Observer analysis	36
1.5.3	Challenge 3: Parameter estimation	37
1.5.4	Challenge 4: Discretization	37
1.5.5	Challenge 5: Applications	38

1.1 Introduction

My research activity is mainly devoted to developing **methodological** aspects of data assimilation in the realm of the biomechanical modeling of tissues and organs, with a particular focus on the cardiovascular system. My work can thus be seen as at the crossroads of several fields among: applied mathematics, mechanical engineering, physiology, cardiology. However, I would say that the most important component of my work is the methodological aspect, hence the applied mathematics aspects with contributions that comprise: (1) modeling components (2) inverse problem methodologies (3) numerical procedures formulated and analysed within the context of direct and inverse simulations, and finally (4) applications to demonstrate that the novelty of the proposed approach offers new perspectives for actual problems. In this context of applied mathematics, I choose to consider data assimilation as a deterministic **inverse problem** in the sense that we infer the classical input – initial condition, parameters, boundary conditions etc. – of the model of a classical system from classical outputs, namely partial measurements. The main originality of this inverse problem is that the models are dynamical models and observed in their natural context without a full experimental access to the system. In this sense, I like to refer to an image stemming from geophysics, namely, *heart forecasting*, to summarize the problem. Considering this inverse problem, I follow the path to develop original contributions that belong more to control theory than optimization. Indeed, as a natural point of view is to solve this inverse problem by a least square minimization of the input to match the given outputs, I propose new developments in the context of **observer theory** where the dynamical model is controlled during its evolution to better match at each time the given outputs and jointly retrieve the uncertainties initially present in the inputs. With this main scientific ambition, the 4 aspects of my research can then be re-enumerated by saying that I (1) investigate original and effective inverse problem methodologies from an observer point of view (2) develop and analyze adapted numerical methods (3) show that they can have an impact within real medical application. And considering (3) we face the classical necessity of (4) improving the modeling components and numerical aspects of the underlying models in order to improve their predictivity, and afterwards the quality of the resulting estimation.

1.2 What is data assimilation ?

In many application fields, a momentous aspect of the modeling chain is to be able to register the conceptualized system on actual measurements at hand, in order to define a predictive model. This key concept is referred to as *estimation* in its most general form, a typical terminology in statistics. In the context that we present here, we adopt the terminology *data assimilation*, a more and more employed terminology, especially but not only when dealing with large dynamical systems.

We can affirm that data assimilation belongs to the **inverse problems** category, in the sense that some data that are generally potential outputs of the system help to retrieve specific inputs of the model: unknown initial conditions, physical parameters, etc.. Historically, the terminology data assimilation has appeared in the 70's in geophysics [Blum et al., 2009] where complex physical models need to be registered on the real data collected. A typical application of data assimilation is weather forecasting. But since data assimilation can be understood

as an inverse problem or an estimation problem, its origins are much older in connection to decision theory, identification, control etc.. Moreover, while it was for several decades focused on geophysics applications, data assimilation has nowadays reached new fields, in particular the concept has now appeared in life sciences and in particular in the cardiovascular context with the first initiatives of [Sainte-Marie et al., 2006] and [28].

Our objective in this introduction is now to show how the data assimilation theory is adressed in the scientific community by showing the various aspects that can be covered by this theory. Following this idea, we believe that we can highlight some classification keywords that show the variety of points of view in data assimilation. But eventually all these points of view are strongly connected, thus unveiling a very profound unified theory. Here are our keywords:

Stochastic / Deterministic – In a statistics context, we consider a hidden random variable \mathbf{y} called the state of a system – with a probability measure $\mathbb{P}(\mathbf{y})$. This variable is observed through an observation or a measurement z . We associate with this realization a random variable denoted by \mathbf{z} with a probability measure $\mathbb{P}(\mathbf{z})$. The purpose of estimation is to find a function of \mathbf{z} – denoted by $\hat{\mathbf{y}} = \varphi(\mathbf{z})$ and called estimator – that summarizes the information on \mathbf{y} observable through \mathbf{z} , hence be in essence a sufficient statistics [Casella and Berger, 2002].

In the literature various estimators have been proposed. Here we recall three of them which often appear in data assimilation:

- **The Minimum Mean-Square Estimator (MMSE):**

$$\hat{\mathbf{y}} = \underset{\phi}{\operatorname{argmin}} \left\{ \mathbb{E}((\mathbf{y} - \phi(\mathbf{z}))^\top (\mathbf{y} - \phi(\mathbf{z}))) \right\}$$

which in fact can be proved to be given by conditional expectation $\hat{\mathbf{y}} = \mathbb{E}(\mathbf{y}|\mathbf{z})$.

- **The The Least Square Estimator (LSE):** which is the statistics defined by

$$\hat{\mathbf{y}} = \underset{\phi}{\operatorname{argmin}} \left\{ \mathcal{J}(\phi) = \begin{pmatrix} \phi \\ \mathbf{z} \end{pmatrix}^\top \mathcal{P}^{-1} \begin{pmatrix} \phi \\ \mathbf{z} \end{pmatrix} \right\},$$

where \mathcal{P}^{-1} is the covariance matrix associated with the couple of random variables (\mathbf{y}, \mathbf{z})

$$\mathcal{P}^{-1} = \begin{pmatrix} P_{yy} & P_{zy} \\ P_{yz} & P_{zz} \end{pmatrix} = \begin{pmatrix} \operatorname{Cov}(\mathbf{y}) & \operatorname{Cov}(\mathbf{y}, \mathbf{z}) \\ \operatorname{Cov}(\mathbf{z}, \mathbf{y}) & \operatorname{Cov}(\mathbf{z}) \end{pmatrix}.$$

- **The Best Linear Unbiased Estimator (BLUE):**

$$\hat{\mathbf{y}} = \mathbb{E}(\mathbf{y}) + G(\mathbf{z} - \mathbb{E}(\mathbf{z}))$$

where

$$G = \underset{\phi}{\operatorname{argmin}} \left\{ \mathbb{E}((\mathbf{y} - \phi)(\mathbf{y} - \phi)^\top) \right\}, \text{ with } \phi = \phi(\mathbf{z}) \text{ linear}$$

and many other estimators can be cited, for instance the *maximum a posteriori estimator* etc. These estimators are defined with their own objectives. However, they are also equivalent in

some situations. Indeed, the *LSE* and the *BLUE* are equivalent and for gaussian variables, the MMSE, the LSE and the BLUE coincide. In that case, the estimate is then given by

$$\hat{\mathbf{y}} = \mathbb{E}(\mathbf{y}|\mathbf{z}) = \mathbb{E}(\mathbf{y}) + \text{Cov}(\mathbf{y}, \mathbf{z}) \text{Cov}(\mathbf{z})^{-1} (\mathbf{z} - \mathbb{E}(\mathbf{z})) \quad (1.1)$$

Note that, as we see in the last expression, $\hat{\mathbf{y}}$ as a function of the random variable \mathbf{z} is itself a random variable. However, for a given real observation z , there exists a realization of the estimation \hat{y} which can be apprehended in a deterministic context.

Imagine now that we can model the measurement procedure by an observation operator C – assumed to be linear to begin with. For instance, we consider a target state \tilde{y} so that the given observations come from

$$z = C\tilde{y} + \chi$$

where χ is an observation error realization. We associate with χ a random variable $\boldsymbol{\chi}$ of zero mean value and covariance $\text{Cov}(\boldsymbol{\chi}) = W$. Moreover, we assume to have some *a priori* knowledge on the state variable given by its first two moments $y_\diamond = \mathbb{E}(\mathbf{y})$ and $P^- = \text{Cov}(\mathbf{y})$. Then, following (1.1) we end up with

$$\hat{\mathbf{y}} = y_\diamond + P^- C^\top (W + C P^- C^\top)^{-1} (z - C y_\diamond),$$

or equivalently

$$\hat{\mathbf{y}} = y_\diamond + ((P^-)^{-1} + C^\top W C)^{-1} C^\top W^{-1} (z - C y_\diamond),$$

and we call *a posteriori* covariance the quantity

$$P^+ = ((P^-)^{-1} + C^\top W C)^{-1}.$$

As a consequence, when we consider a given realization z , we get the corresponding estimate

$$\hat{y} = y_\diamond + P^+ C^\top W^{-1} (z - C y_\diamond). \quad (1.2)$$

The relation (1.2) can be retrieved in a **purely deterministic context** by computing a generalized inverse of C with an additional regularization term based on our *a priori* knowledge on y . Introducing the state space \mathcal{Y} , equipped with its norm $\|\cdot\|_{\mathcal{Y}}$, we introduce a symmetric definite operator N_\diamond bounded and of bounded inverse so that the equivalent norm

$$\|y\|_{\mathcal{Y}, N_\diamond}^2 = \langle y, N_\diamond y \rangle_{\mathcal{Y}},$$

weighs our *a priori* knowledge. We proceed identically with the observation space \mathcal{Z} with the introduction of symmetric definite operator R bounded and of bounded inverse such that

$$\|y\|_{\mathcal{Z}, R}^2 = \langle y, R y \rangle_{\mathcal{Z}}.$$

Then we introduce a least square criterion to be minimized

$$\min_y \left\{ \mathcal{J}(y) = \frac{1}{2} \|y - y_\diamond\|_{\mathcal{Y}, N_\diamond}^2 + \frac{1}{2} \|z - C y\|_{\mathcal{Z}, R}^2 \right\}, \quad (1.3)$$

where the weights are supported by the norms. The resulting minimizer is

$$\hat{y} = y_\diamond + P^+ C^\top R (z - C y_\diamond),$$

which corresponds exactly to the statistical estimator for the measurement realization z when $W = R^{-1}$ and $P^- = N_{\diamond}^{-1}$.

In data assimilation, this compatible stochastic and deterministic description holds in a very general setting, where in addition to very general observation models there exists a dynamical model describing the state evolution up to some modeling error. On the one hand, the model can be formalized as a stochastic dynamics of the form

$$dy = A(y, \theta) dt + B dw, \quad (y(0), \theta) \text{ random}$$

Here the state y is a random process, the model parameters θ a random variable and dw is typically an additive white noise process associated with some modeling error [Bensoussan, 1971, Curtain, 1975]. On the other hand, the model can also be considered as deterministic with unknown functions to be estimated. We define

$$\dot{y} = A(y, \theta) + B\nu, \quad (y(0), \theta, \nu) \text{ unknown,}$$

where the state variable is in an adequate functional space with – possibly – an uncertain initial condition $y(0)$, θ is a set of unknown parameters in some regular space and ν some additional model error depending of the time¹. The introduction of this dynamical model does not modify the estimation purpose which is to estimate the state $y(t), t \in [0, T]$ given some measurements at hand of the form $z(t), t \in [0, T]$. Moreover, there is a strong correspondence in the resulting estimates in the stochastic or deterministic approaches [Bensoussan, 1971]

We choose to focus on the deterministic formulation of the estimation problem.

This means that our framework will be deterministic. However, we will use from time to time some probabilistic interpretation of our results, for instance keeping the vocabulary of covariance operator when meeting some P^+ operators. In so doing, we will also try to report the possible connections between the stochastic and deterministic context.

Variational / Sequential – In the deterministic context, we have seen that the most natural way to estimate the state from the observations is to introduce a least square criterion of the form (1.3) generalized in a dynamical context. To be more specific, let us consider the following class of system solutions²

$$\begin{cases} \dot{y}_{|\zeta, \nu} = A(y_{|\zeta, \nu}, t) + B\nu(t) \\ y_{|\zeta, \nu}(0) = y_{\diamond} + \zeta \end{cases} \quad (1.4)$$

a class of system where we formalize the state dependency with respect to uncertainties ζ and ν . Here, we adopt a classical probability notation with the bar | to underline that the state $y_{|\zeta, \nu}$ can be computed **knowing** ζ, ν . The target trajectory is still denoted by \tilde{y} with

$$\forall t, z(t) = C(\tilde{y}(t), t) + \chi(t).$$

Here, in a deterministic context, χ represents an error between the observation at hand z (that we could write z^x to avoid any ambiguity) that should be considered as small in the norm of the observation space ($\|z^x - \tilde{z}\|_{\mathcal{Z}} \leq \epsilon$).

¹Note that more general modeling errors could be considered

²the question of uncertain parameters will be treated below

We now complete the state and observation spaces introduced in the previous paragraph with the model noise space \mathcal{Q} equipped with the norm $\|\cdot\|_{\mathcal{Q}}$. We also weigh this norm with the introduction of a symmetric definite bounded isomorphism S with bounded inverse in order to define

$$\|\nu\|_{\mathcal{Q},S}^2 = \langle \nu, S\nu \rangle_{\mathcal{Q}}$$

depending of our estimation *a priori*. We can then define the least square criterion to be minimized, namely

$$\min_{\zeta, \nu} \left\{ \mathcal{J}(\zeta, \nu, t) = \frac{1}{2} \|\zeta\|_{N_{\diamond}}^2 + \frac{1}{2} \int_0^t \left(\|z(s) - C(y_{|\zeta, \nu}(s), t)\|_R^2 + \|\nu(s)\|_S^2 \right) ds \right\}. \quad (1.5)$$

The resulting minimizer produces an estimation of the observed trajectory taking into account the *a priori* knowledge. The weights that we have introduced moderate our confidence in the data and in the modeling choices. Quite often, the operators N_{\diamond} and S are only homothetics with small parameters aiming at regularizing the solution reconstructed from the data. But in a general data assimilation context, there is no reason to believe more in the data than in the model, and every weighting operator should be defined with respect to our quantification of the uncertainty on each modeling and data ingredient. In this respect, a history of comparable estimation plus some statistical tools are required, linking again the statistical interpretation to the deterministic interpretation of our estimation problem, and opening the field of uncertainty quantification. Typically in statistics, as previously seen, the inverse of the operator $P_{\diamond} = N_{\diamond}^{-1}$, $W = R^{-1}$ and $Q = S^{-1}$ are understood as error covariance operators.

In the *Data Assimilation* community, minimizing (1.5) is known as the variational approach as reflected in the popular 4D-Var methodology [Le Dimet and Talagrand, 1986], where the criterion gradient is obtained through an adjoint model integration corresponding to the dynamical model constraint under which the criterion is minimized. As a result, the minimization problem is classically solved by a gradient descent algorithm involving numerous iterations of the combination of the model and adjoint dynamics.

Whereas the variational approach is attractive [Le Dimet and Talagrand, 1986, Courtier, 1997, Nassisopoulos and Bourquin, 2010, Cîndea and Munch, 2015] in particular due to its “genericity”, it involves the solution of a costly optimization problem. Original alternatives can be inspired from the point of view of feedback control theory – rather than optimization – leading to possibly more effective strategies, notwithstanding the deep fundamental interrelations of optimal control and feedback theories [Baras and Bensoussan, 1987, Puel, 2008]. The key concept is to define a so-called *observer* – also referred to as sequential *estimator* in the stochastic context – that uses the data as a control to track the actual trajectory, and concurrently retrieve the unknown parameters. This sequential approach gives a coupled model-data system solved similarly to a usual PDE-based model. We thus define a new dynamical system \hat{y} that pursues the target trajectory and parameters via a feedback control G_y only depending of the similarity measure $J(z, y, t) = z(t) - C(y, t)$

$$\begin{cases} \dot{\hat{y}} = A(\hat{y}, \hat{\theta}) + G_y J(z, y, t) \\ \hat{y}(0) = y_{\diamond} \end{cases} \quad (1.6)$$

The objective of this estimator is to converge in time to the target solution \check{y} that originally has produced the measurement z . The objective of a sequential estimator is thus slightly different

from the variational estimator which produces a trajectory estimation on the whole time-window. In particular a sequential estimator is not meant to estimate the initial condition, even if we will see how this apparent limitation can be overcome.

The challenge in sequential estimation is now to propose adequate feedbacks. As a first proposal, a generic feedback can be defined from the variational estimates. Indeed, the so-called *optimal* sequential estimate is defined by

$$\forall t \in \mathbb{R}_+, \quad \hat{y}(t) = y|_{\text{argmin}} \mathcal{J}(\cdot, t)(t). \quad (1.7)$$

In fact – see Section (2.2.1) – the time differentiation of the definition (1.7) leads to a sequential estimate of the form of (1.6) for large classes of model and observation operators. When all these operators are linear, the resulting estimate is the famous Kalman estimator [Kalman and Bucy, 1961], with for instance in the case of state estimation with a dynamics of the form $A(y) = Ay + \beta$,

$$\begin{cases} \dot{\hat{y}} = A\hat{y} + \beta + PC^*(z - C\hat{y}) \\ \dot{P} = AP + PA^* - PC^*RCP + BSB^* \\ \hat{y}(0) = y_\diamond \\ P(0) = P_\diamond \end{cases}$$

The genericity of the optimal sequential estimator has a cost. A definition of the form (1.7) is classical in dynamic programming [Bellman, 1957] with the well known “curse of dimensionality”. Therefore, we will see the limitations of Kalman-like approaches when considering large dimensional systems such as those coming from PDE models. Fortunately, other choices of feedbacks are possible when we limit the objective of the observer to only retrieve asymptotically the target trajectory. This means that in the absence of modeling errors and observation errors we expect that

$$\hat{y}(t) \xrightarrow[t \rightarrow \infty]{} \check{y}(t)$$

Moreover, this asymptotic should be robust to modeling errors and observation errors. In this case we call the resulting observer **an asymptotic observer**. In this class of observer, various new feedbacks can be designed specifically with respect to the model and observation at hand as envisioned by [Luenberger, 1964, Luenberger, 1966, Luenberger, 1971]. In each case, the asymptotic convergence of the observer should be assessed and is generally based on a so-called *observability* condition that ensures that enough information is contained in the measurements. When this condition is not fulfilled, a weaker result is expected, for instance that the distance between the estimator and the target trajectory decreases in time [Krener and Duarte, 1996], or that the observable part of the target system is retrieved [Haine, 2014b]. As examples for various PDE types, we can cite the specific observers for the wave equation [Ramdani et al., 2010], the elasticity system [Li and Xu, 2011], quantum physics [Bonnabel et al., 2009], hyperbolic problems of conservation laws [Auroux and Blum, 2008], or parabolic problems and reaction-diffusion systems etc.. An important result for Luenberger observer design is that the most simple $G = \gamma C^*$ can often be a good feedback candidate due to the stabilization properties associated with γC^*C , see for instance [Haraux, 1989, Liu, 1997].

Considering this landscape of strategies, **our work is clearly focused on sequential estimation with a particular concern for proposing adapted feedback laws for large dimensional systems, hence on asymptotic observers.**

Continuous-time / Discrete-time – Until now, we have presented the estimation problem for continuous-time dynamical systems. However, the estimation objective can also be defined for discrete-time dynamical systems – namely sequences. In the discrete-time framework, the counterpart of (1.4) will be to consider a sequence in \mathcal{Y} defined recursively by

$$\begin{cases} y_{n+1|\zeta, (\nu_k)_{k=0}^n} = A_{n+1|n}(y_{n|\zeta, (\nu_k)_{k=0}^{n-1}}) + B_n \nu_n, & n \in \mathbb{N} \\ y_{0|\zeta, (\nu_k)_{k=0}^n} = y_\diamond + \zeta \end{cases} \quad (1.8)$$

with $A_{n+1|n}$ the transition operator from step n to step $n+1$, $(\nu_k)_{k=0}^n$ a sequence of unknown contributions in \mathcal{Q} that can be seen as a discrete-time model noise and B_n the model noise operator at step n . Here again, we adopt a useful notation $|$ to say that $A_{n+1|n}$ is a forward operator giving the state at $n+1$ *knowing* the state at n . This type of discrete-time model can be considered in itself but – and it is our point of view – can also correspond to a time discretization of continuous-time model of the form (1.4). As an example we could consider – when stable – an explicit discretization of the continuous-time model (1.4) and we would then have

$$A_{n+1|n}(\cdot) = \mathbb{1} + \Delta t A(\cdot, t_n), \quad B_n = \Delta t B.$$

Similarly for an implicit discretization $A_{n+1|n}$ and B_n are defined implicitly – and computed in practice as a limit of the Newton algorithm – then

$$A_{n+1|n}(\cdot) = (\mathbb{1} - \Delta t A(\cdot, t_{n+1}))^{-1}, \quad B_n \simeq \Delta t B.$$

where the second equality is in fact only an approximation at the first order of a non-linear model noise.

Typically, our objective can be summarized as follows. We want to estimate a real trajectory – time-continuous in essence in our case – by extending to our observer the discretization (1.8) that we would consider as made in a direct simulation. To do so, two strategies are possible. The first consists in discretizing directly the time-continuous estimator (1.6) based on classical finite-difference time-discretization in the spirit of what has been done with (1.8). We obtain for state estimation only a scheme of the form

$$\begin{cases} \hat{y}_{n+1} = A_{n+1|n}(\hat{y}_n) + G_{y,n} J(z_n, y_n, t_n) \\ \hat{y}_0 = y_\diamond \end{cases} \quad (1.9)$$

to be analyzed in terms of consistency and stability. Another strategy is to first discretize the model following (1.8) and then apply the estimation formalism to the discrete-time system [Bensoussan, 1971, Kailath et al., 2000, Simon, 2006]. The resulting estimator can then be analyzed as an consistent estimator of the continuous-time model [Dontchev, 1996, Mordukhovich, 1996]. Here also, the classical stability and consistency aspects must be verified, but they can be simplified by the discrete stable operators generated by the discrete-time estimation formalism [Kalman, 1960a, Hager and Horowitz, 1976, Boutayeb et al., 1997]. Moreover, the ultimate objective for an estimator is to prove its convergence with respect to the target system. In this respect, additional properties such as discrete-time observability conditions may be easier to prove when following **a strategy based on estimation principles at the discrete-time level**.

For instance, when considering the variational approach, we can introduce a discrete-time counterpart of the least square criterion. We introduce $J_k : (z, y) \mapsto J_k(z, y, t)$ and the criterion

$$\min_{\zeta, (\nu_k)_{k < n}} \left\{ \mathcal{J}_n^+(\zeta, (\nu_k)_{k < n}) = \frac{1}{2} \|\zeta\|_{N_\circ}^2 + \frac{1}{2} \sum_{k=0}^n \|J_k(z_k, y_k, t_k)\|_{R_k}^2 + \frac{1}{2} \sum_{k=0}^{n-1} \|\nu_k\|_{S_k}^2 \right\}. \quad (1.10)$$

Note that, in order for (1.10) to be consistent with (1.5), we need for instance $R_k = \delta t R$ and $S_k = \delta t S$. When minimizing this criterion over the constraint of the dynamics (1.8), a discrete-time adjoint model appears as the Lagrange multiplier of the constraint, furnishing a direct stable discretization of the continuous-time adjoint. The resulting minimizing trajectory is defined by

$$\forall n \in \mathbb{N}, \forall k \in [0, n], \quad \bar{y}_{k,n}^+ = y_{k|\operatorname{argmin}_\zeta(\mathcal{J}_n^+)},$$

and the optimal observer can be defined by

$$\forall n \in \mathbb{N}, \quad \hat{y}_n^+ = \bar{y}_{n,n}^+.$$

This resulting discrete-time observer will be of the general form (1.9). The interest of such an approach is that the stability of the discretization can be directly inferred from the optimality at the discrete level. This is typically the case when jointly analyzing the two initial estimation results for linear dynamics, namely the discrete-time Kalman filter in [Kalman, 1960b] and its time-continuous counterpart in [Kalman and Bucy, 1961], see for instance a typical example of result in [Aalto, 2014a].

One of the key aspects of our work is **to propose and analyze various discretization strategies combining discrete-time estimation concepts, classical numerical analysis, discrete-time observability condition.**

Finite-dimensional / Infinite-dimensional – Another fundamental classification concerns the state dimension. The methodologies behind estimation are in fact very dependent of the state dimension either for theoretical questions but also for practical matters. To summarize, we can say that the results are more numerous for finite dimensional systems and covered from more than half a century by the control theory. Here we can give some historical perspective with the pioneer works of Wiener [Wiener, 1949] and Kolmogorov [Kolmogorov, 1939] followed by the very important results of [Kalman, 1960b] and [Kalman and Bucy, 1961] that have given birth to a tremendous literature. In optimal filtering we can in particular cite among many others contributions that have inspired our research: [Fleming and Rishel, 1975, James and Baras, 1988, Baras et al., 1988] or [Krener and Hermann, 1977, Krener, 2003a, Krener, 2003b, Kailath et al., 2000] etc.. with influences from dynamic programming, games theory... For specific design, [Luenberger, 1964, Luenberger, 1971] give fundamental results and were originally thought for finite-dimensional systems even if today they have a larger echo³. In finite-dimensional filtering design, there are also many ramifications, in particular when considering non-linear systems [Slotine and Lohmiller, 1998, Bullo, 2005].

The question of estimation has also become popular for infinite dimensional systems. The state $y(t)$ describes the time evolving solution of an evolution PDE $y(\cdot, t)$, the state space is

³however in a less extensive study of infinite dimensional than of finite dimensional systems [Andrieu and Praly, 2006]

a functional space – typically a Hilbert space – and the model operator A even when linear is unbounded. A large community has arisen, extending numerous results obtained for finite dimensional systems to infinite dimensional systems. We can typically cite very inspiring works such as [Lions, 1968, Bensoussan, 1971, Bensoussan et al., 1993, Curtain and Zwart, 1995, Curtain and Pritchard, 1978, Lasiecka and Triggiani, 2000, Zabczyk, 1992, Russell, 1978], again among many others. There are numerous difficulties introduced by the infinite dimension in order to define solutions of the original systems and the observer, but also to prove the observability of the system – namely, the fact that there is enough information in the observations to estimate the uncertainties considered – hence obtaining the convergence of the observer. Note that, as with finite dimensional systems, authors have first started with optimal filtering strategies before developing specific feedbacks adapted to given PDE formulations as previously cited. Moreover PDE dynamical systems are now also studied in the light of notions covered more regularly in finite dimensional systems such as attractors or Lyapunov theory, see for instance the inspiring examples in [Coron, 2007, Joly, 2006, Fridman, 2013].

One fascinating aspect of observer (and also control) theory is that when the theoretical difficulties introduced by the infinite dimension are finally solved, their discretization raises new stabilization questions. Indeed, the classical discretizations have proved to not conserve at the discrete level, the stabilization properties obtained for the initial PDE. Typically, the limitation comes from the fact that, at the discrete level the observability constants depend of the discretization, hence are not uniform. This has led to numerous works for proposing adapted space discretization [Glowinski et al., 1989, Banks and Ito, 1991, Banks and Fabiano, 1998, Zuazua, 2005, Ramdani et al., 2007, Ervedoza, 2009] – and also time discretization as already mentioned – with adapted strategies to prove the convergence of the discretized observer to the real trajectory. Finally, the space discretization of the PDE has also consequences on the practical usability of the designed observer. In fact, numerous designs – in particular those coming from optimal filtering approaches in linear and even more in non-linear settings – are confronted with a curse of dimensionality [Bellman, 1957]. As a consequence, the filters obtained are unpractical for the large dimensional discretization used nowadays. Two ways are then foreseen for circumventing this curse of dimensionality: (1) the Luenberger approach or (2) reduced-order optimal filtering strategy where the optimal feedback is computed and applied on a sub-space of \mathcal{Y} . We have already cited numerous works on (1). Concerning (2), we based our own developments on the inspiring feedback propositions of [Pham et al., 1998a, Pham et al., 1998b, Pham, 2001] with the Singular Evolutive Extended Kalman Filter (SEEK) and the Singular Evolutive Interpolated Kalman Filter (SEIK).

In our work, we have then decided to propose filters for PDEs which can be discretized, hence implemented in a practical numerical environment. Moreover, our objective is to be able to propose the numerical analysis of these discretizations, hence proving that the discretized observer converges to the target trajectory with the discretization refinement.

State estimation / parameter identification – So far we have considered a general class of dynamical model

$$\begin{cases} \dot{y}(t) = A(y(t), t) + B\nu(t), & t \in \mathbb{R}^+ \\ y(0) = y_\diamond + \zeta \end{cases}$$

where the unknown contributions can be seen as a model noise, and the initial condition contribution $\zeta_y - y_\diamond$ being the known *a priori* part. We now discuss how to also estimate – or identify – uncertain parameters in the model operator dynamics $A(y(t), \theta, t)$. We then say that θ is uncertain around an *a priori* θ_\diamond so that $\theta = \theta_\diamond + \zeta_\theta$.

We also introduce a parameter space \mathcal{P} equipped with a norm $\|\cdot\|_{\mathcal{P}}$. Then we consider the symmetric definite operator N_θ , a bounded isomorphism of bounded inverse that weighs the norm

$$\|\theta\|_{\mathcal{P}, N_\theta}^2 = \langle \theta, N_\theta \theta \rangle_{\mathcal{P}}.$$

As a first idea, we can directly extend the variational approach in order to identify parameters [Navon, 1998]

$$\begin{aligned} \min_{\zeta_y, \zeta_\theta, \nu} \{ \mathcal{J}(\zeta_y, \zeta_\theta, \nu, t) \\ = \frac{1}{2} \|\zeta_y\|_{N_\diamond}^2 + \frac{1}{2} \|\zeta_\theta\|_{N_\theta}^2 + \frac{1}{2} \int_0^t \left(\|z(s) - C(y|_{\zeta_y, \zeta_\theta, \nu}(s))\|_R^2 + \|\nu(s)\|_S^2 \right) ds \}. \end{aligned}$$

However, the extension can be less obvious when considering observers. The principle is, in fact, to define a pseudo-dynamics for the parameters. Then an augmented state vector $\begin{pmatrix} y \\ \theta \end{pmatrix}$ is associated with the dynamics

$$\begin{cases} \dot{y}|_{\zeta_y, \zeta_\theta, \nu} = A(y|_{\zeta_y, \zeta_\theta, \nu}, \theta|_{\zeta_\theta}, t) + B\nu \\ \dot{\theta} = 0 \\ y|_{\zeta_y, \zeta_\theta, \nu}(0) = y_\diamond + \zeta_y \\ \theta|_{\zeta_\theta} = \theta_\diamond + \zeta_\theta \end{cases} \quad (1.11)$$

This results in the sequential approach in the definition of a new dynamical system $(\hat{y} \ \hat{\theta})^\top$ that pursues the target trajectory and parameters via a feedback control $G = (G_y \ G_\theta)^\top$ acting on the similarity measure $J(z, y, t)$. The dynamics then reads

$$\begin{cases} \dot{\hat{y}} = A(\hat{y}, \hat{\theta}) + G_y J(z, y, t) \\ \dot{\hat{\theta}} = G_\theta J(z, y, t) \\ \hat{y}(0) = y_\diamond \\ \hat{\theta}(0) = \theta_\diamond \end{cases} \quad (1.12)$$

The second equation in (1.12) enables the identification of parameters through a new dynamics. The final value of the parameter estimation corresponds to the expected identification. Note that the parameter dynamics is obvious to invert, namely the final value coincides with the initial value. This is not the case with the rest of the state initial condition, which can be difficult to reconstruct with observers.

Let us now give some vocabulary and references about joint state and parameter estimation. When assuming perfectly known parameters, we classically refer to state estimation. The question of extending a state observer to a joint state-parameter observer is known as *adaptive observer design*. Adaptive observer is clearly a notion that has been introduced in finite dimensional estimation. But there were some attempts to propose extensions for PDEs, for instance [Baumeister and Scondo, 1987a, Demetriou and Rosen, 1994a, Chapouly and Mirrahimi,

2010]. Finally, we mention that there exist a lot of works where only parameter identification are considered [Chavent, 2010, Banks and Kunisch, 1989]. In the formalism (1.11)-(1.12), it is then quite simple to see that parameter identification only is a singular case where the initial condition confidence is infinite. We have in particular studied the consequences of such asymptotic consideration in terms of theoretical identification results, but also in term of observer design – namely, is the state feedback G_y is null when we only consider uncertain parameters?

All the notions that we have introduced in the previous paragraphs have extensions for joint state-parameter estimation. The observability condition will then express the fact that there is enough information in the measurements to retrieve all the uncertainties including for identifying the parameters, see for instance [Demetriou and Rosen, 1994b, Zhang, 2002, Alves et al., 2009]. Then, the observability condition is often called identification condition.

In our work, **we have proposed a quite general strategy to extend a state observer to a joint state-parameter observer with a convergence proof strategy relying on a joint state-parameter observability condition that can be followed in different cases.** Moreover, we have linked this approach to a least square criterion and proposed original discretizations.

REMARK 1.2.1 (MACHINE LEARNING / DATA ASSIMILATION)

To end this section, we would like to emphasize some subjects that are not covered by data assimilation. Indeed, in data assimilation a fundamental assumption is that we can reasonably describe the system behavior and measurement procedures. In other words, in data assimilation there is a quite strong confidence in our capability to define models of the dynamics and models of the observation. Typically in weather forecasting, since L.F. Richardson (1922), numerous models of the atmospheric circulation have been developed. Considering the cardiac system, complex causal models exist to describe the physiology [Nash and Hunter, 2000]. This is to be opposed to some other organs as for instance brain studies where the physiology is still so complex that there is limited success in describing the causal chain between the brain state (if describable) and observation from a Electroencephalography or a Magnetoencephalography for instance. When models are unknown, we enter in a vast domain of statistical learning where knowledge on observations and corresponding state contribute to learn these models [Hastie et al., 2001]. These theories are not intrinsically incompatible. In a way, data assimilation is more promising as soon as the models are accurate. But an overstep of statistical learning can be considered if some modeling ingredients are unreachable. For instance in cardiology, modeling the environmental impact on the cardiac system as a direct physiological input can be very complex. Then some meta-models, statistical learning and big data concept can be envisioned to cover these aspects. But this goes beyond our presentation.

1.3 The cardiovascular system playground

The heart and more generally the cardiovascular system is a complex system. The heart function is to drive the blood circulation at every beat. It is primarily a muscular pump triggered by electrical signals. Its structure consisting of several admission and ejection chambers and its electromechanical properties make it a biological engine well-adapted to this function. We find in cardiac modeling various biophysical phenomena with

- **electrophysiology** which is a bio-chemical phenomenon typically understood as reaction-diffusion phenomenon. The resulting action-potential is typically diffused up to the skin where it can actually be measured with an electrocardiogram;

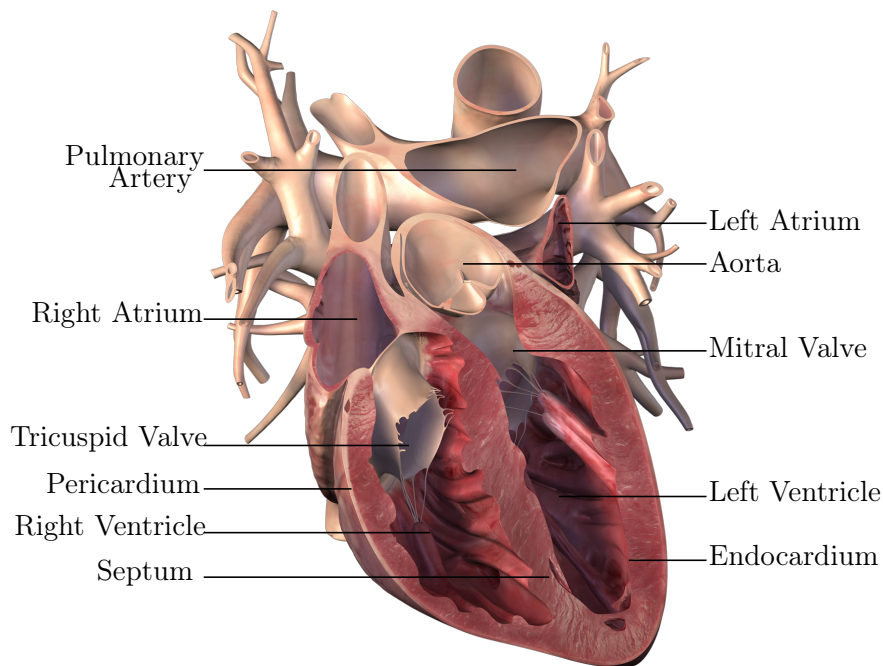


Figure 1.1: Cardiac anatomy

- **cardiac contraction**, resulting from the action-potential propagation, which involves large strain elastodynamics equations with specific micro-macro constitutive laws;
- **fluid-structure interaction**, in the cardiac cavity but also in the arterial systems connected to the cardiac system. Moreover, the heart tissue is also perfused by blood hence is a poro-mechanics system integrating solid and fluid. Finally when the heart is of interest, some simplified fluids models can be envisioned leading to linear or non-linear hyperbolic systems, typically a shallow-water (Saint-Venant) type of systems.
- **Wave equations** in recent data acquisition techniques. In particular much promise resides in the elastography modality [Pernot et al., 2011] that records waves generated by a controlled actuator in a tissue. There, transient elastography – provided by ultrasound (US) devices – leads to wave propagation equations as opposed to Magnetic Resonance Elastography (MRE) that assumes a harmonic regime, hence Helmholtz-like equations.

We see that the cardiovascular system is a beautiful modeling playground involving many different types of PDEs with multi-scale aspects in space and even time – as the heart can be seen during a heart beat up to its remodeling during life. Moreover, we see that this system is indirectly observed by many ways. We have already mentioned the electrocardiogram and introduced the promise of elastography. Clearly, medical images such as echography, Magnetic Resonance Imaging (MRI) or computed tomography (CT) bring a lot of information on the heart contraction. There are also pressure recordings typically by catheters; flow recordings by Doppler or Phase Contrast MRI. Therefore, we see that the cardiovascular system is not only a playground for modeling but also for coupling models and observations.

But eventually it is clearly more than just a playground. Cardiovascular diseases (CVD) have a significant impact on the European society in terms of mortality, morbidity and related healthcare costs. Indeed, they cause over 1.9 million deaths in the EU every year (40% of all

deaths), with a total estimated cost of €196 billion per year. As a consequence, there have been **many attempts to bring multidisciplinary expertise** into medical research, and in particular modern computer sciences tools with the aim of **introducing modeling and simulation capabilities** for such a complex biophysical system [Smith et al., 2011]. In the past years, a growing understanding has appeared on the necessity that these simulations **be personalized on each subject** to really offer diagnosis and prognosis tools. This requires acquiring the specific anatomy, but even more importantly registering the biophysical state – with possibly non-standard conditions associated with a disease. The biophysical personalization is based on the abundant data available for each patient: medical imaging, pressure records, electrocardiograms... Mathematically speaking, this problem directly falls into the data assimilation framework. Indeed, **the principle is to benefit from the data at hand to retrieve the specific state and parameters of the underlying dynamical physical model**, as commonly done in weather forecasting or climatology, hence the possible epithet of *heart forecasting*. At the forefront of the development of original data assimilation strategies of effective use in a real context, we have developed observer strategies to jointly estimate the cardiac state and identify parameters relevant to the diagnosis of certain pathologies.

1.3.1 Electrophysiology

Cardiac electrophysiology describes the electrical phenomena that occur in the cardiac tissue and trigger the cardiac mechanical contraction. Over the past decades, cardiac electrophysiological modeling has made huge progresses, and very realistic modeling and simulations are presented in the literature as reviewed in [Keener and Sneyd, 2004, Colli Franzone et al., 2014], in particular in pathological cases. Various electrophysiological models – based on a reaction-diffusion model – exist as for example the bidomain model and its first approximation the monodomain model. The bidomain equation can be written – in terms of w_e , the extracellular potential and $w_m = w_i - w_e$, the transmembrane potential with w_i , the intracellular potential – as

$$\begin{cases} a_m \left(c_m \partial_t w_m + i_{ion}(w_m, \kappa) \right) - \nabla \cdot (\underline{\sigma}_i \cdot \nabla w_m) \\ \qquad \qquad \qquad = \nabla \cdot (\underline{\sigma}_i \cdot \nabla w_e) + a_m i_{app}, & \text{in } \Omega \times (0, T), \\ \nabla \cdot ((\underline{\sigma}_i + \underline{\sigma}_e) \cdot \nabla w_e) = -\nabla \cdot (\underline{\sigma}_i \cdot \nabla w_m), & \text{in } \Omega \times (0, T), \end{cases}$$

where Ω denotes the domain of interest, and with appropriate boundary conditions

$$\begin{cases} (\underline{\sigma}_i \cdot \nabla w_e) \cdot \underline{n} = -(\underline{\sigma}_i \cdot \nabla w_m) \cdot \underline{n}, & \text{in } \partial\Omega \times (0, T), \\ (\underline{\sigma}_e \cdot \nabla w_e) \cdot \underline{n} = 0, & \text{in } \partial\Omega \times (0, T), \end{cases}$$

where a_m is a positive constant denoting the ratio of membrane area per unit volume, c_m the membrane capacitance per unit surface and i_{app} a given applied stimulus current. The term $i_{ion}(w_m, \kappa)$ – called the reaction term – represents the ionic current across the membrane and depends of internal current variable κ that have their own dynamics [Colli Franzone et al., 2014]. It models the transmembrane potential evolution in the cell over time. The extracellular potential w_e is defined up to a constant. In order to have a well-posed problem, the condition $\int_{\Omega} w_e = 0$ is added. Initially, the cell is at the resting potential around -80mV . Due to a stimulus, the cell becomes depolarized very quickly and the value of the transmembrane potential is around 20mV (1mV in rescaling cases). During the depolarization phase – called the plateau phase – the mechanical contraction of the cell occurs. Then the repolarization of the cell

begins. During this phase, the cell is in refractory phase, which means that a new stimulus cannot trigger a new depolarization. The reaction term $i_{ion}(w_m, \dots)$ governs these different states of the cell. In order to describe this complex process which occurs across the membrane, one (or more) ordinary differential equation(s) can be coupled with the previous bidomain equations. There is a large variety of ionic models which represent the action potential. The existence and uniqueness of the bidomain model has been studied for different ionic models in the literature, see again [Colli Franzone et al., 2014] and references therein. A particular case of the bidomain model is the monodomain model, obtained by assuming that the intra- and extracellular domains have equal anisotropy ratios

$$\begin{cases} a_m \left(C_m \partial_t w_m + i_{ion}(w_m, \kappa) \right) - \nabla \cdot (\underline{\underline{\sigma}}_m \cdot \nabla w_m) = A_m I_{app}, & \text{in } \Omega \times (0, T), \\ (\underline{\underline{\sigma}}_m \cdot \nabla w_m) \cdot \underline{n} = 0, & \text{in } \partial\Omega \times (0, T). \end{cases}$$

Finally we can say that electrophysiological models belongs to the class of reaction-diffusion systems that we can write in the general form

$$\begin{cases} \partial_t w - \nabla \cdot (\underline{\underline{D}} \cdot \nabla w) = kf(w, \kappa), & \text{in } \Omega \times (0, T), \\ \dot{\kappa} = g(\kappa, w) & \text{in } \Omega \times (0, T) \\ (\underline{\underline{D}} \cdot \nabla w) \cdot \underline{n} = 0, & \text{on } \partial\Omega \times (0, T), \\ w(\underline{x}, 0) = w_0(\underline{x}), & \text{in } \Omega. \end{cases}$$

And as a first analysis step we will also consider even simpler reaction diffusion systems where we omit the internal variables.

1.3.2 Cardiac Mechanics

The heart contraction results from the cardiac muscle cells contraction that occurs at the nanoscale of a hierarchical multi-scale structure with the attachment of so-called cross-bridges within sarcomeres, namely, the creation of chemical bonds between myosin heads and specific sites on actin filaments [Tortora and Derrickson, 2009]. Therefore, the subcellular scale is where biochemistry and mechanics are intimately coupled, of consequence at the macroscopic scales with the organ contraction. The objective of a heart model is then to incorporate in a continuum mechanics formulation the active stresses driving the contraction and resulting from the formation of cross-bridges triggered by the activation.

For a continuum mechanics description, we consider the heart domain denoted by $\Omega(t)$ at any time t . This domain is the image of a reference configuration Ω_0 through the solid deformation mapping $\underline{\varphi}$

$$\underline{\varphi} : \begin{cases} \Omega_0 \times [0, T] \longrightarrow \Omega(t), \\ (\underline{\xi}, t) \longmapsto \underline{x} = \underline{\xi} + \underline{u}(\underline{\xi}, t) \end{cases}$$

where \underline{u} is the solid displacement. The solid velocity is given by $\underline{v} = \dot{\underline{u}}$. The deformation gradient \underline{F} is given by $\underline{F}(\underline{\xi}, t) = \underline{\nabla}_{\underline{\xi}} \underline{\phi} = \underline{\mathbb{1}} + \underline{\nabla}_{\underline{\xi}} \underline{u}$, and its determinant is denoted by J . The right Cauchy-Green deformation tensor is defined by $\underline{C} = \underline{F}^\top \cdot \underline{F}$, the Green-Lagrange tensor by $\underline{e} = \frac{1}{2}(\underline{C} - \underline{\mathbb{1}}) = \frac{1}{2}(\underline{\nabla}_{\underline{\xi}} \underline{u} + (\underline{\nabla}_{\underline{\xi}} \underline{u})^\top + (\underline{\nabla}_{\underline{\xi}} \underline{u})^\top \cdot \underline{\nabla}_{\underline{\xi}} \underline{u})$, and its linearization by $\underline{\underline{e}} = \frac{1}{2}(\underline{\nabla}_{\underline{\xi}} \underline{u} + (\underline{\nabla}_{\underline{\xi}} \underline{u})^\top)$.

In the reference configuration, the strong form of the principle of dynamics reads

$$\begin{cases} \rho \partial_t \underline{v} - \operatorname{div}(\underline{T}) = \underline{f}, & \text{in } \Omega_0 \\ \text{Boundary conditions} \end{cases} \quad (1.13)$$

where ρ is the volumic mass, \underline{T} is the first Piola-Kirchhoff stress tensor, and \underline{f} are some volumic forces. In a weak form – also known as the Principle of Virtual Work – we have a balance between the virtual power of inertia forces, of internal forces and of external forces. Namely, with $\mathcal{V}(\Omega_0)$ the space of admissible virtual displacements, we have

$$\forall \underline{v}^b \in \mathcal{V}(\Omega_0), \quad \mathcal{P}_i(\underline{v}^b) + \mathcal{P}_{\text{int}}(\underline{v}^b) = \mathcal{P}_{\text{ext}}(\underline{v}^b)$$

with typically

$$\mathcal{P}_i(\underline{v}^b) = \int_{\Omega_0} \rho \partial_t \underline{v} \cdot \underline{v}^b \, d\Omega, \quad \mathcal{P}_{\text{ext}} = \int_{\Omega_0} \underline{f} \cdot \underline{v}^b \, d\Omega$$

and

$$\mathcal{P}_{\text{int}}(\underline{v}^b) = \int_{\Omega_0} \underline{T} : \underline{\nabla} \underline{v}^b \, d\Omega = \int_{\Omega_0} \underline{\Sigma} : \underline{d}_{\underline{u}} \underline{e}(\underline{u}) \cdot \underline{v}^b \, d\Omega$$

where $\underline{\Sigma} = \underline{F}^{-1} \cdot \underline{T}$ is the second Piola-Kirchhoff stress tensor.

In cardiac mechanics, the objective at the organ level is then to propose a modeling of the stress tensor to include the muscle contraction along the fiber. Hence, in general [Glass et al., 1991, Guccione and McCulloch, 1993, Nash and Hunter, 2000, Rice and de Tombe, 2004] or [Sainte-Marie et al., 2006, Pathmanathan et al., 2010], we end up with

$$\underline{\Sigma} = \underline{\Sigma}_p + \underline{\Sigma}_v + \sigma_a(t) \underline{\tau} \otimes \underline{\tau}$$

where $\underline{\Sigma}_p$ represents the passive – typically hyperelastic – stresses, $\underline{\Sigma}_v$ represents the viscous stresses and $\sigma(t)$ is the active stress along the fiber direction $\underline{\tau}$. In the rest of this manuscript we use $\underline{\Sigma}_v = \eta \underline{\dot{e}}$ and $\underline{\Sigma}_p = \frac{\partial \mathcal{W}}{\partial \underline{e}}$ with \mathcal{W} a function of the invariants [Le Tallec, 1994], for instance for biological tissues [Humphrey, 2003, Holzapfel and Ogden, 2009] propose choice of the form

$$\mathcal{W} = \alpha_0 \exp(\alpha_1 (J_1 - 3)^2) + \alpha_2 \exp(\alpha_3 (J_4(\underline{\tau}) - 3)^2).$$

In this landscape, [Sainte-Marie et al., 2006], [14] have proposed a multi-scale strategy allowing to link microscopic description of the active contraction [Huxley, 1957, Huxley and Simmons, 1971, Eisenberg and Hill, 1978, Panerai, 1980, Bestel et al., 2001, Rice et al., 2003, Marcucci and Truskinovsky, 2010, Guérin et al., 2011] accounting for the number of actin-myosin crossbridges that are generated to the macroscopic description σ_a . A cross-bridge is seen as a special chemical entity having internal mechanical variables – or degrees of freedom [Hill, 2004, Maugin and Muschik, 1994]. For instance in one of the pioneering and most studied work [Huxley, 1957], the cross-bridge is seen as a system with one mechanical degree-of-freedom (dof) corresponding to a linear spring that is under tension as soon as the myosin head attaches to the actin filament.

REMARK 1.3.1 (ACTIVE STRAIN MODELS)

Note that, recently, some works [Rossi et al., 2014] have followed the path of considering models of active contraction through a decomposition of \underline{F} between and active part and a passive part as it is naturally the case when dealing with mechanical models of growth. The advantage of such models is that their

mathematical analysis is facilitated by the fact that they directly induce energy balances. However, the strategy proposed in [14] also allows energy balances and is adapted to stress-based active model, hence benefiting from their large acceptance in the computational engineering but also biomechanics and physiology communities due to their clearer physiological basis.

1.3.3 The cardiovascular system

The main external loading applied to the myocardium is not a volume loading \underline{f} but corresponds to the blood pressure p_v applied on the internal cavity walls. In other words, the virtual power of the external forces corresponds to

$$\mathcal{P}_{\text{ext}} = - \int_{\Gamma_{\text{endo}}} p_v \underline{n} \cdot \underline{F}^{-1} \cdot \underline{v}^b J \, d\Gamma$$

where \underline{n} is the normal vector and Γ_{endo} represents both the left and right endocardiums. Therefore, we need to model the time evolution of p_v . For the heart, we distinguish different phases. When the valves are closed – which corresponds to an isovolumic phase of the heart contraction – the internal pressure is mathematically – as a Lagrange multiplier – the result of the isovolumic constraint in the cavity, see [Sainte-Marie et al., 2006]. However, when the valves are open, the pressure results from a balance with the circulatory system. Then, the pressure can be given when it is measured, or modeled by coupling the solid mechanics with a circulation model. Here, 3 levels of description exist: 0D, 1D or 3D models, and variations by coupling these models are possible [Formaggia et al., 2009, Xiao et al., 2013].

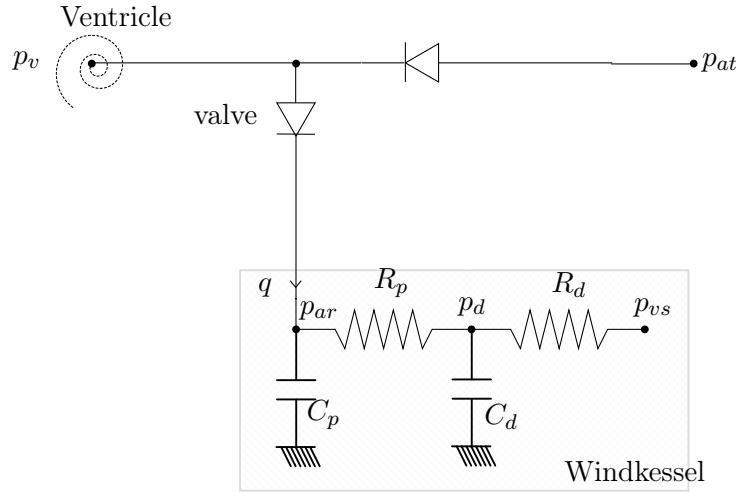


Figure 1.2: A Windkessel model coupled to the ventricle

The 0D models, also called Windkessel models, consist in modeling the pressure in the cavity as uniform and linking it to a simplified model of circulation describing the relation between flow and pressure as an electrical circuit linking current and voltage. For instance, a double Windkessel as in Figure 1.2 gives

$$\begin{cases} C_p \dot{p}_{ar} + \frac{p_{ar} - p_d}{R_p} = q, \\ C_d \dot{p}_d + \frac{p_d - p_{ar}}{R_p} = \frac{p_{vs} - p_d}{R_d}. \end{cases}$$

with q the blood flow ejected by the heart, given by (see Figure 1.3)

$$q = -\frac{d}{dt} \int_{\bar{\Gamma}_{\text{endo}}} \underline{v} \cdot \underline{F}^{-1} \cdot \underline{n} J \, d\Gamma.$$

The ventricular pressure $p_v = p_{ar}$ when the aortic valve is open for the left ventricle – the pulmonary valve is open for the right ventricle, respectively.

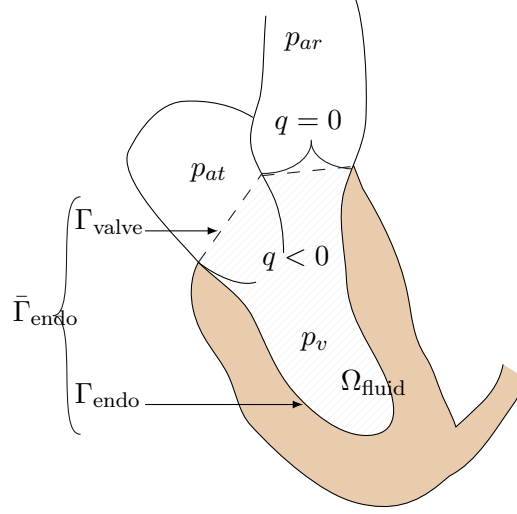


Figure 1.3: Schematic of the ventricular cavity

The 1D models are often considered for modeling arteries as monodimensional systems following the central line of the vessels [Formaggia et al., 2009]. We typically end up with models with an hyperbolic part very similar to what we usually find in shallow water models

$$\begin{cases} \partial_t a + \partial_x(av) = 0, & \text{in } \Omega \\ \partial_t(av) + \partial_x(av^2) + \frac{a}{\rho} \frac{\partial p}{\partial x} + \nu \frac{v}{a} = 0, & \text{in } \Omega \end{cases}$$

where a is the section area of the artery and v is the flow. These models can then be coupled to a 3D model of the intra-cavity circulation or more often a 0D model. Moreover, junctions between vessels are also often modelled with 0D transmission models.

Finally, 3D models of complete fluid structure interaction models can be considered to model the blood within the cardiac cavity, but also to represent arterial blood flows. In this respect, we rapidly summarize the classical formulation of a fluid-structure interaction problem in an artery. We denote the solid and fluid quantities with s and f subscripts, respectively. We adopt an Arbitrary Lagrangian Eulerian (ALE) formulation in the fluid by introducing the mapping

$$\varphi_{\text{ale}} : \Omega_0^f \times [0, T] \rightarrow \Omega^f(t),$$

such that $\varphi_{\text{ale}}|_{\Sigma_0} = \varphi_s|_{\Sigma_0}$, but does not necessarily follow the material trajectories inside the domain. We then associate the corresponding deformation gradient $\underline{F}_f(\xi_f, t) = \underline{\nabla} \varphi_{\text{ale}}(\xi_f, t)$, and determinant $J_f(\xi_f, t) = \det \underline{F}_f(\xi_f, t)$. The fluid domain velocity is denoted by $\underline{v}_{\text{ale}}(\xi_f, t) = \frac{d}{dt} \varphi_{\text{ale}}(\xi_f, t)$. Noting that $\underline{v}_{\text{ale}}|_{\Sigma_0} = \underline{v}_s|_{\Sigma_0}$, we have thus defined an extension map such that

$$\underline{v}_{\text{ale}} = \text{Ext}(\underline{v}_s|_{\Sigma_0}), \quad \text{in } \Omega_0^f.$$

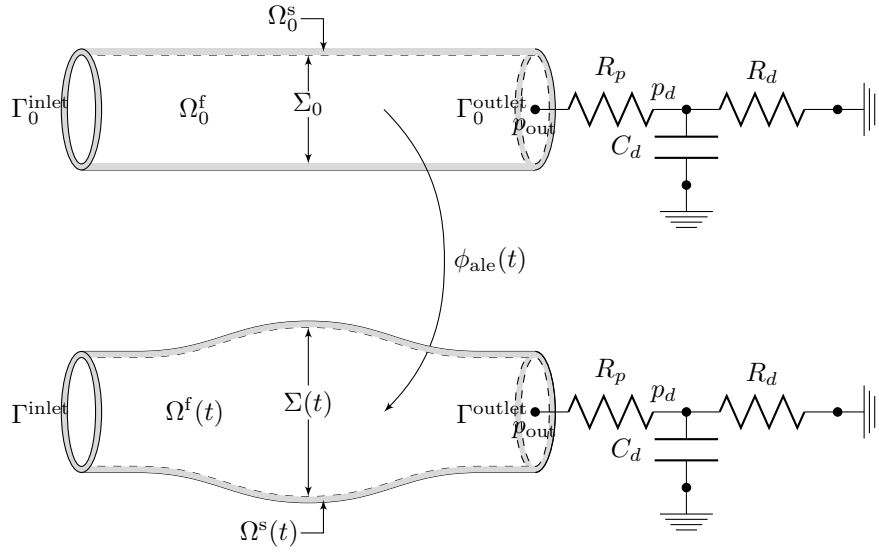


Figure 1.4: Reference (top) and current domain (bottom) in the ALE formulation

The strong form of the coupled fluid-structure problem consists of the two formulations (1.14a),(1.14b) with the coupling conditions on the interface (1.14c)

$$\left\{ \begin{array}{ll} \underline{v}_{\text{ale}} = \text{Ext}(\underline{v}_s|_{\Sigma_0}), & \text{in } \Omega_0^f, \\ \frac{\rho_f}{J_f} \partial_t (J_f \underline{v}_f) \Big|_{\underline{\xi}_f} + \rho_f (\underline{v}_f - \underline{v}_{\text{ale}}) \cdot \underline{\nabla}_{\underline{x}} \underline{v}_f - 2\mu \underline{\nabla}_{\underline{x}} (\underline{\varepsilon}_f(\underline{v}_f)) + \underline{\nabla}_{\underline{x}} p_f = \rho_f \underline{f}_f, & \text{in } \Omega^f(t), \\ \underline{\nabla}_{\underline{x}} \cdot \underline{v}_f = 0, & \text{in } \Omega^f(t) \end{array} \right. \quad (1.14a)$$

$$\left\{ \begin{array}{ll} \rho_s \partial_t \underline{v}_s - \underline{\nabla}_{\underline{\xi}} \cdot \underline{T}_s = 0, & \text{in } \Omega_0^s, \\ \underline{T}_s \cdot \underline{n}_s = -k_s (\underline{u}_s - \underline{u}_b), & \text{on } \Gamma_{\text{in}}^s, \\ \underline{T}_s \cdot \underline{n}_s = -k_s \underline{u}_s - c_s \underline{v}_s, & \text{on } \Gamma_s \end{array} \right. \quad (1.14b)$$

$$\left\{ \begin{array}{ll} \underline{v}_f = \underline{v}_s, & \text{on } \Sigma(t), \\ \underline{T}_s \cdot \underline{n}_s = J_f \underline{\sigma}_f(\underline{v}_f, p_f) \cdot (\underline{F}_f)^{-\top} \cdot \underline{n}_s, & \text{on } \Sigma_0, \end{array} \right. \quad (1.14c)$$

where $\frac{d}{dt} \Big|_{\underline{\xi}}$ represents the ALE time derivative (see [Formaggia et al., 2009] and references therein) and \underline{f}_f is a force per unit mass – for example the gravity that may not be negligible in the blood flow domain for long vertical arteries.

1.4 Past contributions

In order to summarize my research in one sentence my main research objective is *to formulate and mathematically justify original data assimilation strategies that can use data as provided by the measurement procedure, in order to estimate unknown PDE model inputs such as initial*

conditions or parameters. With this objective in mind, the point of view is that of **observer theory in general in a deterministic context** to control the initial PDE model so that it pursues the observed trajectory.

To further classify my results, and more generally to partition the observer research field, we can distinguish **5 fundamental challenges** to be solved for each PDE model and measurement at hand.

Challenge 1: Formulation of adequate similarity measures adapted to the system of interest and design of the control feedback;

Challenge 2: Analysis of the resulting observer: existence, stability, convergence;

Challenge 3: Joint identification of model parameters – namely, adaptive observer formulation – and analysis of identification properties;

Challenge 4: Discretization, numerical strategies and numerical analysis of the observer formulation;

Challenge 5: Applications with real data, in particular in the cardiovascular context.

1.4.1 Data similarity measures and observer design

As recalled in the introduction, optimal filtering is very general in its formulation but its application is limited when considering PDEs, as the covariance operator becomes uncomputable. In order to overcome this difficulty, we have followed two directions depending of the nature of the PDE considered:

- **For dissipative problems**, as the frequencies of interest can be considered as limited we chose to rely on **reduced-order Kalman-based filtering** where the optimal filtering principles are limited to a subspace of interest. In essence, this means that the covariance operator is proved to be decomposed into

$$\forall t, \quad P(t) = L(t)U(t)^{-1}L(t)^*,$$

where L^* is a projection operator on a subspace (potentially finite dimensional) and U is an invertible covariance operator on this subspace. There the dynamics of L and U can be computed. In this respect, our work on reduced-order filtering [16, 22–24] – see [Section 2.3.1.4](#) – has allowed us to experiment with some reduced state filtering design for two examples of systems that are aimed to be discretized with a reduced basis strategy – POD in our case. The POD basis is then also used to decompose the initial condition uncertainty into a small space to be filtered and the rest. The first system example is an over-damped mechanical system as can be the case in cardiac mechanics [13]. The second system was of reaction-diffusion type occurring in electrophysiology [19].

- **For conservative problems**, there is no hope to rely on reduced-order optimal filtering as unfiltered error will increase in the uncontrolled space and irremediably pollute the estimation. Therefore, we must rely on a **Luenberger observer**, which implies to design specifically the feedback for each type of PDE and type of measurement. In this context,

we proposed in particular an original observer feedback for mechanical systems when only the displacement field – as opposed to the velocity field – is partially observed. Indeed, when the velocity is observed, a classical observer for wave-like equations is given by the Direct Velocity Feedback (DVF). Typically, for a wave equation observed on a subdomain Ω_{obs} , the DVF observer reads

$$\begin{cases} \dot{\hat{u}}(x, t) = \hat{v}(x, t), & (x, t) \in \Omega \times (0, \infty) \\ \dot{\hat{v}}(x, t) - \Delta \hat{u}(x, t) = -\gamma \mathbf{1}_{\Omega_{\text{obs}}}(x)(z(t) - \hat{v}|_{\Omega_{\text{obs}}}(x, t)), & (x, t) \in \Omega \times (0, \infty) \\ \hat{u}(x, 0) = u_{\diamond}(x), \quad \hat{v}(x, 0) = v_{\diamond}(x), & x \in \Omega \end{cases}$$

But there was no equivalent when the displacement is directly measured and cannot be differentiated in time without dramatically amplifying the measurement noise. More generally saying, we aim at designing a feedback that can use directly the observed field of a wave-like system and not its time-derivative. In [25] we propose such an original filter in and give several results concerning its practical implementation. It reads

$$\begin{cases} \dot{\hat{u}}(x, t) = \hat{v}(x, t) + \gamma \text{Ext}_{\Omega_{\text{obs}}}(z(t) - \hat{u}|_{\Omega_{\text{obs}}}(x, t)), & (x, t) \in \Omega \times (0, \infty) \\ \dot{\hat{v}}(x, t) - \Delta \hat{u}(x, t) = 0, & (x, t) \in \Omega \times (0, \infty) \\ \hat{u}(x, 0) = u_{\diamond}(x), \quad \hat{v}(x, 0) = \hat{v}_{\diamond}(x), & x \in \Omega \end{cases}$$

with

$$\text{Ext}_{\Omega_{\text{obs}}} : \begin{cases} H^1(\Omega_{\text{obs}}) \rightarrow H_0^1(\Omega) \\ \phi \mapsto \psi \text{ s.t. } : \begin{cases} \Delta \psi = 0, & \text{in } \Omega \setminus \Omega_{\text{obs}} \\ \psi = 0, & \text{on } \partial\Omega \\ \psi = \phi, & \text{in } \overline{\Omega_{\text{obs}}} \end{cases} \end{cases}$$

and we called it the Schur Displacement Feedback (SDF) observer – see Section 2.3.2.

From this first design, we found an important advantage of our SDF when considering **shape measurements** in cardiac mechanics. Indeed, an important question in data assimilation for cardiac mechanics is to be able to handle data that correspond to the contours $\{\mathfrak{S}(t), t \in [0, T]\}$ of the beating heart observed through medical imaging. In that case, we derived in [25, 26] a similarity measure based on the distance to the contour that generalizes the case where we observed the normal displacement at the boundary, namely by derivating the least square functional

$$\mathcal{J}_{\text{data}}(z, y, t) = \int_{\Sigma} |\text{dist}_{\mathfrak{S}}(\underline{\xi} + \underline{u}(\underline{\xi}, t), t)|^2 d\Gamma,$$

where $\text{dist}_{\mathfrak{S}}$ is the signed distance to the contour surface \mathfrak{S} . In fact, from our experience of the SDF definition [25] we prove that a more efficient similarity measure is given by

$$\mathcal{J}_{\text{data}}(z, y, t) = \text{Ext}(\text{dist}_{\mathfrak{S}}(\underline{\xi} + \underline{u}, t); \underline{n}_{\mathfrak{S}}) \|_{\mathcal{E}_t}^2,$$

with $\|\cdot\|_{\mathcal{E}_t}^2$ the norm associated with the linearized elastic energy in the solid, namely equivalent to the H^1 -norm and

$$\underline{\psi}^{\text{ext}} = \text{Ext}(\psi; \underline{\tau}) : \begin{cases} \text{div}(\underline{\underline{A}} : \underline{\underline{\varepsilon}}(\underline{\psi}^{\text{ext}})) = 0 & \text{in } \Omega \\ \underline{\psi}^{\text{ext}} \cdot \underline{\tau} = \psi & \text{in } \Gamma_{\text{obs}}^u \\ (\underline{\underline{A}} : \underline{\underline{\varepsilon}}(\underline{\psi}^{\text{ext}})) \cdot \underline{\tau}_1^\perp = (\underline{\underline{A}} : \underline{\underline{\varepsilon}}(\underline{\psi}^{\text{ext}})) \cdot \underline{\tau}_2^\perp = 0 & \text{in } \Gamma_{\text{obs}}^u \\ \text{same boundary conditions as the model} & \text{on } \partial\Omega \setminus \Gamma_{\text{obs}}^u \end{cases}$$

is a lifting of a scalar data given on the boundary along the direction $\underline{\tau}$, – with $(\underline{\tau}, \underline{\tau}_1^\perp, \underline{\tau}_2^\perp)$ a local orthonormal basis – see Sections 2.3.3.1 & 2.4.1.1.

Therefore our SDF is directly generalized in the non-linear case. We even go further in this aspect by considering an other type of shape observation with the Tagged-MRI modality [33], an imaging modality where a magnetic grid is imprinted on the tissue. We also extend our results to other shape similarity measures with the introduction in a data assimilation framework of the concept of shape descriptors based on the formalism of *currents* popularized by L. Schwartz, a state of the art framework in computational geometry [34], by which surfaces are “embedded” into a Reproducing Kernel Hilbert space (RKHS) with a distance norm of the form

$$\begin{aligned} \|\mathfrak{S}_1 - \mathfrak{S}_2\|^2 = & \iint_{\mathfrak{S}_1} \underline{n}_1(\underline{x}) \cdot k(\underline{x}', \underline{x}) \underline{n}_1(\underline{x}') \, d\Gamma \, d\Gamma + \iint_{\mathfrak{S}_2} \underline{n}_2(\underline{x}) \cdot k(\underline{x}', \underline{x}) \underline{n}_2(\underline{x}') \, d\Gamma \, d\Gamma \\ & - 2 \int_{\mathfrak{S}_1} \int_{\mathfrak{S}_2} \underline{n}_1(\underline{x}) \cdot k(\underline{x}', \underline{x}) \underline{n}_2(\underline{x}') \, d\Gamma \, d\Gamma. \end{aligned}$$

where k is the kernel of the RKHS. When considered in an observer context, \mathfrak{S}_1 is then the deformed boundary of the object and \mathfrak{S}_2 the observed boundary and the discrepancy defined from the norm must be differentiated with respect to the deformation – see Section 2.4.1.2.

Finally, we have developed feedback design principles for non-linear models using transformations that convert the original system into one where feedbacks are well-known. Then we carry over the observer to the underlying non-linear initial equation by an “inverse transformation”:

- In [6] – see Section 2.3.3.3 – we use this principle for non-linear hyperbolic systems such as the shallow-water equations. By using a kinetic representation, we transform our initial system to a linear system – up to the collision term – with an additional kinetic variable, namely a dynamics of the form

$$\frac{\partial}{\partial t} m(t, \mathbf{x}, v) + v \frac{\partial}{\partial \mathbf{x}} m(t, \mathbf{x}, v) = q(t, \mathbf{x}, v)$$

where v is the kinetic velocity variable, m is a particle density and q is a collision operator which satisfies $\int_{\mathbb{R}} q(t, \mathbf{x}, v) \, dv = 0$, $\int_{\mathbb{R}} v q(t, \mathbf{x}, v) \, dv = 0$, $\int_{\mathbb{R}} \frac{v^2}{2} q(t, \mathbf{x}, v) \, dv \leq 0$. The initial system corresponds to the first moments of this generic dynamics, namely

$$h = \int_{\mathbb{R}} m(t, \mathbf{x}, v) \, dv, \quad hu = \int_{\mathbb{R}} vm(t, \mathbf{x}, v) \, dv.$$

On this kinetic representation, a well-designed observer simply reads

$$\partial_t \hat{m} + v \frac{\partial}{\partial \mathbf{x}} \hat{m} = \gamma (m_z - \hat{m}),$$

where m_z is a density reconstructed from the available observations. Then we find the feedback of the initial system by taking the moment of the kinetic representation observer. We end up, for the shallow water system with observed water height $z = \check{h} + \text{noise}$, with the following non-linear observer

$$\begin{cases} \frac{\partial \hat{h}}{\partial t} + \frac{\partial}{\partial \mathbf{x}} (\hat{h} \hat{u}) = \gamma (z - \hat{h}) \\ \frac{\partial}{\partial t} (\hat{h} \hat{u}) + \frac{\partial}{\partial \mathbf{x}} (\hat{h} \hat{u}^2 + \frac{g}{2} \hat{h}^2) = \gamma \hat{u} (z - \hat{h}) \end{cases}$$

The kinetic representation also allows to prove the efficiency of the resulting observer when compared to the literature.

- In [18] and [31] – see Section 2.4.2 – we propose to design an observer for reaction-diffusion system

$$\begin{cases} \frac{\partial w_{|\zeta}}{\partial t} - \nabla \cdot (\underline{D} \cdot \nabla w_{|\zeta}) = kf(w_{|\zeta}), & \underline{x} \in \mathfrak{B}, t \in [0, T] \\ w_{|\zeta}(0) = w_{\diamond} + \zeta \end{cases}$$

presenting traveling waves solutions and where only the front position is observed. The data are therefore typically of the form of an image of the region

$$\forall t \in [0, T], \quad z(t) = \mathfrak{D}_{\hat{w}}(t) = \{\underline{x} \in \Omega, \check{w}(\underline{x}, t) + \text{noise} > c_{\text{th}}\}$$

Here, the model and the data present strong non-linearities. Our strategy is to compare the asymptotic eikonal equation describing the traveling wave propagation in a level set framework

$$\frac{\partial \phi_w}{\partial t} = |\nabla \phi_w| \left(\nabla \cdot \left(\underline{D} \cdot \frac{\nabla \phi_w}{|\nabla \phi_w|} \right) + \alpha_0 \right), \quad (\underline{x}, t) \in \mathfrak{B} \times (0, T).$$

with a similar eikonal equation arising in image processing for regularizing a data-fitting functional. This is typically the case in the Mumford-Shah theory where the eikonal equation appears in the gradient-descent associated with minimization over level sets ϕ of the following type of functional

$$\mathcal{J}_{\text{MS}}(\phi) = \int_{\mathfrak{D}_{\phi}} (z(t) - C_1(\mathfrak{D}_{\phi}))^2 dx + \int_{\mathfrak{B} \setminus \mathfrak{D}_{\phi}} (z(t) - C_2(\mathfrak{D}_{\phi}))^2 dx,$$

with

$$C_1(\mathfrak{D}_{\phi}) = \frac{\int_{\mathfrak{D}_{\phi}} z dx}{\int_{\mathfrak{D}_{\phi}} dx}, \quad C_2(\mathfrak{D}_{\phi}) = \frac{\int_{\mathfrak{B} \setminus \mathfrak{D}_{\phi}} z(t) dx}{\int_{\mathfrak{B} \setminus \mathfrak{D}_{\phi}} dx}.$$

From this analogy, we deduce natural observer for our asymptotic system of the form

$$\begin{aligned} \frac{\partial \phi_{\hat{w}}}{\partial t} &= |\nabla \phi_{\hat{w}}| \left(\nabla \cdot \left(\underline{D} \cdot \frac{\nabla \phi_{\hat{w}}}{|\nabla \phi_{\hat{w}}|} \right) + \alpha_0 \right) \\ &+ \gamma \delta_{\mathfrak{B}} \alpha (|\nabla \phi|) \left(-(z(t) - C_1(\mathfrak{D}))^2 + (z(t) - C_2(\mathfrak{D}))^2 \right) \quad (\underline{x}, t) \in \mathfrak{B} \times (0, T), \end{aligned}$$

that we carry over to the original system by an “inverse asymptotic” procedure to propose the following original observer for reaction diffusion problem

$$\begin{aligned} \frac{\partial \hat{w}}{\partial t} - \nabla \cdot (\underline{D} \cdot \nabla \hat{w}) &= kf(\hat{w}) \\ &+ \gamma \delta_{\mathfrak{B}} \alpha (|\nabla \hat{w}|) \left(-(z(t) - C_1(\mathfrak{D}))^2 + (z(t) - C_2(\mathfrak{D}))^2 \right), \quad (\underline{x}, t) \in \mathfrak{B} \times (0, T). \end{aligned}$$

1.4.2 Observer analysis results

Once the observer has been envisioned, we can proceed to its analysis. Here, we must define the necessary framework to prove that (1) the observer dynamics is well posed (2) the observer converges asymptotically to the target trajectory in the absence of observation errors and (3) the estimation is robust to noise.

In [10], we have demonstrated (1) and (2) on our original SDF observer by linking the observer asymptotic convergence to an observability condition of the type

$$\exists c > 0, \quad \forall T > T_0, \quad \int_0^{T_0} \|u|_{\zeta_u, \zeta_v}(\cdot, t)\|_{H^1(\Omega_{\text{obs}})}^2 dt \geq c \left(\|\zeta_u\|_{H^1(\Omega)}^2 + \|\zeta_v\|_{L^2(\Omega)}^2 \right),$$

$$\forall (\zeta_u, \zeta_v) \in H_0^1(\Omega) \times L^2(\Omega)$$

and $u|_{\zeta_u, \zeta_v}$ a solution of the wave equation with initial condition ζ_u, ζ_v . **This observability is not proved in the literature** and we propose a demonstration where by local equirepartition of the energy we directly link this condition to the classical geometric control condition (GCC) that, usually, justifies an observability condition for velocity measurements, hence for the DVF observer, – see Section 2.3.3.1. We generalized this results to a beam equation in [11] and to elasticity in a subsequent paper (see [Imperiale, 2013]). In the latter – of original interest for us having the cardiac application in mind – the GCC is replaced by the elastic geometric control condition stating that every combination of pressure (P) and shear (S) waves ray should encounter the subdomain of observation, knowing that these rays are independent in the domain interior and coupled on the boundary as any (P) ray reflects on the boundary to give a (P) ray and (S) ray, and conversely for the (S) rays.

We also investigate the stabilization property of the SDF in a fluid-structure interaction formulation [4]. In this case, we do not have a complete mathematical proof for the observability condition. However, we show by a spectral sensitivity analysis the type of observability condition that can and can-not be expected in this coupled problem – see Section 2.3.3.2.

In [24] – see Proposition 2.3.6 – we investigate the point (3) for the classical DVF observer. More precisely when the stabilized operator can be shown to be Riez Spectral, namely that the eigenelements of the stabilized system generate a Riez basis, we evaluate the impact of a white measurement noise on the estimation error.

In [6] (see Theorem 2.3.11), we also propose several analysis results concerning (1), (2) and (3) concerning the observer design of hyperbolic conservation laws based on a kinetic description. Indeed we analyse convergence of the observer with respect to a scalar gain multiplying the feedback and we investigate the impact of noisy observation, which shows to be not negligible in the strong L_2 norm because of its high oscillations, but is smaller in a weaker $H^{-\alpha}$ norm. It remains, however, to have a complete understanding of the asymptotic convergence with respect to time, in particular for partial measurements.

In [18] (Propositions 2.4.1 & 2.4.2), we show a stabilizing property – a prerequisite of (2) – of our reaction-diffusion estimator based on front data. In this non-linear case, we show that, as soon as the data are sufficiently contrasted – namely, the front is sharp enough in the data – our feedback allows a decrease of the linearized estimation error. This implies that our observer can converge for small estimation errors. However, on this last observer, there are still numerous open questions to finalize our analysis. In particular, the necessary condition of existence of the observer remains as the observer involves a singularity in the feedback term.

1.4.3 Parameter estimation results

In [24], we study the question of adaptive parameter estimation in order to propose a strategy of parameter identification that can be coupled to any state observer. In other words, our

objective is to propose **for any state observer of the original system, a generic additional parameter feedback allowing to jointly identify some parameters**. In this respect, we demonstrate that an efficient approach is to combine, with the initial state feedback \check{G} , a reduced-order optimal estimator restricted to the parameter space. Indeed, the state estimate allows to stabilize the error on the parameter subspace justifying to limit the Kalman-like covariance operator on this subspace. In a fully linear context, we have a joint estimator of the form

$$\begin{cases} \dot{\hat{y}} = A\hat{y} + D\hat{\theta} + \check{G}(z - C\hat{y}) + L\dot{\hat{\theta}}, & \hat{y}(0) = y_\diamond, \\ \dot{\hat{\theta}} = U^{-1}L^*C^*R(z - C\hat{y}), & \hat{\theta}(0) = \theta_\diamond, \\ \dot{L} = (A - \check{G}C)L + D, & L(0) = 0, \\ \dot{U} = L^*C^*RCL, & U(0) = P^\theta. \end{cases}$$

We analyse this strategy in a linear context with the change of variable

$$(\tilde{y}, \tilde{\theta}) \mapsto (\eta, \tilde{\theta}) = (\tilde{y} - L\tilde{\theta}, \tilde{\theta}),$$

that gives the following error dynamics

$$\begin{cases} \dot{\eta} = (A - \check{G}C)\eta \\ \dot{\tilde{\theta}} = -U^{-1}L^*C^*RCL\tilde{\theta} - U^{-1}L^*C^*RC\eta + U^{-1}L^*C^*R\chi, \end{cases}$$

This error system is luminous as it partially decouples a typical state estimation error dynamics $\dot{\eta} = (A - \check{G}C)\eta$ and a typical parameter identification error dynamics of the form $\dot{\tilde{\theta}} = -U^{-1}L^*C^*RCL\tilde{\theta}$. In particular our proof allows to understand that a classical simple parameter identification approach cannot be robust to any state error including initial condition, discretization errors or modeling errors when $\check{G} = 0$ as η can be excited by various errors, hence pollute the parameter error $\tilde{\theta}$. Therefore, we advise to always consider a state observer and rely in any identification problem on a joint state-parameter estimator much more robust to errors. In a non-linear context for the coupled state and parameters – which is very common when considering parameter identification – the operators in the dynamics of L and U are the tangent of dynamics and/or the observation model in the spirit of the EKF filter, hence we propose a Reduced Order Extended Kalman Filter (ROEKF) applied to the parameter space. Here, we propose elements of analysis based on the linearization of error dynamics where our arguments obtained for linear systems can be reused. For further details see [Section 2.3.4](#).

From the results obtained in [24] we derive two important extensions by replacing the ROEKF applied to the parameters by a Reduced Order H^∞ Filter in [16] ([Sections 2.3.4.3](#)) and a Reduced Order Unscented Kalman Filter (ROUKF) in [22, 23] ([Section 2.3.4.4](#)). On the one hand, the H^∞ version allows to present an original alternative analysis, in particular in a deterministic context as it represents a worst case scenario. On the other hand, the UKF version is very useful in practice as it computes the parameter sensitivity from a stencil of particles, hence is model tangent free. This has shown to very interesting when dealing with complex models – for instance fluid-structure interaction problems [5] or electromechanical problems [19] – and non-linear discrepancy measurements as in [33, 34]. Note that, in order to rely on UKF, we manage to formulate the reduced-order version of the UKF estimator in its most general form [22] ([see Section 2.3.1.4](#)).

It is also important to underline that our principle of coupling Luenberger observers with reduced-order optimal filters has also allowed us in [19] to formulate an adapted estimator for a

coupled parabolic and hyperbolic problem. On the one hand, the Luenberger observer is devoted to the hyperbolic system where the complete space must be stabilized, and on the other hand the reduced-order optimal filter increases the stabilization of the low frequencies of the parabolic system.

1.4.4 Discretization Results

The first objective is to propose adequate discretizations in terms of consistency and stability.

- In this respect, we put a lot of effort in demonstrating on realistic cases the computational efficiency of our new formulated state observer in [25] or [33, 34] where we propose conservative time-schemes, but also splitting methods which are both convenient for practical implementations but also for numerical analysis. Indeed, with a splitting strategy we can separate the initial model discretization, the feedback discretization and eventually some additional numerical viscosity to enforce the stabilization rate to be robust with respect to the discretization and avoid spurious high frequencies (see Section 2.3.2.3).
- Concerning our reduced-order optimal filter in [16, 23, 24], we also propose adequate discretizations based on the time-discrete optimal filter theory, hence we formulate the Reduced-Order time-discrete optimal filter (see Section 2.3.4.2).
- Moreover, we assess the consistency of our new formulated ROUKF by comparison with the ROEKF of the linearized error system. In [6], we also cover the discretization question. Here we show the potential of the kinetic representation to propose adequate discretizations of our observer of hyperbolic systems. In fact, we are able to obtain a stabilization result at the discretized level.
- Finally, in an upcoming paper [37] (see Section 2.2.1), we propose a time-discrete version of the exact optimal filter for non-linear systems. For time-continuous systems, the Mortensen filter extends the Kalman filter by

$$\begin{cases} \dot{\hat{y}}(t) = A(\hat{y}, t) - (\nabla^2 \mathcal{V}(\hat{y}(t), t))^{-1} \mathrm{d}_y J(\hat{y}(t), t)^\top R J(\hat{y}(t), t), & t \in \mathbb{R}^+ \\ \hat{y}(0) = y_\diamond \end{cases}$$

where a *cost-to-come* \mathcal{V} is the solution of a Hamilton Jacobi Bellman equation of the form

$$\begin{cases} \partial_t \mathcal{V}(y, t) - \mathcal{H}(y, \nabla \mathcal{V}(y, t), t) = 0, & (y, t) \in \mathcal{Y} \times \mathbb{R}^+ \\ \mathcal{V}(y, 0) = \frac{1}{2} \|y - y_\diamond\|_{\mathcal{Y}, N_\diamond}^2 \end{cases}$$

with $\mathcal{H}(y, q, t) = \frac{1}{2} \|J(y, t)\|_{\mathcal{Z}, R}^2 - \frac{1}{2} q^\top B Q B^\top q - q^\top A(y, t)$. However, there is no equivalent result for time-discrete system. In [37], we prove that for a large class of non-linear systems, the extension of the time-discrete Kalman filter for non-linear systems is given by the following procedure: From the costs-to-come solutions of the following Bellman equation

$$\begin{cases} \mathcal{V}_n^+(y) = \mathcal{V}_n^-(y) + \frac{1}{2} \|J_n(y)\|_{R_n}^2, \\ \mathcal{V}_{n+1}^-(y) = \mathcal{V}_n^+(\check{y}) + \frac{1}{2} \nabla \mathcal{V}_{n+1}^-(y)^\top B_n Q_n B_n^\top \nabla \mathcal{V}_{n+1}^-(y) \\ \quad \text{with } y = A_{n+1|n}(\check{y}) + B_n Q_n B_n^\top \nabla \mathcal{V}_{n+1}^-(y), \\ \mathcal{V}_0^-(y, 0) = \frac{1}{2} \|y - y_\diamond\|_{\mathcal{Y}, N_\diamond}^2, \end{cases}$$

compute

$$\left\{ \begin{array}{l} \text{Initialization:} \\ \hat{y}_0 = y_0, \\ \mathcal{V}_0^- = \frac{1}{2} \|y - \hat{y}_0^-\|_{\mathcal{Y}, \mathcal{N}_0}; \\ \text{Correction:} \\ \text{Starting from initial guess } \hat{y}_n^- \text{ which satisfies} \\ \nabla \mathcal{V}_n^+(\hat{y}_n^-) = \text{d}J_n(\hat{y}_n^-)^\top R_n J_n(\hat{y}_n^-), \\ \text{compute (by Newton's method) for } n \in \mathbb{N}, \hat{y}_n^+ \text{ such that} \\ \nabla \mathcal{V}_n^+(\hat{y}_n^+) = 0; \\ \text{Prediction:} \\ \hat{y}_{n+1}^- = A_{n+1|n}(\hat{y}_n^+), \quad n \in \mathbb{N} \text{ which satisfies} \\ \nabla \mathcal{V}_{n+1}^-(\hat{y}_{n+1}^-) = 0; \end{array} \right.$$

Our second objective is to propose complete numerical analyses of the state observers and then of the joint state-parameter observers. Our most important result appears in [11] – see [Theorem 2.3.5](#) – where we prove that the observer can be a better approximation of a real system than the usual discretized system. In essence, our result restarts from the usual numerical convergence estimates for the full discretization of the a wave equation with a spatial discretization of order h^θ and temporal discretization of order Δt^α , namely

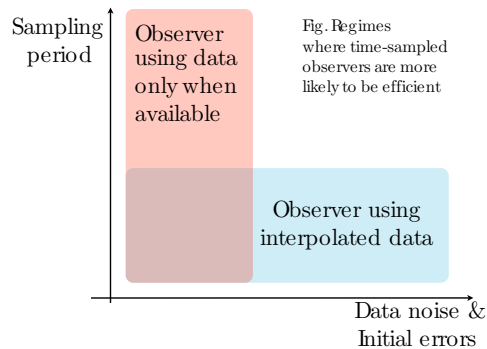
$$\|\hat{y}_h^n - \check{y}(n\Delta t)\|_{\mathcal{Y}} \leq c(y_0, n\Delta t) \max(h^\theta, \Delta t^\alpha), \quad \forall n \in \mathbb{N}$$

This estimates deteriorates when time increases. However with the observer we manage to obtain with $\epsilon = \max\{\Delta t, h^\theta\}$

$$\|\hat{y}_h^n - \check{y}(n\Delta t)\|_{\mathcal{Y}} \leq c(y_0) \max(\epsilon, \epsilon^2 h^{-1} \Delta t), \quad \forall n \in \mathbb{N}.$$

Therefore, **when data are available, it is always positive to incorporate them in the numerical simulation through the definition of an observer.** In order to prove the result in [11], we demonstrate an exponential stability result uniform with respect to the discretization – space or time. When this result is added to the usual paradigm of consistency and stability in numerical analysis, then we can show that the observer is a better approximation of a real system than the usual discretized system since the use of the available data allows to counterbalance the effect of time in classical numerical estimates. We point out that this result obtained for the wave equation can be generalized to several other systems, as we did for instance for a beam equation [11].

In [17] we investigate the fundamental question of assimilating time-sampled data. This question is very sensitive when considering medical imaging data as for instance MRI techniques that are known to have a strong resolution in space but not as strong in time as opposed to ultrasound technics that have a good resolution in time but not as good in



space. Mathematically speaking, we improve the result of [11] by incorporating a data time-sampling parameter – see [Theorem 2.3.7](#). Then we compare two choices of data assimilation. On the one hand the estimation uses interpolated data at each time-step of the model discretization. On the other hand, an observer uses the data only when they are available. The resulting optimal strategy depends of the level of data noise and of the data sampling period. Note that we also investigate the question of data space discretization in the particular case of tagged-MRI data [Imperiale, 2013] – see [Section 2.4.1.3](#).

Finally we show in [13] that when parameter estimation is defined as a second stage of a system discretized by reduced basis approaches – in our paper we consider the case of Proper Orthogonal Decomposition – the question of the stability of the state discretization with respect to the parameter variation must be assessed carefully. More precisely, we prove that the POD basis must be built from trajectory snapshots generated from a sampling of the parameter space where the target parameter is expected.

1.4.5 Modeling and application results

From the beginning of our work on data assimilation we aim at convincing the cardiovascular community of the potential of using data assimilation, and more precisely sequential strategies, in order to build patient-specific models [28] and [33, 39–41] – see [Section 3.4](#). In a first step, we proceed by presenting our methods on realistic synthetic examples [5, 6, 18, 19, 25] or [33, 40]. Then we succeed in presenting complete cardiovascular applications with real data on two cases:

- In [8] we estimate the contractility of a pig infarcted heart using Cine-MRI segmentations of the left ventricle. On a controlled animal experiment we are able to quantify the infarct by identifying a contractility parameter in the model using as data only the deforming contours of the geometry extracted from the image sequence segmentation. Up to our knowledge, this article is the first article integrating a complete data assimilation framework with real data for a cardiovascular application.
- In [21], we identify the boundary condition representing the tethering of external organs on an aorta fluid-structure interaction model and using CT segmentations of the aortic walls. The deformation of arteries is very much impacted by the surrounding organs, as for instance the aorta that is partially tethered to the spine. To avoid too much complexity in the modeling of such external organs we propose to replace them by a simpler model of boundary conditions that then need to be identified. We again use real data segmentations of medical images assimilated in the complete fluid-structure interaction model to perform a joint state and parameter estimation. There is also [3] where *in-vitro* estimation results on a controlled real experiment mimicking a vascular system are excellent.

The efficiency of our ROUKF method has motivated other international groups to use sequential strategies for identification in a cardiac context, see for instance our collaborations in [3, 20, 29]. In [29] the collaboration has allowed to illustrate how UKF-based estimation can be used to identify a parameter of a quasi-static hyperelastic model. In [20] the ROUKF filter developed in our opensource Library Verdandi⁴ is used in a large collaboration in a clinical

⁴developed in collaboration with Inria-project Clime

context. Qualitatively the results are interesting but remain to be improved quantitatively due to modeling issues. A similar type of collaboration has also been set-up in [3] for stiffness identification in a blood-flow FSI model. This effort toward the cardiovascular community is finally summarized in the two review papers [9, 12].

Note that in order to apply our observer strategy in a real context, we faced the necessity to improve the quality of our cardiac and cardiovascular models in terms of formulation [7, 14, 15], discretization [14, 15], boundary conditions [26], experimental calibration [7] or even clinical predictivity with respect to a given pathology [27]:

- **Original models** – In [14] (see Section 3.2.1.1), we complement the first model of cardiac contraction proposed in [Sainte-Marie et al., 2006] by improving the coupling between the microscopic model and the macroscopic formulation. In particular we obtain in this paper a complete energy balance between the macroscopic kinetic energy and hyperelastic energy and the microscopic elastic energy of the cardiac actin-myosin bridges. In [7] (see Section 3.3.1), we proposed an asymptotic formulation of the 3D cardiac model in order to define an adequate 1D model of cardiac fiber and 0D model of cardiac cavity. These two models are very interesting as they contain the same constitutive law as the 3D model. Therefore, we prove in [7] that they are very useful for calibration purposes. In [15] (see Section 3.2.2), we propose a new poromechanics formulation that is adapted to the large deformations and rapid flows present in the heart. This general model reads

$$\left\{ \begin{array}{l} \rho_{s0}(1 - \phi_0) \frac{dv_s}{dt} - \nabla_{\underline{\xi}} \cdot (\underline{F} \cdot \underline{\Sigma}_s) - J\phi^2 \underline{k}_f^{-1} \cdot (v_f - v_s) \\ \quad + pJ\underline{F}^{-T} \cdot \nabla_{\underline{\xi}} \phi = \rho_{s0}(1 - \phi_0) \underline{f}, \quad \text{in } \Omega_0 \\ \frac{1}{J} \frac{d}{dt} (J\rho_f \phi v_f) + \nabla_{\underline{x}} \cdot (\rho_f \phi v_f \otimes (v_f - v_s)) - \theta v_f + \phi^2 \underline{k}_f^{-1} \cdot (v_f - v_s) \\ \quad + \phi \nabla_{\underline{x}} p - \nabla_{\underline{x}} \cdot (\phi \underline{\sigma}_{vis}) = \rho_f \phi \underline{f}, \quad \text{in } \Omega_t \\ \frac{1}{J} \frac{d}{dt} (J\rho_f \phi) + \nabla_{\underline{x}} \cdot (\rho_f \phi (v_f - v_s)) = \theta, \quad \text{in } \Omega_t \end{array} \right.$$

with ϕ the volume fraction of fluid phase. These equations present an interesting structure of Fluid-Structure interaction where the solid velocity plays the role of an ALE – here not arbitrary, however. We prove that the system is energy balanced as was not the case for a more classical coupling involving a structure with a Darcy fluid.

- **Boundary conditions** – In [26], we propose to use viscoelastic boundary conditions for the solid in order to easily integrate the tethering of external tissue around the system. Therefore, we have in general on the solid boundary

$$\underline{T}_s \cdot \underline{n}_s = -k_s(\underline{u}_s - \underline{u}_b) - c_s \underline{v}_s, \quad \text{on } \partial\Omega_0^s$$

where k_s is an elastic coefficient, \underline{u}_b is a given displacement and c_s a viscous coefficient. These simple boundary conditions have shown to be quite effective on our cardiac and arterial modeling [26] and are now well adopted in the community. Note that it is also possible to consider these boundary conditions on the deformed configuration and not the reference configuration.

- **Discretization** – In [14] for our cardiac model (see Theorem 3.2.3) and in [15] for our poromechanics model (see Theorem 3.2.5), the energy balance that we obtained at the continuous level have allowed us to formulate energy balanced time-discretization of these non-linear systems. Therefore, these discretizations offer a chance to prove convergence, at least in their linearized version.
- **Experimental calibration** In [7] (see Section 3.3.1.2), we complete the intricate work of making our 1D asymptotic model to fit complex sets of experimental data obtained by Y. Lecarpentier on mice. This work is then for the team an important validation and calibration step of the original model that we have proposed. It was also a necessary step before pursuing our application objective of inverse problems on real data.
- **Clinical predictivity** In [27] we prove that cardiac modeling can now be of practical use, for instance in order to optimize the pacemaker lead positions. To this end, we based the simulation of [27] on *heartLab*, the cardiac FEM code with data assimilation capabilities that we have specifically developed.

Note finally that we have also decided to better understand some measurement procedures such as ultrasound [32], tagged-MRI [33] or electro-cardiograms (ECG) [30] etc. In fact we believe that there is a real need in combining model and data for both estimating the models, but also understanding and filtering the measurement procedure.

1.4.6 Other Results

Finally, the paper [2] concerned a classical “static” inversion problem about the Radon transform from partial measurement and numerical methods associated with it. This result is not strictly devoted to observer theory or cardiovascular applications. However, it corresponds to a first experience in inverse problems and has some interesting echos in my actual work.

1.5 Perspectives: Research Project

We conclude this chapter by giving some perspectives and future works and here again we believe that the matrix of our 5 challenges in observer theory naturally classifies our future research.

1.5.1 Challenge 1: From Data similarity measures to observer design

We have formulated – *in specific cases [18, 25] and [31, 33, 34]*– some original observers strategies which can tackle **shape-based measurements**. These observer formulations combine **image analysis considerations, shape optimization methods and control theory**. Some of them have already have led to original formulations that were *numerically assessed in synthetic cases*. We now believe that we are at the forefront of developing a general theory on observers based on shape data. In particular, we think that our Mumford-Shah approach (see [18] and [31] and Section 2.4.2) can be further analyzed and generalized to multiple PDEs. We have in mind two interesting model examples with potential cardiac applications.

- The first one is a biomechanical model of the contraction where we replace our distance-based or currents-based feedback term by a feedback based on the Mumford-Shah functional. One difficulty is that the Mumford-Shah similarity measure must be adapted in a H^1 context in order to extract the maximal observability from the data, hence to envision stability results at least for small errors in a H^1 context.
- A second class of system concerns wave-like systems in infinite domains with application to elastography. Wave propagation in acoustics or elasticity can also be observed via wavefronts as with new echographic devices that image the wave propagation [Pernot et al., 2011] (see Fig. 1.5). In this case, whereas the detailed values of the propagating wave are unknown, the pattern associated with the propagation is visible and provides a wealth of information on the wave and the underlying medium. In cardiac applications, this novel measurement modality has a tremendous potential. Indeed, the local properties of the tissue can be assessed by focusing on a small volume of tissue at high frequencies uncoupled from the heart rate. After rewriting a wave equation in a first-order hyperbolic

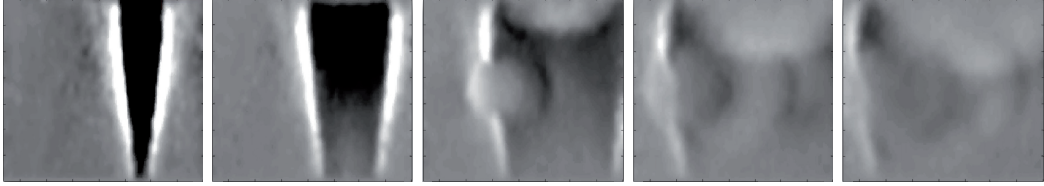


Figure 1.5: Wave propagation echography in a medium with a penetrable inclusion (courtesy M. Pernot)

system with $y = (u \ v)^\top$, our starting strategy will be to introduce a Mumford-Shah feedback of the form

$$\begin{cases} \rho \partial_t \hat{u}(x, t) - \nabla \cdot \hat{v}(x, t) = -\frac{\beta \delta_{\mathbb{R}^+}(x, t)}{|\nabla \hat{y}|} \left((\mathcal{I}[\hat{y}](x, t) - C_1(t))^2 - (\mathcal{J}[\hat{y}](x, t) - C_2(t))^2 \right), & x \in \mathbb{R}^n, \\ \mu^{-1} \partial_t \hat{v}(x, t) - \nabla \hat{u}(x, t) = 0, & x \in \mathbb{R}^n. \end{cases}$$

Note that this system is unbounded and, having in mind its implementation, we must take into account the necessity to impose transparent boundary conditions, or at least absorbing boundary conditions. However, the question of transparent boundary conditions is already challenging for standard wave-like equations, and we will now face the situation to make them compatible with our observer definition.

In the spirit of our design principle by transformation and inverse transformation, with Marie Doumic – and our PhD Student Aurora Armiento – we recently started a collaboration concerning the estimation of models of population dynamics, and more precisely Lifschitz-Slyozov models of depolymerization [1]. In this model, a concentration u of polymers reacts with a concentration v of monomers leading to the dynamics

$$\begin{cases} \frac{\partial}{\partial t} u(x, t) + \frac{\partial}{\partial x} \left((k_o(x)v(t) - k_d(x))u(x, t) \right) = 0, & x \in \mathbb{R}^+, t \geq 0, \\ v(t) = \int_{\mathbb{R}^+} x u(x, t) dx = \rho > 0 \\ u(x, 0) = u_0(x), \\ v(0) = v_0 \end{cases}$$

where k_o is a polymerization rate, k_d a depolymerization rate, and ρ the total mass of monomers. In this context, the measurements considered by the biologists are the moments of u of order $k = 0, 1$ or 2

$$z = \int_0^\infty x^k u(x, t) dx.$$

Here again, we aim at defining a joint state and parameter estimator. To do so, we project to reduce the Lifschitz-Slyozov system by considering the dynamics of its moments with adequate closure relations, hence defining a finite dimensional non-linear system where the measurements at hands are direct observations of the state. Then, combining the existing theory of observation of non-linear system in finite dimension, we believe that we can propose and justify original state estimators. The parameters estimation design will follow naturally from our previous works.

1.5.2 Challenge 2: Observer analysis

Reaction-diffusion with shape observations – We have formulated for reaction-diffusion problems original observer strategies that can tackle shape-based measurements [18] [31]. From this first step of design, we now want to further analyze the formulated observer. The question is to give a sense to the singular data-driven term. In a starting collaboration with Romain Joly, we find that this question is close to similar problems formulated around the Mumford-Shah functionals and related Gradient Flow systems [Gobbino, 1998, Feng and Prohl, 2004]. Therefore, starting from our first result of stability for small errors [18], we believe that a more complete analysis can be performed to show that asymptotically the observer converges to a propagating wave solution with accurate front velocity.

Observer for wave-like equations in unbounded domain – The extension of our front based feedback to wave equations imposed to first develop a theory of observers for wave equations in unbounded domain, a work in close collaboration with Sonia Fliss, Sebastien Imperiale and Antoine Tonnoir. Here, our formulation should take into account the specificity of control theory for unbounded domain, as for instance when the Geometric Control Condition in exterior domain replaces the classical GCC. An alternative is to develop transparent boundary conditions compatible with the observer in order to re-introduce a bounded domain. In the latter, we think that there is then an opportunity to consider the transparent boundary condition – for instance based on Dirichlet-to-Neumann condition – as a supplementary stabilization operator that controls the energy within the bounded domain. Therefore, we believe that there a fruitful dialog can emerge between control theory and transparent boundary condition theory, as both fields can bring new ideas and principles to each other.

Observer for population dynamics models – Concerning our work with Marie Doumic, we recall that the Lifschitz-Slyozov system is non-linear, hence any proposed observer will be difficult to analyze. However, considering the measurement at hand, an idea is to rely on a moment-based reduction that allows to define with an adequate closure relation a finite dimensional system that approximates the Lifschitz-Slyozov model. This system, as it is finite dimensional, can be analyzed with classical results of non-linear control-observation, in particular with Lie brackets to justify the observability of the system.

Recently, the paper [Ramdani et al., 2015] has introduced an original observer for an age-structured population model, an integro-differential model where the non-local term appears this time in the initial condition. This model presents the characteristics of having an unstable subspace of finite dimension. We believe that this system offers a very interesting setup for formulating, but more importantly analyzing intensively our reduced-order filtering methods.

Finally, chemotaxis models are systems of growing interest [Perthame, 2004] where patterns appear and where a shape observer could be proposed and analyzed.

1.5.3 Challenge 3: Parameter estimation

In [24], we propose a joint state and parameters estimation procedure using a space-discretized form. The proof is written in a form that could be naturally extended to infinite dimensional systems. However, the complete analysis in this context remains to be done. More precisely, the article is based on an observability condition that has to be verified for each system of interest. One important goal of our future work is then to link this particular observability condition to more classical observability inequalities appearing in identification problems for specific partial differential equations, such as Carleman inequalities. One target class of systems for carrying on the complete analysis are wave-like systems – including elastodynamical systems – where we typically identify the wave velocity or an additive potential.

In rare situations, a parameter identification can be obtained with a more direct method than a Carleman inequality. This is typically the case in [Cristofol et al., 2014] where it is proved that a front velocity measurement allows to identify the reaction term in a reaction-diffusion model presenting front propagations. This result is also a typical target for completing the proof of convergence of a joint state and parameter estimator for a reaction-diffusion system observed through front data.

1.5.4 Challenge 4: Discretization

We believe that there is still a lot of work in the complete understanding of observer theory, in particular linking the nudging approach in data assimilation to control results. Moreover, the sequential estimation approach has known a strong development in data assimilation around the EnKF formulations, but the optimal control description envisioned in the 80s is now less studied, at least theoretically. We also believe that the links between the stochastic approaches and the deterministic approaches can be reinforced in particular to envision new discretization methods. For instance, in the continuity of our work [37], we are concerned with a tractable “space” discretization of the deterministic Mortensen estimator for nonlinear systems, hence breaking the curse of dimensionality. In this respect, we can study the connection between the Mortensen filter and the corresponding stochastic filter, namely the Zakai filter [James and Baras, 1988, Fleming and McEneaney, 2000]. A motivation for this arises from the numerous efficient Monte Carlo strategies developed for the implementation of the Zakai filter. Therefore, we expect to be able to extend the use of Monte Carlo methods to adequately approximate the Hamilton-Jacobi-Bellman (HJB) equation formulated in the Mortensen filter. Similar uses of Monte Carlo based HJB approximations are already known in control theory [Desai et al., 2003], but the approach has not been carefully defined and analyzed for observers.

We also think that the stability results with respect to noise can be improved. Numerous works treat the noise as stochastic, leading for instance to the strong results obtained in [Bensoussan, 1971] but at the cost of a quite complex formalism. By contrast, we aim at complementing our deterministic approach by introducing a more systematic treatment of our noise, as apprehended with H^s with $s < -\frac{1}{2}$ function of time [Nussbaum and Pereverzev, 1999]. This noise enters in the observer as a source term and we want to mathematically analyze the impact of such a perturbation, potentially by defining less regular solutions as initiated in [6].

Finally, we think that concerning the numerical aspects of observer design, there is still a lot of work to popularize their use in actual applications. This is why we have made a lot of efforts in developing – with Vivien Mallet and other members of the Inria Project-Team Clime – the generic open-source Library Verdandi that integrates state of the art data assimilation methods in a generic formalism such that it can be directly linked to numerous model implementations [12]. However, there is still a lot to do, in particular with the growing need of compatibility with parallel architectures. Indeed, more and more models are developed to be run on parallel architectures. This has led to the popularization of numerical approaches such as domain-decomposition, and time-parallelism. As a consequence, a new challenge appears – as illustrated by the CEMRACS 2016 that we co-organize on this topic – of having data assimilation methods that do not slow down this parallel implementation, and even benefit from this parallelism. Note that this question is by far not limited to computational aspects, but implies to develop original numerical methods, as illustrated for instance by our ROUKF design.

1.5.5 Challenge 5: Applications

As we strongly believe that real applications are a very important trigger for developing efficient methods, we aim at continuing our work on cardiac modeling and data coupling. For instance, concerning our historic focus on cardiac estimation from segmentation sequences, we think that there is now an opportunity to introduce our Mumford-Shah based discrepancy measure instead of our distance-based discrepancy measure. Moreover, we plan to continue our investigation on coupling multiple modality observations, for instance coupling image modalities to some signals modalities such as ECG, peripheral pressure signals, sismo-cardiograms that measure the acceleration of the chest during the heart contraction, ballisto-cardiograms etc.. Here, our objective is to evaluate the observability gain offered by these modalities in the spirit of our work [19], but also to see the potential of these signals to monitor a simplified heart model [7] over long time evolutions. Up to now, we liked to refer to *heart forecasting* to summarize our applications of data assimilation in cardiac estimation. When moving from the time-scale of the heart beat to the time-scale of the heart evolution, we could now use the image of *heart climatology* to summarize the new modeling challenges that we will face, and also the new data assimilation challenges, as we will surely need to couple multiple scales in the estimation procedure.

Moreover, we believe that the most ambitious project about cardiac modeling concerns the new imaging modality of elastography. As a measurement of the mechanical behavior of the heart, much promise resides in this modality, which consists in measuring waves induced by a controlled actuator in a tissue. Two techniques are now considered. On the one hand, transient

elastography is performed using ultrasound (US) devices generating an impulse and recording the resulting traveling waves. On the other hand, magnetic resonance imaging (MRI) allows to measure harmonic vibrations in a tissue submitted to periodic excitation. Originally designed for breast cancer detection, elastography is now used for various other organs like the liver, and has recently been applied to the heart [Pernot et al., 2011]. This measurement is intrinsically very different from kinematics measurements coming from other medical imaging modalities. Here, indeed, we access the mechanical properties of the tissue by submitting it to controlled excitations. Therefore, we believe that the observability provided by these measurements is very strong. Hence, we have a big opportunity to couple our state of the art model of contractions with new observers-based model of the wave propagation in the tissue, in order to propose very original approaches to identify mechanical parameters in cardiac laws. On this subject, we have initiated a collaboration with M. Pernot from ESPCI among the most promising techniques of transient ultrasound elastography that are being developed.

But our work is not restricted to cardiac applications. First of all, our approach on shape-based feedback design can be of interest in numerous applications. We have already talked about chemotaxis models and also wave propagation which can be useful in non-destructive control. There are also potential applications in geophysics where satellite images also present shape data [Chabot et al., 2015]. For instance, our collaboration with Jacques Sainte-Marie concerns the observations of propagating sea-waves and topography estimation in shallow water systems. There are also potential applications in ice-sheet models where we observe the front of the ice sheets that have been losing mass at an increasing rate for more than two decades. In this context, there is still the challenge of having complex models presenting all the required physical ingredients, but with data in a form of moving front [Gillet-Chaulet et al., 2012]. The same type of question arises with wild fire propagation [Rochoux et al., 2013].

Finally, our work with Marie Doumic is also based on real experiments analysis as Marie Doumic has been collaborating for a long time with Human Rezai, a biologist from Inra who realizes depolymerization experiments.

PART II

Detailed presentation of my past contributions

Data assimilation contributions

Tout est dans le contrôle

— M. Platini

Chapter contents

2.1	Introduction	44
2.2	Toward a unified theory in optimal filtering of non-linear finite dimensional systems	44
2.2.1	Least square estimation and corresponding optimal estimator	44
2.2.2	Principle of the time-discretization and related time-discrete estimator	48
2.2.3	Approximated optimal filters in the light of the discrete-time Mortensen filter	51
2.3	Control-based sequential estimation strategies for PDEs	56
2.3.1	Optimal-control-based strategies	56
2.3.2	Luenberger observers formulations – The wave equation case	66
2.3.3	Luenberger observers: other models	81
2.3.4	Hybrid feedback design	92
2.4	Shape-based data assimilation	100
2.4.1	Motion extraction from images by sequential estimation based on a biomechanical model	101
2.4.2	A Luenberger observer for reaction-diffusion models with front position data	112

2.1 Introduction

This chapter consolidates my various results on sequential estimation. Some results concern optimal estimation with the formulation of the new deterministic optimal observer for non-linear time-discrete systems, and (with K. Mauffrey) some review contributions of formulating and analysing a Kalman-like observer for parabolic problems. Then there are contributions to Luenberger observers: (1) First for wave equation with their analysis (with D. Chapelle, N. Cîndea, M. de Buhan, A. Imperiale); (2) Then for mechanical systems with complex observations (with D. Chapelle, A. Imperiale, P. Le Tallec) or in FSI (with C. Bertoglio, D. Chapelle, M.A. Fernández, J.-F. Gerbeau); (3) For hyperbolic systems (with A.-C. Boulanger, B. Perthame, J. Sainte-Marie); (4) For reaction-diffusion observation (with A. Collin, D. Chapelle). Finally I have worked intensively on formulating, analyzing and discretizing so-called reduced-order optimal strategies that allow to apply a Kalman-like optimal observer on a subsystem of interest with applications on state estimation for parabolic problems (with C. Corrado, D. Chapelle, A. Gariah, J.-F. Gerbeau, J. Sainte-Marie) or for joint state and parameter estimation (with D. Chapelle, P. Le Tallec).

2.2 Toward a unified theory in optimal filtering of non-linear finite dimensional systems

In this section, our objective is to introduce to some extent the principles behind optimal filtering design in a quite general non-linear framework. In this context, even if the subject has been much studied since the second part of the last century, numerous challenges remain in the light of the various dual visions that we have presented in Chapter 1. Indeed, to some extent, these visions – variational/sequential, stochastic/deterministic, discrete-time/continuous-time or finite-dimensional/infinite-dimensional – were proved to be consistent with each other, hence to form a unified estimation framework. This is particularly true for linear systems around the Kalman filter theory [Kalman, 1960a, Kalman and Bucy, 1961]. However, for non-linear systems, we still encounter some open questions. For instance, the variational/sequential equivalence is well understood in the deterministic framework with the Mortensen filter [Mortensen, 1968, Fleming, 1997]. Moreover, some comparisons have been made between stochastic and deterministic approaches for continuous-time dynamical systems [Hijab, 1982, Hijab, 1984, Daum, 1986, Baras et al., 1988, James and Baras, 1988]. However, there were very few results linking the discrete-time and continuous-time sequential estimator (except with the time-scale approach [Peng et al., 2010]). In fact, there was no optimal filter for discrete-time deterministic systems, a question to which I have endeavored to contribute [37].

2.2.1 Least square estimation and corresponding optimal estimator

We consider a general class of dynamical model on a finite dimensional space $\mathcal{Y} \sim \mathbb{R}^{N_y}$

$$\begin{cases} \dot{y}_{|\zeta, \nu}(t) = A(y_{|\zeta, \nu}(t), t) + B\nu(t), & t \in \mathbb{R}^+ \\ y_{|\zeta, \nu}(0) = y_\diamond + \zeta \end{cases} \quad (2.1)$$

where y is the state variable, A is the dynamical operator, ν represents an unknown contribution that can be seen as a model noise, y_\diamond is the known part of the initial condition but ζ is to be determined. In other words, the initial condition of this system is considered potentially uncertain around an *a priori* y_\diamond .

Considering this class of system, we assume to have at our disposal some measurements – or observations – on a particular instance of this model leading to a target trajectory $\{\check{y}(t), t \in \mathbb{R}^+\}$. We model the measurement generation in a general form

$$\forall t \in \mathbb{R}^+, \quad z(t) = C(\check{y}(t), t) + \chi(t),$$

where C is called the observation operator from \mathcal{Y} to the observation space $\mathcal{Z} \sim \mathbb{R}^{N_{\text{obs}}}$ and χ is an unknown function assimilated to a measurement noise. Using these measurements $\{z(t), t \in \mathbb{R}^+\}$, we seek to reconstruct a complete trajectory without knowing initially $(\check{\zeta}, \check{\nu})$.

We have seen in Chapter 1 that there are two classes of estimation strategies. First, the variational strategy consists in minimizing the least square criterion often through an adjoint model integration associated with the dynamical model constraint under which the cost function is minimized. We define the least square estimator (LSE) minimizing the criterion defined on a specific time window $[0, t]$

$$\min_{\zeta, \nu(\cdot)} \left\{ \mathcal{J}(\zeta, \nu(\cdot), t) = \frac{1}{2} \|\zeta\|_{\mathcal{Y}, N_\diamond}^2 + \frac{1}{2} \int_0^t \left(\|J(y|_{\zeta, \nu}(s), s)\|_{\mathcal{Z}, R}^2 + \|\nu(s)\|_{\mathcal{Q}, S}^2 \right) ds \right\}, \quad (2.2)$$

where the discrepancy between the model and the measurement is computed through

$$\forall t \in \mathbb{R}^+, \forall y \in \mathcal{Y}, \quad J(y, t) = z(t) - C(y, t),$$

and $\|\cdot\|_{\mathcal{Y}, N_\diamond}$, $\|\cdot\|_{\mathcal{Z}, R}$ and $\|\cdot\|_{\mathcal{Q}, S}$ define norms characterizing the initial condition uncertainty, the observation noise and the model noise, respectively, by bounded invertible symmetric operators of bounded inverse

$$\|y\|_{\mathcal{Y}, N_\diamond} = \langle y, N_\diamond y \rangle_{\mathcal{Y}}^{\frac{1}{2}}, \quad \|z\|_{\mathcal{Z}, R} = \langle z, Rz \rangle_{\mathcal{Z}}^{\frac{1}{2}}, \quad \|\nu\|_{\mathcal{Q}, S} = \langle \nu, S\nu \rangle_{\mathcal{Q}}^{\frac{1}{2}}.$$

Therefore, the inverse of these three weighting operators

$$P_\diamond = N_\diamond^{-1}, \quad W = R^{-1}, \quad \text{and} \quad Q = S^{-1},$$

are related to error covariances in the probabilistic framework [Kailath et al., 2000]. For the sake of compactness, we classically introduce the Lagrangian functional

$$\mathcal{L} : \begin{cases} \mathcal{Y} \times \mathcal{Q} \times \mathbb{R}^+ \rightarrow \mathbb{R} \\ (y, \nu, t) \mapsto \frac{1}{2} \|J(y, t)\|_{\mathcal{Z}, R}^2 + \frac{1}{2} \|\nu\|_{\mathcal{Q}, S}^2 \end{cases}$$

We denote by $\{\bar{y}_t(s), s \in [0, t]\}$ the trajectory associated with the minimizers $\bar{\zeta}_t, \bar{\nu}_t$. Clearly the more t increases the better the minimizing trajectory should approximate the target trajectory. The most common approach for solving this least square problem consists in minimizing the criterion with the help of the adjoint equation associated with the dynamics constraint under which we minimize the criterion. In fact, defining the adjoint variable from a given trajectory $\{y_t(s), s \in [0, t]\}$ by

$$\begin{cases} \dot{q}_t(s) + d_y A(y_t(s), s)^\top q_t = d_y J(y_t(s), s)^\top R J(y_t(s), s), & s \in [0, t] \\ q_t(t) = 0 \end{cases}$$

the variational estimator dynamics can be summarized by introducing the system Hamiltonian

$$\mathcal{H} : \begin{cases} \mathcal{Y} \times \mathcal{Y} \times \mathcal{Q} \times \mathbb{R}^+ \rightarrow \mathbb{R} \\ (y, q, \nu, t) \mapsto \mathcal{L}(y, \nu, t) - q^\top (A(y, t) + B\nu) \end{cases}$$

since we have for all $s \in [0, t]$

$$\dot{\bar{y}}_t = -\nabla_q \mathcal{H}(\bar{y}_t, \bar{q}_t, \bar{\nu}_t, s), \quad \dot{\bar{q}}_t = \nabla_y \mathcal{H}(\bar{y}_t, \bar{q}_t, \bar{\nu}_t, s), \quad \nabla_\nu \mathcal{H}(\bar{y}_t, \bar{q}_t, \bar{\nu}_t, s) = 0.$$

By Pontryagin's principle and dynamic programming [Bellman, 1957, Fleming and Rishel, 1975], this minimization problem can be characterized through the solution of a Hamilton-Jacobi-Bellman (HJB) equation. Let us introduce the *cost-to-come* associated with the initial minimization

$$\forall (y, t) \in \mathcal{Y} \times \mathbb{R}^+, \quad \mathcal{V}(y, t) = \min_{\nu|_{y(t)=y}} \mathcal{J}(\zeta(y, \nu), \nu, t),$$

in the sense that the initial condition of the trajectory is imposed by the final state and the choice of the model noise function. Assuming that the minimization problem (2.2) has a unique solution then the *cost-to-come* is a solution of the Hamilton-Jacobi-Bellman equation

$$\partial_t \mathcal{V}(y, t) - \min_\nu \mathcal{H}(y, \nabla \mathcal{V}(y, t), \nu, t) = 0. \quad (2.3)$$

For the sake of simplicity, we consider a linear dependency of the model with respect to the model noise. Therefore the HJB equation (2.3) can be simplified by directly finding the minimum in ν . We introduce for all $(y, q, t) \in \mathcal{Y}^2 \times \mathbb{R}^+$,

$$\bar{\mathcal{H}}(y, q, t) = \min_\nu \mathcal{H}(y, q, \nu, t) = \frac{1}{2} \|J(y, t)\|_{\mathcal{Z}, R}^2 - \frac{1}{2} q^\top B Q B^\top q - q^\top A(y, t),$$

and the *cost-to-come* is solution of

$$\begin{cases} \partial_t \mathcal{V}(y, t) - \bar{\mathcal{H}}(y, \nabla \mathcal{V}(y, t), t) = 0, & (y, t) \in \mathcal{Y} \times \mathbb{R}^+ \\ \mathcal{V}(y, 0) = \frac{1}{2} \|y - y_\diamond\|_{\mathcal{Y}, N_\diamond}^2 \end{cases} \quad (2.4)$$

Then, when the *cost-to-come* is a C^1 solution, the adjoint variable can be characterized by

$$\forall s \in [0, t], \quad \nabla \mathcal{V}(\bar{y}_t(s), s) = \bar{q}_t(s). \quad (2.5)$$

The relation (2.5) is the starting point of a fundamental unification between variational and sequential approaches. Indeed, a very effective observer candidate can be derived from the least square criterion by considering at every time t the least square estimate minimizing the criterion aggregating the data up to the time t , namely we define the sequential optimal¹ \hat{y} by

$$\hat{y}(t) = \bar{y}_t(t).$$

From the final condition satisfied by the adjoint variable $\bar{q}_t(t) = 0$, we can characterize \hat{y} with (2.5) to get

$$\forall t \in \mathbb{R}^+, \quad \nabla \mathcal{V}(\hat{y}(t), t) = 0,$$

¹denoted as optimal because of its link with the optimal criterion estimator

where the time-window value t associated with $\mathcal{J}(\cdot, \cdot, t)$ is no longer fixed. Hence, using again the chain rule we get for $t \in \mathbb{R}^+$,

$$\begin{aligned} 0 &= \frac{d}{dt} \left(\nabla \mathcal{V}(\hat{y}(t), t) \right) = \nabla \partial_t \mathcal{V}(\hat{y}(t), t) + \nabla^2 \mathcal{V}(\hat{y}(t), t) \cdot \dot{\hat{y}}(t) \\ &= \nabla \bar{\mathcal{H}}(\hat{y}(t), \nabla \mathcal{V}(\hat{y}(t), t), t) \\ &\quad \nabla^2 \mathcal{V}(\hat{y}(t), t) \cdot \nabla_q \bar{\mathcal{H}}(\hat{y}(t), \nabla \mathcal{V}(\hat{y}(t), t), t) + \nabla^2 \mathcal{V}(\hat{y}(t), t) \cdot \dot{\hat{y}}(t), \end{aligned}$$

and from the partial derivatives of $\bar{\mathcal{H}}$, we finally obtain the filter dynamics

$$\begin{cases} \dot{\hat{y}}(t) = A(\hat{y}(t), t) - (\nabla^2 \mathcal{V}(\hat{y}(t), t))^{-1} d_y J(\hat{y}(t), t)^\top R J(\hat{y}(t), t), & t \in \mathbb{R}^+ \\ \hat{y}(0) = y_\diamond \end{cases} \quad (2.6)$$

and the optimal gain is given by

$$G = (\nabla^2 \mathcal{V}(\hat{y}(t), t))^{-1} d_y J(\hat{y}(t), t)^\top R.$$

This deterministic non-linear optimal observer was first introduced by [Mortensen, 1968] – who called his filter the Maximum Likelihood filter – with several in depth-studies in [Fleming, 1997, James and Baras, 1988, Krener, 2003b]. Following [Fleming, 1997], we will call the optimal observer in a non-linear framework the *Mortensen observer*.

REMARK 2.2.1 (INFINITE DIMENSIONAL SYSTEMS)

The validity of this formulation for infinite dimensional systems is an intricate problem that goes far beyond the formal replacement of the transposition by a general duality notation. We refer to the [Barbu and Da Prato, 1985] for general HJB solutions in Hilbert spaces.

In a linear framework, namely when all operators are assumed to be linear

$$\forall t \in \mathbb{R}^+, \quad A : y \rightarrow A(t)y + \beta(t), \quad C : y \rightarrow C(t)y,$$

it is well known that the optimal observer is given by the popular Kalman filter [Kalman and Bucy, 1961]

$$\begin{cases} \dot{\hat{y}}(t) = A(t)\hat{y}(t) + \beta(t) + P(t)C(t)^\top R(z(t) - C(t)\hat{y}(t)), & t \in \mathbb{R}^+ \\ \hat{y}(0) = y_\diamond \end{cases} \quad (2.7)$$

where P satisfies the following Riccati equation

$$\begin{cases} \dot{P}(t) = A(t)P(t) + P(t)A(t)^\top - P(t)C(t)^\top R C(t)P(t) + BQB^\top, & t \in \mathbb{R}^+ \\ \hat{P}(0) = P_\diamond \end{cases} \quad (2.8)$$

and can be interpreted in a probabilistic standpoint as the state estimation covariance. It is easy to prove that the Kalman filter formulation is in fact consistent with the non-linear filter formulation (2.6) since, in that case, the *cost-to-come* is given by

$$\forall (y, t) \in \mathcal{Y} \times \mathbb{R}^+, \quad \mathcal{V}(y, t) = \frac{1}{2}(y - \hat{y}(t))^\top P^{-1}(t)(y - \hat{y}(t)) + \frac{1}{2} \int_0^t \|z(s) - C(s)\hat{y}(s)\|_{Z,R}^2 ds.$$

2.2.2 Principle of the time-discretization and related time-discrete estimator

From the starting point of the time-continuous Mortensen filter, our problem is then to understand how the Mortensen filter can be discretized. A standard discretization approach would be to propose an accurate discretization of the cost-to-come based on classical adapted non-linear time-discretization for hyperbolic systems, with for instance a Godunov discretization of (2.4). Then, the discretized cost-to-come must be introduced in a discretization of the Mortensen observer (2.6) depending of the discretization constraint imposed by the operator dynamics A . Our point of view in [37] is different and inspired from what has been done for linear dynamics when passing from the continuous-time Kalman filter to the discrete-time Kalman filter. Everything starts by first considering a discrete-time version of (2.1)

$$\begin{cases} y_{n+1|\zeta, (\nu_k)_{k=0}^n} = A_{n+1|n}(y_{n|\zeta, (\nu_k)_{k=0}^{n-1}}) + B_n \nu_n, & n \in \mathbb{N} \\ y_{0|\zeta, (\nu_k)_{k=0}^n} = y_\diamond + \zeta \end{cases} \quad (2.9)$$

with $A_{n+1|n}$ the transition operator from step n to step $n+1$, $(\nu_k)_{k=0}^n$ a sequence of unknown contribution in \mathcal{Q} that can be seen as a discrete-time model noise definition, and B_n the model noise operator at step n . Note that this discrete-time system can be considered in itself or as a consistent and stable discretization of (2.1). In this respect, we introduce a sequence of times $(t_n)_{n \in \mathbb{N}}$ and a discretization parameter Δt considered here to be constant for simplicity, *i.e.* $\Delta t = t_{n+1} - t_n$. Then the transition operator and the model noise operator would typically satisfy

$$\lim_{\Delta t \rightarrow 0, t_n \rightarrow t} \frac{1}{\Delta t} (A_{n+1|n}(y) - \mathbb{1}) = A(y, t), \quad \lim_{\Delta t \rightarrow 0, t_n \rightarrow t} \frac{B_n}{\Delta t} = B(t).$$

As an example we could consider – when stable – an explicit discretization of the continuous-time model (2.1) and we would then have

$$A_{n+1|n}(\cdot) = \mathbb{1} + \Delta t A(\cdot, t_n), \quad B_n = \Delta t B,$$

but similar definitions hold for implicit scheme. We also note that in the context of discretization we can assume that $A_{n+1|n}$ is a bijection without being too restrictive since it corresponds to a perturbation of the identity, at least for Δt small enough.

In this discrete-time context, we consider the target sequence $(\check{y}_n)_{n \in \mathbb{N}}$ and an observation operator C_n at each time step, so that some measurements z_n are given by

$$z_n = C_n(\check{y}_n) + \chi_n,$$

with an additive noise sequence (χ_n) . Note that, in general, measurement procedures are in essence time-sampled and the observation discrete-time model should be more directly defined than the observation continuous-time model. Then the latter is regenerated by interpolation from the sampled measurements with a measurement error ν integrating some interpolation error. Eventually, we can consider the two frameworks independently or assuming that for all $t \in [t_n, t_{n+1}]$, we have $\|C(y, t) - C_n(y)\| = O(\Delta t)$.

One way to propose a discrete-time estimator compatible with (2.9) – *i.e.* the discretization of (2.1) – hence propose a discretization of (2.6), is to rely on least square estimation at the discrete-time level. Typically, one least square criterion minimization considers

$$\min_{\zeta, (\nu_k)_{k < n}} \left\{ \mathcal{J}_n^+(\zeta, (\nu_k)_{k < n}) = \frac{1}{2} \|\zeta\|_{\mathcal{Y}, N_\diamond}^2 + \frac{1}{2} \sum_{k=0}^n \|J_k(y_k)\|_{R_k}^2 + \frac{1}{2} \sum_{k=0}^{n-1} \|\nu_k\|_{S_k}^2 \right\}.$$

with, by extension,

$$\mathcal{J}_0^+(\zeta) = \frac{1}{2} \|\zeta\|_{\mathcal{Y}, N_\diamond}^2 + \|J_0(y_k)\|_{R_0}^2.$$

or another²

$$\min_{\zeta, (\nu_k)_{k \leq n}} \left\{ \mathcal{J}_{n+1}^-(\zeta, (\nu_k)_{k \leq n}) = \frac{1}{2} \|\zeta\|_{\mathcal{Y}, N_\diamond}^2 + \frac{1}{2} \sum_{k=0}^n \|J_k(y_k)\|_{R_k}^2 + \frac{1}{2} \sum_{k=0}^n \|\nu_k\|_{S_k}^2 \right\}.$$

Here again, the continuous-time criterion and the discrete-time criterion are defined in contexts which can be completely independent or related as the time-discrete framework is defined after time-discretization of the continuous-time system. In the latter, the two criteria should be defined consistently as Δt goes to 0. In this respect, we could for instance consider

$$R_n = \Delta t R, \quad S_n = \Delta t S \quad \text{or equivalently} \quad W_n = \frac{1}{\Delta t} W, \quad Q_n = \frac{1}{\Delta t} Q,$$

so that $\lim_{\Delta t \rightarrow 0} \mathcal{J}_n^+(\cdot, \cdot) = \mathcal{J}(\cdot, \cdot, n\Delta t)$.

As we denoted the trajectory associated with the minimizing arguments in the time-continuous context by

$$\forall s \in [0, t], \quad \bar{y}_t(s) = y_{|\operatorname{argmin}(\mathcal{J}(\cdot, t))}(t),$$

we now define in a discrete-time context

$$\forall 0 \leq k \leq n, \quad \bar{y}_{k,n}^+ = y_{k|\operatorname{argmin}_\zeta(\mathcal{J}_n^+)}.$$

Moreover, the optimal sequential estimator defined from the trajectory associated with the minimizer by

$$\forall t \in \mathbb{R}^+, \quad \hat{y}(t) = y_{|\operatorname{argmin}(\mathcal{J}(\cdot, t))}(t),$$

becomes in a time-discrete context

$$\hat{y}_n^+ = \bar{y}_{n,n}^+ = y_{n|\operatorname{argmin}_\zeta(\mathcal{J}_n^+)} \quad (2.10)$$

and equivalently for a \hat{y}_n^- .

The question is now to formulate the resulting recursive equation governing the dynamics of \hat{y}_n^+ or \hat{y}_n^- , and then to show how these discrete-time dynamics correspond to consistent and stable discretizations of (2.6).

This question is solved since [Kalman, 1960a, Kalman and Bucy, 1961] in the case of *linear* time-discrete dynamics and observation operators

$$\forall n \in \mathbb{N}, \quad A_{n+1|n} : y \mapsto A_{n+1|n}y + \beta_n, \quad C_n : y \mapsto C_n y,$$

Indeed it is well known that the discrete-time optimal estimator – discretizing (2.7) – is given by

$$\left\{ \begin{array}{l} \text{Initialization:} \\ \hat{y}_0^- = y_\diamond \\ \text{Correction:} \\ \hat{y}_n^+ = \hat{y}_n^- + G_n(z_n - C_n \hat{y}_n^-), \quad n \in \mathbb{N} \\ \text{Prediction:} \\ \hat{y}_{n+1}^- = A_{n+1|n} \hat{y}_n^+ + \beta_n, \quad n \in \mathbb{N} \end{array} \right.$$

²the interest of the *plus* subscript notation will appear shortly.

where the (discrete-time) Kalman filter is given by prediction-correction dynamics

$$G_n = P_n^+ C_n^\top R_n = P_n^- C_n^\top (W_n + C_n^\top P_n^- C_n)^{-1}$$

with the state covariances P_n^\pm satisfying the discrete-time Riccati equation

$$\left\{ \begin{array}{l} \text{Initialization:} \\ \quad P_0^- = P_\diamond \\ \text{Correction:} \\ \quad P_n^+ = P_n^- - P_n^- C_n^\top (C_n P_n C_n + R_n) C_n P_n, \quad n \in \mathbb{N} \\ \text{Prediction:} \\ \quad P_{n+1}^- = A_{n+1|n} P_n^+ A_{n+1|n}^\top + B_n Q_n B_n^\top, \quad n \in \mathbb{N} \end{array} \right.$$

Here we use a classical notation in Kalman filter theory [Simon, 2006] where the predicted state is denoted by a *minus* superscript whereas the correction step is identified by a *plus* superscript. It is optimal in the sense of (2.10) since, here, it can be easily proven [Kailath et al., 2000, Simon, 2006] that

$$\hat{y}_n^+ = \bar{y}_{n|n}^+ = y_{n|\text{argmin}_\zeta(\mathcal{J}_n^+)}.$$

Moreover, we can also prove

$$\hat{y}_n^- = \bar{y}_{n|n}^- = y_{n|\text{argmin}_\zeta(\mathcal{J}_n^-)}.$$

Finally the consistency is quite straightforward to obtain and the stability analysis comes directly from the stability property of the least square estimate, hence the interest to satisfy variational criteria at the discrete-time level.

Our contribution aims at extending this result in the case of **non-linear** dynamics and observation operator by introducing the exact counterpart of (2.6) in the discrete-time context. We call this new estimator *the discrete-time Mortensen estimator*. This estimator is presented with *ad-hoc* regularity assumptions to facilitate its definition.

PROPOSITION 2.2.1 (DISCRETE-TIME MORTENSEN FILTER (MOIREAU, P.))

We assume that for all n $A_{n+1|n} \in \mathcal{C}^1(\mathcal{Y})$ with $dA_{n+1|n}(\cdot)$ invertible, B_n is bounded, $C_n \in \mathcal{C}^1(\mathcal{Y})$ with $d_y C_n(\cdot)$ bounded. Moreover $dA_{n+1|n}(\cdot)$, B_n and $d_y C_n(\cdot)$, are supposed to be bounded with respect to n . Considering the two optimal criteria

$$\min_{\zeta, (\nu_k)_{k \leq n}} \left\{ \mathcal{J}_{n+1}^-(\zeta, (\nu_k)_{k \leq n}) = \frac{1}{2} \|\zeta\|_{\mathcal{Y}, N_\diamond}^2 + \frac{1}{2} \sum_{k=0}^n \|J_k(y_k)\|_{R_k}^2 + \frac{1}{2} \sum_{k=0}^n \|\nu_k\|_{S_k}^2 \right\},$$

$$\min_{\zeta, (\nu_k)_{k < n}} \left\{ \mathcal{J}_n^+(\zeta, (\nu_k)_{k < n}) = \frac{1}{2} \|\zeta\|_{\mathcal{Y}, N_\diamond}^2 + \frac{1}{2} \sum_{k=0}^n \|J_k(y_k)\|_{R_k}^2 + \frac{1}{2} \sum_{k=0}^{n-1} \|\nu_k\|_{S_k}^2 \right\},$$

we assume that they have unique minimizers. We introduce two discrete costs-to-come functions – called the prediction cost-to-come and the correction cost-to-come – defined for all $n \in \mathbb{N}$

$$\left\{ \begin{array}{l} \mathcal{Y}_n^+(y) = \min_{\substack{(\nu_k)_{k < n} \\ y_n = y}} \mathcal{J}_n^+(\zeta, (\nu_k)_{k < n}) \\ \mathcal{Y}_{n+1}^-(y) = \min_{\substack{(\nu_k)_{k \leq n} \\ y_{n+1} = y}} \mathcal{J}_{n+1}^-(\zeta, (\nu_k)_{k \leq n}), \quad \mathcal{Y}_0^-(y) = \frac{1}{2} \|y - y_\diamond\|_{\mathcal{Y}, N_\diamond}^2, \end{array} \right.$$

Then, assuming that \mathcal{V}_n^- and \mathcal{V}_n^+ are smooth enough – namely $\mathcal{C}^2(\mathcal{Y})$ – for all n , they are solutions of the following system

$$\begin{cases} \mathcal{V}_n^+(y) = \mathcal{V}_n^-(y) + \frac{1}{2}\|J_n(y)\|_{R_n}^2, \\ \mathcal{V}_{n+1}^-(y) = \mathcal{V}_n^+(\check{y}) + \frac{1}{2}\nabla\mathcal{V}_{n+1}^-(y)^\top B_n Q_n B_n^\top \nabla\mathcal{V}_{n+1}^-(y) \\ \quad \text{with } y = A_{n+1|n}(\check{y}) + B_n Q_n B_n^\top \nabla\mathcal{V}_{n+1}^-(y), \\ \mathcal{V}_0^-(y, 0) = \frac{1}{2}\|y - y_\diamond\|_{\mathcal{Y}, N_\diamond}^2, \end{cases}$$

and the estimators built from the prediction sequence $(\hat{y}_n^-)_{n \in \mathbb{N}}$ and the correction sequence $(\hat{y}_n^+)_{n \in \mathbb{N}}$ defined by

$$\forall n \in \mathbb{N}, \begin{cases} \hat{y}_n^+ = \bar{y}_{n,n}^+ = \bar{y}_{n,n+1}^-, \\ \hat{y}_n^- = \bar{y}_{n+1,n}^+ = \bar{y}_{n+1,n+1}^-, \end{cases}$$

can be computed by the recursive procedure

$$\left\{ \begin{array}{l} \text{Initialization:} \\ \quad \hat{y}_0 = y_\diamond, \\ \quad \mathcal{V}_0^- = \frac{1}{2}\|y - \hat{y}_0^-\|_{\mathcal{Y}, N_\diamond}; \\ \text{Correction:} \\ \quad \text{Starting from initial guess } \hat{y}_n^- \text{ which satisfies} \\ \quad \nabla\mathcal{V}_n^+(\hat{y}_n^-) = dJ_n(\hat{y}_n^-)^\top R_n J_n(\hat{y}_n^-), \\ \quad \text{compute (by Newton's method) for } n \in \mathbb{N}, \hat{y}_n^+ \text{ such that} \\ \quad \nabla\mathcal{V}_n^+(\hat{y}_n^+) = 0; \\ \text{Prediction:} \\ \quad \hat{y}_{n+1}^- = A_{n+1|n}(\hat{y}_n^+), \quad n \in \mathbb{N} \text{ which satisfies} \\ \quad \nabla\mathcal{V}_{n+1}^-(\hat{y}_{n+1}^-) = 0; \end{array} \right. \quad (2.11)$$

In particular, when $A_{n+1|n}$, B_n and C_n are linear we retrieve the Kalman estimator prediction-correction sequence introduced in [Kalman, 1960a].

2.2.3 Approximated optimal filters in the light of the discrete-time Mortensen filter

As we see, the Mortensen filter and its corresponding time-discrete version are condemned to be used with systems of very small dimension. We have implemented a version in [37] that can be used for 2-dimensional or 3-dimensional systems, hence implying 2-dimensional or 3-dimensional Bellman equations to be solved. We believe that with state-of-the-art spatial discretizations, for instance using Sparse-Grids we can reach up to 10 dimensions at the extreme limit as it is a typical barrier for people confronted to similar problems [Fleming and McEneaney, 2000, Bokanowski et al., 2013]. Therefore, for larger systems, we must rely on approximated optimal filters. In our application cases we have worked on two such filters:

- The Extended Kalman Filter (EKF),
- The Unscented Kalman Filter (UKF).

These two filters, EKF and UKF, will be present in numerous results presented in this manuscript. Thus, it is the occasion to see their structure in the light of (2.6) and (2.11).

REMARK 2.2.2 (ENKF)

Nowadays, there is a huge research effort going on the alternative Ensemble Kalman Filter (EnKF) that, however, we have not considered. In fact, the UKF filter is close to the EnKF, at least algebraically. We will see in the next paragraph that, in spirit, the UKF is more deterministic than the EnKF, hence its interest in our research.

The Extended Kalman Filter – The initial principle of the Extended Kalman Filter is to replace the linear operators appearing in the Kalman estimator by the tangent of the non-linear dynamics of interest. Therefore, the continuous-time EKF is formally given by

$$\begin{cases} \dot{\hat{y}}(t) = A(\hat{y}, t) + P(t) \, dC(\hat{y}, t)^\top R (z(t) - C(\hat{y}, t)) \\ \dot{P}(t) = dA(\hat{y}, t)P(t) + P(t) \, dA(\hat{y}, t)^\top - P(t) \, dC(\hat{y}, t)^\top R \, dC(\hat{y}, t)(t)P(t) + BQB^\top \\ \hat{y}(0) = y_\diamond \\ \hat{P}(0) = P_\diamond \end{cases} \quad (2.12)$$

with obvious extension for infinite dimensional system using the proper adjoint operators. Note that the EKF can also be rewritten using the discrepancy operator J . It is a less classical form but very useful in practice when dealing with an implicit observation operator as in Section 2.4.

$$\begin{cases} \dot{\hat{y}}(t) = A(\hat{y}, t) - P(t) \, dJ(\hat{y}, t)^\top R J(\hat{y}, t) \\ \dot{P}(t) = dA(\hat{y}, t)P(t) + P(t) \, dA(\hat{y}, t)^\top - P(t) \, dJ(\hat{y}, t)^\top R \, dJ(\hat{y}, t)(t)P(t) + BQB^\top \\ \hat{y}(0) = y_\diamond \\ \hat{P}(0) = P_\diamond \end{cases}$$

We understand that the principle of the EKF is to replace the cost-to-come second derivative by a computable operator solution of a Riccati equation.

Moreover the non-linear discrete-time version is given by

$$\begin{cases} \text{Initialization:} \\ \hat{y}_0^- = y_\diamond \\ P_0^- = P_0 \\ \text{Correction:} \\ \hat{y}_n^+ = \hat{y}_n^- + G_n (z_n - C_n(\hat{y}_n^-)) \\ G_n = P_n^+ \, dC_n(\hat{y}_n^+)^\top R_n = P_n^- \, dC_n(\hat{y}_n^+)^\top (W_n + dC_n(\hat{y}_n^+)^\top P_n(\hat{y}_n^-) \, dC_n(\hat{y}_n^+))^{-1} \\ P_n^+ = P_n^- - P_n^- \, dC_n(\hat{y}_n^+)^\top (dC_n(\hat{y}_n^+) P_n \, dC_n(\hat{y}_n^+) + W_n)^{-1} \, dC_n(\hat{y}_n^+) P_n \\ \text{Prediction:} \\ \hat{y}_{n+1}^- = A_{n+1|n}(\hat{y}_n^+) \\ P_{n+1}^- = dA_{n+1|n}(\hat{y}_n^+) P_n^+ \, dA_{n+1|n}(\hat{y}_n^+)^\top + B_n Q_n B_n^\top \end{cases}$$

and it is consistent and stable time discretization of the (2.12) as soon as the stability of the estimator (2.12) can be established. Here again, when compared to (2.11), we see that the Newton iterations of $\nabla \mathcal{V}_n^+(\hat{y}_n^+)$ is limited to their first iteration, whereas the propagation of the cost-to-come is simplified by the time-discrete Riccati equation with tangent operators.

The Unscented Kalman Filter – Another approximate optimal filter is given by the UKF filter. This filter was originally introduced in [Julier et al., 1995, Julier et al., 2000] with the objective to better represent how a non-linear transformation φ acts on the first two moments of a random variable \mathbf{y} . As we also recall in [23], it is possible to generate some sampling points – called *sigma*-points in UKF – centered around $\mathbb{E}(\mathbf{y})$ to propagate them with φ and then compute the first two moments of the random variable $\varphi(\mathbf{y})$ from the empirical moments of the sampling points. Let N_p be the number of sigma-point to be considered; we define N_p weight coefficients $\alpha = (\alpha_i)_{1 \leq i \leq N_p}$ and a set of sigma-points $\mathbf{y} = (y_i)_{1 \leq i \leq N_p}$ such that

$$\left\{ \begin{array}{l} \sum_{i=1}^{N_p} \alpha_i = 1 \\ \mathbb{E}_\alpha(\mathbf{y}) = \sum_{i=1}^{N_p} \alpha_i y_i = \mathbb{E}(\mathbf{y}) \\ \text{Cov}_\alpha(\mathbf{y}) = \mathbb{E}_\alpha((\mathbf{y} - \mathbb{E}_\alpha(\mathbf{y}))(\mathbf{y} - \mathbb{E}_\alpha(\mathbf{y}))^\top) \\ \quad = \sum_{i=1}^{N_p} \alpha_i (y_i - \mathbb{E}_\alpha(\mathbf{y}))(y_i - \mathbb{E}_\alpha(\mathbf{y}))^\top = \text{Cov}(\mathbf{y}) \end{array} \right.$$

Introducing a deviation of each particle with respect to the mean value

$$y_i = \mathbb{E}_\alpha(\mathbf{y}) + \tilde{y}_i,$$

with $\mathbb{E}_\alpha(\tilde{y}) = 0$ we get the conditions that

$$\left\{ \begin{array}{l} \sum_{i=1}^{N_p} \alpha_i \tilde{y}_i = 0 \\ \sum_{i=1}^{N_p} \alpha_i \tilde{y}_i \tilde{y}_i^\top = \text{Cov}(\mathbf{y}) \end{array} \right.$$

which allows to approximate the first two moments of the random variable \mathbf{y}^φ from the *propagated sigma points* $\mathbf{y}^\varphi = (y_i^\varphi)_{1 \leq i \leq N_p} = (\varphi(y_i))_{1 \leq i \leq N_p}$. Indeed, we easily show

$$\begin{aligned} \mathbb{E}_\alpha(\mathbf{y}^\varphi) &= \sum_{i=1}^{N_p} \alpha_i y_i^\varphi \\ &= \varphi(\mathbb{E}(\mathbf{y})) + d^2 \varphi(\mathbb{E}(\mathbf{y})) : \text{Cov}(\mathbf{y}) + o(\mathbb{E}(\|\mathbf{y}\|^2)), \end{aligned}$$

and

$$\begin{aligned} \text{Cov}_\alpha(\mathbf{y}^\varphi) &= \sum_{i=1}^{N_p} \alpha_i (y_i^\varphi - \mathbb{E}_\alpha(\mathbf{y}^\varphi))(y_i^\varphi - \mathbb{E}_\alpha(\mathbf{y}^\varphi))^\top \\ &= d\varphi(\mathbb{E}(\mathbf{y})) \cdot \text{Cov}(\mathbf{y}) \cdot d\varphi(\mathbb{E}(\mathbf{y})) + o(\mathbb{E}(\|\mathbf{y}\|^2)). \end{aligned}$$

Therefore the UKF filter in [Julier et al., 1995], uses that the discrete-time Kalman correction on a random state \mathbf{y} using a random measurement \mathbf{z} is a BLUE of the form (1.1) but computed with the empirical covariances, namely

$$\hat{\mathbf{y}} = \mathbb{E}_\alpha(\mathbf{y}) + \text{Cov}_\alpha(\mathbf{y}, \mathbf{z}) \text{Cov}_\alpha(\mathbf{z})^{-1} (\mathbf{z} - \mathbb{E}(\mathbf{z})),$$

where the empirical mean and covariance are applied to a random variable from the sigma-points generated around it. This implies that the discrete-time UKF estimator is of the form

$$\left\{ \begin{array}{l}
 \text{Initialization:} \\
 \hat{y}_0^- = y_\diamond \\
 P_0^- = P_0 \\
 \text{Sampling:} \\
 \hat{y}_{n,i}^- = \hat{y}_n^- + \sqrt{P_n^-} \tilde{y}_i \\
 \text{Correction:} \\
 \hat{z}_{n,i}^- = C_n(\hat{y}_{n,i}^-) \\
 \hat{y}_n^+ = \hat{y}_n^- + G_n(z_n - \mathbb{E}_\alpha(\hat{z}_n^-)) \\
 G_n = \text{Cov}_\alpha(\hat{y}_n^-, \hat{z}_n) (\text{Cov}_\alpha(\hat{z}_n^-) + W_n)^{-1} \\
 P_n^+ = P_n^- - \text{Cov}_\alpha(\hat{y}_n^-, \hat{z}_n) (\text{Cov}_\alpha(\hat{z}_n^-) + W_n)^{-1} \text{Cov}_\alpha(\hat{y}_n^-, \hat{z}_n) \\
 \text{Re-Sampling:} \\
 \hat{y}_{n,i}^+ = \hat{y}_n^+ + \sqrt{P_n^+} \tilde{y}_i \\
 \text{Prediction:} \\
 \hat{y}_{n+1,i}^- = A_{n+1|n}(\hat{y}_{n,i}^+) \\
 \hat{y}_{n+1}^- = \mathbb{E}_\alpha(\hat{y}_{n+1}^-) \\
 P_{n+1}^- = \text{Cov}_\alpha(\hat{y}_{n+1}^-) + B_n Q_n B_n^\top
 \end{array} \right. \quad (2.13)$$

Considering now (2.13) and the discrete-time Mortensen filter (2.11), we can have a completely deterministic interpretation of UKF as already pointed out in [23]. The objective of UKF and EKF are very close. In EKF we define a modified discrete-time Riccati equation based on an operator computed from the non-linear dynamics tangent. In UKF, the modified discrete-time Riccati equation is based on an operator computed from multi-dimensional finite difference approximations using the *sigma*-points as a stencil – see also the UKF interpretation given in [Lefebvre et al., 2002]. As a consequence, the UKF filter and the EKF filter coincide with the Kalman Filter when all the operators are actually linear. Moreover, as the EKF in [Reif and Unbehauen, 1999, Krener, 2003a, Bonnabel and Slotine, 2015], the UKF can be analyzed identically for small errors – in the spirit of [23] – leading to the diagram Figure 2.1.

REMARK 2.2.3 (ENKF)

Considering the stochastic interpretation of the UKF filter, it is close to the EnKF imagined by [Evensen, 2007] at the same period. However, the specificity of the sampling points involved in UKF defined and in a smaller number implies that UKF is in practice more deterministic in spirit than EnKF.

Finally, the discrete-time UKF reveals to be very useful in practice as (1) it is much easier to develop since it is tangent free, (2) for linearized errors, it has the same stabilizing properties as the EKF and (3) for very non-linear systems, as described in [Julier et al., 1995], the heuristics shows that UKF can behave more efficiently than EKF. Having in mind the discrete-time Mortensen filter, this is clearly understandable for a similar reason to when using a secant method instead of a gradient based Newton when choosing a root-finding algorithm.

REMARK 2.2.4 (CONSTRUCTION OF THE UNITARY SIGMA-POINTS)

There exist several choices of points that allow to create a finite-difference stencil in dimension N_r , that we report here for futur use in this manuscript. For instance we have the:

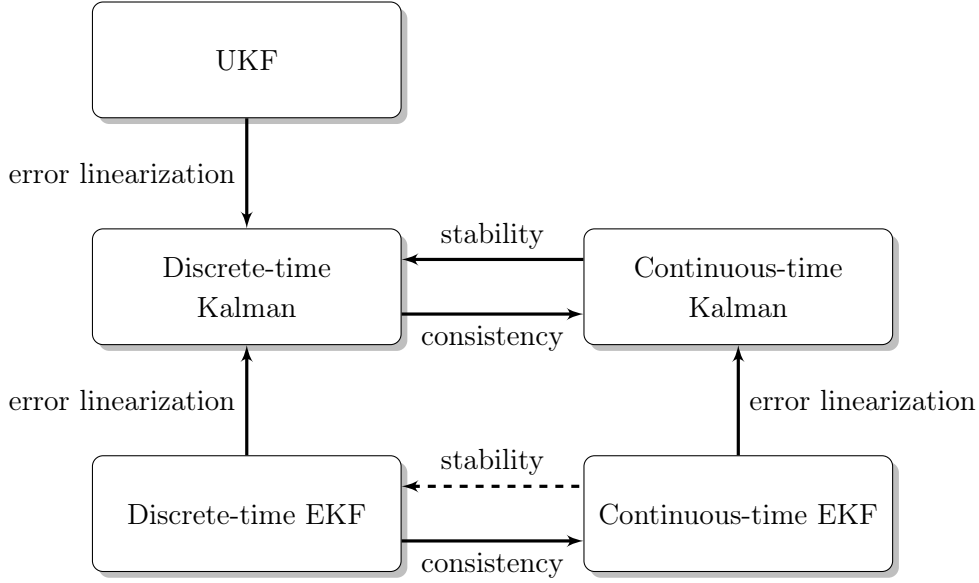


Figure 2.1: Relations between filtering procedures

- CANONICAL SIGMA-POINTS – they are $N_p = 2N_y$ particles defined from the canonical basis of the space \mathbb{R}^{N_y} of each side of the origin. Therefore we define

$$e_i = \begin{cases} \sqrt{N_y} & \text{if } 1 \leq i \leq N_y \\ -\sqrt{N_y} & \text{if } N_y + 1 \leq i \leq 2N_y \end{cases}$$

with the corresponding weight $\alpha_i = \frac{1}{N_y}$

- STAR SIGMA-POINTS – they are $N_p = 2N_y + 1$ particles defined from the canonical basis of the space \mathbb{R}^{N_y} of each side of the origin plus the origin. We define

$$e_i = \begin{cases} \sqrt{N_y} & \text{if } 1 \leq i \leq N_y \\ -\sqrt{N_y} & \text{if } N_y + 1 \leq i \leq 2N_y \\ 0 & \text{if } i = 2N_y + 1 \end{cases}$$

and the corresponding weight can be $\alpha_i = \frac{1}{N_y + 1}$. In [Julier et al., 2000], the origin weight is bigger than others. For example choosing

$$\alpha_i = \begin{cases} a_i & \text{if } 1 \leq i \leq 2N_y \\ b_i & \text{if } i = 2N_y + 1 \end{cases}$$

allows to also approximate the next third and fourth moments of \mathbf{y}^φ .

- SIMPLEX SIGMA POINTS – they corresponds to the minimum number of sigma-points to define the covariance of \mathbf{y} , *i.e.* $N_p = N_y + 1$. The unitary simplex sigma points are typically positioned on a regular simplex of radius $\sqrt{N_p}$ [Uhlmann and Julier, 2002]. Eventually, the associated weights are uniform $\alpha_i = \frac{1}{N_y + 1}$.

2.3 Control-based sequential estimation strategies for PDEs

2.3.1 Optimal-control-based strategies

2.3.1.1 Observer formulation for parabolic problems

We have discussed in Section 2.2 the principles underlying optimal filtering, where optimal means that the feedback is derived from a least square criterion optimization. The presentation in Section 2.2 was limited to finite dimensional dynamical system. Our objective here is then to understand the interest of possible extensions to infinite dimensional systems such as systems associated with evolution PDEs. In a recent work with K. Mauffrey [35], we investigated and reviewed the different aspects of optimal observer design consolidating results for the definition of the minimization problem, the existence of Riccati solutions and observer trajectory, and more importantly proving the asymptotic convergence of the observer to the target trajectory at least in the absence of measurement noise. These results complete the theory presented in [Baras and Bensoussan, 1987].

To present our result, we restart with a linear system of the form

$$\begin{cases} \dot{y}_{|\zeta, \nu}(t) = A(t)y_{|\zeta, \nu}(t) + \beta(t) + B(t)\nu(t), & t \in \mathbb{R}^+ \\ y_{|\zeta, \nu}(0) = y_{\diamond} + \zeta \end{cases} \quad (2.14)$$

where y is the state variable in a Hilbert space \mathcal{Y} , A is a perfectly known time-varying dynamical operator defined in the next paragraph. Moreover $\beta(t) \in L^2(0, +\infty; \mathcal{Y})$ is a time-dependent source term. Additionally $\nu \in L^2(0, +\infty; \mathcal{Q})$ – with \mathcal{Q} a Hilbert space – represents an unknown contribution that can be seen as a model noise acting on the dynamics through a model noise operator B . Finally the initial condition contribution $y_{\diamond} \in \mathcal{Y}$ is the known part of the initial condition, whereas $\zeta_y \in \mathcal{Y}$ is to be determined.

In fact, for infinite dimensional state and observation spaces, the definition of the initial system, the Riccati solution and the observer can be quite intricate. We cannot investigate here all the cases when (2.14) defines a dynamical system with an underlying PDE structure, hence we will focus on one example of interest: a simple generalized heat equation.

First, we may consider that the model dynamics is a time-independent operator A which is self-adjoint for a parabolic (dissipative) system. Then typically $A : D(A) \subset \mathcal{Y} \rightarrow \mathcal{Y}$ is the infinitesimal generator of a C^0 -semigroup $(\mathbb{T}_t)_{t \geq 0}$ on the Hilbert space \mathcal{Y} . Actually, we can be more general by considering time varying model operators $A(t)$ following [Tanabe, 1979, Baras and Bensoussan, 1987]. Then A is defined through a mapping $a : [0, +\infty) \times \mathcal{V} \times \mathcal{V} \rightarrow \mathbb{R}$ – with \mathcal{V} a dense subspace of \mathcal{Y} – which satisfies the following properties:

- for a.e. $t \geq 0$, $a(t; \cdot, \cdot)$ is bilinear on $\mathcal{V} \times \mathcal{V}$,
- $a(t; \cdot, \cdot)$ is bounded on $\mathcal{V} \times \mathcal{V}$ uniformly with respect to t , i.e. there exists $M > 0$ such that:

$$|a(t; u, v)| \leq M \|u\|_{\mathcal{V}} \|v\|_{\mathcal{V}}, \quad \forall (u, v) \in \mathcal{V} \times \mathcal{V}, \quad \forall t \in [0, +\infty),$$

- $a(t; \cdot, \cdot)$ is \mathcal{V} -elliptic with respect to \mathcal{Y} , uniformly with respect to a.e. t , i.e. there exists $\nu > 0$ and $\lambda \geq 0$ such that:

$$a(t; v, v) + \lambda \|v\|_{\mathcal{Y}}^2 \geq \nu \|v\|_{\mathcal{Y}}^2, \quad \forall v \in \mathcal{V}, \text{ a.e. } t \in [0, +\infty),$$

- for each bounded interval $[t_0, t_1] \subset [0, +\infty)$, there exist $\alpha_0 \in (0, 1]$ and $M_0 > 0$ such that

$$|a(t; u, v) - a(s; u, v)| \leq M_0 |t - s|^{\alpha_0} \|u\|_{\mathcal{V}} \|v\|_{\mathcal{V}},$$

for all t, s in $[t_0, t_1]$ and all u, v in \mathcal{V} .

A is then defined by:

$$\langle A(t)u, v \rangle_{\mathcal{V}', \mathcal{V}} = -a(t; u, v),$$

for $(u, v) \in \mathcal{V} \times \mathcal{V}$ and $t \in [0, +\infty)$. In particular, $A \in L^\infty(0, +\infty; \mathcal{L}(\mathcal{V}, \mathcal{V}'))$.

With a time-varying parabolic system, we can expect for all t a solution $y \in L^2([0, t], \mathcal{V})$ with also $\dot{y} \in L^2([0, t], \mathcal{V}')$. For all (t, s) , we denote by $\Upsilon(t, s)$ the mild evolution operator from time s to time t generated by A [Tanabe, 1979].

Second, we consider a bounded observation operator $C \in L^\infty(0, +\infty, \mathcal{L}(\mathcal{Y}, \mathcal{Z}))$ with \mathcal{Z} a Hilbert space. Note that boundary operators are often not bounded but still very useful in practice. We refer to [Weiss, 1989, Lasiecka and Triggiani, 2003, Tucsnak and Weiss, 2009] for the numerous specificities raised by these operators that we do not treat here for the sake of clarity. The observations are still given by $z \in L^2(0, +\infty, \mathcal{Z})$. Finally, we also consider a bounded model noise operator $B \in L^\infty(0, +\infty, \mathcal{L}(\mathcal{Q}, \mathcal{V}'))$.

The least square criterion remains the same as (2.2) for finite-dimensional systems. Note that, as in finite dimension, we assume that $P_\diamond \in \mathcal{L}(\mathcal{Y})$, $S \in \mathcal{L}(\mathcal{Q})$ and $R \in \mathcal{L}(\mathcal{Z})$ are self-adjoint, non-negative and invertible operators. The adjoint system can be directly defined since it is based on $-A^*$ in reverse time, which is also dissipative. Therefore the adjoint variable has the same regularity. In order to formalize the Kalman observer in this case, we must then give a proper definition of the so-called *covariance* operator solution of the Riccati equation. In fact, the covariance operator can be intrinsically defined as the bounded operator on \mathcal{Y} associated with the mapping $q \mapsto \bar{y}_{t,\lambda}(t)$

$$\bar{y}_{t,\lambda}(t) = P(t)\lambda, \quad \forall \lambda \in \mathcal{Y}.$$

where

$$\begin{cases} \dot{\bar{y}}_{s,\lambda}(s) = A(s)\bar{y}_{s,\lambda}(s) + B(s)QB(s)^*\bar{q}_{t,\lambda}(s), & \text{in } (0, t), \\ -\dot{\bar{q}}_{t,\lambda}(s) = A(s)^*\bar{q}_{t,\lambda}(s) - C(s)^*RC(s)\bar{y}_{t,\lambda}(s), & \text{in } (0, t), \\ \bar{y}_{t,\lambda}(0) = P_\diamond\bar{q}_{t,\lambda}(0), \\ \bar{q}_{t,\lambda}(t) = \lambda. \end{cases}$$

and can be shown to satisfy the Riccati equation (2.8) in the mild sense, namely

$$\begin{aligned} P(t)\lambda = & \Upsilon(t, 0)P_\diamond\Upsilon(t, 0)^*\lambda + \int_0^t \Upsilon(t, s)B(s)QB(s)^*\Upsilon(t, s)^*\lambda \, ds \\ & - \int_0^t \Upsilon(t, s)P(s)C(s)^*RC(s)P(s)\Upsilon(t, s)^*\lambda \, ds. \end{aligned}$$

In the case where the model dynamics is associated with a semi-group generator, we have $y \in C^1([0, t], \mathcal{Y}) \cap C^0([0, t], D(A))$ and we can justify that the covariance operator P satisfies the Riccati equation (2.8) in a weak sense, namely

$$\frac{d}{dt} \langle p, P(t)q \rangle_{\mathcal{Y}} = \langle A^*p, P(t)q \rangle_{\mathcal{Y}} + \langle P(t)p, A^*q \rangle_{\mathcal{Y}} - \langle CP(t)p, CP(t)q \rangle_R + \langle B^*p, B^*q \rangle_Q.$$

and also as strong solution $C^1(\mathbb{R}, \mathbb{S}^+(\mathcal{Y}))$ where $\mathbb{S}^+(\mathcal{Y})$ is the space of positive symmetric operators.

Once the covariance operator is defined as a proper Riccati solution, we can then prove that the Kalman observer \hat{y} (see (2.7) with a duality $*$ replacing the transpose \top) exists with the same regularity as the target y .

As a typical example of (2.14), we can think of a classical heat equation.

$$\begin{cases} \partial_t u(\underline{x}, t) - \Delta u = f, & \underline{x} \text{ in } \Omega \\ u(\underline{x}, t) = 0, & \underline{x} \text{ on } \partial\Omega \end{cases}$$

where f is a source term, typically in $L^2(\Omega)$. We consider $\mathcal{Y} = L^2(\Omega)$ and $\mathcal{V} = H_0^1(\Omega)$. We can now consider an simple observation operator associated with the measurement of the solution on a subdomain $\Omega_{\text{obs}} \subset \Omega$

$$\forall t \in \mathbb{R}^+, \quad C : y(t) \mapsto z(t) = \mathbb{1}_{\Omega_{\text{obs}}}(\cdot)u(\cdot, t).$$

and a model noise operator which applies to the complementary subset $\Omega \setminus \overline{\Omega_{\text{obs}}}$

$$\forall t \in \mathbb{R}^+, \quad B : \nu(t) \mapsto r(t) = \mathbb{1}_{\Omega \setminus \overline{\Omega_{\text{obs}}}}(\cdot)u(\cdot, t).$$

In [Bensoussan, 1971, Lions, 1968] it is asserted that we can associate with the covariance operator $P(t)$ a function called kernel $\pi(\cdot, \cdot, t) \in L^2(\Omega \times \Omega)$ such that

$$\forall y \in L^2(\Omega), \quad (P(t)y)(\underline{x}) = \int_{\Omega} \pi(\underline{x}, \underline{x}', t) u(\underline{x}', t) \, d\underline{x}'.$$

It is even possible to derive the integro-differential equation satisfied by the kernel. We show that

$\pi \in L^2(0, t; H_0^1(\Omega \times \Omega)) \cap L^\infty(0, t; L^2(\Omega \times \Omega))$ and

$$\begin{cases} \partial_t \pi(t; \underline{x}, \underline{x}') = (\Delta_{\underline{x}} + \Delta_{\underline{x}'})\pi(t; \underline{x}, \underline{x}') - \gamma \int_{\Omega_{\text{obs}}} \pi(t; \underline{x}, \underline{x}'')\pi(t; \underline{x}'', \underline{x}') \, d\underline{x}'' + \beta \mathbb{1}_{\Omega \setminus \overline{\Omega_{\text{obs}}}}(\underline{x})\delta(\underline{x} - \underline{x}'), \\ \hspace{15em} \text{in } \mathcal{D}'((0, t)), \quad (\underline{x}, \underline{x}') \in \Omega \times \Omega, \\ \pi(0; \underline{x}, \underline{x}') = \pi_0(\underline{x}, \underline{x}'), \quad (\underline{x}, \underline{x}') \in \Omega \times \Omega, \\ \pi(t; \underline{x}, \underline{x}') = \pi(t; \underline{x}', \underline{x}), \quad \forall t \in [0, t], \quad (\underline{x}, \underline{x}') \in \Omega \times \Omega, \end{cases}$$

Moreover, we have

$$\int_{\Omega \times \Omega} \pi(t; \underline{x}, \underline{x}') \varphi(\underline{x}) \varphi(\underline{x}') \, d\underline{x} d\underline{x}' \geq 0, \quad \forall \varphi \in L^2(\Omega), \quad \forall t \in [0, t].$$

Using the kernel π , the observer \hat{y} is now a strong solution of the PDE

$$\begin{cases} \partial_t \hat{u}(\underline{x}, t) - \Delta \hat{u} = f + \gamma \int_{\Omega_{\text{obs}}} \pi(t; \underline{x}, \underline{x}') (\hat{u}(\underline{x}', t) - \hat{u}(\underline{x}, t)) \, d\underline{x}', & \underline{x} \text{ in } \Omega \\ u(\underline{x}, t) = 0, & \underline{x} \text{ on } \partial\Omega \end{cases}$$

REMARK 2.3.1 (KERNEL FORMULATION VALIDITY)

This formulation is quite appealing in itself but numerous questions are raised here to justify it completely. In fact the kernel existence cited by [Lions, 1968] is intricate to justify. Even if it is clear for distributions with the Schwartz kernel Theorem [Gask, 1960], then it is less obvious for the covariance operator solution of the Riccati equation, see for instance [Temam, 1971, Rosen, 1991]. In [Temam, 1971], the existence of the kernel is demonstrated only for $C = \mathbb{1}$ which, in the case of observation theory, is rather restrictive. In particular in [Rosen, 1991], the kernel existence is demonstrated in a quite general context for the operator C^*RC , but, in practice, the hypotheses are still difficult to verify even in a simple case like the one presented below leading still to ongoing work.

2.3.1.2 Analysis

The question is now to prove that the observer \hat{y} converges in time to the target trajectory \tilde{y} at least with no measurement noise

$$z = C\tilde{y},$$

namely the so-called asymptotic convergence sought for any observer formulation.

To this end, we equivalently prove that the estimation error $\tilde{y} = \tilde{y} - \hat{y}$ is stable to 0.

To obtain the convergence we need some observability and controllability conditions as in finite dimension. In our work, we need the following assumptions directly related to observability and controllability conditions :

1. There exist a time $T_C > 0$ and a positive constant $C_C(T_C)$ for which we have

$$c_C(T_C) \|\Upsilon(T + T_C, T)\zeta\|_{\mathcal{Y}}^2 \leq \int_T^{T+T_C} \|C(t)\Upsilon(t, T)\zeta\|_{\mathcal{Z}}^2 dt, \quad \forall \zeta \in \mathcal{Y},$$

for every $T \geq 0$.

2. There exists a positive constant C_B such that

$$C_B \|\lambda\|_{\mathcal{Y}}^2 \leq \|\Upsilon(t_2, t_1)^* \lambda\|_{\mathcal{Y}}^2 + \int_{t_1}^{t_2} \|B(t)^* \Upsilon(t_2, t)^* \lambda\|_{\mathcal{Q}}^2 dt, \quad \forall \lambda \in \mathcal{Y}, \quad (2.15)$$

for every interval $[t_1, t_2] \subset [t_0, +\infty)$.

3. $\sup_{t \geq t_0} \|P(t)^{-1}\|_{\mathcal{L}(\mathcal{Y})} < +\infty$.

THEOREM 2.3.1 (MAUFFREY-MOIREAU)

Under the model hypotheses and the additional observability and controllability conditions 1-3, we have

$$\|\tilde{y}(t)\|_{\mathcal{Y}} \leq c_1 e^{-c_2(t-t_0)} \|\zeta\|_{\mathcal{Y}}, \quad \forall t > t_0,$$

where $c_1 = \|P_{\diamond}^{-1}\|_{\mathcal{L}(\mathcal{Y})}^{1/2} \|P\|_{\infty}^{1/2} \gamma^{-1/2}$, $c_2 = \ln(\gamma^{-1})/(2T_C)$ and $\gamma \in (0, 1)$ is a constant which only depends on c_B , λ , T_C , $c_C(T_C)$, $\|B\|_{\mathcal{L}(\mathcal{Q}, \mathcal{Y})}$, $\|C\|_{\mathcal{L}(\mathcal{Z})}$, $\|S\|_{\mathcal{L}(\mathcal{Q})}$, $\|S^{-1}\|_{\mathcal{L}(\mathcal{Q})}$, $\|R\|_{\mathcal{L}(\mathcal{Z})}$, $\|R^{-1}\|_{\mathcal{L}(\mathcal{Z})}$ and $\|P^{-1}\|_{\infty}$.

The conditions to obtain the exponential convergence are rather classical and the of result obtained in (2.3.1) is announced in numerous work but we did not find it in a clear and complete statement. Note however that the controllability condition (2.15) is even weaker than the classical controllability condition.

2.3.1.3 Discretization and curse of dimensionality

Once the analysis of the estimator has been performed, we can now consider its space and time discretization. We have already seen a strategy to time-discretize the system based on the discrete-time Kalman filter. Hence, we focus here on space discretization aspects. Let us consider a Galerkin discretization – in a space \mathcal{V}_h – of the heat equation. For a function $u_h \in \mathcal{V}_h$ we associate the vector of degrees of freedom $\mathbf{u} \in \mathbb{R}^{N_{\text{dof}}}$. We have the following finite dimensional dynamical systems

$$\mathbf{M}\dot{\mathbf{u}} + \mathbf{K}\mathbf{u} = \mathbf{f}.$$

In this simple case, the state is directly given by $\mathbf{y} = \mathbf{u}$, the dynamics operator $\mathbf{A} = -\mathbf{M}^{-1}\mathbf{K}$, and the right hand side $\boldsymbol{\beta} = \mathbf{M}^{-1}\mathbf{f}$ such that we can write

$$\dot{\mathbf{y}} = \mathbf{A}\mathbf{y} + \boldsymbol{\beta} + \mathbf{B}\boldsymbol{\nu}.$$

For this class of system we consider a target trajectory $\{\tilde{\mathbf{y}}(t), t \in \mathbb{R}^+\}$ which corresponds to the space-discretization of the time-continuous trajectory $\{\tilde{y}(t), t \in \mathbb{R}^+\}$ and a space-discretized observations operator \mathbf{C} such that a discretized version of the observations \mathbf{z} are given by

$$\mathbf{z} = \mathbf{C}\tilde{\mathbf{y}} + \boldsymbol{\chi},$$

where $\boldsymbol{\chi}$ contains now the measurement noise and the space discretization error. Let us now consider the natural discretized space norm. For example for all $(u_h, z_h, \nu_h) \in \mathcal{V}_h \times \mathcal{Z}_h \times \mathcal{W}_h$ we have

$$\langle \mathbf{C}^* z_h, u_h \rangle_{\mathcal{Y}} = \langle z_h, \mathbf{C}u_h \rangle_{\mathcal{Z}} = \mathbf{z}^T \mathbf{M}_{\Omega_{\text{obs}}} (\mathbf{C}\mathbf{u}) = (\mathbf{z}^T \mathbf{M}_{\Omega_{\text{obs}}} \mathbf{C}\mathbf{u})^T = \mathbf{u}^T \mathbf{C}^T \mathbf{M}_{\Omega_{\text{obs}}} \mathbf{z},$$

and

$$\langle \mathbf{B}^* u_h, \nu_h \rangle_{\mathcal{Y}} = \langle u_h, \mathbf{B}\nu_h \rangle_{\mathcal{Y}} = \mathbf{u}^T \mathbf{M} (\mathbf{B}\boldsymbol{\nu}) = (\mathbf{u}^T \mathbf{M} (\mathbf{B}\boldsymbol{\nu}))^T = \boldsymbol{\nu}^T \mathbf{B}^T \mathbf{M}\mathbf{u}.$$

In other words, the natural norms after space discretization appear as symmetric matrix operators \mathbf{M} and $\mathbf{M}_{\Omega_{\text{obs}}}$ that weigh the usual euclidian norm. We can now apply the optimal observer formalism to the finite dimensional system followed by \mathbf{y} and observed through \mathbf{z} and get

$$\begin{cases} \mathbf{M}\dot{\hat{\mathbf{y}}}(t) = -\mathbf{K}\hat{\mathbf{y}}(t) + \gamma \mathbf{M}\mathbf{P}(t)\mathbf{M}^{-1}\mathbf{C}^T \mathbf{M}_{\Omega_{\text{obs}}} (\mathbf{z}(t) - \mathbf{C}\hat{\mathbf{y}}(t)), & t > 0, \\ \hat{\mathbf{y}}(0) = \mathbf{y}_{\diamond}, \end{cases}$$

where the finite dimensional covariance operator satisfies

$$\begin{cases} \dot{\mathbf{M}}\mathbf{P}(t) = -\mathbf{K}\mathbf{P}(t) - \mathbf{M}\mathbf{P}(t)\mathbf{M}^{-1}\mathbf{K}^T - \gamma \mathbf{M}\mathbf{P}(t)\mathbf{M}^{-1}\mathbf{C}^T \mathbf{M}_{\Omega_{\text{obs}}} \mathbf{C}\mathbf{P}(t) \\ \quad + \beta \mathbf{M}\mathbf{B}\mathbf{M}^{-1}\mathbf{B}^T \mathbf{M}, & t > 0, \\ \mathbf{P}(0) = \mathbf{P}_0. \end{cases}$$

We then realize that this equations leads to a full matrix operator – in fact \mathbf{P}_{ij} is directly related to the discretization of the kernel π . Therefore, the space discretization drastically limits the use of the Kalman filter for infinite dimensional systems in particular for PDEs in dimension 2 or 3. This is again a *curse of dimensionality* example for these filters coming from dynamic programming paradigms.

REMARK 2.3.2

The complete analysis of a space and time discretization of the Kalman filtering for infinite dimensional systems has been investigated in different works. For instance in [Bensoussan, 1971], some Galerkin

approximation strategies are used to prove the existence of the continuous covariance operator, giving by this way some discretization analysis arguments. We can also cite the convergence work of [Hager and Horowitz, 1976] the recent works [Aalto, 2014a, Aalto, 2014b] which analyses intensively the space discretization and time discretization of the Kalman filter in a stochastic context.

2.3.1.4 Reduced-Order strategies

Principles – A way to circumvent the curse of dimensionality consists in assuming a specific reduced-order form for the covariance operators. For example, when forgetting the model noise we can consider the ansatz

$$\forall t, \quad P(t) = L(t)U(t)^{-1}L(t)^* \quad (2.16)$$

with U is an isomorphism and L an extension operator – hence $L(t)^*$ is a projection operator. As we have shown in [24] – strictly speaking in the finite dimensional case but with clear extension in the infinite dimensional case – the solution of the Riccati equation form reduces to

$$\dot{L} = AL \text{ and } \dot{U} = L^*C^*RCL, \quad (2.17)$$

Since A stable, it is straightforward to define L . Moreover, U is a positive definite operator as soon as its initial condition is. This, by the way, illuminates the analysis of the initial Riccati solution P .

The initialization of this dynamics is based on the following initial decomposition. We define by $\mathcal{V}_r \subset \mathcal{Y}$ a space where the initial condition uncertainty – denoted by ζ_r – is reduced and Π_r is the projector on this subspace. Therefore we should parametrize the initial condition as

$$y = y_\diamond + \Pi_r^* \zeta_r.$$

There, we aim at defining $L(0) = \Pi_r^*$ and $U(0) = U_0$ as the inverse of an error covariance operator on \mathcal{V}_r – namely an operator weighting the natural norm of \mathcal{V}_r . We end up with a Reduced Order Kalman Filter (ROKF) estimator of the form

$$\begin{cases} \dot{\hat{y}} = A\hat{y} + f + LU^{-1}L^*C^*(z - C\hat{y}) \\ \dot{L} = AL \\ \dot{U} = L^*C^*RCL \\ \hat{y} = y_\diamond \\ L(0) = \Pi_r^* \\ U(0) = U_0 \end{cases}$$

The principle of this reduction is not new as it can be envisioned in the square-root approaches of optimal filtering in finite dimensional systems [Kailath et al., 2000]. Moreover, the Singular Evolutive Extended Kalman filter proposed in the data assimilation community is exactly based on the same decomposition [Pham et al., 1998a]. We can also cite [Le Bris and Rouchon, 2013] where the question of Riccati decomposition is intensively studied. Note that similar reduction strategies have also been proposed in [Aalto, 2014b].

In our work [24], we complete the previous works on reduced-order strategy by two remarks. First and taking inspiration from [Pham et al., 1998a], we have that the resulting observer can still be associated with an optimal criterion. In that case, we easily show that the Reduced

Order Kalman Filter (ROKF) obtained from (2.17) is associated with the minimization of the criterion

$$\min_{\zeta_r} \left\{ \mathcal{J}(\zeta_r, t) = \frac{1}{2} \|\zeta_r\|_{U_0}^2 + \frac{1}{2} \int_0^t \left(\|z(s) - C(y_{|\zeta_r}(s))\|_R^2 \right) ds \right\}. \quad (2.18)$$

The second result is a convergence analysis principle inspired from the observer analysis in [Zhang, 2002]. We first proceed formally in a general setting before specifying some results for our initial parabolic problem. For any $y \in \mathcal{Y}$, let us introduce $y_\perp = (\mathbb{1} - \Pi_r)y$ the projection of y on the supplementary space \mathcal{V}_\perp so that $\mathcal{Y} = \mathcal{V}_\perp \oplus \mathcal{V}_r$. Hence every $y \in \mathcal{Y}$ is characterized by $(y_\perp \ y_r)$. Accordingly we decompose $L = (L_\perp \ L_r)$ with in particular $L_\perp(0) = 0$. We then introduce the estimation error $\tilde{y} = \hat{y} - y = (\tilde{y}_\perp \ \tilde{y}_r)$. By construction the error dynamics is the same as for the Kalman filter, namely

$$\dot{\tilde{y}} = (A - PC^*RC)\tilde{y} + PC^*R\chi,$$

with P decomposed as in (2.16). Then we proceed (when valid) to the change of variable

$$(\tilde{y}_\perp, \tilde{y}_r) \mapsto (\eta, \mu) = (\tilde{y}_\perp - L_\perp L_r^{-1} \tilde{y}_r, (L_r)^{-1} \tilde{y}_r), \quad (2.19)$$

that leads to the rewriting of the error dynamics in

$$\begin{cases} \dot{\eta} = (A_{\perp\perp} - L_\perp L_r^{-1} A_{r\perp})\eta \\ \dot{\mu} = -U^{-1} L^* C^* R C L \mu - U^{-1} L^* C^* R C (\mathbb{1} - \Pi_r)(\eta + \chi), \end{cases} \quad (2.20)$$

We point out that (2.20) is obtained when formally assuming that L_r is an isomorphism for all t . The remarkable consequence of our change of variable – inspired from [Pham et al., 1998a] and then completed in our work [38] and [19, 24] – is that (2.20) is tridiagonal. Thus, if we can obtain that η is exponential stable to 0, the stability of μ is defined by its homogeneous part $\dot{\mu} = -U^{-1} L^* C^* R C L \mu$ which is characteristic of Kalman-based error dynamics where a quadratic term $L^* C^* R C L$ is weighed by a covariance operator U^{-1} , reduced in our case.

The specific configuration where $A_{r\perp} = 0$ is worth studying. It corresponds to the configuration where the dynamics on the reduced space is decoupled from the dynamics on the supplementary space, at least in the sense that the part of the state on \mathcal{V}_\perp has no impact in the dynamics on the reduced space. In this configuration, the dynamics of the error (2.20) is then easier to analyze. First, L_r is solution of

$$\dot{L}_r = A_{rr} L_r, \quad L_r(0) = \mathbb{1},$$

a simple autonomous system. Then the dynamics of η is also autonomous

$$\dot{\eta} = A_{\perp\perp} \eta, \quad \eta(0) = \tilde{y}_\perp(0),$$

in the unfiltered space.

Let us look at the consequence of this assumption in our heat equation example. We consider the eigen-decomposition $(\lambda_i, \varphi_i)_{i \in \mathbb{N}}$ of the laplacian

$$-\Delta \varphi_i = \lambda_i \varphi_i,$$

and define $\mathcal{V}_r = \text{span}\{\varphi_i\}_{1 \leq i \leq N_r}$ the finite dimensional space of N_r lower order frequencies. In that case, we have indeed $A_{r\perp} = 0$, L_r an invertible matrix – even if ill-conditioned – and η

exponentially stable to 0. The reduced optimal filter is computable in practice and we can manage the exponential stability constant by choosing carefully the number of low frequencies.

We point out that the decomposition of the state into a stable part and a part to be controlled is a rather general idea. It has been used in control with optimal control design, see a nice example in [Breiten and Kunisch, 2015] with a cardiac application. A general definition of the projector can be found in [Curtain and Zwart, 1995] and we also invite the interested reader to read in [Ramdani et al., 2015] the very precise review of this problem for observer design.

REMARK 2.3.3 (EXTENSION TO MODEL NOISE)

The reduced order decomposition is incompatible with general model noise operator B unless we assume that it can be decomposed on the same controlled and uncontrolled spaces. Otherwise, an artificial projection on the controlled space can be envisioned, leading to

$$BQB^\top \rightarrow L(L^\top L)^{-1}L^\top BQB^\top L(L^\top L)^{-1}L^\top,$$

giving a modified dynamics of the reduced covariance inverse

$$\dot{U} = L^\top C^\top RCL - UL(L^\top L)^{-1}L^\top BQB^\top L(L^\top L)^{-1}L^\top U,$$

certainly more intricate to analyze.

Extension to non-linear systems – The heat equation is a rather simple example and our objective is typically to design efficient feedbacks for more general models such as those encountered with the cardiac system. Typical models of interest for us are reaction diffusion models, hence non-linear models, a topic on which we have only made some formal investigations. The idea is to formally derive an extension of the ROKF for non-linear systems based on the Extended Kalman Filter principles. The resulting estimator is called Reduced-Order Extended Kalman Filter (ROEKF). This idea takes its origin in [Pham et al., 1998a] for discrete-time dynamical systems but can be also developed for continuous-time systems as we have shown in [24]. As the derivation is only formal, we limit our presentation to finite dimensional systems typically obtained after spatial discretization. Besides, our formalism is directly compatible with non-linear observation operators. Indeed, the estimator dynamics reads

$$\begin{cases} \dot{L} = (dA)L \\ \dot{U} = L^\top (dC)^\top R (dC)L, \\ L(0) = \Pi \\ U(0) = U_0 \end{cases}$$

As we have seen in Section 2.2.3, the EKF filter is a simplification of optimal filter equations based on a linearization approximation. Then it has been analyzed for – and only for – small estimation errors as for instance in [Reif and Unbehauen, 1999, Krener, 2003a]. We believe that the same type of analysis can be conducted for the ROEKF as we initiate in [38] and then [19, 24]. There we consider the dynamics of the linearized error δy , and a change of variable similar to (2.19) gives

$$\begin{cases} \dot{\eta} = (dA_{\perp\perp} - L_\perp L_r^{-1} dA_{r\perp})\eta \\ \dot{\mu} = -U^{-1}L^* dC^* R dC L \mu - U^{-1}L^* dC^* R dC(\mathbb{1} - \Pi)\eta, \end{cases}$$

where the differentials of the operators are taken with respect to the observer trajectory or to the target trajectory.

The applicability of such an estimator has been numerically investigated in [13, 19] in conjunction with reduced basis strategies based on Proper Orthogonal Decomposition (POD) to define the reduced space. We briefly recall that, with POD, the order reduction is achieved by using pre-computed solutions to generate a well-chosen subspace within which an approximate solution is then sought, e.g. by Galerkin projection. We refer to [Chapelle et al., 2012] and references therein for an introduction to POD strategies, also recalling that a POD approximation corresponds to a modal decomposition when the dynamics operator is linear, hence a POD decomposition can be seen as a natural non-linear extension of the modal reduction that we introduced for the heat equation. This POD extension and the resulting ROEKF strategy have been applied to a reaction-diffusion model in [19]. In [13] the numerical investigations cover a damped mechanical model of cardiac contraction. In both cases, the initial condition uncertainty reduction on the POD basis is efficient with a number of POD vectors from 10 to 40.

Time-discretization of the ROEKF – Concerning the time discretization of these reduced-order strategies, here again the principle is to discretize the initial model, and then consider the minimization of a discretized version of (2.18). We obtained a discrete-time Reduced-Order Kalman Filter which can then be extended to a discrete-time ROEKF (similar to the SEEK of [Pham et al., 1998a]).

1. Initialization:

$$\begin{cases} \hat{y}_0^- &= y_\diamond \\ L_0 &= \Pi \\ U_0 &= U_\diamond \end{cases}$$

2. Correction:

$$\begin{cases} G_n &= L_n U_n^{-1} L_n^T dC_n^{-T} R_n \\ \hat{y}_n^+ &= \hat{y}_n^- + G_n (z_n - C_n(\hat{y}_n^-)) \\ P_n^+ &= L_n U_n^{-1} L_n^T \end{cases}$$

3. Prediction:

$$\begin{cases} \hat{y}_{n+1}^- &= A_{n+1|n}(y_n^+) \\ L_{n+1} &= dA_{n+1|n} L_n \\ U_{n+1} &= U_n + L_{n+1}^T dC_{n+1}^{-T} R_{n+1} dC_{n+1} L_{n+1} \\ P_{n+1}^- &= L_n U_{n+1}^{-1} L_n^T \end{cases}$$

The ROUKF alternative – Moreover, we can use other types of approximated optimal filters for non-linear systems as alternatives to the discrete-time estimator (2.21). In this respect we

have introduced in [23] a new reduced-order filter based on the UKF principles. The central idea behind a ROUKF formulation is the possibility that there exist a decomposition of the form

$$P_n^+ = \Gamma_n^+ \Delta_n^+ \Gamma_n^{+\top} \text{ and } P_{n+1}^- = \Gamma_{n+1}^- \Delta_{n+1}^+ \Gamma_{n+1}^{-\top}.$$

This is due to the following proposition demonstrated in our paper [23]. We refer to Section 2.2.3 for the notation.

PROPOSITION 2.3.2 (CHAPELLE-MOIREAU)

Let $\mathbf{y} \in \mathbb{R}^d$ be a random variable with mean and covariance represented by the empirical mean and empirical covariance of sigma-points $\mathbf{y} = (y^{(i)})_{1 \leq i \leq r}$ respecting the construction rules of a given family of – i.e. canonical, stars, simplex etc. – sigma points $\mathbf{v} = (v^{(i)})_{1 \leq i \leq r}$ with associated weights $\alpha = (\alpha_i)_{1 \leq i \leq N_p}$. Denoting by \mathbf{d}_α the diagonal matrix construct from the vector α , we have the identity

$$\text{Cov}_\alpha(\mathbf{y}) = \mathbf{y} \mathbf{d}_\alpha \mathbf{v}^\top (\mathbf{v} \mathbf{d}_\alpha \mathbf{v}^\top)^{-1} \mathbf{v} \mathbf{d}_\alpha \mathbf{y}^\top$$

Using Proposition 2.3.2, we propose in [23] a ROUKF estimator distinguishing two cases: (1) the simplex sigma-points case, and (2) the case of general sigma-points. The simplified formulation for simplex sigma-points is due to the following remarks. Simplex sigma-points correspond to the minimum number of particles – namely $N_p = N_r + 1$ – to define a stencil of dimension N_r . Therefore, when the covariance operator P of reduced rank is decomposed with simplex sigma-points, we are certain that after any non-linear transform φ , the resulting covariance operator P^φ computed from the φ -propagated sigma-points is at most of rank N_r and therefore can still be decomposed with a reduced operator of size N_r and corresponding projection operators. This is not the case anymore for generalized sigma-points since the resulting space generated by the propagated sigma-points is in general of dimension $N_p - 1 > N_r$. In this case a supplementary singular value decomposition where we keep only the biggest N_r eigenvalues of the propagated covariance operator must be performed to project the propagated covariance operator on the space of operator of rank N_r in the Frobenius norm sense.

Consequently, the resulting estimator for simplex sigma-points is very natural as exposed in [23] (we denote by $\mathbf{e} = (e_i)_i$ are unitary simplex sigma points)

1. Initialization:

$$\begin{cases} \hat{\mathbf{y}}_n^- &= \mathbf{y}_\diamond \\ \mathbf{L}_0 &= \mathbf{\Pi} \sqrt{U_\diamond^{-1}} \\ U_0 &= \mathbf{1} \end{cases}$$

2. Sampling

$$\begin{cases} \Gamma_n &= \sqrt{U_n^{-1}} \\ \hat{\mathbf{y}}_{n,i}^- &= \hat{\mathbf{y}}_n^- + \mathbf{L}_n e_i \end{cases}$$

3. Correction:

$$\begin{cases} \hat{z}_{n,i}^- &= C_n(\hat{y}_{n,i}^-) \\ \Upsilon_n &= \hat{z}_n^- \mathbf{d}_\alpha \mathbf{e}^\top \\ U_n &= \mathbb{1} + \Upsilon_n^\top \mathbf{R}_n \Upsilon_n \\ G_n &= L_n U_n \Upsilon_n^\top \mathbf{R}_n \\ \hat{y}_n^+ &= \hat{y}_n^- + G_n(z_n - \mathbb{E}_\alpha(\hat{z}_n^-)) \\ P_n^+ &= L_n^\top U_n^{-1} L_n \end{cases}$$

4. Re-Sampling

$$\begin{cases} \Gamma_n &= \sqrt{U_n^{-1}} \\ \hat{y}_{n,i}^+ &= \hat{y}_n^+ + L_n \Gamma_n e_i \end{cases}$$

5. Prediction:

$$\begin{cases} \hat{y}_{n+1,i}^- &= A_{n+1|n}(y_{n,i}^+) \\ \hat{y}_{n+1}^- &= \mathbb{E}_\alpha(\hat{y}_{n+1}^-) \\ L_{n+1} &= \hat{y}_{n+1}^- \mathbf{d}_\alpha \mathbf{e}^\top \\ P_{n+1}^- &= L_{n+1}^\top L_{n+1} \end{cases}$$

The most general form with the additional SVD can be found in [22], generalizing a first presentation in [23].

We point out that the reduced-order filter called the Singular Evolutive Interpolated Kalman Filter (SEIK) that has been proposed in the seminal works [Pham et al., 1998b, Pham, 2001]³ can be reinterpreted as a ROUKF. Indeed, our contribution proves that SEIK is a special form of ROUKF with a particular choice – potentially suboptimal – of simplex sigma-points and corresponding weights. From this fundamental remark, we deduce the generalized version in [22] and introduce some principle of analysis at the discrete-time level but also at the continuous-time level. In fact, we prove in [22] that the algorithms (2.21) and (2.22) are exactly equivalent when considering linear operators as it was the case for UKF and EKF. This is summarized by the Diagram 2.2 similar to the Diagram 2.1 in Section 2.2.3.

As a conclusion, our unified theory allows to understand that, in practice, the ROUKF is a very interesting alternative to ROEKF as it is (1) tangent free, (2) has the same stabilization property for linearized errors and (3) is heuristically robust to large non-linearities. This last property is particularly true with enough sampling points, and the SVD projection.

2.3.2 Luenberger observers formulations – The wave equation case

In the previous section, we have seen the so-called optimal estimators in the sense that they are linked to a variational criterion. Then, we have seen that this can imply an asymptotic property for the observer, namely that

$$\hat{y}(t) \xrightarrow[t \rightarrow \infty]{} y(t)$$

³The SEEK mentioned in the ROEKF section was also formulated by D.T. Pham

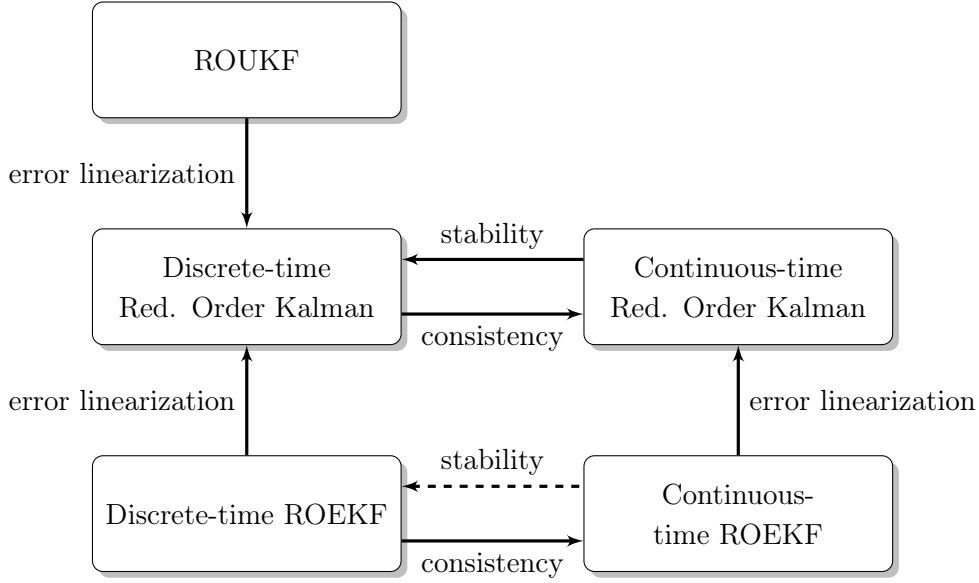


Figure 2.2: Relations between reduced order filtering procedures

at least when no noise and modelling errors are present. This asymptotic property is a fundamental objective for an observer, meaning that the homogenous dynamics of the observer is stable. Then, this must be completed by some robustness results concerning the impact of the modeling errors and measurement noises. This robustness is typically provided in optimal filtering by the underlying variational criterion. One critical aspect of optimal filtering is the curse of dimensionality for practical numerical implementations. This has led us to define reduced-order optimal filters where the controlled space is of reduced dimension (potentially finite). This requires that the uncontrolled space be stable by itself, otherwise no robustness with respect to noise and errors could be obtained. This reduced-order approach was presented for dissipative systems where the uncontrolled space is made of highly damped substates. However, this is not appropriate for conservative systems such as wave-like equations (wave, elasticity, beams) or even general hyperbolic problems. In this case, the need of whole state-space stability is incompatible with the dimensionality limitation imposed by optimal filtering. Therefore, we need to base our observer design on alternative approaches where we keep the asymptotic properties and relax the need for a variational criterion. In other words, we thus seek a filter G such that the observer

$$\dot{\hat{y}} = A\hat{y} + \beta + G(z - C\hat{y})$$

tends to the target trajectory \tilde{y} as time increases. This implies to devise G for linear systems so that the error $\tilde{y} = \tilde{y} - \hat{y}$

$$\dot{\tilde{y}} = (A - GC)\tilde{y} + \text{errors}$$

is stable to 0 when no errors are present and robust to these errors. Requiring only this stability property for designing G is typically what has driven [Luenberger, 1964, Luenberger, 1971] in his observer design strategy. Hence, we use the denomination *Luenberger observers* for characterizing this approach.

With the objective of our cardiac mechanics applications, the wave equation reveals to be a fundamental case for observer design and analysis. Hence, it has been for us a subject of intensive

research with many different papers [10, 11, 17, 24, 25]. In fact on the wave equation, we have been contributing to all of the 5 problems mentioned in Section 1.4). In [10, 25] we formulate an original observer for wave equations using field measurements (Problem 1). In [10, 24] we prove the exponential convergence of some observers (Problem 2). In [25], we propose a strategy to also estimate some parameters for wave-like equations (Problem 3). In [11, 17] we proceed to the numerical analysis of the observers (Problem 4). Note finally that the original observer formulated in [25] for wave-like equations has been applied to a complex mechanical problem in cardiac modeling with real data in our work [8] (Problem 5).

REMARK 2.3.4 (VARIATIONAL APPROACHES)

The optimal filtering strategy is cursed for wave equations but a direct minimization of the variational criteria can be performed. In [Cîndea and Munch, 2015] their solution of the extremal problem by duality allows to define an estimator of the wave equation with adequate discretization.

2.3.2.1 Observer formulation

We consider a bounded domain Ω of \mathbb{R}^n with a regular boundary $\partial\Omega$. Given a known source term $f \in L^1(\mathbb{R}^+, L^2(\Omega))$ with \dot{f} – namely, the time derivative of f – also in $L^1(\mathbb{R}^+, L^2(\Omega))$, we consider the general wave equation

$$\begin{cases} \ddot{u}|_{\zeta_u, \zeta_v}(\underline{x}, t) - \Delta u|_{\zeta_u, \zeta_v}(\underline{x}, t) = f(\underline{x}, t), & (\underline{x}, t) \in \Omega \times (0, \infty) \\ u|_{\zeta_u, \zeta_v}(\underline{x}, t) = 0, & (\underline{x}, t) \in \partial\Omega \times (0, \infty) \\ u|_{\zeta_u, \zeta_v}(\underline{x}, 0) = u_0(\underline{x}) + \zeta_u(\underline{x}), & x \in \Omega \\ \dot{u}|_{\zeta_u, \zeta_v}(\underline{x}, 0) = v_0(\underline{x}) + \zeta_v(\underline{x}), & x \in \Omega \end{cases} \quad (2.23)$$

with uncertainties ζ_u, ζ_v on the initial condition.

To define a first order state form of (2.23) we introduce $y_\zeta(t) = \begin{pmatrix} u(t) \\ v(t) \end{pmatrix}$ (with $\zeta = \begin{pmatrix} \zeta_u \\ \zeta_v \end{pmatrix}$) such that

$$\begin{cases} \dot{y}|_\zeta(t) = Ay|_\zeta(t) + \beta(t), & t > 0 \\ y|_\zeta(0) = y_\diamond + \zeta, \end{cases} \quad (2.24)$$

where $y_0 = \begin{pmatrix} u_0 \\ v_0 \end{pmatrix}$ and $A : \mathcal{D}(A) \rightarrow \mathcal{Y}$ with

$$\mathcal{D}(A) = \mathcal{D}(-\Delta) \times \mathcal{D}(-\Delta^{\frac{1}{2}}), \quad \mathcal{Y} = \mathcal{D}(-\Delta^{\frac{1}{2}}) \times \mathcal{H}, \quad A = \begin{pmatrix} 0 & I \\ \Delta & 0 \end{pmatrix}, \quad \beta = \begin{pmatrix} 0 \\ f \end{pmatrix},$$

for $\mathcal{H} = L^2(\Omega)$ here. Note that with the boundary conditions considered in (2.23) we have $\mathcal{D}(-\Delta^{\frac{1}{2}}) = H_0^1(\Omega)$ and $\mathcal{D}(-\Delta) = H^2(\Omega) \cap H_0^1(\Omega)$. The operator A generates a group and for all $y_0 \in \mathcal{Y}$ then $(u, \dot{u}) \in C((0, T); \mathcal{Y})$ for any $T > 0$, see e.g. [Pazy, 1983].

This model is entirely defined by its initial condition and in particular the trajectory of interest $\{\tilde{y}(t), t > 0\}$ is defined by an unknown $\check{\zeta} = (\check{\zeta}_u, \check{\zeta}_v)$. However, some measurements associated with the trajectory \tilde{y} are available. For instance, we consider that we know the target solution at every time t in $\Omega_{\text{obs}} \subset \Omega$, an open and non-empty subset of Ω . These measurements can be produced from a target trajectory with the use of the following observation operator

$$\forall t \geq 0, \quad \left| \begin{array}{l} L^2(\Omega) \rightarrow L^2(\Omega_{\text{obs}}) \\ v(\cdot, t) \mapsto z(t) = \check{v}(\cdot, t)|_{\Omega_{\text{obs}}} \end{array} \right. \quad (2.25)$$

or more interestingly

$$\forall t \geq 0, \quad \left\{ \begin{array}{l} H_0^1(\Omega) \rightarrow H^1(\Omega_{\text{obs}}) \\ u(\cdot, t) \mapsto z(t) = \tilde{u}(\cdot, t)|_{\Omega_{\text{obs}}} \end{array} \right.$$

We point out that due to measurement noise the second case can not be derived in any case from the first one by a simple time-derivation. Moreover, we expect a higher space regularity in the second case.

In each case, introducing the observation space $\mathcal{Z} = L^2(\Omega_{\text{obs}})$ or $\mathcal{Z} = H^1(\Omega_{\text{obs}})$, we can define an observation operator $C \in \mathcal{L}(\mathcal{Y}, \mathcal{Z})$ by

$$C = \begin{pmatrix} 0 & \mathfrak{h}C \end{pmatrix}, \text{ or } C = \begin{pmatrix} \mathfrak{h}C & 0 \end{pmatrix}, \quad (2.26)$$

respectively, with $\mathfrak{h}C$ the restriction operator on Ω_{obs} . We aim to define an observer of the form

$$\left\{ \begin{array}{l} \dot{\hat{y}}(t) = A\hat{y}(t) + \beta + G(z(t) - C\hat{y}(t)), \quad t > 0 \\ \hat{y}(0) = y_\diamond \end{array} \right.$$

with G a gain operator to be defined in $\mathcal{L}(\mathcal{Z}, \mathcal{Y})$ in our case. Hence, the dynamics followed by the error $\tilde{y} = \check{y} - \hat{y}$ reads

$$\left\{ \begin{array}{l} \dot{\tilde{y}} = (A - GC)\tilde{y}(t), \quad t > 0 \\ \tilde{y}(0) = \check{\zeta} \end{array} \right.$$

and then G should stabilize \tilde{y} to 0.

Considering time-derivative measurements associated with (2.25), a convenient, and still efficient, choice is to choose $G = \gamma \begin{pmatrix} 0 \\ \mathbb{1}_{\Omega_{\text{obs}}} \end{pmatrix}$ for any $\gamma > 0$. The corresponding observer is built from a *Direct Velocity Feedback (DVF)* giving

$$\left\{ \begin{array}{ll} \ddot{\hat{u}}(x, t) - \Delta \hat{u}(x, t) = f + \gamma \mathbb{1}_{\Omega_{\text{obs}}}(x)(z(x, t) - \dot{\hat{u}}|_{\Omega_{\text{obs}}}(x, t)), & (x, t) \in \Omega \times (0, \infty) \\ \hat{u}(x, t) = 0, & (x, t) \in \partial\Omega \times (0, \infty) \\ \hat{u}(x, 0) = u_\diamond(x), \quad \dot{\hat{u}}(x, 0) = v_\diamond(x), & x \in \Omega \end{array} \right.$$

and the error follows

$$\left\{ \begin{array}{ll} \ddot{\tilde{u}}(x, t) - \Delta \tilde{u}(x, t) + \gamma \mathbb{1}_{\Omega_{\text{obs}}}(x)\dot{\tilde{u}}(x, t) = 0, & (x, t) \in \Omega \times (0, \infty) \\ \tilde{u}(x, t) = 0, & (x, t) \in \partial\Omega \times (0, \infty) \\ \tilde{u}(x, 0) = \tilde{u}_0(x), \quad \dot{\tilde{u}}(x, 0) = \tilde{v}_0(x), & x \in \Omega \end{array} \right. \quad (2.27)$$

a system whose stability properties have been intensively studied in different communities [Lions, 1968, Tucsnak and Weiss, 2009, Preumont, 2002, Zuazua, 2005].

When the measurements are directly the wave field, we propose in [10, 25] an observer that does not necessitate a time-differentiation of the measurement, hence avoids amplifying measurements errors. In return, we will see that the strategy necessitates some measurements spatial regularity. To formulate the observer, we introduce $\text{Ext}_{\Omega_{\text{obs}}}$ a harmonic lifting operator

$$\text{Ext}_{\Omega_{\text{obs}}} : \left\{ \begin{array}{l} H^1(\Omega_{\text{obs}}) \rightarrow H_0^1(\Omega) \\ \phi \mapsto \psi \text{ s.t. } : \left\{ \begin{array}{ll} \Delta\psi = 0, & \text{in } \Omega \setminus \Omega_{\text{obs}} \\ \psi = 0, & \text{on } \partial\Omega \\ \psi = \phi, & \text{in } \overline{\Omega_{\text{obs}}} \end{array} \right. \end{array} \right. \quad (2.28)$$

We easily verify that $\text{Ext}_{\Omega_{\text{obs}}}$ is bounded from $H^1(\Omega_{\text{obs}})$ to $H_0^1(\Omega)$ using the trace and lifting properties to write

$$\|\text{Ext}_{\Omega_{\text{obs}}}(\phi)\|_{H_0^1(\Omega)}^2 \leq \|\nabla\phi\|_{L^2(\Omega_{\text{obs}})}^2 + c_1\|\phi\|_{H^{1/2}(\partial\Omega_{\text{obs}})}^2 \leq c_2\|\phi\|_{H^1(\Omega_{\text{obs}})}^2.$$

As a candidate observer, we propose to choose $G = \gamma \begin{pmatrix} \text{Ext}_{\Omega_{\text{obs}}} \\ 0 \end{pmatrix}$ which gives the following first-order system with $\gamma > 0$.

$$\begin{cases} \dot{\hat{u}}(x, t) = \hat{v}(x, t) + \gamma \text{Ext}_{\Omega_{\text{obs}}}(z(t) - \hat{u}|_{\Omega_{\text{obs}}}(x, t)), & (x, t) \in \Omega \times (0, \infty) \\ \dot{\hat{v}}(x, t) - \Delta\hat{u}(x, t) = f, & (x, t) \in \Omega \times (0, \infty) \\ \hat{u}(x, t) = 0, & (x, t) \in \partial\Omega \times (0, \infty) \\ \hat{u}(x, 0) = u_\diamond(x), \quad \hat{v}(x, 0) = v_\diamond(x), & x \in \Omega \end{cases}$$

This observer is original in the control theory community since the feedback correction is applied on the primary equation linking originally the time-derivative of the field to its velocity. This observer was first formulated in [25] in a general wave-like context after a Galerkin spatial discretization. The feedback was named ‘‘Schur Displacement Feedback’’ (SDF). The strong formulation was then introduced in [10]. Note that in essence the filter proposed by [Li and Xu, 2011] for the beam equation is close to our formulation, in particular our beam formulation of the SDF [11]. Ultimately we derive the error dynamics with

$$\begin{cases} \dot{\tilde{u}}(x, t) = \tilde{v}(x, t) - \gamma \text{Ext}_{\Omega_{\text{obs}}}(\tilde{u}|_{\Omega_{\text{obs}}}(x, t)), & (x, t) \in \Omega \times (0, \infty) \\ \dot{\tilde{v}}(x, t) - \Delta\tilde{u}(x, t) = 0, & (x, t) \in \Omega \times (0, \infty) \\ \tilde{u}(x, t) = 0, & (x, t) \in \partial\Omega \times (0, \infty) \\ \tilde{u}(x, 0) = \zeta_u(x), \quad \tilde{v}(x, 0) = \zeta_v(x), & x \in \Omega \end{cases}$$

These observer extend to boundary measurements on Γ_{obs} where we originally have Neumann boundary conditions. For the DVF, the resulting observer is also well known with a generalized Robin boundary condition on Γ_{obs} of the form

$$\frac{\partial u}{\partial n} = -\gamma v, \quad \text{on } \Gamma_{\text{obs}}$$

However, the analysis of this observer is known to be quite intricate since the observation operator is not bounded anymore, hence we must prove that the observation operator is admissible. In our case of direct field measurement, the resulting observer is directly compatible with boundary measurement by considering this time the extension (2.28) from the boundary. Moreover, we point out that the observation operator remains bounded in this case.

2.3.2.2 Observer Analysis

The question is now to analyze the convergence of the resulting observer. For the DVF, the error system (2.27) has been extensively studied. A first remark is that the error system is dissipative since the system energy

$$\mathcal{E}(y, t) = \frac{1}{2} \left(\int_{\Omega} |\nabla u|^2 \, d\Omega + \int_{\Omega} |v|^2 \, d\Omega \right),$$

decreases for the error with

$$\frac{d}{dt} \mathcal{E}(\tilde{y}, t) = -\gamma \int_{\Omega_{\text{obs}}} |\tilde{v}|^2 \, d\Omega = -\gamma \|\tilde{v}\|_{L^2(\Omega_{\text{obs}})}^2. \quad (2.29)$$

This can be considered as the minimal requirement for the observer. In essence it also means that there is no side effect in using the observer instead of the initial system to model and simulate the target trajectory. This point of view has been mathematically translated into the observer objective definition of [Krener and Duarte, 1996].

To obtain a stronger property of convergence for the observer, the objective is now to prove that the dissipation in (2.27) which appears only on a small subdomain is sufficient to stabilize the solution on the whole domain. In this respect and taking the example of the well studied DVF error system we enumerate the various available strategies. First we need to distinguish two types of stability: the exponential stability and a weaker stability where the rate is not exponential.

Proving the asymptotic stability without any convergence rate can be done with a very nice combination of spectral analysis of the uncontrolled model operator A and unique continuation principles “à la Holmgren” [Tataru, 1995]. We refer to the monograph [Burq and Gérard, 2002] where this widespread idea has been consolidated under the name of “weak stability”.

THEOREM 2.3.3 (ASYMPTOTIC STABILITY THEOREM [BURQ AND GÉRARD, 2002])
Considering an error system for wave equations of the form

$$\begin{cases} \dot{\tilde{y}} = (A - \gamma C^* C)\tilde{y}(t), & t > 0 \\ \tilde{y}(0) = \check{\zeta} \end{cases}$$

Any solution verifies

$$\lim_{t \rightarrow +\infty} \mathcal{E}(\tilde{y}, t) = 0$$

if one of the following equivalent condition is satisfied:

1. for all initial condition $\check{\zeta} = \tilde{\phi}$ with $\tilde{\phi}$ an eigenvector of $A - C^*C$, $\lim_{t \rightarrow +\infty} \mathcal{E}(\tilde{y}_{|\tilde{\phi}}, t) = 0$;
2. for all eigenvectors $\tilde{\phi}$ of $A - C^*C$ we have $C\tilde{\phi} = 0 \Rightarrow \tilde{\phi} = 0$;
3. for all eigenvectors ϕ of A we have $C\phi = 0 \Rightarrow \phi = 0$;
4. for all eigenvectors φ of $-\Delta$, we have ${}^{\natural}C\varphi = 0 \Rightarrow \varphi = 0$.

Theorem 2.3.3 is fundamental to understand the minimum requirement for observer convergence. Moreover, unique continuation results are compatible with potential time and space-varying coefficients in the equations [Tataru, 1995].

The exponential stability corresponds to an exponential decay of the error energy. Remember that we prove an exponential stability with optimal filter approaches in Theorem 2.3.1. For any skew-adjoint model operator as in the wave equation case, it is directly related to the observability condition⁴ [Haraux, 1989, Ramdani et al., 2005] satisfied by system (2.24)

$$\exists(c_0, T_0) \text{ s.t } \forall T > T_0, \quad \int_0^T \|Cy_{|\zeta}\|_Z dt \geq c_0 \|y_{|\zeta}(0)\|_Y. \quad (2.30)$$

Note that proving the exponential stability is not obvious when comparing (2.30) and (2.29). Indeed in (2.30), the conditions involves the initial system that is conservative. However in

⁴the conservative property of the operator implies that there is no need of a controllability results to excite the system as in 2.3.1

(2.29), we need a controllability condition on the error system, a system which is exponentially decreasing, hence a more difficult condition – but still true – to prove. Let us now give various methods developed in the literature to prove this identifiability condition:

- **Spectral methods** – Numerous works are based on spectral analysis of the couple (A, C) to obtain the exponential stability of the error system, hence for us the convergence of the observer. Here we see two classes of results: (1) abstract spectral results analyzing the impact of the observation operator on the A spectral elements and (2) computing and analyzing the spectral elements of the closed loop operator $A - GC$ operators. For the first case, the idea is to extend the weak stability property from a spectral analysis of A . When A is skew-adjoint as it is the case for wave-like equations, the question is more intricate. A well developed answer is based on a resolvent condition [Burq and Zworski, 2004, Miller, 2005, Ramdani et al., 2005] which consists in proving that there exist two positive constants m_1 and m_2 such that

$$\forall \varphi, \quad \|\mathfrak{h}A^{\frac{1}{2}}\varphi\| \leq m_2 \|(\mathfrak{h}A - \lambda I)\varphi\|^2 + m_1 \|\mathfrak{h}C\varphi\|$$

with here $\mathfrak{h}A = -\Delta$. Concerning (2), the objective is to directly perform a spectral analysis of the closed loop system and prove that the resulting operator is spectral in the sense of [Curtain and Zwart, 1995], namely that it can be decomposed over its spectral elements. The main difficulty is here to prove that the spectral elements of $A - GC$ which are different from A form a complete basis. This has only been done in specific 1D or 2D cases in [Cox and Zuazua, 1994, Shubov, 1997]. Note that in [24], we have given an interesting numerical criterion to understand the distance between the subspace of generated by the spectral elements of A – where the complete basis property is easily obtained – with the subspace generated by the spectral elements of $A - GC$. When the operator is spectral, its analysis is considerably simplified since the growth abscissa

$$\mu_0(A) = \inf_{t>0} \ln \frac{\mathbb{T}_t}{t},$$

and the spectral abscissa of the system

$$\sigma(A) = \sup\{\Re(\lambda) \mid \lambda \in \mathfrak{G}(A)\}.$$

coincide as it is the case for operators with compact resolvent, see Remark 2.3.5.

- **Multiplier method** – The principle of the multiplier method takes was given in [Lions, 1968] to demonstrate controllability results. The principle is to use specific test functions of the form $q\nabla w$ in the weak form of the dynamics in order to prove and observability condition. The resulting observability condition is typically obtained for boundary observation [Komornik, 1994] through the condition that there exists a point \underline{x}_0 such that the domain of observation is seen from this point. Concerning the interior observation problem, the multiplier techniques can easily be Extended when the subdomain Ω_{obs} is a neighborhood of $\Gamma(\underline{x}_0)$ [Zuazua, 2005].
- **Carleman estimates** – More complete and general inequalities can be obtained through Carleman estimates strategies – see for instance [Lasiecka et al., 1999, Baudouin et al., 2013] and the references therein. Here again the boundary observations are more classically

considered but not necessarily. Moreover, it can produce results with Neumann boundary conditions. We also point out that one important application of Carleman estimates is to prove some uniqueness continuation results – see for instance [Tataru, 1996] – hence allowing to obtain some weak stability results when the exponential stability is not valid [Lebeau, 1996].

- **Microlocal analysis** – Finally the last approach and certainly the most precise is given by microlocal analysis which aims at studying the high frequency behavior of wave-like equations in order to understand the propagation of singularities in the domain. The idea is to show that the information is supported by optic geometric rays. Hence, in [Bardos et al., 1988, Lebeau et al., 1992] the Geometric Control Condition (GCC) is introduced – also valid for Neumann boundary conditions as shown in [Bardos et al., 1988] – testing if there exists a time T_0 such that every optical ray encounters the observation domain under which the observability condition is fulfilled with $T > T_0$. Recently, the original microlocal approach of [Lebeau et al., 1992] has been greatly simplified [Burq and Gérard, 1997] by using the microlocal defect measures introduced by [Gérard, 1991]. This allows to prove very elegantly the geometric control condition sufficient for exact controllability for domains of class C^3 and equations with C^2 coefficients.

REMARK 2.3.5 (COMPARISON WITH DISSIPATIVE SYSTEMS)

We point out that for an operator A with compact resolvent, the exponential stability can directly be obtained from spectral analysis with the Holmgren continuation principle. Indeed, there exists in this case a generalization – see [Ramdani et al., 2015] – of the famous Hautus test for finite dimension systems [Hautus, 1970] saying that if

$$(\phi \in \mathcal{D}(A) \cup \mathcal{Y} \mid A\phi = \lambda\phi \text{ and } C\phi = 0) \Rightarrow \phi = 0$$

is satisfied then A, C is detectable, namely there exists G such that $A - GC$ generates an exponential semi-group. For conservative systems, we have just seen that the link with a spectral analysis inspired from finite dimensional analysis is much more intricate as the Hautus test in Theorem (2.3.3) gives only an asymptotic stability but not necessarily exponential. We understand anyway why the spectral properties of A is so crucial to deduce the stability of the error system.

Concerning our original observer formulation using field measurements, we prove in [10] the exponential stability when the GCC is satisfied. Our proof starts from the classical results obtained for the DVF and that we convert for the SDF. The next proposition considers without loss of generality that $y_\diamond = 0$.

PROPOSITION 2.3.4 (CHAPELLE-DE BUHAN-CÎNDEA-MOIREAU)

Assume that the geometric control condition of Bardos, Lebeau and Rauch [Bardos et al., 1988] is satisfied for some Ω_{obs}^b strict subset of Ω_{obs} such that $\text{dist}(\Omega \setminus \Omega_{obs}, \Omega_{obs}^b) > 0$, in the time interval $]0, T_0[$ for $T_0 > 0$. Then the observability condition

$$\int_0^{T_0} \|u|_{\zeta_u, \zeta_v}(\cdot, t)\|_{H^1(\Omega_{obs})}^2 dt \geq C \left(\|\zeta_u\|_{H^1(\Omega)}^2 + \|\zeta_v\|_{L^2(\Omega)}^2 \right), \quad \forall (u_0, v_0) \in H_0^1(\Omega) \times L^2(\Omega), \quad (2.31)$$

holds for the same time T_0 . As a consequence, there exist strictly positive constants c and μ such that the energy $\tilde{\mathcal{E}}$ of the error system decreases with

$$\tilde{\mathcal{E}}(t) \leq ce^{-\mu t} \tilde{\mathcal{E}}(0), \quad \forall t > 0.$$

To prove (2.31), we demonstrate an interesting equirepartition over time of the local energy localized within the subdomain Ω_{obs} between the kinetic and potential contributions. This type of equirepartition properties typically appears in [Zhang, 2000] and in Carleman estimates – with additional weighting and more complex functions. Note that we believe that a direct proof with micro-local analysis with H^1 -defect measures could also be conducted. We underline the fact that (2.31) is not valid with $\|u|_{\zeta_u, \zeta_v}(\cdot, t)\|_{L_2(\Omega_{\text{obs}})}$ without relaxing the norms on the right hand side. Hence, **this means that for the wave equation in its natural spaces, we must have some spatial regularity in the data if we do not want to rely on time-derivative of measurements.**

2.3.2.3 Observer discretization and numerical analysis

The first difficulty is to propose a discretization that preserves the dissipative property for the estimation error, hence ensuring there is eventually no arm in using the observer. In this respect, standard discretization principles allow to propose adequate discretizations as soon as the feedback is based on the “physical” properties of the underlying system, as opposed to the genericness offered by Kalman-based approaches. For instance, let us consider the discretization of the wave equation (2.23) where we decide to rely on a standard finite element space discretization and a Newmark time-scheme for the time discretization.

We consider for instance a Lagrange discretization and denote by \mathbf{u} the vector of degrees of freedom associated with u_h the finite element approximation of the field u . We introduce the mass and stiffness matrix operators associated with the finite element discretization

$$\mathbf{u}^\top \mathbf{M} \mathbf{w} = \int_{\Omega} u_h w_h \, d\Omega, \quad \mathbf{u}^\top \mathbf{K} \mathbf{w} = \int_{\Omega} \nabla u_h \cdot \nabla w_h \, d\Omega$$

and the Newmark scheme reads as a mid-point rule on both the field and its time-derivative

$$\begin{cases} \frac{\mathbf{u}_{n+1} - \mathbf{u}_n}{\delta t} = \frac{\mathbf{v}_{n+1} + \mathbf{v}_n}{2} \\ \mathbf{M} \frac{\mathbf{v}_{n+1} - \mathbf{v}_n}{\delta t} + \mathbf{K} \frac{\mathbf{u}_{n+1} + \mathbf{u}_n}{2} = \mathbf{f} \end{cases} \quad (2.32)$$

In the rest of the document we will use the mid-point notation $*_{n+\frac{1}{2}} = \frac{*_{n+1} + *_{n}}{2}$.

We recall that the Newmark time-scheme is more common for the elastodynamics problem discretization and furnishes a direct first-order system discretization. In practice however, it is solved by

$$\left(\frac{\mathbf{M}}{\delta t} + \frac{\mathbf{K}}{2}\right) \mathbf{u}_{n+1} = \left(\frac{\mathbf{M}}{\delta t} - \frac{\mathbf{K}}{2}\right) \mathbf{u}_n + \frac{\mathbf{M}}{\delta t} \mathbf{v}_n + \mathbf{f} \quad (2.33)$$

followed by

$$\mathbf{v}_{n+1} = \frac{2}{\delta t} (\mathbf{u}_{n+1} - \mathbf{u}_n) - \mathbf{v}_n, \quad (2.34)$$

and we will see the importance of these aspects when examining the performances and complexity of our observer implementation. We also recall that the Newmark scheme can be rewritten as a – maybe more classical – θ -scheme with $\theta = \frac{1}{4}$

$$\mathbf{M} \frac{\mathbf{u}_{n+1} - 2\mathbf{u}_n + \mathbf{u}_{n-1}}{2\delta t^2} + \mathbf{K} \frac{\mathbf{v}_{n+1} + 2\mathbf{v}_n + \mathbf{v}_{n-1}}{4} = \mathbf{f}.$$

This scheme is conservative. Indeed, by computing the energy

$$\mathcal{E}(y) = v^\top Mv + u^\top Ku = \|u_h\|_{L^2(\Omega)} + \|\nabla u_h\|_{L^2(\Omega)},$$

we directly infer $\mathcal{E}_{n+1} = \mathcal{E}_n$ for the homogenous system.

Considering the DVF case, a natural observer discretization is based on a mid-point discretization of the feedback so that

$$\begin{cases} \frac{\hat{u}_{n+1} - \hat{u}_n}{\delta t} = \hat{v}_{n+\frac{1}{2}} \\ M \frac{\hat{v}_{n+1} - \hat{v}_n}{\delta t} + K \hat{u}_{n+\frac{1}{2}} = f + \gamma \mathring{C}^\top M_{\Omega_{\text{obs}}} \left(z_{n+\frac{1}{2}} - \mathring{C} \hat{v}_{n+\frac{1}{2}} \right) \end{cases}$$

where \mathring{C} is the interpolation operator from the discretized space of the velocity field to the discretized space of observation. Moreover $M_{\Omega_{\text{obs}}}$ is the L^2 mass operator associated with the Ω_{obs} subdomain. To evaluate the relevance of this discretization, let us consider for now that z_n is in fact a velocity field associated with the discretized wave equation (2.32). In other words, let us assume – which is only exact up to discretization errors added to measurement errors – that

$$z_{n+\frac{1}{2}} = \mathring{C} \check{v}_{n+\frac{1}{2}}.$$

Then, by considering the error $y_n = \check{y}_n - \hat{y}_n$, we easily verify that

$$\frac{\tilde{\mathcal{E}}_{n+1} - \tilde{\mathcal{E}}_n}{\delta t} = -\gamma \check{v}_{n+\frac{1}{2}} \mathring{C}^\top M_{\Omega_{\text{obs}}} \mathring{C} \check{v}_{n+\frac{1}{2}},$$

which proves the dissipative property at the discretized level.

Considering now the SDF case, we introduced in [25] a comparable discretization as for the DVF. We introduce the discrete operator $K_{\Omega_{\text{obs}}}$ associated with the extension problem. We consider for all $\phi \in \text{Im} \mathring{C}$, the extension ψ solution of the mixed problem associated with

$$\begin{pmatrix} K & \mathring{C}^\top \\ \mathring{C} & 0 \end{pmatrix} \begin{pmatrix} \psi \\ \lambda \end{pmatrix} = \begin{pmatrix} 0 \\ \phi \end{pmatrix} \quad (2.35)$$

Provided this system is solvable in λ , we define $K_{\Omega_{\text{obs}}}$ such that $\lambda = -K_{\Omega_{\text{obs}}} \phi$, hence

$$K\psi = \mathring{C}^\top K_{\Omega_{\text{obs}}} \phi.$$

Therefore, after spatial discretization, we have

$$\begin{cases} K \dot{\hat{u}} = K \hat{v} + \gamma \mathring{C}^\top K_{\Omega_{\text{obs}}} (z - \mathring{C} \hat{u}) \\ K \dot{\hat{v}} + K \hat{u} = f \end{cases}$$

giving that the energy error decays as

$$\frac{d\tilde{\mathcal{E}}}{dt} = -\gamma \tilde{u} \mathring{C}^\top K_{\Omega_{\text{obs}}} \mathring{C} \tilde{u}.$$

Then after time discretization,

$$\begin{cases} K \frac{\hat{u}_{n+1} - \hat{u}_n}{\delta t} = K \hat{v}_{n+\frac{1}{2}} + \gamma \mathring{C}^\top K_{\Omega_{\text{obs}}} \left(z_{n+\frac{1}{2}} - \mathring{C} \hat{u}_{n+\frac{1}{2}} \right) \\ M \frac{\hat{v}_{n+1} - \hat{v}_n}{\delta t} + K \hat{u}_{n+\frac{1}{2}} = f \end{cases}$$

leading to a similar decay as for the DVF

$$\frac{\tilde{\mathcal{E}}_{n+1} - \tilde{\mathcal{E}}_n}{\delta t} = -\gamma \tilde{\mathbf{u}}_{n+\frac{1}{2}} \mathfrak{h} \mathbf{C}^\top \mathbf{K}_{\Omega_{\text{obs}}} \mathfrak{h} \mathbf{C} \tilde{\mathbf{u}}_{n+\frac{1}{2}}.$$

We now understand that the DVF and SDF formulations are meant to be very similar both at the continuous and discrete level. Typically, we consider the discrete state $\mathbf{y} = \begin{pmatrix} \mathbf{u} \\ \mathbf{v} \end{pmatrix} \in \mathcal{Y}_h$ equipped with the norm of \mathcal{Y} represented by the operator

$$\mathbf{N} = \begin{pmatrix} \mathbf{K} & \mathbf{0} \\ \mathbf{0} & \mathbf{M} \end{pmatrix} = \mathbf{P}_0^{-1}$$

Then the observation operators acting on the state are given by

$$\mathbf{C}_{\text{DVF}} = \begin{pmatrix} \mathbf{0} & \mathfrak{h} \mathbf{C} \end{pmatrix} \quad \text{or} \quad \mathbf{C}_{\text{SDF}} = \begin{pmatrix} \mathfrak{h} \mathbf{C} & \mathbf{0} \end{pmatrix}$$

with the associated observation norms $\mathbf{R}_{\text{DVF}} = \gamma \mathbf{M}_{\Omega_{\text{obs}}}$ and $\mathbf{R}_{\text{SDF}} = \gamma \mathbf{K}_{\Omega_{\text{obs}}}$. We have in both cases a time scheme of the form

$$\frac{\hat{\mathbf{y}}_{n+1} - \hat{\mathbf{y}}_n}{\delta t} = \mathbf{A} \hat{\mathbf{y}}_{n+\frac{1}{2}} + \mathbf{P}_0 \mathbf{C}^\top \mathbf{R} \left(z_{n+\frac{1}{2}} - \mathbf{C} \hat{\mathbf{y}}_{n+\frac{1}{2}} \right), \quad (2.36)$$

with the energy balance

$$\frac{\tilde{\mathcal{E}}_{n+1} - \tilde{\mathcal{E}}_n}{\delta t} = -\tilde{\mathbf{y}}_{n+\frac{1}{2}}^\top \mathbf{C}^\top \mathbf{R} \mathbf{C} \tilde{\mathbf{y}}_{n+\frac{1}{2}}.$$

The discretizations are compatible with energy balances. Hence, we could expect to have the observer convergence property transposed to the discrete level.

To finalize a full convergence analysis we need to convert the dissipative properties at the discrete level into an exponential stabilization of the system. In this respect, we therefore seek an observability condition at the discrete level of the form

$$\sum_{k=1}^n \tilde{\mathbf{y}}_{n+\frac{1}{2}}^\top \mathbf{C}^\top \mathbf{R} \mathbf{C} \tilde{\mathbf{y}}_{n+\frac{1}{2}} \quad \text{vs} \quad \tilde{\mathbf{y}}_0^\top \mathbf{N} \tilde{\mathbf{y}}_0.$$

Exponential stability at the discrete level – However, the discretization difficulties do not end here, since even for natural discretizations it is now well known that the observability condition is not verified at the discrete level [Zuazua, 2005]– namely, the operator $\mathbb{T}_{n+\frac{1}{2}|0}^\top \mathbf{C}^\top \mathbf{R} \mathbf{C} \mathbb{T}_{n+\frac{1}{2}|0}$ is not coercive with a constant independent of the discretization– due to high spurious frequencies. These non-physical high frequencies are not controlled by the observation and may pollute the observer convergence as soon as the initial condition discretization excites them.

Here, there is a tremendous literature on possible remedies to this difficult problem, see for instance [Glowinski et al., 1989, Banks et al., 1991, Banks and Fabiano, 1998, Ramdani et al., 2007, Tebou and Zuazua, 2007, Ervedoza et al., 2008, Ervedoza, 2009, Ervedoza and Zuazua, 2009b, Abdallah et al., 2012]. In essence, we can classify the remedies into 2 categories: additional numerical viscosity methods and mixed formulation discretization methods.

In [11], we have thus followed the strategy of adding some numerical viscosity to damped the high frequencies. Let us first introduce the span of all eigenvectors of the space-discretized dynamics

$$\mathcal{C}_h = \text{span}\{\phi_h \text{ such that } \mu_j \leq \eta\}.$$

then we define for any ϵ , an *viscosity* operator A_ϵ as defined in [Ervedoza and Zuazua, 2009b] that damped the system in \mathcal{C}_h^\perp .

. Using this prediction correction scheme we can then assess the convergence of the observer.

THEOREM 2.3.5 (CHAPELLE-CINDEA-MOIREAU)

Let $\mathbb{A} : \mathcal{D}(\mathbb{A}) \rightarrow \mathcal{H}$ be a self-adjoint, definite positive operator with compact resolvent and let $C \in \mathcal{L}(\mathcal{D}(\mathbb{A}^{\frac{1}{2}}), \mathcal{Z})$ be a bounded linear operator such that System (2.23) is exactly observable with (2.26). Let $(\mathcal{U}_h)_{0 < h < h^*}$ be a family of finite dimensional subspaces of $\mathcal{D}(\mathbb{A}^{\frac{1}{2}})$ (associated with standard assumptions (2.6)-(2.11) of [11]), and let $\Delta t \in (0, \Delta t^*)$ be the time discretization step. Set $\epsilon = \max\{\Delta t, h^\theta\}$ and let $A_\epsilon \in \mathcal{L}(\mathcal{Y}_h)$ be a viscosity operator as in [Ervedoza and Zuazua, 2009b]. Then, considering the discrete system

$$\begin{cases} \frac{\hat{y}_{n+1}^- - \hat{y}_n^+}{\Delta t} = A \frac{\hat{y}_{n+1}^- + \hat{y}_n^+}{2} + \mathbb{C}^\top \mathbb{R} \left(z_{n+\frac{1}{2}} - \mathbb{C} \frac{\hat{y}_{n+1}^- + \hat{y}_n^+}{2} \right) \\ \frac{\hat{y}_{n+1}^+ - \hat{y}_{n+1}^-}{\Delta t} = -A_\epsilon \hat{y}_{n+1}^+ \end{cases}$$

for an initial condition $y_0 \in \mathcal{D}(\mathbb{A}^{\frac{3}{2}}) \times \mathcal{D}(A_0)$ there exists a positive constant $c(y_0)$, independent of h , Δt and n , such that

$$\|\hat{y}_h^n - \check{y}(n\Delta t)\|_{\mathcal{Y}} \leq c(y_0) \max(\epsilon, \epsilon^2 h^{-1} \Delta t), \quad \forall n \in \mathbb{N}. \quad (2.37)$$

In essence, the above theorem shows more than the observer convergence. It ensures that the observer converges to the target trajectory better than a classical standard discretization, starting from the exact initial condition but not using the observations. **This result is fundamental: it justifies to rely on observers in numerical simulation to always benefit from all the data sources available on a problem.** We note that there are still some efforts to simplify the assumptions on the viscosity operators. An important result is to show that physical damping operators are sufficient (for example of Rayleigh type) to handle the spurious high frequency. Therefore, we could rely on the viscosity already present in the system.

Observation sampling and noise – Until now, we have only considered perfect measurements, namely measurements that are direct outputs of the model. However in practice, the observation are corrupted by noise coming from the measurement procedure. We have investigated this question with two main results.

The first results are published in [24] where we consider a wave-like equation with velocity measurements corrupted by white noise. In order to avoid the introduction of cylinder set measures – see the very complete [Bensoussan, 1971] on this respect – we define a finite dimensional observation operator sampling the space. More precisely, the observation operator is made of N_{obs} non-overlapping contiguous measurement cells generating a subdomain Ω_{obs} . The resulting measurement corresponds to an average on each cell $\int_{\Omega_{\text{obs}}} s_i \check{v} d\Omega$ using weight functions $(s_i)_{i=1}^{N_{\text{obs}}}$ centered on each cell and such that $\|s_i\|_{L^2(\Omega_{\text{obs}})} = 1$. Then we say that the measurement is defined by

$$z = Cv + \chi$$

with a white noise $\chi \in \mathbb{R}^{N_{\text{obs}}}$ of covariance $W = \text{diag}(\alpha_i^2)_{i=1}^{N_{\text{obs}}}$. With such an observation operator, we consider a DVF observer on a time window $[0, T]$ and prove the following proposition.

PROPOSITION 2.3.6 (MOIREAU-CHAPELLE-LE TALLEC)

Let us introduce μ_0 and τ , a constant and a characteristic time τ such that

$$\begin{cases} \mu_0 \cdot T \gg 1 & \text{if uniformly exponential stability} \\ \mu_0 = 0 & \text{if only stability} \end{cases}$$

and

$$\tau = \begin{cases} \frac{1}{\mu_0} \ll T & \text{if uniformly exponential stability} \\ T & \text{if only stability} \end{cases}$$

Then we have

$$\mathbb{E}(\|\tilde{y}\|_{\mathcal{E}}) \leq c \left(e^{-2\mu_0 t} \mathbb{E}(\|\tilde{\zeta}\|_{\mathcal{E}}) + \tau \gamma^2 \|y - y_h\|_{L^2([0,T],\mathcal{E})} + \tau \gamma^2 \sum_{i=1}^{N_{\text{obs}}} \alpha_i^2 \right).$$

Note that the estimation is not necessarily sharp with respect to the discretization as [24] was published before [11]. Moreover in [24], we show that even when only stability is available it is still possible to obtain an exponential stability on the initial condition part $\mathbb{E}(\|\tilde{\zeta}\|_{\mathcal{E}})$ by assuming further regularity on it.

The second type of results concerns the fundamental question of the data sampling which is inherent to every measurement procedure. In particular, we are concerned by coarse data in time with respect to the model discretization. As an illustration, we can cite the case of the assimilation of image sequences for cardiovascular systems – described *e.g.* in [8, 21] or [33] – where the time-sampling of the data is of one or two orders of magnitude larger than the model time-step discretization. This example justifies our need of an observer that directly uses the field measurements and not their time derivatives, but it also imposes to understand the impact of the data time sampling in an estimation of the type (2.37).

Facing this situation, there exist two alternatives. The first one – considered for example in [25] – consists in interpolating the data in time in order to regenerate a time-continuous sequence which can then be compatible with any time discretization of the model. This approach is very attractive from an abstract standpoint but at the price of an additional time-interpolation error perturbing the observer dynamics as any other measurement noise. Moreover, this perturbation has the consistency of the data sampling period. A second approach – often used in practice without even mentioning it – is to compute the discrepancy only when the data are available. This intermittent correction is potentially error free but may induce correction shocks that limit the stabilization of the error between the observer trajectory and the pursued trajectory. In order to evaluate these two alternatives, we consider in [17] a splitting time-discretization of the observer inspired from [Ervedoza and Zuazua, 2009a]. Once the time discretization of the observer is chosen, we define $(j_r)_{r \in \mathbb{N}} \subset \mathbb{N}$ as a strictly increasing sequence of natural numbers so that the available measurements are

$$z_r = z(j_r \delta t), \quad r \in \mathbb{N}.$$

We then consider two strategies to introduce these time-sampled data in a discrete observer. The first one is to consider the data only when they are available, hence in essence $\gamma_n = 0$ when

the data z^n is not available. The second one consists in interpolating the data to generate an approximated z^n for all n . We summarize these two strategies by (we choose here $\Lambda_\epsilon = \mathcal{U}_t A^2$)

$$\begin{cases} \frac{\hat{y}_{n+1}^- - \hat{y}_n^+}{\delta t} = A \frac{\hat{y}_{n+1}^- + \hat{y}_n^+}{2}, & n > 0 \\ \frac{\hat{y}_{n+1}^+ - \hat{y}_{n+1}^-}{\delta t} = \delta^{n+1} \gamma C^* (d_{n+1} - C \hat{y}_{n+1}^+) + \mathcal{U}_t A^2 \hat{y}_{n+1}^+, & n > 0 \\ \hat{y}_+^0 = \hat{y}_0, \end{cases} \quad (2.38)$$

where $(\delta^n)_{n \in \mathbb{N}}$ and $(d^n)_{n \in \mathbb{N}}$ will be referred to as the switching coefficients and the interpolated data respectively. For the first idea – named *on/off switch* and where the correction term only appears when measurements are available – we have

$$\delta^n = \begin{cases} 1 \\ 0 \end{cases} \quad d_n = \begin{cases} z_r & \text{if } \exists r \in \mathbb{N} : n = j_r \\ 0 & \text{otherwise.} \end{cases}$$

The second choice where we interpolate in time the data reads, in the particular case of linear interpolation,

$$\delta^n = 1 \quad \forall n, \quad d_n = \frac{n - j_r}{j_{r+1} - j_r} z_{r+1} + \left(1 - \frac{n - j_r}{j_{r+1} - j_r}\right) z_r \quad j_r \leq n \leq j_{r+1}.$$

We can now give the convergence estimate for the on/off observer.

THEOREM 2.3.7 (CÎNDEA-IMPERIALE-MOIREAU)

Let A be a skew-adjoint operator with compact resolvent and $C \in \mathcal{L}(\mathcal{Y}, \mathcal{Z})$ be a bounded linear observation operator such that the observability inequality (2.30) holds. Assume that there exists a strictly positive integer N such that $j_r = rN\delta t, n \in \mathbb{N}$. Then, for every $y_0 \in \mathcal{D}(A_0^2) \times \mathcal{D}(A_0^{\frac{3}{2}})$ there exist positive constants $M_0, \mu_0(N), c_1$ and c_2 , independent of $\delta t \in (0, 1)$ and n , such that \tilde{y}_+^n solution of estimation error for the on-off scheme satisfies

$$\|\tilde{y}_n^+\|_{\mathcal{Y}} \leq M_0 \exp(-\mu_0 \alpha_n \delta t) \|\tilde{y}_0\|_{\mathcal{Y}} + \frac{\delta t}{1 - \exp(-\mu_0 \rho \Delta t)} (\delta t^2 c_1 + \mathcal{U}_t c_2).$$

where $\alpha_n = \text{card}\{j, 1 \leq j \leq n, \delta_j = 1\} = \lfloor \frac{n}{N} \rfloor$, and $\rho = \frac{c_n}{n}$. By comparison, the estimation error in the case of interpolated data is given by positive constants $\tilde{M}_0, \tilde{\mu}_0, \tilde{c}_1, \tilde{c}_2$ and \tilde{c}_3 , independent of $\delta t \in (0, 1)$ and n , such that,

$$\|\tilde{y}_n^+\|_{\mathcal{Y}} \leq \tilde{M}_0 \exp(-\tilde{\mu}_0 n \delta t) \|\tilde{y}_0\|_{\mathcal{Y}} + \frac{\delta t}{1 - \exp(-\tilde{\mu}_0 \delta t)} (\delta t^2 \tilde{c}_1 + \mathcal{U}_t \tilde{c}_2 + \gamma \tilde{c}_3 |\varepsilon_d|).$$

where $|\varepsilon_d| = \max_{1 \leq i \leq n} \|\varepsilon_d^i\|_{\mathcal{Z}}$ is the maximum of the interpolation errors $\varepsilon_d^i = C\check{y}(i\delta t) - d_i$.

In the light of Theorem 2.3.7 we understand that choosing a strategy – interpolated or on/off – relies on a compromise between stability and consistency. On the one hand, the observer with intermittent correction phases bear an exact consistency with respect to the data, however corrections shocks may occur thus leading to potential instabilities. On the other hand, the observer fed with interpolated data admits a correction phase at each model time-step – hence its greater stability – but artificially induces noise in the observer dynamical system due to data interpolation error. **In practice, the on/off switch has shown an incredible robustness to large data time steps** compared to the second observer whose efficiency, in that case, is

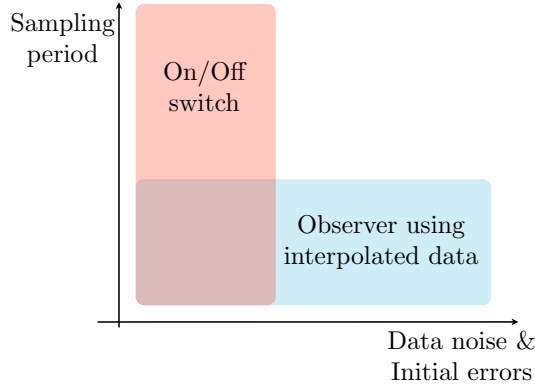


Figure 2.3: Illustration of the different regimes where observers are more likely to be efficient.

deteriorated by a significant amount of interpolation error. **However, in the case of high initial errors or high data noise, it appears to be more efficient to interpolate the data**, since the subsequently obtained dynamical system will benefit from a stabilizing operator at each time step. This trade-off is summarized in Figure 2.3.

Computational issues – Even if the presented observer is attractive, there are various technicalities to be handled in order to propose an efficient numerical method following Theorem 2.3.5 in the case of the SDF. Most of them were addressed in [25] and [Imperiale, 2013].

The first issue concerns the need for solving an additional mixed formulation (2.35) to compute the SDF feedback. We easily see that this mixed problem corresponds in fact to the minimization of

$$\min_{\psi | {}^{\natural}C\psi = \phi} \left\{ \frac{1}{2} \psi^{\top} K \psi \right\}$$

As an alternative, we propose in [25] to solve a penalized problem

$$\min \left\{ \frac{\epsilon}{2} \psi^{\top} K \psi + \frac{1}{2} \|\phi - {}^{\natural}C\psi\|_{M_{\Omega_{\text{obs}}}} \right\}$$

Then the computation of $K_{\Omega_{\text{obs}}}$ can be approximated by

$$K(\epsilon K + {}^{\natural}C^{\top} M_{\Omega_{\text{obs}}} {}^{\natural}C)^{-1} {}^{\natural}C^{\top} M_{\Omega_{\text{obs}}} \xrightarrow{\epsilon \rightarrow 0} {}^{\natural}C^{\top} K_{\Omega_{\text{obs}}}.$$

This allows to rewrite the resolution as

$$\begin{cases} (\epsilon K + {}^{\natural}C^{\top} M_{\Omega_{\text{obs}}} {}^{\natural}C) \frac{\hat{u}_{n+1} - \hat{u}_n}{\delta t} = (\epsilon K + {}^{\natural}C^{\top} M_{\Omega_{\text{obs}}} {}^{\natural}C) \hat{v}_{n+\frac{1}{2}} + \gamma {}^{\natural}C^{\top} M_{\Omega_{\text{obs}}} \left(z_{n+\frac{1}{2}} - {}^{\natural}C \hat{u}_{n+\frac{1}{2}} \right) \\ M \frac{\hat{v}_{n+1} - \hat{v}_n}{\delta t} + K \hat{u}_{n+\frac{1}{2}} = f + \gamma {}^{\natural}C^{\top} M_{\Omega_{\text{obs}}} \left(z_{n+\frac{1}{2}} - {}^{\natural}C \hat{v}_{n+\frac{1}{2}} \right) \end{cases} \quad (2.39)$$

which is much more direct to solve. We point out that finally the systems continues to read as in (2.36), but with a modified operator P_0 .

One drawback of the SDF discretization (2.39) is that it imposes to solve a $2N_{\text{dof}}$ degrees of freedom system instead of solving the N_y dof system (2.33) followed by (2.34). First in [25] we show that an iterative scheme over systems of size N_{dof} can be quite effective. We

started to investigate prediction-correction – namely splitting – strategies in [Imperiale, 2013]. In addition to their possible analysis as in (2.38), these prediction-correction time-schemes are also numerically attractive. In essence they read

$$\begin{cases} \frac{\hat{y}_{n+1}^- - \hat{y}_n^+}{\delta t} = A \frac{\hat{y}_{n+1}^- + \hat{y}_n^+}{2} \\ \frac{\hat{y}_{n+1}^+ - \hat{y}_{n+1}^-}{\delta t} = P_0 C^T R (z_{n+1} - C \hat{y}_{n+1}^+) - P_0 \Lambda_\epsilon \hat{y}_{n+1}^+ \end{cases}$$

which allows to limit the computational impact of the correction as an extra-step. We further mention that the correction can also be rewritten in the form

$$\hat{y}_{n+1}^+ = \hat{y}_{n+1}^- + P_{0,\delta t}^+ C^T R (z_{n+1} - C \hat{y}_{n+1}^-) - P_{0,\delta t}^+ \Lambda_\epsilon \hat{y}_{n+1}^-$$

with

$$P_{0,\delta t}^+ = P_0 (N + \delta t C^T R C + \delta t \Lambda_\epsilon)^{-1}$$

which is exactly a classical BLUE correction as available in data assimilation codes and library such as Verdandi [12].

Therefore, **our observer formulation has also been carefully designed from a computational stand-point to be easily integrated in simulation codes.**

Initial condition estimation remark – We have investigated many subjects on observer design for wave equations. However, we never had the opportunity to study the reconstruction of the initial condition uncertainty. Indeed, one drawback of classical observer formulations with respect to standard variational approaches is that we filter the initial condition uncertainty but do not reconstruct it. In cardiovascular problems, most of the examples we have dealt with are periodic, hence, the asymptotic reconstruction allows to retrieve the initial condition. In all other cases, we want to rely on the back and forth strategy proposed by [Ramdani et al., 2010] and analysed on various aspects (convergence, discretization) in the literature [Ito et al., 2011, Haïne and Ramdani, 2012, Haïne, 2014b]. This strategy uses the time-reverse property of the wave generator to reconstruct the initial condition via an observer of the time-reverse equation. This back and forth strategy has also been designed for other conservative system in [Auroux and Blum, 2008] with the appellation *back and forth nudging (BFN)*. We point out that our SDF strategy is completely compatible with a back and forth observer approach as already used in [Haïne, 2014a].

2.3.3 Luenberger observers: other models

We have presented on the wave-like equation the various challenges related to the state observer design, analysis and discretization. We can now move slightly closer to the cardiac application by showing how our design for the wave equation leads to extensions for mechanical problems. In this respect, we will present here formulations derived for elasticity, then cardiac non-linear mechanics and finally fluid-structure interaction. We have not reached on this problem the same level of mathematical analysis as most of these problems are non-linear, but numerical investigations will show that the strategy is still strongly relevant. Finally, at the very end of this section we present a Luenberger observer for a vast class of hyperbolic systems that admit a kinetic representation.

2.3.3.1 Observer in structure mechanics

The elastodynamics case – First, we should start with elastodynamics in small displacement

$$\begin{cases} \partial_t \underline{u} = \underline{v}, & \text{in } \Omega \\ \rho \partial_t \underline{v} - \operatorname{div}(\underline{\sigma}) = \underline{f}, & \text{in } \Omega \\ \text{boundary conditions} & \text{on } \partial\Omega \end{cases} \quad (2.40)$$

where $\underline{\sigma} = \underline{\underline{A}} : \underline{\underline{\varepsilon}}(\underline{u})$. We will also use $\Delta_e = \operatorname{div}(\underline{\underline{A}} : \underline{\underline{\varepsilon}})$. The mechanical energy reads

$$\|\underline{u}\|_{\mathcal{E}_m} = \int_{\Omega} \underline{\underline{\varepsilon}}(\underline{u}) : \underline{\underline{A}} : \underline{\underline{\varepsilon}}(\underline{u}) \, d\Omega,$$

and is equivalent to an H^1 semi-norm. If we assume to have some measurements on a subdomain, for instance some velocity measurements on Ω_{obs}^v and displacement measurements on Ω_{obs}^u then our wave observer directly extends to elasticity by simply considering [25]

$$\begin{cases} \partial_t \hat{\underline{u}} = \hat{\underline{v}} + \gamma_u \underline{\text{Ext}}_{\Omega_{\text{obs}}^u}(\underline{z}_u - \hat{\underline{u}}|_{\Omega_{\text{obs}}^u}), & \text{in } \Omega \\ \rho \partial_t \hat{\underline{v}} - \operatorname{div}(\hat{\underline{\sigma}}) = \underline{f} + \gamma_v \mathbb{1}_{\Omega_{\text{obs}}^v}(\underline{z}_v - \hat{\underline{v}}_{\Omega_{\text{obs}}^v}), & \text{in } \Omega \\ \text{same boundary conditions as (2.40)} & \text{on } \partial\Omega \end{cases}$$

where the extension is given by

$$\underline{\psi}^{\text{ext}} = \underline{\text{Ext}}_{\Omega_{\text{obs}}^u}(\underline{\psi}) : \begin{cases} \operatorname{div}(\underline{\underline{A}} : \underline{\underline{\varepsilon}}(\underline{\psi}^{\text{ext}})) = 0 & \text{in } \Omega \setminus \Omega_{\text{obs}}^u \\ \underline{\psi}^{\text{ext}} = \underline{\psi} & \text{in } \Omega_{\text{obs}}^u \\ \text{same boundary conditions as (2.40)} & \text{on } \partial\Omega \end{cases}$$

If the measurements are on the boundary, we then have

$$\begin{cases} \partial_t \hat{\underline{u}} = \hat{\underline{v}} + \gamma_u \underline{\text{Ext}}_{\Gamma_{\text{obs}}^u}(\underline{z}_u - \hat{\underline{u}}|_{\Gamma_{\text{obs}}^u}), & \text{in } \Omega \\ \rho \partial_t \hat{\underline{v}} - \operatorname{div}(\hat{\underline{\sigma}}) = \underline{f}, & \text{in } \Omega \\ \hat{\underline{\sigma}} \cdot \underline{n} = \gamma_v(\underline{z}_v - \hat{\underline{v}}_{\Gamma_{\text{obs}}^v}) & \\ \text{same boundary conditions as (2.40)} & \text{on } \partial\Omega \setminus \Gamma_{\text{obs}}^v \end{cases}$$

where this time

$$\underline{\psi}^{\text{ext}} = \underline{\text{Ext}}_{\Omega_{\text{obs}}^u}(\underline{\psi}) : \begin{cases} \operatorname{div}(\underline{\underline{A}} : \underline{\underline{\varepsilon}}(\underline{\psi}^{\text{ext}})) = 0 & \text{in } \Omega \\ \underline{\psi}^{\text{ext}} = \underline{\psi} & \text{in } \Gamma_{\text{obs}}^u \\ \text{same boundary conditions as (2.40)} & \text{on } \partial\Omega \setminus \Gamma_{\text{obs}}^u \end{cases}$$

Note again that the feedback associated with velocity measurements is the classical DVF [24], whereas on the displacement part we rely on our SDF design. With mechanical formulations, this SDF is quite similar to the feedback imagined concurrently on the beam problem in [Li and Xu, 2011] when compared to our formulation for the beam problem in [11, Appendix]. We also point out that all these formulations correspond to the semi-group formulation

$$\dot{\hat{\underline{y}}} = A\hat{\underline{y}} + C^*R(\underline{z} - C\hat{\underline{y}}),$$

with R a simple scaling operator by γ^v and γ^u in each subspace of observation.

On the elastodynamics problem, the analysis of the observer is very similar to the analysis performed for the scalar wave equation. To our best knowledge, however, few results exist on geometric control condition for elasticity problems when the boundary conditions are not of Dirichlet type. In this case, [Khenissi et al., 2010] consolidate the elastic geometric control conditions stating that every combination of pressure (P) and shear (S) waves rays should encounter the subdomain of observation, knowing that these rays are independent in the domain interior and coupled on the boundary, as any (P) ray reflects on the boundary to give a (P) ray and (S) ray, and conversely for the (S) rays. The specific cases of glancing rays etc. are completely defined. We then can follow the same path as for the wave equation to prove [Imperiale, 2013]

THEOREM 2.3.8 (CHAPELLE-IMPERIALE-MOIREAU)

We assume that there exists a constant C and a time T such that every solution of

$$\begin{cases} \dot{\underline{u}} = \underline{v}, & \text{in } \Omega \\ \rho \dot{\underline{v}} - \Delta_e \underline{u} = 0, & \text{in } \Omega \\ \underline{u} = 0, & \text{on } \partial\Omega \end{cases}$$

satisfies the elastic geometric condition for a domain Ω_{obs}^b slightly smaller than Ω_{obs} , namely, with $\Omega_{obs}^b \subset \Omega_{obs}$ and $\text{dist}(\Omega \setminus \Omega_{obs}, \tilde{\Omega}_{obs}) > 0$. Therefore the observer

$$\begin{cases} \partial_t \hat{\underline{u}} = \hat{\underline{v}} + \gamma \underline{Ext}_{\Omega_{obs}}(z_u - \hat{\underline{u}}|_{\Omega_{obs}^b}), & \text{in } \Omega \\ \rho \partial_t \hat{\underline{v}} - \Delta_e \hat{\underline{u}} = \underline{f}, & \text{in } \Omega \\ \hat{\underline{u}} = 0 & \text{on } \partial\Omega \end{cases}$$

converges exponentially to the target system

$$\begin{cases} \dot{\underline{u}} = \underline{v}, & \text{in } \Omega \\ \rho \dot{\underline{v}} - \Delta_e \underline{u} = \underline{f}, & \text{in } \Omega \\ \underline{u} = 0, & \text{on } \partial\Omega \end{cases}$$

such that $z = \tilde{\underline{u}}|_{\Omega_{obs}^b}$.

We point out that our proof is still based on energy equi-repartition, manipulation whereas a direct proof using H^1 micro-local defect measures for elasticity [Burq and Lebeau, 2001] should allow to avoid the definition of Ω_{obs}^b .

Non-linear mechanics – The question is now to propose an observer for non-linear mechanics of the form

$$\begin{cases} \partial_t \underline{u} = \underline{v}, & \text{in } \Omega_0 \\ \rho \partial_t \underline{v} - \text{div}(\underline{T}) = \underline{f}, & \text{in } \Omega_0 \\ \text{boundary conditions} & \text{on } \partial\Omega_0 \end{cases}$$

where \underline{T} is the first tensor of Piola-Kirchhoff and Ω_0 is the reference configuration. Concerning the DVF, the feedback is the same but, for the SDF, the question is now to understand in which

sense the extension should be considered. As explained in [25], after spatial discretization, the analysis of the linearized error between the observer and the target system indicates that the extension should be considered with the linearized stress tensor around the trajectory. However this tensor is not necessarily associated with a well-posed problem since coercivity is not always satisfied, for instance in compression. In these cases it may be more robust to stick with a time-constant extension based on the linearized tensor with respect to the reference configuration. In fact, the practical results in [25] show some very good observer convergence with these two choices.

2.3.3.2 Fluid-structure interaction

A common data assimilation problem in blood flow modeling consists in considering a fluid-structure interaction model of a part of an artery that must be registered on measurements of the wall displacement. In that case the question remains to design an observer using structure displacements, but this time for coupled problems. We address this question in [4] where we simply define the observer as the coupling of the structure mechanics observer and a non observed fluid. We then try to understand how this coupled problem – hyperbolic for the solid and parabolic for the fluid in essence – is then controlled by observation on the structure. This type of question of controlling coupled system by actioning only on one them is becoming a more and more intensive field of research that remains particularly intricate. We can cite for instance [Zhang and Zuazua, 2006, Duyckaerts, 2007, Raymond and Vanninathan, 2010, Court, 2014, Badra and Takahashi, 2014] – see also references therein – for results on FSI stabilization and control that should give the necessary tools for an extensive mathematical analysis of this problem. As it was a preliminary analysis, we have limited our approach by simply showing the additional stability brought by the observer and trying to quantify it by a spectrum sensitivity analysis.

Energetic balance associated with the observer – We consider a standard FSI model as given in (1.14) (Section 1.3.3) coupled to a RCR-Windkessel model. On the solid part, we assume to have at our disposal some interior measurements or boundary measurements on the external part of the wall boundary (the uncoupled boundary). First, we prove that our coupled observer brings no unstable perturbation to the non-linear Navier-Stokes-Elasticity problem.

PROPOSITION 2.3.9 (BERTOGGIO-CHAPELLE-FERNÁNDEZ-GERBEAU-MOIREAU)

Defining

$$\begin{aligned}\hat{\mathcal{E}}(t) &= \frac{\rho_f}{2} \|\hat{v}_f\|_{L^2(\Omega_f(t))}^2 + \frac{\rho_s}{2} \|\hat{v}_s\|_{L^2(\Omega_0)}^2 + \frac{1}{2} \|\hat{u}_s\|_{\mathcal{E}_{m,s}}^2 + \frac{C}{2} \hat{p}^2, \\ \hat{\mathcal{D}}(t) &= 2\mu_f \|\varepsilon_f(\hat{v}_f)\|_{L^2(\Omega_f(t))}^2 + \eta_s \|\hat{v}_s\|_{\mathcal{E}_{m,s}}^2 + \frac{\hat{p}^2}{R_d} + R_p \hat{Q}^2,\end{aligned}$$

for the DVF observer, the energy balance reads

$$\frac{d}{dt} \hat{\mathcal{E}}(t) \leq -\hat{\mathcal{D}}(t) - \frac{\gamma_v}{2} \|\hat{v}_s\|_{L^2(*)}^2 + \frac{\gamma_u}{2} \|z_v\|_{L^2(*)}^2 - \int_{\Gamma^{\text{in}} \cup \Gamma^{\text{out}}} \frac{\rho_f}{2} \hat{v}_f \cdot \underline{n}_f |\hat{v}_f|^2 d\Gamma,$$

whereas for the SDF observer, we have

$$\frac{d}{dt} \hat{\mathcal{E}}(t) \leq -\hat{\mathcal{D}}(t) - \frac{\gamma_u}{2} \|\text{Ext}_*^s(\hat{u}_s)\|_{\mathcal{E}_{m,s}}^2 + \frac{\gamma_u}{2} \|\text{Ext}_*^s(z_u)\|_{\mathcal{E}_{m,s}}^2 - \int_{\Gamma^{\text{in}} \cup \Gamma^{\text{out}}} \frac{\rho_f}{2} \hat{v}_f \cdot \underline{n}_f |\hat{v}_f|^2 d\Gamma,$$

with $*$ standing for the domain of observation namely either Ω_{obs} or Γ_{obs} .

Sensitivity analysis – We now proceed to a sensitivity analysis in the spirit of [Preumont, 2002]. Let us start by the solid only when we add a DVF or a SDF. To simplify the presentation we consider a Galerkin spatial discretization. As originally done in this case in [38], we compute the sensitivity to the feedback by introducing the quadratic eigenvalue problem of the DVF

$$\text{Find } (\phi_u, \lambda) \text{ such that } \left(\lambda^2 M_s + \lambda(\Lambda_s + \gamma_v \mathbb{d} C_v^T R_v \mathbb{d} C_v) + K_s \right) \phi_u = 0. \quad (2.41)$$

The solution (λ, ϕ_u) of this problem (2.41) is a function of γ_v and we denote by $(\lambda_{|0}, \phi_{u|0})$ the solutions when $\gamma_v = 0$. Recalling that in our case we choose $\Lambda_s = \eta_s K_s$, they verify

$$K_s \phi_{u|0} = \omega^2 M_s \phi_{u|0}, \text{ and } \lambda_{|0}^2 + \eta_s \omega^2 \lambda_{|0} + \omega^2 = 0,$$

and we can normalize them such that $\phi_{u|0}^T M_s \phi_{u|0} = 1$ (note that we can consider real-only eigenmodes in our case). Then we can compute the Fréchet derivative of λ with respect to γ_v to compute a sensitivity. We obtain

$$\left(2\lambda_{|0} \frac{\partial \lambda}{\partial \gamma_v} \Big|_{\gamma_v=0} M_s + \lambda_{|0} \mathbb{d} C_v^T R_v \mathbb{d} C_v + \frac{\partial \lambda}{\partial \gamma_v} \Lambda_s \right) \phi_{u|0} + \left(\lambda_{|0}^2 M_s + \lambda_{|0} \Lambda_s + K_s \right) \frac{\partial \phi_u}{\partial \gamma_v} \Big|_{\gamma_v=0} = 0.$$

Finally, left-multiplying by $\phi_{u|0}^T$ and using that, by definition, $(\lambda_{|0}^2 M_s + \lambda_{|0} \Lambda_s + K_s) \phi_{u|0} = 0$, we obtain

$$\left(2 + \eta_s \frac{\omega^2}{\lambda_{|0}} \right) \frac{\partial \lambda}{\partial \gamma_v} \Big|_{\gamma_v=0} = -\phi_{u|0}^T (\mathbb{d} C_v^T R_v \mathbb{d} C_v) \phi_{u|0}.$$

Then for an initially undamped structure the initial eigenvalues on the imaginary axis $\lambda_{|0}^2 = -\omega^2$ are moved to the half plane of negative real parts by

$$\frac{\partial \lambda}{\partial \gamma_v} \Big|_{\gamma_v=0} = -\frac{\phi_{u|0}^T (\mathbb{d} C_v^T R_v \mathbb{d} C_v) \phi_{u|0}}{2} = -\frac{1}{2} \frac{\|\mathbb{d} C_v \phi_{u|0}\|_{L^2(\Omega_{obs})}^2}{\|\phi_{u|0}\|_{L^2(\Omega_s)}^2}.$$

Therefore, when we have an observability inequality of the form: there exist two positive constants T_0 and α such that

$$\forall T \geq T_0, \quad \int_0^T \|\mathbb{d} C_v v_s(t)\|_{L^2(\Omega_{obs})}^2 dt \geq \alpha (\|u(0)\|_{\mathcal{E}_{s,m}}^2 + \|v(0)\|_{L^2(\Omega)}^2),$$

then we see that

$$\frac{\partial \lambda}{\partial \gamma_v} \Big|_{\gamma_v=0} \leq -\frac{\alpha}{2T_0}.$$

In [4] we then develop the same computation for the SDF observer to retrieve the same sensitivity

$$\frac{\partial \lambda}{\partial \gamma_d} \Big|_{\gamma_d=0} \leq -\frac{\alpha}{2T_0},$$

as indeed in [25] we design the SDF with this objective.

A typical illustration of the poles behavior is given in Figure 2.4 inspired from [4]. Note also that the pole representation allows to understand the over-damping phenomena, namely, the fact that large values of the gain are counter productive with respect to the stabilization rate – see [38] for a more complete description on this aspect.

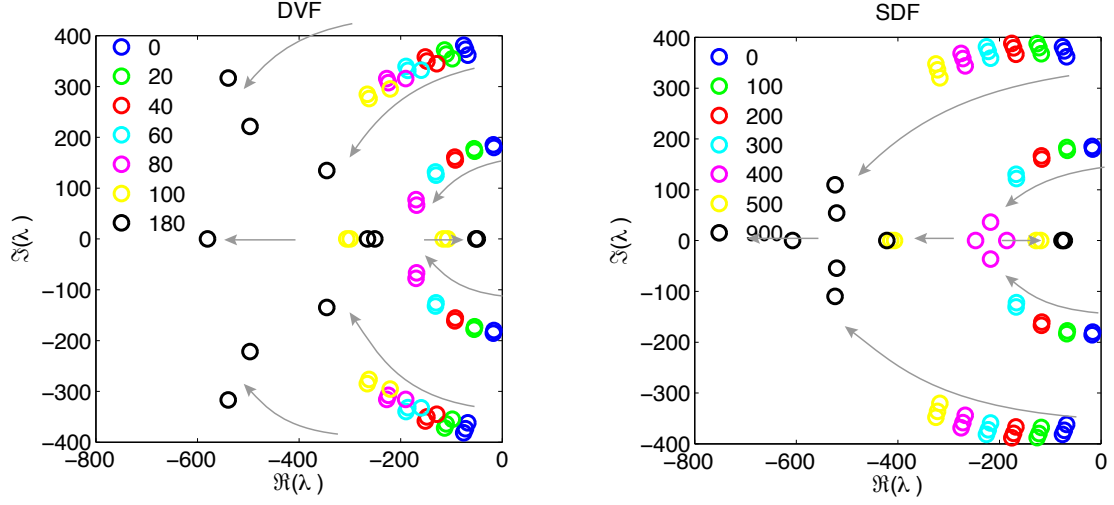


Figure 2.4: Poles of the DVF (left) and the SDF (right) estimators in elastodynamics with boundary observation and for different values of the gain. The grey arrows sketch the trajectories of the poles when increasing the feedback gain

We can now investigate the impact of the fluid on the SDF observer. We start by considering only an inviscid incompressible fluid. Hence, the forcing pressure p is driven by an elliptic problem with interface coupling conditions reducing to

$$\begin{cases} -\Delta p = 0, & \text{in } \Omega_f \\ \nabla p \cdot \underline{n}_f = 0, & \text{on } \Gamma_{\text{in}} \\ p = 0, & \text{on } \Gamma_{\text{out}} \end{cases}$$

with the coupling condition

$$\begin{cases} \nabla p \cdot \underline{n}_f = -\rho_f \partial_t \underline{\sigma}_s \cdot \underline{n}_f, & \text{on } \Sigma \\ \eta_s \underline{\sigma}_s(\underline{v}_s) \cdot \underline{n}_s + \underline{\sigma}_s(\underline{u}_s) \cdot \underline{n}_s - p \underline{n}_f = 0, & \text{on } \Sigma \end{cases}$$

By eliminating the pressure variable by a Schur complement we end up with the discretized problem

$$\begin{bmatrix} \mathbf{K}_s & 0 \\ 0 & \mathbf{M}_s + \mathbf{M}_a \end{bmatrix} \begin{bmatrix} \dot{\mathbf{u}}_s \\ \dot{\mathbf{v}}_s \end{bmatrix} = \begin{bmatrix} 0 & \mathbf{K}_s \\ -\mathbf{K}_s & -\Lambda_s \end{bmatrix} \begin{bmatrix} \mathbf{u}_s \\ \mathbf{v}_s \end{bmatrix}$$

where \mathbf{M}_a is the so-called added mass operator given by

$$\mathbf{M}_a = \rho_f \mathbf{B}_f \mathbf{K}_s \mathbf{B}_f^\top \text{ with } \forall p_h \in \mathcal{V}_{p,h}, \mathbf{v}_{s,h} \in \mathcal{V}_{\underline{v},h}, \quad \mathbf{v}_s \mathbf{B}_f \mathbf{p} = \int_{\Sigma} p_h \mathbf{v}_{s,h} \cdot \underline{n}_f \, d\Gamma.$$

Then, the sensitivity analysis gives for the SDF

$$\left. \frac{\partial \lambda}{\partial \gamma_d} \right|_{\gamma_v=0} \leq -\frac{1}{2} \frac{\|C_v \phi_{u|0}\|_{L^2(\Omega_{\text{obs}})}^2}{\|\phi_{u|0}\|_a^2 + \|\phi_{u|0}\|_{L^2(\Omega_s)}^2},$$

with $\|\phi_{u|0}\|_a = \Phi_{a,d}^\top M_a \phi_{a,d}$. For the DVF however, we have

$$\frac{\partial \lambda}{\partial \gamma_v} \Big|_{\gamma_v=0} \leq -\frac{1}{2} \left(1 - \frac{\|C_d \phi_{u|0}\|_a^2}{\|\phi_{u|0}\|_a^2 + \|\phi_{u|0}\|_{L^2(\Omega_s)}^2} \right)$$

Here, we see that the SDF is still very efficient whereas the DVF sensitivity is close to 0 as for some modes $\Phi_{a,d}^\top M_a \phi_{a,d}$ is close to 1. In fact, the DVF must be changed in this FSI configuration to take into account the added mass-effect by changing

$$\mathfrak{C}_v^\top M_{\text{obs}} \mathfrak{C}_v \rightarrow \mathfrak{C}_v^\top (M_s + \mathfrak{C}_v M_a \mathfrak{C}_v^\top) \mathfrak{C}_v$$

in order to retrieve a good sensitivity. We see here the interest of the sensitivity analysis to design efficient feedbacks.

To go further in the analysis we consider an FSI problem where the outflow pressure condition is given by a coupled lumped-parameter model – namely a Windkessel model – as it is often the case in blood flow modeling. In [4], we proceed again to a sensitivity analysis combining exact computation and order of magnitude analysis to determine the sensitivity of our feedback in actual situation. Our conclusion is that the SDF can still be very effective in that case whereas the DVF is limited intrinsically by the quasi-static nature of the Windkessel pole, which makes it impossible to stabilize with velocity-based strategies.

We finally move to the evaluation of the sensitivity for an Elastodynamics-Stokes coupling problem. Here we are exactly in the case of the parabolic-hyperbolic situation [Duyckaerts, 2007]. In [4] we again combine pole analysis and numerical computations to justify how the fluid pole are stable but rather unaffected by the observer on the solid part. This indicates that an objective for fluid-structure interaction data assimilation problems is to rely on measurements on both the solid and the fluid part. In blood flows, this is typically achieved by combining standard MRI with phase contrast MRI where the flow is recorded, or Doppler images.

2.3.3.3 Hyperbolic problems with kinetic representation/interpretation

As we have seen with the wave equation, data assimilation offers an effective strategy to deal with the various sources of error entering and propagating during a simulation and restricting the performance of a numerical prediction. This is in fact true for hyperbolic systems in general, and especially for conservative systems where, in the absence of dissipation, every type of errors – model errors, numerical errors – propagate and possibly expand in time. We thus want to consider here a general class of conservation laws that may contain non-linearities as for instance transport equations, Burgers equation, shallow water or Euler systems for gas dynamics, and we focus on non-viscous configurations. The presence of non-linearities introduces a new step of difficulty for the formulation of observers as compared to what we have seen with the wave equation [Bardos and Pironneau, 2005]. However, we propose in [6] an original approach based on a kinetic description [Perthame, 2004] to circumvent the difficulty brought by the non-linearities. Indeed, the kinetic description is formalized by a linear – up to the collision term – transport equation in which the advection velocity is an additional free variable. Hence, we can easily design a Luenberger observer at the kinetic level leading to a BGK (Bhatnagar–Gross–Krook) type equation. Then, we derive the observer of the original system by computing the macroscopic variable from the kinetic observer. The resulting observer feedback can be non-linear and proves to be more effective than other nudging operator computed directly at the macroscopic level.

A first simple result on transport equations Let us first study the simple configuration of a transport equation model defined on $[0, 1]$ with periodic boundary conditions

$$\begin{cases} \frac{\partial u}{\partial t} + \alpha \frac{\partial u}{\partial x} = 0 \\ u(x, 0) = u_0(x) \end{cases} \quad (2.42)$$

We further assume that α is constant. We choose as the state space $L^2([0, 1])$ and easily prove that (2.42) is associated with the group generator $A = -\alpha \frac{\partial}{\partial x}$ of domain

$$D(A) = \{H^1((0, 1)) \text{ s.t. } u(0) = u(1)\}.$$

On this system, we follow a target trajectory $\{\check{u}\}$ starting from $\check{u}_0 = u_\diamond + \zeta$ and we consider that we have at our disposal partial observations of the target trajectory over time up to some measurement errors

$$z(x, t) = \mathbb{1}_\omega(x)\check{u} + \chi$$

with typically $\omega = (a, b) \subset [0, 1]$. The observation space is defined by $\mathcal{Z} = L^2((a, b))$ and the observation operator $C = \mathbb{1}_\omega(x) \cdot$ is bounded.

We define the observability condition for this transport equation as the existence of a time T_0 and constant c such that

$$\forall T \geq T_0, \quad \int_0^T \|u\|_{L^2(\omega)} dt \geq c \|u_0\|_{L^2([0,1])}.$$

We directly verify the observability condition from the equation characteristics.

PROPOSITION 2.3.10

We denote by $\{x_{x,t}(s), s \geq 0\}$ the characteristics passing by x at time t . The time passed into ω when following a characteristic is denoted by $\tau_{x_0} = \frac{1}{\alpha} \int_0^t \mathbb{1}_\omega(x_{x_0,0}(s)) ds$. If $\tau_{\min} = \min_{x_0} \tau_{x_0} > 0$, then the observability condition is satisfied for all $t > T_0 = \tau_{\min}$.

Then we directly infer an effective observer

$$\begin{cases} \frac{\partial \hat{u}}{\partial t} + \alpha \frac{\partial \hat{u}}{\partial x} = \gamma \mathbb{1}_\omega(z - \hat{u}) \\ \hat{u}(x, 0) = u_\diamond(x) \end{cases}$$

and with the following estimation error

$$\begin{cases} \frac{\partial \tilde{u}}{\partial t} + \alpha \frac{\partial \tilde{u}}{\partial x} = -\gamma \mathbb{1}_\omega \tilde{u} + \gamma \mathbb{1}_\omega \chi \\ \tilde{u}(x, 0) = \zeta(x) \end{cases} \quad (2.43)$$

The homogeneous part of system (2.43) is exponentially stable. Indeed, we have on every characteristics

$$\frac{d\tilde{u}}{dt}(x_{x_0,0}(t)) = -\gamma \mathbb{1}_\omega \tilde{u}(x_{x_0,0}(t))$$

which implies that for all $t > T_0$

$$\|\tilde{u}\| \leq \exp\left(-\gamma \int_0^t \mathbb{1}_\omega(x_{x_0,0}(s)) ds\right) \leq e^{-\lambda \tau_{\min}},$$

with easy extension with measurement errors.

Kinetic description of systems of conservation laws From this simple example we can now propose an observer strategy for a wide class of hyperbolic systems. Considering the following scalar conservation law

$$\begin{cases} \partial_t u + \sum_{i=1}^d \partial_{x_i} A_i(u) = 0 \\ u(t=0, x) = u_\diamond(\underline{x}) + \zeta_u(\underline{x}) \end{cases}$$

with the entropy inequalities, for any convex function $\mathcal{S}(\cdot)$ and corresponding entropy flux η_i ,

$$\partial_t \mathcal{S}(u) + \sum_{i=1}^d \partial_{x_i} \eta_i(u) \leq 0,$$

the kinetic description can be written

$$\begin{cases} \partial_t m(t, \underline{x}, \underline{v}) + \alpha(\underline{v}) \cdot \nabla_{\underline{x}} m(t, \underline{x}, \underline{v}) = q(t, \underline{x}, \underline{v}) \\ m(0, x, \underline{v}) = m_\diamond(\underline{x}, \underline{v}) + \zeta_m(\underline{x}, \underline{v}) \end{cases}$$

with u is the macroscopic variable, m is the density function which is related to u by its first moment:

$$u(t, \underline{x}) = \int_{\mathbb{R}^d} m(t, \underline{x}, \underline{v}) d\underline{v},$$

q is the collision operator. Nonlinearities are hidden in the density function m , and shocks are confined in the collision operator. But we emphasize the fact that for fixed \underline{v} , the kinetic equation can be handled as a linear equation. The equivalence proof is based on simple integration of the kinetic equations. Then, the observer equations at the macroscopic level

$$\begin{cases} \partial_t \hat{u} + \nabla_{\underline{x}} \cdot A(\hat{u}) = \gamma(u - \hat{u}) \\ \hat{u}(0) = u_\diamond \end{cases}$$

are formulated at the kinetic level

$$\begin{cases} \partial_t \hat{m} + \alpha(\underline{v}) \cdot \nabla_{\underline{x}} \hat{m} = \gamma(m_z - \hat{m}) \\ \hat{m}(0) = m_\diamond \end{cases}$$

At the macroscopic level, the nonlinearity of the flux A is the main obstacle to easy convergence proofs of \hat{u} towards u . Possible techniques are based on L^1 contraction principle in the scalar case, but do not easily extend to systems. At the kinetic level, the equation gains linearity and we can even have the explicit solution:

$$\hat{m}(t, x, v) = \hat{m}_0(x - \alpha(\underline{v})t, v) e^{-\gamma t} + \int_0^t e^{-\gamma s} m_z(t-s, x - \alpha(\underline{v})s, v) ds,$$

as soon as $m_z(t, x, v)$ can be generated from the measurements z . This leads to theoretical convergence results, consolidated in [6] with and without measurement noise.

The Saint-Venant example and its kinetic description – We consider the illustrative example of the Saint-Venant system (or shallow-water system), that reads in 1D after simplifying the source term

$$\begin{cases} \frac{\partial h}{\partial t} + \frac{\partial}{\partial x} (hu) = 0 \\ \frac{\partial}{\partial t} (hu) + \frac{\partial}{\partial x} (hu^2 + \frac{g}{2}h^2) = 0 \end{cases} \quad (2.44)$$

where h stands for the water height, u for the water velocity and g is typically the gravity parameter. For now we do not mention any boundary condition. Note that a similar type of model also appeared in Section 1.3.3 as a 1d asymptotic model of the cardiovascular circulation in arteries.

System (2.44) naturally comes with an entropy inequality for the so-called energy

$$\mathcal{E}(h, u) = h \frac{u^2}{2} + g \frac{h^2}{2},$$

which satisfies for weak solutions

$$\frac{\partial \mathcal{E}}{\partial t} + \frac{\partial}{\partial x} \left(u \left(\mathcal{E} + \frac{gh}{2} \right) \right) \leq 0.$$

On this system we consider the configuration where we measure the water height at every point of the domain. Thus we have on the target trajectory $\{(\check{h}, \check{u}), t > 0\}$,

$$z = \check{h} + \chi. \quad (2.45)$$

In the literature [Auroux and Blum, 2008, Auroux and Nodet, 2008], the following observer has been proposed

$$\begin{cases} \frac{\partial \hat{h}}{\partial t} + \frac{\partial}{\partial x} (\hat{h} \hat{u}) = \gamma(z - \hat{h}) \\ \frac{\partial}{\partial t} (\hat{h} \hat{u}) + \frac{\partial}{\partial x} \left(\hat{h} \hat{u}^2 + \frac{g}{2} \hat{h}^2 \right) = 0 \end{cases}$$

which satisfies the energy balance (even without observation error)

$$\frac{\partial \hat{\mathcal{E}}}{\partial t} + \frac{\partial}{\partial x} \left(\hat{u} \left(\hat{\mathcal{E}} + \frac{g\hat{h}}{2} \right) \right) \leq -\gamma \hat{h} \left(\frac{\hat{u}^2}{2} - g\hat{h} \right)$$

where the right hand side is of uncontrolled sign.

Instead we propose to introduce a kinetic representation of (2.44). Formally, we have an equivalence between the macroscopic conservation law plus its energy inequality and a kinetic formulation of the form

$$\frac{\partial}{\partial t} m(t, x, v) + v \frac{\partial}{\partial x} m(t, x, v) = q(t, x, v) \quad (2.46)$$

where v is the kinetic velocity variable, m is a particle density and q is a collision operator which satisfies

$$\int_{\mathbb{R}} q(t, x, v) dv = 0, \quad \int_{\mathbb{R}} v q(t, x, v) dv = 0, \quad \int_{\mathbb{R}} \frac{v^2}{2} q(t, x, v) dv \leq 0.$$

A density of interest is given by

$$m(t, x, v) = \frac{h}{c} \psi \left(\frac{v - u}{c} \right), \quad \text{with } c = \sqrt{\frac{gh}{2}} \text{ and } \psi(x) = \frac{1}{\pi} \sqrt{1 - \frac{x^2}{4}} \mathbb{1}_{|x| \leq 2}. \quad (2.47)$$

so that in particular the density moments give

$$h = \int_{\mathbb{R}} m(t, x, v) dv, \quad hu = \int_{\mathbb{R}} v m(t, x, v) dv.$$

Then in the kinetic theory [Perthame, 2004], it is known that a system of the form

$$\frac{\partial}{\partial t} f(h, u - v) + v \frac{\partial}{\partial x} f(h, u - v) = \gamma (f(h, u - v) - m(h, u - v))$$

will converge to the solution of (2.46). In [6], we prove that by replacing m with $m_z = \frac{z}{c} \psi(\frac{v-u}{c})$ computed only from the measurement z given in (2.45), we have the same property. In the absence of measurement noise $z = \check{h}$, we end up with the following theorem.

THEOREM 2.3.11 (BOULANGER–MOIREAU–PERTHAME–SAINTE-MARIE)

Let $h(t, x) \in L^\infty([0, T] \times \mathbb{R}_x)$ be solution of (2.44), and $m_z = \frac{z}{c} \psi(\frac{v-u}{c})$. Let $\hat{m}(t, x, v)$ solution of

$$\frac{\partial}{\partial t} \hat{m} + v \frac{\partial}{\partial x} \hat{m} = \gamma (m_z - \hat{m})$$

with the constraint of being of the form (2.47). Assuming some regularity on m_z defined by

$$\frac{\partial}{\partial t} m_z + v \frac{\partial}{\partial x} m_z \left(\frac{v-u}{c^2} \right) m_z = q \in C([0, T], L^1(\mathbb{R}_x \times \mathbb{R}_v))$$

then, there exists $\gamma' > 0$ such that for all $T > 0$

$$\begin{aligned} \|\hat{m}(T) - m_z(T)\|_{L^1(\mathbb{R}_x \times \mathbb{R}_v)} &\leq \|\hat{m}(0) - m_z\|_{L^1(\mathbb{R}_x \times \mathbb{R}_v)} e^{-(\gamma-\gamma')T} \\ &\quad + \sup_{0 \leq t \leq T} \|q(t)\|_{L^1(\mathbb{R}_x \times \mathbb{R}_v)} \frac{1 - e^{-(\gamma-\gamma')T}}{\gamma - \gamma'}. \end{aligned}$$

Note that in our article [6], we also investigate the effect of noise by combining the result from Theorem 2.3.11 and a comparison between the exact $\check{m}_z = \frac{\check{z}}{c} \psi(\frac{v-u}{c})$ and the noisy density $m_z = \frac{z}{c} \psi(\frac{v-u}{c})$.

By taking the moments of the kinetic observer, we then obtain an observer at the macroscopic level, namely here

$$\begin{cases} \frac{\partial \hat{h}}{\partial t} + \frac{\partial}{\partial x} (\hat{h} \hat{u}) = \gamma (z - \hat{h}) \\ \frac{\partial}{\partial t} (\hat{h} \hat{u}) + \frac{\partial}{\partial x} (\hat{h} \hat{u}^2 + \frac{g}{2} \hat{h}^2) = \gamma \hat{u} (z - \hat{h}) \end{cases} \quad (2.48)$$

which, this time, satisfies a controlled energy balance of the form

$$\frac{\partial \hat{\mathcal{E}}}{\partial t} + \frac{\partial}{\partial x} \left(\hat{u} \left(\hat{\mathcal{E}} + \frac{g \hat{h}}{2} \right) \right) \leq -\gamma (\mathcal{E} - \hat{\mathcal{E}}).$$

The advantage of the kinetic representation to design an effective observer (2.48) is now clear. It allows to benefit from the “linearity” to formulate and analyse observers with properties conserved (despite the non-linearity) at the macroscopic level. Moreover the kinetic representation is also well adapted to the formulation of conservative time-schemes [Bristeau et al., 2011]. Hence, in [6], we present an observer discretization that satisfies an energy balance at the discretized level.

2.3.4 Hybrid feedback design

So far we have presented two different alternatives for sequential estimation. The first one is based on optimal control, whereas the second one is more related to approximate controllability. The main advantage of the optimal approach is its genericity, hence the Kalman-like feedback can be designed for any dynamics. However, it faces the “curse of dimensionality” that binds its application with PDEs when not relying on reduced-order strategies. On the contrary, the approach inspired from Luenberger allows to propose effective feedbacks which are easily implementable but necessitate to specifically design the feedback for each dynamics and observations at hand. In our opinion, this is particularly technical when the observation operator gives a very indirect measurement of a state variable as in the two following situations:

- the sequential identification of some parameters using an observation operator which generally acts only on the state,
- the estimation of coupled systems where the measurements are related to only one sub-variable of the state.

For instance, to our best knowledge, the design of Luenberger estimator for parameter identification is limited to very specific situations where typically the whole state is observed [Hoffmann and Sprekels, 1985, Baumeister and Scondo, 1987b, Demetriou and Rosen, 1994a]. For coupled systems, it is classical to limit the action of the feedback on the sub-system which is observed as we did with fluid-structure interaction formulations. To overcome this difficulty, we have proposed a hybrid sequential strategy that combines a Luenberger observer – when available – with a reduced-order optimal feedback on the remaining un-controlled space. We have investigated the potential of this strategy for identification purposes mainly, but also in the context of a weakly coupled system.

2.3.4.1 Joint state and parameter estimator continuous formulation

We first consider a dynamical system where the source term depends of some parameter θ to be estimated. The system then reads

$$\begin{cases} \dot{y}_{|\zeta_y, \nu} = A(t)y_{|\zeta_y, \zeta_\theta} + D(t)\theta_{|\zeta_\theta} \\ y_{|\zeta_y, \zeta_\theta}(0) = y_\diamond + \zeta_y \\ \theta_{|\zeta_\theta} = \theta_\diamond + \zeta_\theta \end{cases}$$

On this system we assume to have the following observation $z = C(t)\check{y} + \chi^5$, about the target solution \check{y} , and we want to jointly estimate the initial condition unknown ζ_y and parameter unknown ζ_θ – see the same question covered in [Alves et al., 2009].

Let us now further assume that we have already designed an effective Luenberger feedback \check{G} for the state dynamics. We denote by \check{y} this state estimator following the dynamics

$$\dot{\check{y}} = A\check{y} + D\check{\theta} + \check{G}(z - C\check{y}), \quad \check{y}(0) = y_\diamond.$$

⁵In the rest of the section the time-dependency of the operators is discarded to ease the reading, but generalization to time-dependent operator is straightforward

We then propose in [24] to extend the state estimation to a joint state-parameter estimation by using a ROKF on the remaining uncontrolled space, namely the parameter space. This is inspired by – hence it unifies – two different works, one on adaptative estimation [Zhang, 2002] and one on reduced-order Kalman approaches [Pham et al., 1998a]. Following our description in Section 2.3.1.4, we end up with the estimator defined by

$$\begin{cases} \dot{\hat{y}} = A\hat{y} + D\hat{\theta} + \check{G}(z - C\hat{y}) + L\dot{\hat{\theta}}, & \hat{y}(0) = y_\diamond, \\ \dot{\hat{\theta}} = U^{-1}L^*C^*R(z - C\hat{y}), & \hat{\theta}(0) = \theta_\diamond, \\ \dot{L} = (A - \check{G}C)L + D, & L(0) = 0, \\ \dot{U} = L^*C^*RCL & U(0) = P^\theta. \end{cases} \quad (2.49)$$

Let us first give some insight on this estimator. The operator L – described in Section 2.3.1.4 as an extension operator – can here be conceived more intuitively as a sensitivity operator. Indeed we have

$$L(t) = d_\theta \check{y}(t), \quad t \geq 0,$$

as they follow the same dynamics starting from the same initial condition. We then understand that the ROKF formulation introduces in the state dynamics of (2.49) a correction $L\dot{\hat{\theta}}$ that integrates the parameter dynamics through the state dynamics.

The analysis of the estimator convergence is based on a similar change of variable as in (2.19)

$$(\tilde{y}, \tilde{\theta}) \mapsto (\eta, \tilde{\theta}) = (\tilde{y} - L\tilde{\theta}, \tilde{\theta}),$$

that leads to the rewriting of the error dynamics into

$$\begin{cases} \dot{\eta} = (A - \check{G}C)\eta, \\ \dot{\tilde{\theta}} = -U^{-1}L^*C^*RCL\tilde{\theta} - U^{-1}L^*C^*RC\eta + U^{-1}L^*C^*R\chi. \end{cases} \quad (2.50)$$

With (2.50) we understand precisely the key element of the joint estimator convergence. First we see that η follows the same error as the state observer error dynamics $\check{y} - \hat{y}$, and η should converge to 0 as soon as the state observer is properly designed. Therefore we can focus on the parameter error by demonstrating that $U^{-1}L^*C^*RC\eta$ converges to 0. The homogeneous part of the parameter error

$$\dot{\tilde{\theta}} = -U^{-1}L^*C^*RCL\tilde{\theta},$$

follows a Grammian-based dynamics remarkable of a Kalman-like approach with U a covariance operator and L^*C^*RCL a positive operator feeding the covariance dynamics. For instance, a Liapunov approach [Zhang and Xu, 2001] gives the convergence of this homogenous part under an identifiability condition of the form

$$\exists(c_1, c_2, T), \quad c_1 \|\theta\|_{\mathcal{P}, N_\theta}^2 \geq \int_0^T \|C(L\theta)\|_{\mathcal{Z}, \mathbb{R}}^2 dt \geq c_2 \|\theta\|_{\mathcal{P}, N_\theta}^2, \quad (2.51)$$

Following this intuitive strategy, we proceed in [24] to the complete analysis of the estimation error. We consider a stochastic set-up for the noise but limit our proof to a spatially discretized system to avoid the technicalities of cylinder set measures that would have been introduced with a space- and time-continuous white noise. Hence, we recall that in [24] the observation

operator measures the average velocity on set of q cells with weights α_i as described above Proposition 2.38. However, we believe that similar results can be obtained on a deterministic infinite dimensional set-up.

THEOREM 2.3.12 (MOIREAU-CHAPELLE-LE TALLEC)

We define $\lambda_{\inf}(t)$ as as the smallest solution of the generalized eigenvalue problem

$$L^T C^T R C L \theta = \lambda U \theta,$$

then, if the state estimator is exponentially stable, we have that

$$\begin{aligned} \mathbb{E}(\|\tilde{\theta}\|_{U(0)}^2) \leq & \frac{c}{(1 + \lambda_{\inf}(t))^2} \left\{ 1 + \|L\|_{L^2([0,T];\mathcal{L})}^2 \left[c_{\text{obs}}^2 \left(\sum_{i=1}^q (\alpha_i)^2 \sum_{j=1}^3 \|v_i^j\|_{\mathbb{R}}^2 \right) \right. \right. \\ & \left. \left. + (c_{\text{obs}})^4 \left(\tau \mathbb{E}(\|\zeta_y\|_{\mathcal{Y}}^2) + (1 + t \tau \gamma^2) \|\check{y} - \check{y}_h\|_{L^2([0,T];\mathcal{Y})}^2 + t \tau \gamma^2 \sum_{i=1}^q \alpha_i^2 \right) \right] \right\}, \end{aligned} \quad (2.52)$$

where τ is the time constant directly related to the exponential stability of the chosen state observer and given in Proposition 2.3.6.

We further underline that the condition (2.51) is a natural condition for identification purposes exploited in the literature [Zhang, 2002, Demetriou and Rosen, 1994b]. It is very similar to an observability condition applied to the parameter through the use of the sensitivity operator L . Therefore, we believe that this condition can be precisely stated in various configurations as it is for instance – in a similar form – in [Alves et al., 2009].

Another important remark concerns the crucial role of the state estimator in our joint estimation. Numerous identification approaches are based on a variational criterion that only takes into account the parameter uncertainties [Chavent, 2010]

$$\mathcal{J}(\zeta_\theta, T) = \frac{1}{2} \|\theta\|_{\mathcal{P}, N_\theta}^2 + \frac{1}{2} \int_0^T \|z - C y_{|\zeta_\theta}\|_{\mathcal{Z}, \mathbb{R}}^2 dt. \quad (2.53)$$

Sometimes, it is even proved that the identification problem is then well posed under the condition of perfectly well known initial state condition. With our approach, we see that this kind of result can be shown to be very sensitive to any state errors: initial condition errors but also discretization errors or model errors. Indeed, one fundamental advantage of relying on ROKF is that we know that ROKF is equivalent to the minimization of a variational criterion on the reduced space. For our parameter estimation, we then show in [24] that our joint state-parameter estimation is equivalent to the minimization of

$$\mathcal{J}(\zeta_\theta, T) = \frac{1}{2} \|\theta\|_{\mathcal{P}, N_\theta}^2 + \frac{1}{2} \int_0^T \|z - C \check{y}_{|\zeta_\theta}\|_{\mathcal{Z}, \mathbb{R}}^2 dt, \quad (2.54)$$

where now it is the state observer which appears in the minimization. Now, if we choose $G_y = 0$ we retrieve the classical criterion (2.53) but end up in our observer convergence analysis with an autonomous dynamics for η i.e. $\dot{\eta} = A\eta$. Hence if A is skew-symmetric as for example for the wave equation, then η does not converge to 0 as soon as $\eta(0) = \tilde{y}(0) \neq 0$ and the parameter-only estimator does not converge anymore. **This means that the state observer is almost mandatory to ensure the robustness of any parameter identification problem.**

REMARK 2.3.6 (INITIAL CONDITION ESTIMATION)

We point out that such an adaptive observer allows to identify the initial condition even for parabolic problems as in this case we define $y_{|\zeta_y, \zeta_\theta}(0) = y_\circ + \Pi \zeta_\theta$. We use this strategy in [18] with a reaction-diffusion problem.

2.3.4.2 Joint state and parameter estimator discretizations

A second fundamental advantage on relying on ROKF to formulate the adaptive observer (2.49) is that we directly know an efficient discretization. First, we consider a uniformly convergent discretization for the state observer such as we did for the wave equation in Section 2.3.2.3

$$\begin{cases} \check{y}_{n+1|\zeta_\theta} = A_{n+1|n}\check{y}_{n|\zeta_\theta} + D_n\theta_{|\zeta_\theta} + \check{G}_n(z - C_n\check{y}_n) \\ \check{y}_{0|\zeta_\theta} = y_\diamond \\ \check{\theta}_{0|\zeta_\theta} = \theta_\diamond + \zeta_\theta \end{cases}$$

We can then use the discrete-time ROKF to formulate a consistent and stable discretization of the parameter dynamics hence of the joint state-parameter estimation. We end up with a prediction correction scheme on top of the state discretization – which, by the way, can also use a splitting time-scheme. The complete estimator reads

1. Initialization:

$$\begin{cases} \hat{y}_0^- &= y_\diamond \\ \hat{\theta}_0^- &= \theta_\diamond \\ L_0 &= 0 \\ U_0 &= U_\diamond \end{cases}$$

2. Prediction:

$$\begin{cases} \hat{y}_{n+1}^- &= A_{n+1|n}y_n^+ + D_n\hat{\theta}_n^+ + \check{G}_n(z - C_n\hat{y}_n^+) \\ \hat{\theta}_{n+1}^- &= \hat{\theta}_{n+1}^+ \\ L_{n+1} &= A_{n+1|n}L_n \\ U_{n+1} &= U_n + L_{n+1}^\top C_{n+1}^{-\top} R_{n+1} C_{n+1} L_{n+1} \\ (P_{y,n+1}^- &= L_n U_{n+1}^{-1} L_n^\top) \end{cases}$$

3. Correction:

$$\begin{cases} G_{\theta,n+1} &= U_{n+1}^{-1} L_{y,n+1}^\top C_{n+1}^\top R_{n+1} \\ \hat{y}_{n+1}^+ &= \hat{y}_{n+1}^- + L_{n+1} G_{\theta,n+1} (z_{n+1} - C_{n+1} \hat{y}_{n+1}^-) \\ \hat{\theta}_{n+1}^+ &= \hat{\theta}_{n+1}^- + G_{\theta,n+1} (z_{n+1} - C_{n+1} \hat{y}_{n+1}^-) \\ (P_{y,n+1}^+ &= L_{n+1} U_{n+1}^{-1} L_{n+1}^\top) \end{cases}$$

Note that here the scheme starts with a prediction since the first correction would have been null.

2.3.4.3 H^∞ extensions

Another strong advantage of the optimal control structure of our adaptive observer is that the H^2 criterion (2.54) can be replaced by a H^∞ criterion as we propose in [16]. The principle is to define the reduced-order parameter estimator by seeking

$$\sup_{z, \zeta_\theta} \frac{\int_0^T \|\hat{y} - \check{y}_{|\zeta_\theta}\|_{O_y}^2 + \|\hat{\theta} - \zeta_\theta\|_{O_\theta}^2 dt}{\|\zeta_\theta\|_{N_\theta}^2 + \int_0^T \|z - C\check{y}_{|\zeta_\theta}\|_R^2 dt} \leq \frac{1}{\varrho},$$

Then – as is classical in H^∞ theory, see e.g. [Başar and Bernhard, 1995] – we replace the inf-sup criterion by the following cost function

$$\mathcal{J}^\varrho(\zeta_\theta, T) = \frac{1}{2} \int_0^T \|\hat{y} - \check{y}_{|\zeta_\theta}\|_{O_y}^2 + \|\hat{\theta} - \zeta_\theta\|_{O_\theta}^2 dt - \frac{1}{2\varrho} \left(\|\zeta_\theta\|_{N_\theta}^2 + \int_0^T \|z - C\check{y}_{|\zeta_\theta}\|_R^2 dt \right).$$

on which we seek stationary points. We easily end up with a reduced-order H^∞ filter to be applied to the parameter space modifying (2.49) into

$$\begin{cases} \dot{\hat{y}} = A\hat{y} + D\hat{\theta} + \check{G}(z - C\hat{y}) + L\dot{\hat{\theta}}, & \hat{y}(0) = y_\diamond \\ \dot{\hat{\theta}} = U^{-1}L^*C^*R(z - C\hat{y}), & \hat{\theta}(0) = \theta_\diamond \\ \dot{L} = (A - \check{G}C)L + D, & L(0) = 0 \\ \dot{U} = L^*C^*RCL - \varrho(L^\top O_y L + O_\theta) & U(0) = P^\theta \end{cases}$$

Here, we emphasize that the essential difference with the observer formulated in (2.49) lies in the dynamics of U , namely, with the “negative” term associated with ϱ in the right-hand side.

Then in [16] the same type of error analysis as in Theorem 2.3.12 is carried on.

2.3.4.4 Non-linear extensions

One final interest of the ROKF setting is its easy generalization in non-linear situation. In [23,24] we typically studied the case where

$$\begin{cases} \dot{y}_{|\zeta, \nu} = A(\theta_{|\zeta_\theta}, t)y_{|\zeta_y, \zeta_\theta} + \beta(t) \\ y_{|\zeta_y, \zeta_\theta}(0) = y_\diamond + \zeta_y \\ \theta_{|\zeta_\theta} = \theta_\diamond + \zeta_\theta \end{cases}$$

Then the prediction steps of joint-state estimator is directly modified into

1. Prediction:

$$\begin{cases} \hat{y}_{n+1}^- & = A_{n+1|n}(y_n^+, \hat{\theta}_n^+) + \check{G}_n(z - C_n \hat{y}_n^+) \\ \hat{\theta}_{n+1}^- & = \hat{\theta}_{n+1}^+ \\ L_{n+1} & = dA_{n+1|n} L_n \\ U_{n+1} & = U_n + L_{n+1}^\top C_{n+1}^- \check{R}_{n+1} C_{n+1} L_{n+1} \\ (P_{y,n+1}^- & = L_n U_{n+1}^{-1} L_n^\top) \end{cases}$$

Concerning the analysis, one possible strategy is to use the EKF stability property for small errors [Reif and Unbehauen, 1999, Krener, 2003a, Bonnabel and Slotine, 2015] to obtain an extended result of (2.52). Then two major difficulties remain: (1) we will need to prove a persistent excitation property in a non-linear system configuration and (2) the convergence of the state estimator needs to be robust with respect to the parameter dependency as the operator dynamics is now a function of uncertain parameters.

When seeking a discretization, we can consider the discrete-ROEKF. But since the analysis should be based on linearization, we can also rely on a ROUKF formulation at the time-discretized level as sketched in Figure 2.2.

We then end up with the following discrete estimator, proposed in [23]

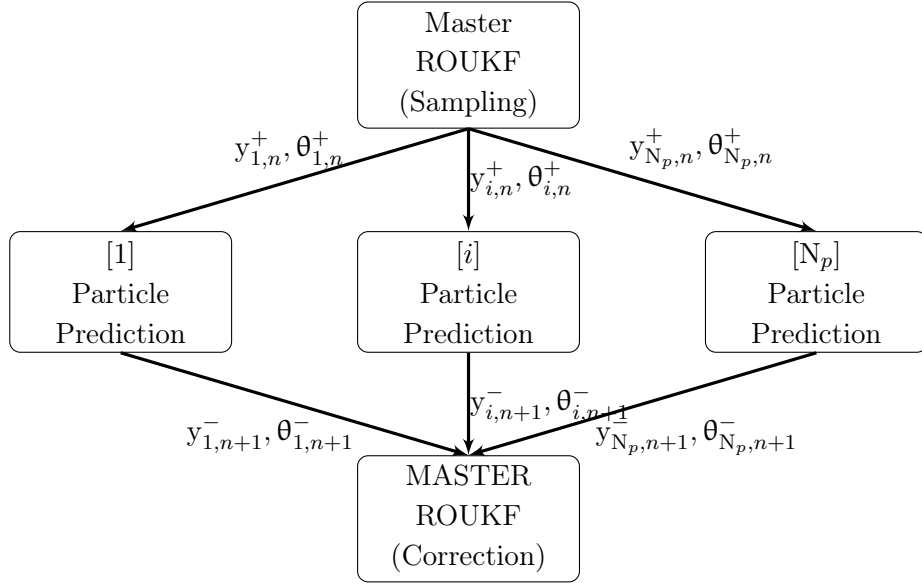


Figure 2.5: Estimation algorithm

1. Initialization:

$$\begin{cases} \hat{y}_n^- &= y_\diamond \\ L_{y,0} &= 0 \\ L_{\theta,0} &= \mathbb{1} \\ U_0 &= U_0 \end{cases}$$

2. Sampling

$$\begin{cases} \Gamma_n &= \sqrt{U_n^{-1}} \\ \hat{y}_{n,i}^- &= \hat{y}_n^- + L_{y,n} \Gamma_n e_i \\ \hat{\theta}_{n,i}^- &= \hat{\theta}_n^- + L_{\theta,n} \Gamma_n e_i \end{cases}$$

3. Prediction:

$$\begin{cases} \hat{y}_{n+1,i}^- &= A_{n+1|n}(y_{n,i}^+, \theta_{n,i}^+) + \check{G}_n(z - C_n y_{n,i}^+) \\ \hat{y}_{n+1}^- &= \mathbb{E}_\alpha(\hat{y}_{n+1}^-) \\ L_{y,n+1} &= \hat{y}_{n+1}^- d_\alpha e^\top \\ L_{\theta,n+1} &= \hat{\theta}_{n+1}^+ d_\alpha e^\top \end{cases}$$

4. Re-Sampling (possibly)

$$\begin{cases} \Gamma_{n+1} &= \sqrt{U_{n+1}^{-1}} \\ \hat{y}_{n+1,i}^- &= \hat{y}_{n+1}^- + L_{y,n+1} e_i \end{cases}$$

5. Correction:

$$\begin{cases} \hat{z}_{n+1,i}^- &= C_{n+1}(\hat{y}_{n+1,i}^-, \hat{\theta}_{n+1,i}^-) \\ \Upsilon_{n+1} &= \hat{z}_{n+1}^- \mathbf{d}_\alpha \mathbf{e}^\top \\ U_{n+1} &= \mathbb{1} + \Upsilon_{n+1}^\top \mathbf{R}_{n+1} \Upsilon_{n+1} \\ \hat{y}_{n+1}^+ &= \hat{y}_{n+1}^- + L_{y,n+1} \Upsilon_{n+1}^\top \mathbf{R}_{n+1} (z_{n+1} - \mathbb{E}_\alpha(\hat{z}_{n+1}^-)) \\ \hat{\theta}_{n+1}^+ &= \hat{\theta}_{n+1}^- + L_{\theta,n+1} \Upsilon_{n+1}^\top \mathbf{R}_{n+1} (z_{n+1} - \mathbb{E}_\alpha(\hat{z}_{n+1}^-)) \end{cases}$$

which leads to the same error analysis as for (2.55) after linearization of the operators. In fact, in [23] we prove that the change of variable should be in this case

$$(\tilde{y}_n, \tilde{\theta}_n) \mapsto (\eta_n, \mu_n) = (\tilde{y}_n - L_{y,n} L_{\theta,n}^{-1} \tilde{\theta}_n, L_{\theta,n}^{-1} \tilde{\theta}_n).$$

The advantage of this formulation is its simplicity of implementation following the algorithm illustrated in Figure 2.5. Here again the scheme starts with a prediction since the correction would have been null. **The simplicity and parallel structure of this scheme allows its used with a variety of models, see for instance [3, 20] or [Marchesseau et al., 2012, Lombardi, 2013, Xiao, 2013].**

2.3.4.5 An estimator for a weakly coupled system appearing in cardiac electromechanics

One final example of hybrid observer is the one formulated in [19] for a weakly coupled system appearing in cardiac electromechanics. We recall that the electrical activation of the cardiac tissue is the input of the heart contraction. Moreover, numerous works neglect the mechanical effects and the domain deformation on the cardiac action potential propagation. Eventually, we end up with a formulation

$$\begin{cases} \dot{y}^\ell = A^\ell(y^\ell), & y^\ell(0) = y_\diamond^\ell + \zeta^\ell, \\ \dot{y}^m = A^m(y^m, y^\ell), & y^m(0) = y_\diamond^m + \zeta^m. \end{cases}$$

written after spatial discretization to ease the presentation. On this system we assume to have at our disposal a measurement of the mechanical displacement field on a subdomain typically extracted from tagged-MRI – see Section 2.4.1.3

$$z^m(t) = C^m y^m + \chi^m.$$

Moreover, on the electrical part we consider to have the ECG signal that we recall to correspond to the measurement at the surface of the skin of the electrical potential diffused through the thorax

$$z^\ell(t) = C^\ell y^\ell + \chi^\ell.$$

Having in mind these two types of observations, we can envision a Luenberger observer on the mechanical part as described in Section 2.3.3.1 and a POD-based reduced-order Kalman-like filter (see Section 2.3.1.4) for the electrical part. One possibility to design the resulting observer is to introduce a block-diagonal feedback for the coupled system. However, a more involved

approach consists in incorporating the mechanical measurement directly into the control of the electrical part with our hybrid observer strategy.

In the sequel, we use the notation “ d_m ” et “ d_ℓ ” for the partial derivative with respect to y^m and y^ℓ , respectively, whereas d is used for the total derivative. We introduce in our ROEKF $L = \begin{pmatrix} L^\ell \\ L^m \end{pmatrix}$, $C = \begin{pmatrix} C^\ell & 0 \\ 0 & C^m \end{pmatrix}$ and $z = \begin{pmatrix} z^\ell \\ z^m \end{pmatrix}$, so that the dynamics reads

$$\begin{cases} \dot{\hat{y}}^\ell = A^\ell(\hat{y}^\ell) + L^\ell U^{-1} L^\top dC^\top R(z - C(\hat{y})) \\ \dot{\hat{y}}^m = A^m(\hat{y}^m, \hat{y}^\ell) + \check{G}^m(z^m - C^m(\hat{y}^m)) + L^m U^{-1} L^\top dC^\top R(z - C(\hat{y})) \\ \dot{L}^\ell = (dA^\ell(\hat{y}^\ell))L^\ell \\ \dot{L}^m = (d_m A^m(\hat{y}^m, \hat{y}^m) - \check{G}^m dC^m(\hat{y}^m))L^m + (d_\ell A^m(\hat{y}^m, \hat{y}^\ell))L^\ell \\ \dot{U} = L^\top (dC)^\top R (dC) L \end{cases} \quad (2.58)$$

starting from $\hat{y}^\ell(0) = y_\diamond^\ell$, $\hat{y}^m(0) = y_\diamond^m$, $L^m = 0$, $L^\ell = \mathbb{1}$ and $U(0) = U_\diamond^\ell$.

Note that in the dynamics (2.58), the Luenberger filter applies only on the mechanical part. However, the optimal filter corrects the electrophysiology evolution from the electrical measurements and the mechanical measurement. This correction is then reverberated

$$\dot{\hat{y}}^m = A^m(\hat{y}^m, \hat{y}^\ell) + \check{G}^m(z^m - C^m(\hat{y}^m)) + L^m (L^\ell)^{-1} \dot{\hat{y}}^\ell,$$

when assuming (L^ℓ) invertible.

To obtain some element of analysis, we get after linearization of the error dynamics, the following system of the linearized error

$$\begin{cases} \delta \tilde{y}^\ell &= -U^{-1} L^\top (dC)^\top R (dC) \delta \tilde{y}, \\ \delta \tilde{y}^m &= (d_m A - \check{G}^m d_m C^m) \delta \tilde{y}^m + (d_\ell A) \delta \tilde{y}^\ell + L^m (L^\ell)^{-1} \delta \tilde{y}^\ell \end{cases}$$

starting from $\delta \tilde{y}^\ell(0) = \zeta^\ell$ et $\delta \tilde{y}^m(0) = \zeta^m$.

Here we introduce the change of variables

$$(\delta \tilde{y}^m, \delta \tilde{y}^\ell) \mapsto (\delta \eta, \delta \mu) = (\delta \tilde{y}^m - L^m (L^\ell)^{-1} \delta \tilde{y}^\ell, (L^\ell)^{-1} \delta \tilde{y}^\ell),$$

and obtain

$$\begin{cases} \dot{\delta \eta} &= (d_m A - \check{G}^m d_m C^m) \delta \eta, \quad \delta \eta(0) = \zeta^m \\ \dot{\delta \mu} &= -U^{-1} L^\top (dC)^\top R (dC) L \delta \mu, \\ &\quad -U^{-1} L^\top (d_m C^m)^\top R^m (d_m C^m) \delta \eta, \quad \delta \tilde{y}^\ell(0) = \zeta^\ell. \end{cases}$$

The first equation corresponds to the dynamics of the linearized error studied for the mechanical system. Hence it converges to 0. Therefore the second term in the second equation tends to 0. The homogeneous part of the second equation can then be proved to converge to 0 if the following observability condition (2.59) is satisfied with our linear observation operator – namely, $dC = C$ in our particular example. Namely, we expect for all initial error $\delta \tilde{y}^\ell(0)$ that

$$\exists(C, T_0), \quad \forall T \geq T_0, \quad \int_0^T \|C(L\delta\mu\|_{\mathbb{R}}^2 \geq C \|\delta \tilde{y}^\ell(0)\|_{U_\diamond^\ell}^2, \quad (2.59)$$

which can be at least verified numerically. In the last observability condition, we have that $L\delta\mu = L(L^\ell)^{-1} \delta \tilde{y}^\ell$ represents the effect of a variation on $\delta \tilde{y}^\ell$ on both the electrophysiology and the mechanics. This effect is then observed through C . The observability is thus expected to be improved with respect to the situation where only the electrophysiology is considered. This will be confirmed numerically.

2.4 Shape-based data assimilation

In recent works, the question has been raised of taking into account more **indirect** observations than $z = C\tilde{y} + \chi$, as in an **image** $\mathcal{I}[\tilde{y}]$ that gives the shape of the solution pattern, *i.e.* not a direct measurement of the state. For instance, in weather forecasting numerous contributions deal with information contained in satellite images where we can track moving clouds, hence compute wind flows [Titaud et al., 2010]. In cardiac medical imaging, it is common to image the beating heart under time sequences of 2D or 3D images. By processing these images, one hopes to extract a flow field or a displacement field of the heart [Carranza-Herrezuelo et al., 2010, Le Guyader and Vese, 2011], see Figure 2.6.

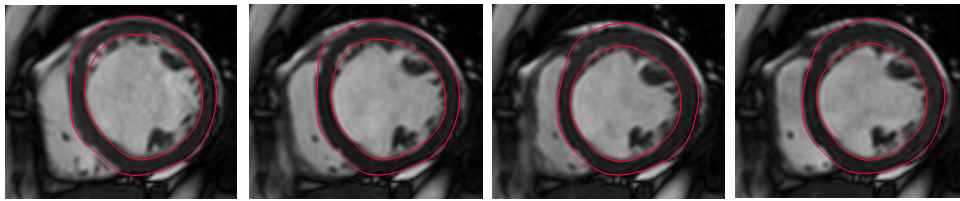


Figure 2.6: A cine-MRI sequence with segmented left ventricle

In wildfire propagation, images data allow to follow the front propagation of the fire. Similarly, in electrophysiology, actual reconstruction of the heart electrical activity from body surface potential (ECGI) aims at building at the epicardium a map of the depolarization time, hence a measurement of the propagating depolarization front [Ramanathan et al., 2004]. We can also think of ice sheet forming observations, species dispersion monitoring *etc.* where shapes associated with the PDE solutions are observed, see Figure 2.7.

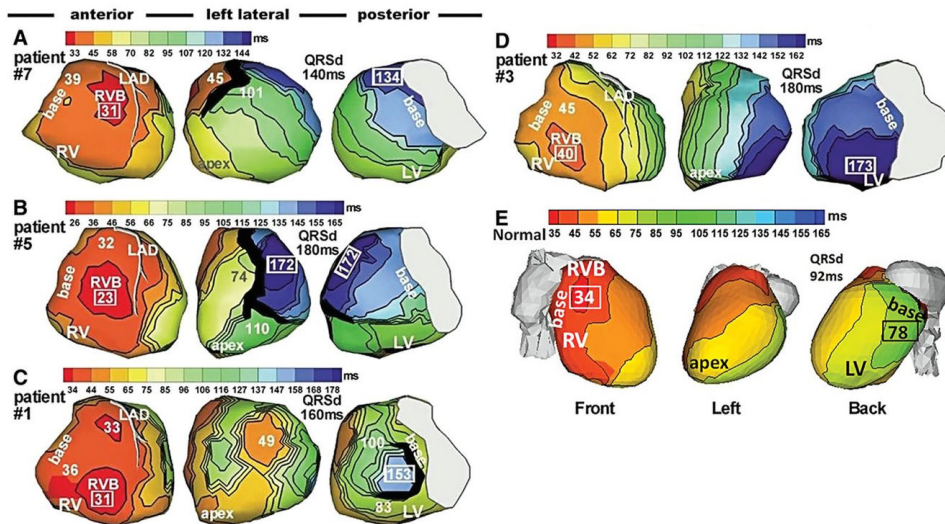


Figure 2.7: Epicardial isochrone maps reconstructed from ECGI for 4 representative heart failure – reproduced from [Rudy, 2013]

In fact, we believe that these complex observations will represent the future of data assimilation and we have tried so far to initiate this research direction in cardiac applications with two contributions:

- how to use a time-sequence of images of deforming organs to jointly estimate the state and parameters of a mechanical model,
- how to estimate a full bidomain model (reaction-diffusion) from front data typically obtained from time-depolarization maps.

2.4.1 Motion extraction from images by sequential estimation based on a biomechanical model

2.4.1.1 Estimation from segmentation of moving object based on simple distances computations

In the work [8] – resp. [21] – we consider the case where the wall motion of the heart – resp. an artery – is tracked *via* a time-sequence of segmented 3D images – MRI in [8], in CT [21]. These segmentations generate a sequence of surface objects $(\mathfrak{S}_k)_{1 \leq k \leq N_j}$ representing the boundary of the system to be modeled. From a practical point of view, we can consider that these surfaces are numerically stored as triangular meshes $(\mathfrak{T}_k)_{1 \leq k \leq N_j}$.

In correspondence with these observations, we assume to have a model of the mechanical behavior of the system of interest such as in Section 1.3.2. Namely, we assume that we can simulate a model of the solid displacement

$$\begin{cases} \partial_t \underline{u} = \underline{v}, & \text{in } \Omega_0 \\ \rho \partial_t \underline{v} - \operatorname{div}(\underline{T}) = 0, & \text{in } \Omega_0 \end{cases} \quad (2.60)$$

As it is not straightforward to compare a surface object from the state solution of the mechanical system (2.60), we do not introduce in [25] a standard observation operator of the form $z = C\hat{y} + \chi$. Instead, we notice that in estimation, an observation alone is never considered since it is always compared to the model with the computation of the innovation $z - C\hat{y}$. More generally in data assimilation, we only need to define a discrepancy operator – or similarity operator depending of the point of view – J generalizing the comparison

$$J(z, y) = z - Cy,$$

when the subtraction operation can not be defined. We thus decide to rely on distance operators to define the discrepancy between the surfaces object and the state of our mechanical system. First, assuming that the surfaces are available for all time, we introduce the signed distance field

$$\underline{\operatorname{dist}}_{\mathfrak{S}} : \begin{cases} (L^2(\Sigma))^3 \mapsto (L^2(\Sigma))^3 \\ \underline{x}(\underline{\xi}) \rightarrow \operatorname{dist}_{\mathfrak{S}}(\underline{x}(\underline{\xi})) \end{cases}$$

Note that the signed distance allows to determine on which side of the surface the model lies. Based on these distance fields, we can build a discrepancy measure defined for example as the $L^2(\Sigma)$ -norm of the distance on the surface

$$J(z, y) = \operatorname{meas}_{L^2(\Sigma)}\{\mathfrak{S}\}(y, t) = \int_{\Sigma} |\operatorname{dist}_{\mathfrak{S}}(\underline{\xi} + \underline{u}(\underline{\xi}, t), t)|^2 d\Gamma, \quad (2.61)$$

which is null for the pursued actual displacement field. Therefore, if this discrepancy vanishes, then the given state is consistent with the observations. The nudging direction is then obtained

by differentiating the distance with respect to the state, namely $\underline{n}_{\mathfrak{S}}(\underline{\xi} + \underline{u}, t)$ which is directly related to be the tangent field of the distance [25].

The distance (2.61) considers an L^2 -norm on the interface Σ , but other norms are possible. However, we have seen in Section 2.3.3.1 – see also the spectral comparison in [25] – for linear elasticity that an $H_{\frac{1}{2}}$ -norm defined with a lifting operator Ext is a more effective norm for the state observer. The question is now to generalize this idea for non-linear discrepancy operators. We then propose in [25] the following extension

$$\text{meas}_{H^{\frac{1}{2}}(\Sigma)}\{\mathfrak{S}\}(y, t) = \int_{\Omega_0} \|\text{Ext}(\text{dist}_{\mathfrak{S}}(\underline{\xi} + \underline{u}, t); \underline{n}_{\mathfrak{S}})\|_{\mathcal{E}_l}^2 d\Omega,$$

with $\|\cdot\|_{\mathcal{E}_l}^2$ the norm associated with the linearized elastic energy in the solid, namely, equivalent to the H^1 -norm and

$$\underline{\psi}^{\text{ext}} = \text{Ext}(\psi; \underline{\tau}) : \begin{cases} \text{div}(\underline{\underline{A}} : \underline{\underline{\varepsilon}}(\underline{\psi}^{\text{ext}})) = 0 & \text{in } \Omega \\ \underline{\psi}^{\text{ext}} \cdot \underline{\tau} = \psi & \text{in } \Gamma_{\text{obs}}^u \\ (\underline{\underline{A}} : \underline{\underline{\varepsilon}}(\underline{\psi}^{\text{ext}})) \cdot \underline{\tau}_1^\perp = (\underline{\underline{A}} : \underline{\underline{\varepsilon}}(\underline{\psi}^{\text{ext}})) \cdot \underline{\tau}_2^\perp = 0 & \text{in } \Gamma_{\text{obs}}^u \\ \text{same boundary conditions as the model} & \text{on } \partial\Omega \setminus \Gamma_{\text{obs}}^u \end{cases}$$

is a lifting of a scalar data given on the boundary along the direction $\underline{\tau}$, – with $(\underline{\tau}, \underline{\tau}_1^\perp, \underline{\tau}_2^\perp)$ giving a local orthonormal basis. Therefore its corresponding discrepancy operator becomes

$$\mathcal{P}_{H^{\frac{1}{2}}(\Sigma)}\{\mathfrak{S}\}(y, t)(\underline{u}^b) = \int_{\Omega_0} \left\langle \text{Ext}(\text{dist}_{\mathfrak{S}}(\underline{\xi} + \underline{u}, t); \underline{n}_{\mathfrak{S}}), \text{Ext}((\underline{u}^b \cdot \underline{n}_{\mathfrak{S}}); \underline{n}_{\mathfrak{S}}) \right\rangle_{\mathcal{E}_l} d\Omega, \quad \underline{u}^b \in \mathcal{V}.$$

This operator can be shown to be close for small distances to

$$\mathcal{P}_{H^{\frac{1}{2}}(\Sigma)}\{\mathfrak{S}\}(y, t)(\underline{u}^b) = \int_{\Omega_0} \left\langle \text{Ext}(\text{dist}_{\mathfrak{S}}(\underline{\xi} + \underline{u}, t); \underline{n}_{\mathfrak{S}}), \underline{u}^b \right\rangle_{\mathcal{E}_l} d\Omega,$$

using the extension characterization– see [Imperiale, 2013]. The discrepancy is used as a correction term in the equation relating the solid displacement time derivative to the solid velocity to ensure the stabilization of the state estimator as described for linear elastodynamics system. In [25], we also develop some linearization arguments to justify the extension in non-linear formulations. One remaining difficulty lies in the linearization of non-linear mechanical formulations that are known to be ill-posed around certain trajectories (for instance around compression). Hence the complete analysis remains to be done. Eventually, we propose the following observer correction in weak form

$$\forall \underline{u}^b \in \mathcal{V}, \int_{\Omega_0} \left\langle \frac{\partial \hat{\underline{u}}}{\partial t}, \underline{u}_s^b \right\rangle_{\mathcal{E}_l} d\Omega = \int_{\Omega_0} \langle \hat{\underline{v}}, \underline{u}^b \rangle_{\mathcal{E}_l} d\Omega + \gamma \int_{\Omega_0} \left\langle \text{Ext}(\text{dist}_{\mathfrak{S}}(\underline{\xi} + \hat{\underline{u}}, t); \underline{n}_{\mathfrak{S}}), \underline{u}^b \right\rangle_{\mathcal{E}_l} d\Omega,$$

where γ represents the gain parameter to adjust the nudging. Hence in strong formulation we substitute

$$\frac{\partial \hat{\underline{u}}}{\partial t} = \hat{\underline{v}} + \gamma \text{Ext}(\text{dist}_{\mathfrak{S}}(\underline{\xi} + \hat{\underline{u}}, t); \underline{n}_{\mathfrak{S}}),$$

replacing the canonical identity $\frac{\partial u}{\partial t} = v$.

Concerning the space discretization of such observers, the non-linear extension of what we propose in the linear case in Section 2.3.3.1 is quite straightforward and is presented in [25]

$$(\epsilon \mathbf{K} + \mathbf{d}_u \mathbf{J} \mathbf{M}_\Sigma \mathbf{d}_u \mathbf{J}) \frac{\partial \hat{\underline{u}}}{\partial t} = (\epsilon \mathbf{K} + \mathbf{d}_u \mathbf{J} \mathbf{M}_\Sigma \mathbf{d}_u \mathbf{J}) \hat{\underline{v}} - \gamma \mathbf{d}_u \mathbf{J}^\top \mathbf{M}_\Sigma \mathbf{J}(\underline{z}, \hat{\underline{u}}). \quad (2.62)$$

Concerning the time discretization, one key aspect of our observer formulation is to limitate the cost of the feedback computation. We propose in [25] an elegant mid-point scheme of the form

$$(\epsilon\mathbf{K} + \mathbf{d}_u\mathbf{J}\mathbf{M}_\Sigma \mathbf{d}_u\mathbf{J})\frac{\hat{\mathbf{u}}_{n+1} - \hat{\mathbf{u}}_n}{\Delta t} = (\epsilon\mathbf{K} + \mathbf{d}_u\mathbf{J}\mathbf{M}_\Sigma \mathbf{d}_u\mathbf{J})\hat{\mathbf{v}}_{n+\frac{1}{2}} - \gamma \mathbf{d}_u\mathbf{J}^\top\mathbf{M}_\Sigma\mathbf{J}(z_{n+\frac{1}{2}}, \hat{\mathbf{u}}_{n+\frac{1}{2}})$$

We point out that there is no need to compute the second derivative of \mathbf{J} related to curvature computations to obtain a stable feedback for small errors at the discrete level. Then we propose in [33, 34] – see details in [Imperiale, 2013] – an even more efficient prediction-correction time scheme

$$\text{Correction: } \hat{\mathbf{u}}_{n+1}^+ = \hat{\mathbf{u}}_{n+1}^- - \gamma\Delta t(\epsilon\mathbf{K} + \mathbf{d}_u\mathbf{J}\mathbf{M}_\Sigma \mathbf{d}_u\mathbf{J})^{-1} \mathbf{d}_u\mathbf{J}^\top\mathbf{M}_\Sigma\mathbf{J}(z_{n+1}, \hat{\mathbf{u}}_{n+1})$$

interpretable as a BLUE algorithm with *a priori* covariance $\epsilon\mathbf{K}^{-1}$, an observation covariance $\gamma\Delta t\mathbf{M}_\Sigma$ and a tangent observation operator $-\mathbf{d}_u\mathbf{J}$.

In the beginning of this section, we mentioned that in practice a sequence of images is finite with a certain sampling. As we discussed for the linear wave equation, we face the alternative: (1) use the data only when they are available or (2) interpolate the data information. The question is now to give a sense to the solution (2) when the data are in fact surfaces. We show in [25] that the good definition of the notion of interpolation is to interpolate not the data – namely the surfaces – but the discrepancies. For instance the L^2 -measure (2.61) becomes

$$J(\underline{u}, t) = \text{meas}_{L^2(\Sigma)}\{\mathfrak{S}_k\}(y, t) = \int_{\Sigma} |\text{dist}_{\{\mathfrak{S}_k\}}(\underline{\xi} + \underline{u}, t)|^2 d\Gamma,$$

with

$$\underline{\text{dist}} : \begin{cases} L^2(\Sigma) \times [0, T] \mapsto L^2(\Sigma) \\ (\underline{x}(\underline{\xi}), t) \rightarrow \left(\frac{t_{k+1}-t}{\Delta T}\right)\text{dist}_{\mathfrak{S}_k}(\underline{x}(\underline{\xi})) + \left(\frac{t-t_k}{\Delta T}\right)\text{dist}_{\mathfrak{S}_{k+1}}(\underline{x}(\underline{\xi})), \quad t \in [t_k, t_{k+1}] \end{cases}$$

and a nudging direction $\left(\frac{t_{k+1}-t}{\Delta T}\right)\underline{n}_{\mathfrak{S}_k}(\underline{x}(\underline{\xi})) + \left(\frac{t-t_k}{\Delta T}\right)\underline{n}_{\mathfrak{S}_{k+1}}(\underline{x}(\underline{\xi}))$ when $t \in [t_k, t_{k+1}]$. Note that again this choice implies that the feedback is no more causal.

2.4.1.2 Estimation from segmentation of moving object based on the theory of Currents

In the previous section, we built a discrepancy measure using a simple signed distance between the given surface data and the corresponding deformed model geometries. However, computing simple distances is not (by far) the state of the art strategy to compare shapes [Younes, 1998, Younes, 2010]. Hence, we may suffer from standard disadvantages as illustrated in Figure 2.8. The efficiency of the data assimilation procedure can then be deteriorated in complex geometrical situations. In order to avoid these matching difficulties, we consider the formalism of surface currents [Vaillant and Glaunès, 2005, Durrleman et al., 2009, Younes, 2010] which has been successfully used in the field of medical image analysis, and represents one of the state-of-the-art *geometrical data representation*. In fact we investigate in [34] – see more details in [Imperiale, 2013] – how the obtained observability is improved. Naturally, this improvement has a price in terms of mathematical complexity, but also in terms of numerical complexity as we will see in the sequel.

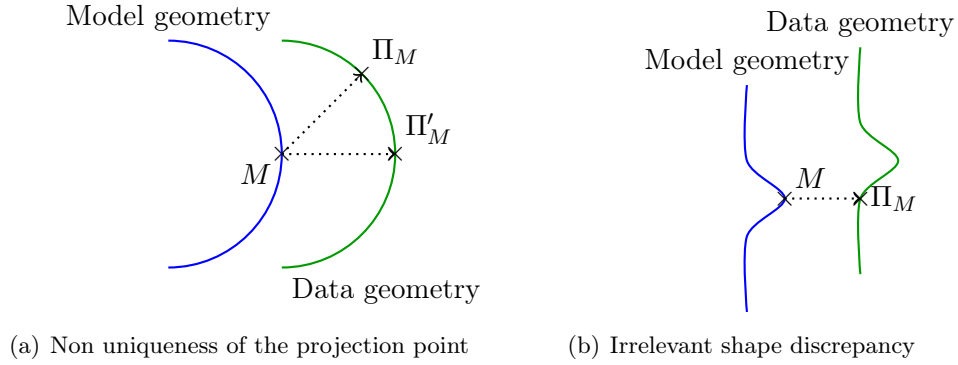


Figure 2.8: Disadvantages of the signed distance operator.

The formalism of *currents* is based on the idea that, through its normal vector field, any surface can be represented as a computational support. More precisely, if we consider a test vector field \underline{w} defined in the ambient space and a surface \mathfrak{S} admitting $\underline{n}_{\mathfrak{S}}$ as its normal then one can consider the following operation resulting in the scalar value:

$$S_{\mathfrak{S}}(w) = \int_{\mathfrak{S}} \underline{w} \cdot \underline{n}_{\mathfrak{S}} \, d\Gamma. \quad (2.63)$$

The validity of this expression is entirely conditioned by the regularity of the involved vector fields and the relationship between \mathcal{W} , the space of test vector fields, and \mathcal{N} , the space of admissible normal vector fields, is a recurrent topic when dealing with currents. One appealing example is when we expect the least regularity on \mathcal{W} , that is to say the trace of any test vector field is defined allowing (2.63) to make sense. This leads to $w \in \mathcal{W} = H^1(\mathbb{R}^3, \mathbb{R}^3)$ and $n_{\mathfrak{S}} \in \mathcal{N} \subset L^2(\mathfrak{S}, \mathbb{R}^3)$. In the following we will say that a surface \mathfrak{S} is *represented as a current* if its normal n belongs to \mathcal{N} and if the couple $(\mathcal{W}, \mathcal{N})$ is such that $S_{\mathfrak{S}}$ belongs to \mathcal{W}^* , the dual of the space of test vector fields. Additionally, if \mathcal{W} is a Hilbert space, then for any surface \mathfrak{S} represented as a current we can define its Riesz representation $s \in \mathcal{W}$ such that

$$\forall w \in \mathcal{W} \quad S_{\mathfrak{S}}(w) = \langle S_{\mathfrak{S}}, w \rangle_{\mathcal{W}^*, \mathcal{W}} = (s_{\mathfrak{S}}, w)_{\mathcal{W}} = \int_{\mathfrak{S}} \underline{w} \cdot \underline{n}_{\mathfrak{S}} \, d\Gamma.$$

It is clear that if we want to rely on the theory of currents in our data assimilation procedure, we need to define \mathcal{W} according to the level of regularity of the surfaces \mathfrak{S} that can be generated by a mechanical model. Up to now this constitutes an open question and even if we are able to define this space precisely, we may find spaces where the computation of currents is very intricate. We believe that there may be a path in considering target solutions regular enough so that these currents can be easily defined and computed. Then the observer relying on this currents should be proved to have some hidden regularity to generate surfaces in the same space. Avoiding this question, we proceed formally on this topic, and adopt a very convenient space \mathcal{W} for practical implementations.

In order to provide numerically tractable forms for currents, we follow [Vaillant and Glaunès, 2005, Durrleman et al., 2009, Younes, 2010] and define \mathcal{W} as a Reproducing Kernel Hilbert Space

(RKHS)⁶ where the evaluation functions

$$\forall \underline{x} \in \mathbb{R}^3, \forall \underline{\alpha} \in \mathbb{R}^3 \quad \delta_{\underline{x}}^{\underline{\alpha}} \left| \begin{array}{l} \mathcal{W} \rightarrow \mathbb{R} \\ w \mapsto \delta_{\underline{x}}^{\underline{\alpha}}(w) = \underline{\alpha} \cdot \underline{w}(\underline{x}), \end{array} \right.$$

are continuous linear forms, namely $\delta_{\underline{x}}^{\underline{\alpha}} \in \mathcal{W}^*$. As an example, we can think of Gaussian kernels of the form $k(\underline{x}, \underline{x}') = \exp\left(-\frac{\|\underline{x}-\underline{x}'\|^2}{\mu^2}\right)$. Applying the reproducing property in the definition of the operator $S_{\mathfrak{S}}$, we obtain for any test vector field $w \in \mathcal{W}$

$$\langle S_{\mathfrak{S}}, w \rangle_{\mathcal{W}^*, \mathcal{W}} = \int_{\mathfrak{S}} \underline{w} \cdot \underline{n} \, d\Gamma = \int_{\mathfrak{S}} (k(\underline{x}', \cdot) \underline{n}, w)_{\mathcal{W}} \, d\Gamma = (s_{\mathfrak{S}}, w)_{\mathcal{W}},$$

which easily gives the Riesz representer $s = \int_{\mathfrak{S}} k(\underline{x}', \cdot) \underline{n} \, d\Gamma$.

If \mathfrak{S}_1 and \mathfrak{S}_2 are two surfaces represented as currents, then, using the expression of their Riesz representers, we have

$$\begin{aligned} (\mathfrak{S}_1, \mathfrak{S}_2) &= (s_{\mathfrak{S}_1}, s_{\mathfrak{S}_2})_{\mathcal{W}} = \langle S_{\mathfrak{S}_1}, S_{\mathfrak{S}_2} \rangle_{\mathcal{W}^*} = \langle S_2, s_1 \rangle_{\mathcal{W}^*, \mathcal{W}} \\ &= \int_{\mathfrak{S}_1} \int_{\mathfrak{S}_2} \underline{n}_{\mathfrak{S}_2}(\underline{x}) \cdot k(\underline{x}', \underline{x}) \underline{n}_{\mathfrak{S}_1}(\underline{x}') \, d\Gamma \, d\Gamma, \end{aligned}$$

and the norm between these objects can be computed by

$$\begin{aligned} \|\mathfrak{S}_1 - \mathfrak{S}_2\|^2 &= \|S_1\|_{\mathcal{W}^*}^2 - 2\langle S_1, S_2 \rangle_{\mathcal{W}^*} + \|S_2\|_{\mathcal{W}^*}^2 \\ &= \iint_{\mathfrak{S}_1} \underline{n}_1(\underline{x}) \cdot k(\underline{x}', \underline{x}) \underline{n}_1(\underline{x}') \, d\Gamma \, d\Gamma + \iint_{\mathfrak{S}_2} \underline{n}_2(\underline{x}) \cdot k(\underline{x}', \underline{x}) \underline{n}_2(\underline{x}') \, d\Gamma \, d\Gamma \\ &\quad - 2 \int_{\mathfrak{S}_1} \int_{\mathfrak{S}_2} \underline{n}_1(\underline{x}) \cdot k(\underline{x}', \underline{x}) \underline{n}_2(\underline{x}') \, d\Gamma \, d\Gamma. \end{aligned}$$

We now understand that we can define elegant discrepancies between surfaces. In fact, the surfaces are embedded into a vector space, hence we can rely on to classical observation operators. In order to exploit this new discrepancy in an observer formalism, we rely on the same type of manipulation as for the distance. When we see the final formulation (2.62) after spatial discretization, we understand that we need to compute

$$\begin{aligned} d_u J(\underline{\delta u}) &= -\langle d_u \Sigma_t(\underline{u})(\underline{\delta u}), \mathfrak{S}_t - \Sigma_t \rangle = -\langle d_u \Sigma_t(\underline{u})(\underline{\delta u}), s_{\mathfrak{S}_t} - s_{\Sigma_t}(\underline{u}, t) \rangle_{\mathcal{W}^*, \mathcal{W}} \\ &= - \int_{\Sigma_t} \left(\underline{\nabla} (s_{\mathfrak{S}_t} - s_{\Sigma_t}(\underline{u}, t)) \cdot \underline{\delta u} \right) \cdot \underline{n} \, d\Gamma - \int_{\Sigma_t} (s_{\mathfrak{S}_t} - s_{\Sigma_t}(\underline{u}, t)) \cdot d_{\underline{u}}(\underline{n} \, d\Gamma)(\underline{\delta u}). \end{aligned}$$

The term $d_{\underline{u}}(\underline{n} \, d\Gamma)(\underline{\delta u})$ is classical in shape optimization but also in shell theory [Chapelle and Bathe, 2011]. Following the notation introduced in [Chapelle and Bathe, 2011], we can show that

$$d_{\underline{u}}(\underline{n} \, d\Gamma)(\underline{\delta u}) = (\underline{\nu}(\underline{\delta u}) + \underline{\tau}(\underline{\delta u})) \, d\Gamma$$

with $\underline{\nu}$ the normal derivative operator

$$\begin{aligned} \underline{\nu}(\underline{\delta u}) &= d\underline{n}(\underline{\delta u}) = - \sum_{i=1,2} (\underline{n} \cdot \underline{\delta u}_{,i}) \underline{a}^i \\ &= -\underline{a}_1 \otimes \underline{n} \cdot \underline{\delta u}_{,1} - \underline{a}_2 \otimes \underline{n} \cdot \underline{\delta u}_{,2}, \end{aligned}$$

⁶Concerning the question of admissible regularity we believe that a $\mathcal{H}^s(\Omega_0, \mathbb{R}^3)$ with $s \geq 2$ could be a good candidate for the admissible displacements space compatible with the use of RKHS spaces

and $\underline{\tau}$ the surface derivative

$$\underline{\tau}(\underline{\delta u}) \, d\Gamma = -\left(\underline{n} \otimes \underline{a}^1 \cdot \underline{\delta u}_{,1} + \underline{n} \otimes \underline{a}^2 \cdot \underline{\delta u}_{,2}\right) \, d\Gamma.$$

Therefore $d_u J(\underline{\delta u})$ can be computed if for all t Σ_t is represented by a triangulation $\mathfrak{T} = (\mathfrak{T}_i)_{1 \leq i \leq N_{\mathfrak{T}}}$ with [Imperiale, 2013]

$$\begin{aligned} d_u J(\underline{\delta u}) &= \sum_{i=1}^{N_{\mathfrak{T}}} \int_{\mathfrak{T}_i} \left(\underline{\nabla} (s_{\mathfrak{E}_t} - s_{\Sigma_t}(u, t)) \cdot \underline{\delta u} \right) \cdot \frac{\partial \underline{x}_i}{\partial r} \wedge \frac{\partial \underline{x}_i}{\partial s} \, dr \, ds \\ &\quad - \int_{\mathfrak{T}_i} (s_{\mathfrak{E}_t} - s_{\Sigma_t}(u, t)) \cdot \left(\frac{\partial \underline{\delta u}}{\partial r} \wedge \frac{\partial \underline{x}_i}{\partial s} + \frac{\partial \underline{x}_i}{\partial r} \wedge \frac{\partial \underline{\delta u}}{\partial s} \right) \, dr \, ds. \end{aligned}$$

which leads to the same terms as in [Vaillant and Glaunès, 2005] when integrals are numerically approximated by evaluating each integrand at the center of the deformed triangle.

Then in order to propose adequate discretizations of the form (2.62), we need to compute the bilinear form

$$\begin{aligned} (d_u \Sigma_t(\underline{\delta u}_1), d_{\Sigma_t}(\underline{\delta u}_2)) &= \int_{\Sigma_t} \int_{\Sigma_t} \left(\underline{\nabla}_2 k(\underline{x}', \underline{x}) \right) \cdot \underline{u}_1^b(\underline{x}) \underline{n}(\underline{x}) \cdot \left(\underline{\nu}(\underline{u}_2^b) + \underline{\tau}(\underline{u}_2^b) \right) \Big|_{\underline{x}'} \, d\Gamma \, d\Gamma \\ &\quad + \int_{\Sigma_t} \int_{\Sigma_t} \left(\underline{\nabla}_1 k(\underline{x}', \underline{x}) \cdot \underline{u}_2^b(\underline{x}') \right) \underline{n}(\underline{x}') \cdot \left(\underline{\nu}(\underline{u}_1^b) + \underline{\tau}(\underline{u}_1^b) \right) \Big|_{\underline{x}} \, d\Gamma \, d\Gamma \\ &\quad + \int_{\Sigma_t} \int_{\Sigma_t} \left(\underline{\nabla}^2 k(\underline{x}', \underline{x}) : (\underline{u}_1^b(\underline{x}) \otimes \underline{u}_2^b(\underline{x}')) \right) \underline{n}(\underline{x}') \cdot \underline{n}(\underline{x}) \, d\Gamma \, d\Gamma \\ &\quad + \int_{\Sigma_t} \int_{\Sigma_t} k(\underline{x}', \underline{x}) \left(\underline{\nu}(\underline{u}_2^b) + \underline{\tau}(\underline{u}_2^b) \right) \Big|_{\underline{x}'} \cdot \left(\underline{\nu}(\underline{u}_1^b) + \underline{\tau}(\underline{u}_1^b) \right) \Big|_{\underline{x}} \, d\Gamma \, d\Gamma. \end{aligned} \tag{2.64}$$

which computation on a triangulation is fully developed in [Imperiale, 2013].

To evaluate the performance of this new discrepancy and feedback with respect to that obtained with the standard distances, some numerical evaluation are presented in [Imperiale, 2013] and reproduced here see Figure 2.9. The dynamics is considered as linear with a damping proportional to the stiffness in order to avoid the spurious high frequencies. We solve the eigenvalue problem

$$\begin{bmatrix} (\epsilon K + d_u J M_{\Sigma} d_u J) & d_u J M_{\Sigma} d_u J \\ 0 & M \end{bmatrix} \begin{bmatrix} \dot{\underline{u}} \\ \dot{\underline{v}} \end{bmatrix} = \begin{bmatrix} 0 & (\epsilon K + d_u J M_{\Sigma} d_u J) \\ -K & -\Lambda \end{bmatrix} \begin{bmatrix} \underline{u} \\ \underline{v} \end{bmatrix}$$

The first plot in Figure 2.9 corresponds to the complete displacement feedback on the whole surface Σ as described in Section 2.3.3.1. The next two plots concern the feedback of the normal component displacement and the linearized signed distance operator. We clearly see here the loss of observability induced by observation only on the normal displacement compared to the complete displacement feedback on the boundary. Moreover, we also illustrate that the tangent operator associated with the distance discrepancy is a normal displacement on the boundary operator.

The last three plots concerns the observer based on the *current* formalism. The difference between the three plots is that we start from a large value of the kernel width – in the first plot $\mu = 50$ – and we evolve towards smaller values, namely $\mu = 10$ and $\mu = 0.1$. These plots illustrate a crucial concept of the discrepancy measure based on currents. Namely, as the kernel

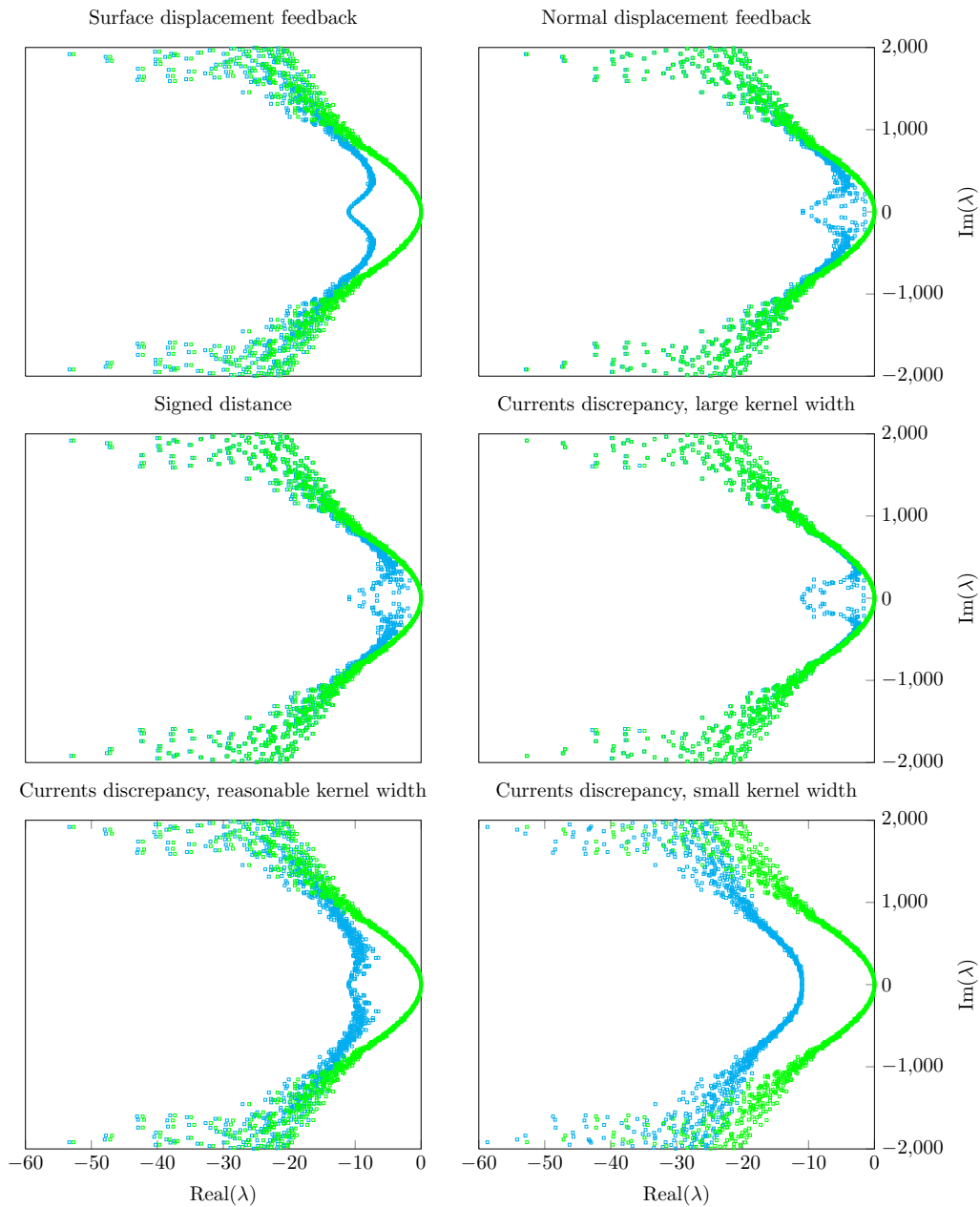


Figure 2.9: Spectral analysis and comparison of the various observers. (From [Imperiale, 2013])

width decreases the stabilization property appears to significantly improve. This is due to the fact that the kernel width directly controls the sensitivity of the metrics to shape variations and any shape dissimilarities of characteristic length below μ will not be perceived by the discrepancy measure. Therefore, when $\mu \rightarrow 0$, the stability seems to be as good as when we observe the total displacement on the surface, whereas we only compare surface objects. In fact, we see in (2.64) that in the stabilization operator associated with the *currents*, the total displacement appears. However, nothing is really magical in the sense that when $\mu \rightarrow 0$, the kernel focuses so much that the stabilization is strong but the innovation coming from the discrepancy is null. In other words, when $\mu \rightarrow 0$, the kernel acts as a Dirac delta function. Hence the Riesz representation of the data surface can be assimilated to

$$s_{\mathfrak{S}} \underset{\mu \rightarrow 0}{\sim} \delta_{\mathfrak{S}} \underline{n}_{\mathfrak{S}},$$

entailing

$$\mathfrak{S} - \Sigma \underset{\mu \rightarrow 0}{\rightarrow} 0,$$

which could be interpreted as a non-visibility of the data from the model standpoint. To conclude, this spectral analysis shows that the choice of the kernel width is of prime importance and corresponds to a compromise between stability and observability.

For a reasonable value of the bandwidth, we observe that the stability is not as good as when the complete displacement is observed. But still we obtain a significant improvement of the damping of the system compared with the distance-based observer. This property justifies numerically the interest of the formalism of *currents* as a state-of-the-art surface discrepancy operator.

2.4.1.3 Estimation from tagged-MRI sequences

Despite all our efforts, it was very clear from the spectra computed in [25] that boundary observations will have a limited observability with respect to interior observations. This very intuitive idea is in fact the reason for the development of new imaging modalities such as tagged-MRI. Tagged-MR is often considered to be the “gold standard” in cardiac imaging, in particular as regards the assessment of so-called “cardiac mechanical indicators”, namely, indicators pertaining to displacements, strains, and volumes [Axel et al., 2005]. As a matter of fact, tagged-MR images visualize the deformations of grids associated with the actual tissues, which is of course most valuable for clinical purposes, both from a qualitative standpoint as assessed by the physician’s eye, and with a view to obtaining such quantitative indicators. From tagged-MRI, numerous image processing works have the ambition to reconstruct 3D material displacements [Denney and Prince, 1995, Pan et al., 2005, Chen et al., 2010, Carranza-Herrezuelo et al., 2010]. In that case, the linear observation operator of the form $C : u \mapsto u|_{\omega}$ can directly be used with the SDF observer. However, the problem of extracting actual 3D material displacements from a tagged-MR sequence gives rise to serious difficulties, and in fact in many cases only 2D “apparent” displacements are obtained [Clarysse et al., 2000], which may introduce specific inaccuracies in the displacement-based quantitative indicators, in addition to usual inaccuracies pertaining to image processing. In [33] – with details in [Imperiale, 2013] – our objective was then to show that the tagged-MR data can be more directly used – without relying on field reconstruction – in an observer, so that the observer reconstructs “online” the 3D displacement. Again, our

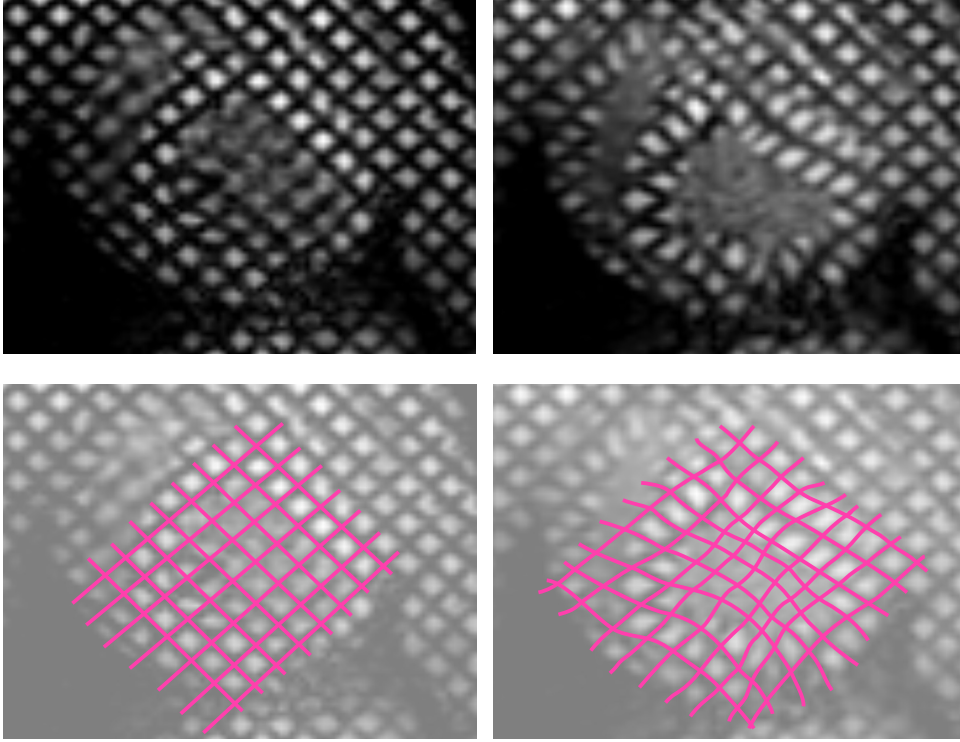


Figure 2.10: Tagged-MRI at marking time and at systole (full heart contraction) and corresponding tag grids

strategy is to avoid unnecessary data processing by using the data as they are, and define an observation operator adapted to them.

We believe that a good target for the data processing is to assume that a first step of image processing leads to the construction of geometrical objects taking the form of tag grids or tag planes and following in time the deformations of the tag patterns – see [Young, 1999] for an example of tag planes construction and [Chen et al., 2010] for tag grids.

Tag planes First, let us consider that the data consist in a set of $N_{\mathfrak{P}}$ tag planes $\mathfrak{T} = \bigcup_i^{N_{\mathfrak{P}}} \mathfrak{P}^i$ deforming over time. Then the discrepancy between the model and the data will be measured using the signed distances between the tag planes and the corresponding synthetic data, namely, deforming surfaces obtained by applying the model displacements to the initial configuration of the tag planes. Note that we should also be able to define a discrepancy with the formalism of current but since the grids are narrow, we believe that we should have more relevant shape discrepancy with tagged than with boundary segmentations. Let us then denote by $\mathfrak{T}_0 = \bigcup_i^{N_{\mathfrak{P}}} \mathfrak{P}_0^i$ the set of tag planes in the reference configuration, mapped by the estimated trajectory \hat{u} to $\hat{\mathfrak{T}} = \bigcup_i^{N_{\mathfrak{P}}} \hat{\mathfrak{P}}^i$. For any point in a synthetic tag plane $\hat{\mathbf{x}} = \underline{\xi} + \hat{u}(\underline{\xi}) \in \hat{\mathfrak{P}}^i$ for some $\underline{\xi} \in \mathfrak{P}_0^i$, we can compute the signed distance to the corresponding actual tag plane by

$$\text{dist}(\hat{\mathbf{x}}, \mathfrak{P}^i) = (\hat{\mathbf{x}} - \Pi_{\mathfrak{P}^i} \hat{\mathbf{x}}) \cdot \mathbf{n}_{\mathfrak{P}^i} .$$

The discrepancy operator is then the application mapping the displacement field to this collection of (scalar) distance fields defined over the planes of \mathfrak{T}_0 – see Figure 2.10. When differentiating

with respect to the displacement field we have

$$d_{\underline{u}} \text{dist}(\hat{\underline{x}}, \mathfrak{P}^i)(\delta \underline{u}) = \underline{n}_{\mathfrak{P}^i} \cdot \delta \underline{u},$$

hence, the application of the above-described strategy gives an observer that follows the mechanical system of equations (1.14b), except for the first equation modified into

$$\dot{\underline{u}} = \hat{\underline{v}} - \gamma \sum_{i=1}^{N_{\mathfrak{P}}} \text{Ext}_{\mathfrak{P}_0^i}(\text{dist}(\hat{\underline{x}}, \mathfrak{P}^i); \underline{n}_{\mathfrak{P}^i}(\hat{\underline{x}})).$$

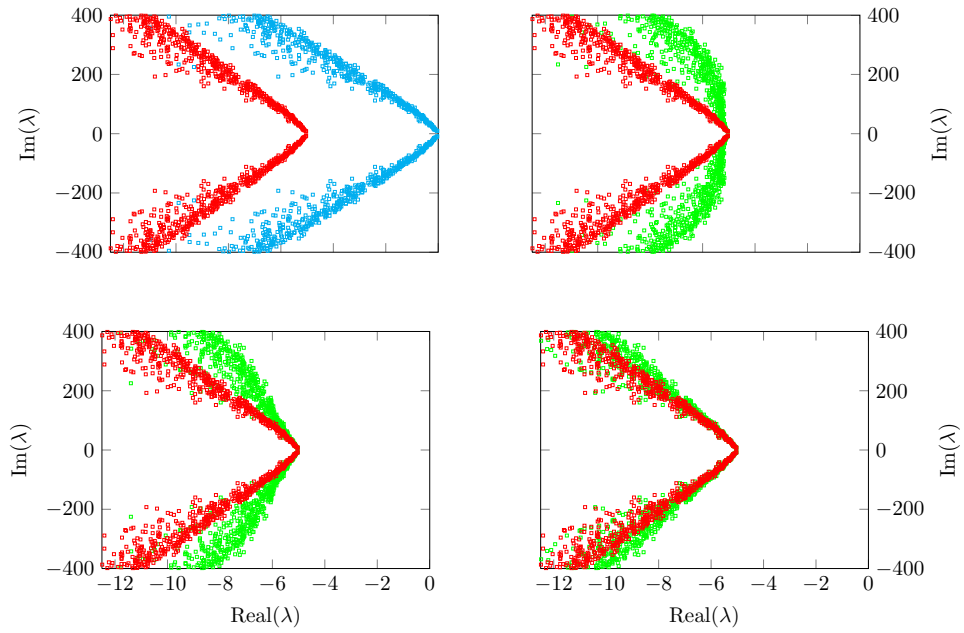


Figure 2.11: Spectra of the time continuous operators. (up-left) : In (cyan) operators without filter, in (red) complete displacement observer. (up-right): In (green) (3D) tag planes with spacing 8 mm. (down-left): In (green) (3D) tag planes with spacing 3.5 mm. (down-right): In (green) (3D) tag planes with spacing 0.25 mm

Tag grids We now consider the data in the form of a collection of tag lines deforming within a set of (2D) image slices. We thus assume that we have $N_{\mathfrak{P}}$ such lines $(\mathfrak{L}^{ij})_{i=1}^{N_{\mathfrak{P}}}$ in each 2D image \mathfrak{I}^j , with $1 \leq j \leq N_{\mathfrak{J}}$. We cannot directly design the discrepancy operator based on the corresponding model lines, since displacement fields are not well-defined along lines in the variational space, hence this would not give a well-posed observer problem. To circumvent this difficulty, we again consider the tag planes in the model and project each point of the planes onto the neighboring image slices – by the Euclidean orthogonal projection denoted by $\Pi_{\mathfrak{J}^j}$ for image \mathfrak{I}^j – and compute the signed distance of the projected point to the corresponding tag line within each image, *i.e.*

$$\text{dist}(\Pi_{\mathfrak{J}^j} \hat{\underline{x}}, \mathfrak{L}^{ij}) = (\Pi_{\mathfrak{J}^j} \hat{\underline{x}} - \Pi_{\mathfrak{L}^{ij}} \Pi_{\mathfrak{J}^j} \hat{\underline{x}}) \cdot \underline{n}_{\mathfrak{L}^{ij}}.$$

Then, we can interpolate the signed distances thus-obtained in the various images concerned – which provides interpolated distance fields over the model tag planes as a discrepancy operator, namely,

$$J_i(\hat{\underline{u}}, z) = I(\text{dist}(\Pi_{\mathcal{J}j} \hat{\underline{x}}, \mathcal{L}^{ij})),$$

for each plane \mathfrak{P}_0^i , where I denotes the interpolation operator. When differentiating this expression, we have

$$\underline{d}_u \text{dist}(\Pi_{\mathcal{J}j} \hat{\underline{x}}, \mathcal{L}^{ij})(\delta u) = \underline{n}_{\mathcal{L}^{ij}} \cdot \delta u,$$

but we also have a contribution coming from the interpolation operator derivative. Since this interpolation only depends on the coordinate of the point considered along the axis orthogonal to all image slices, denoting by I' the derivative with respect to this coordinate, a straightforward computation finally yields

$$\underline{d}_u J_i(\hat{\underline{u}}, z)(\delta u) = \left(I(\underline{n}_{\mathcal{L}^{ij}}) + I'(\text{dist}(\Pi_{\mathcal{J}j} \hat{\underline{x}}, \mathcal{L}^{ij})) \underline{n}_{\mathcal{J}} \right) \cdot \delta u,$$

where $\underline{n}_{\mathcal{J}}$ denotes the director vector of the orthogonal axis. Note that when considering a linear interpolation between the two adjacent planes, the derivative I' is directly given by the finite difference expression computed between these two adjacent planes. This finally gives for the observer correction equation

$$\hat{\underline{u}} = \underline{v} - \gamma \sum_{i=1}^{N_{\mathfrak{P}}} \text{Ext}_{\mathfrak{P}_0^i} \left(I(\text{dist}(\Pi_{\mathcal{J}j} \hat{\underline{x}}, \mathcal{L}^{ij})); \underline{e}^i \right),$$

with $\underline{e}^i = I(\underline{n}_{\mathcal{L}^{ij}}) + I'(\text{dist}(\Pi_{\mathcal{J}j} \hat{\underline{x}}, \mathcal{L}^{ij})) \underline{n}_{\mathcal{J}}$.

We thus understand that there are strategies to use directly the tags as shapes hence to avoid some unnecessary processing. The question is then to understand the observability content of these raw data. In [Imperiale, 2013] elements of analysis are given to show that having 3 sets of orthogonal tagged planes is similar to having the 3D displacement fields discretized on a grid of same spacing parameter as the tags. In fact, if we consider tagged planes, we should get after linearization an observability inequality with a term of the form

$$\forall \varphi, \|\varphi\|_{\mathcal{Z}}^2 = \sum_{i=1}^{N_{\mathfrak{P}}} \|\text{Ext}_{\mathfrak{P}_0^i}(\varphi)\|_{H^1(\Omega_{\text{obs}})}^2,$$

where Ω_{obs} is the region spanned by the tag grid. In a first stage of analysis, we consider this expression for a discrete function $\varphi_{\tilde{h}}$ constructed based on piecewise-bilinear shape functions associated with the regular tagged grid, \tilde{h} denoting the distance between two adjacent planes in any direction. We denote this discrete space by $Q_1^{\tilde{h}}(\Omega_{\text{obs}})$. Then, straightforward scaling arguments – as is standard in finite element analysis, see *e.g.* [Chapelle and Bathe, 2011] – show that we have the following equivalence of norms

$$\|I_{\tilde{h}}(\varphi_h|_{\Omega_{\text{obs}}})\|_{\mathcal{Z}}^2 \geq C \|I_{\tilde{h}}(\varphi_h|_{\omega_0})\|_{\mathcal{H}^1(\Omega_{\text{obs}})}^2 \geq C_{\tilde{h}, h} \|\varphi_h\|_{\mathcal{H}^1(\Omega_{\text{obs}})}^2,$$

where $I_{\tilde{h}}$ denotes the interpolation operator into the tag grid discrete space. Then we believe that we can complete a convergence analysis with two levels of discretization: one coming from the model and the one coming from the data. Note that we have already encountered two levels of sampling when we considered that the data time-sampling did not correspond to the time-discretization. Here, the consequence will be the same, *i.e.* if the data sampling is too coarse

then the observer would not be able to stabilize modes with variations smaller than the data grid. The remaining modes must therefore be damped by the natural damping of the system see Figure 2.11.

2.4.2 A Luenberger observer for reaction-diffusion models with front position data

Last but not least, we want to present another shape-based observer applied this time to a reaction-diffusion problem such as one encountered in electrophysiology. Our objective here is to propose an effective strategy for performing estimation in an electrophysiology model with data in the form of isochrones of the depolarization front. These data are typically reconstructed in electrocardiographic imaging [Ramanathan et al., 2004, Rudy, 2013] from body surface potentials – the same type of signals as those producing ECGs but typically gathered from a complete thoracic vest. From these isochrones of the depolarization front we can generate a sequence of level sets of the electrical potential separating the depolarized zone from the repolarized zone. Therefore we propose to design an observer that can consider a reaction-diffusion class of model of the form

$$\begin{cases} \frac{\partial w_{|\zeta}}{\partial t}(\underline{x}, t) - \nabla \cdot \underline{D}(\underline{x}) \nabla w_{|\zeta}(\underline{x}, t) = k(\underline{x})f(w_{|\zeta}, t), & \underline{x} \in \mathfrak{B}, t > 0 \\ w_{|\zeta}(0) = w_{\diamond} + \zeta \end{cases} \quad (2.65)$$

with propagating solutions [Keener and Sneyd, 2004]. On an unknown target solution \check{w} we assume to have at our disposal the time evolution of the front

$$\mathfrak{F}_{\check{w}}(t) = \{\underline{x} \in \mathfrak{B}, \check{w}(\underline{x}, t) = c_{\text{th}}\},$$

where c_{th} is a threshold value characterizing the front, and the already traveled-through region is given by

$$\mathfrak{D}_{\check{w}}(t) = \{\underline{x} \in \Omega, \check{w}(\underline{x}, t) > c_{\text{th}}\},$$

up to some measurement noise. These data can be represented as a sequence of images $(\mathcal{J})_{1 \leq k \leq N_j}$ that essentially take two different values inside and outside the traveled-through region. In the rest of this section we will thus define our observation z as a field given on \mathfrak{B} and taking two different values, or a regularized version thereof. We propose in [18] to show how a Luenberger observer of \check{w} can be designed to use these data.

Inspiration from image-processing strategies – When seeking a propagating solution for reaction-diffusion models, it is now common to derive the so-called eikonal-curvature equation, an asymptotic formulation designed to follow the front over time. As shown in [Keener and Sneyd, 2004], a level set ϕ_w of the front \mathfrak{F}_w follows the dynamics

$$\frac{\partial \phi_w}{\partial t} = |\nabla \phi_w| \left(\nabla \underline{D} \cdot \frac{\nabla \phi_w}{|\nabla \phi_w|} + b_0 \right), \quad (\underline{x}, t) \in \mathfrak{B} \times (0, T). \quad (2.66)$$

with b_0 a constant depending of f . We see that the front propagation is driven by a term along the normal of the front $\sqrt{\underline{D}k} c_0 |\nabla \phi_w|$ and a curvature term $|\nabla \phi_w| \nabla \underline{D} \cdot \frac{\nabla \phi_w}{|\nabla \phi_w|}$.

On this model, the use of the data is more natural since the state of the eikonal-curvature equation is a front as for the data. In fact, eikonal-curvature models are very popular in image processing to segment objects. Our idea is thus to get inspiration from the data similarity compatible in image processing with an eikonal-curvature equation. This lead us naturally to Mumford-Shah-based data driven terms, and in particular the data-fitting term of the piecewise-smooth Mumford-Shah functional of [Chan and Vese, 2001]

$$\mathcal{J}_{\text{MS}} = \int_{\mathcal{D}_\phi} (z(t) - C_1(\mathcal{D}_\phi))^2 dx + \int_{\mathfrak{B} \setminus \mathcal{D}_\phi} (z(t) - C_2(\mathcal{D}_\phi))^2 dx,$$

where

$$C_1(\mathcal{D}_\phi) = \frac{\int_{\mathcal{D}_\phi} z dx}{\int_{\mathcal{D}_\phi} dx}, \quad C_2(\mathcal{D}_\phi) = \frac{\int_{\mathfrak{B} \setminus \mathcal{D}_\phi} z(t) dx}{\int_{\mathfrak{B} \setminus \mathcal{D}_\phi} dx}.$$

Following similar computations as in [Delfour and Zolésio, 2011, Hintermüller and Ring, 2004] based on the shape derivation of \mathcal{J}_{MS} , a good observer candidate for (2.66) can be

$$\begin{aligned} \frac{\partial \phi_{\hat{w}}}{\partial t} &= |\underline{\nabla} \phi_{\hat{w}}| \left(\underline{\nabla} \underline{D} \cdot \frac{\underline{\nabla} \phi_{\hat{w}}}{|\underline{\nabla} \phi_{\hat{w}}|} + b_0 \right) \\ &\quad + \gamma \delta_{\mathfrak{F}} \alpha(|\underline{\nabla} \phi|) \left(-(z(t) - C_1(\mathcal{D}))^2 + (z(t) - C_2(\mathcal{D}))^2 \right) \quad (\underline{x}, t) \in \mathfrak{B} \times (0, T). \end{aligned} \quad (2.67)$$

where $\delta_{\mathfrak{F}}$ is the single layer distribution associated with the front \mathfrak{F} , γ is the nudging gain and α is any positive function.

Shape based observer – The system (2.67) is a good candidate as an observer for the eikonal-curvature model (2.66). However our objective is to propose a feedback for (2.65) where all the physical content is present. Therefore, we carry over the observer to the initial reaction-diffusion model by an inverse asymptotic analysis, namely by intuitively designing the reaction-diffusion observer so that, after an asymptotic analysis similar to [Keener and Sneyd, 2004], we end up with (2.67). We easily end up – see [18] – with

$$\begin{aligned} \frac{\partial \hat{w}}{\partial t} - \underline{\nabla} \cdot \underline{D} \underline{\nabla} \hat{w} &= kf(\hat{w}) \\ &\quad + \gamma \delta_{\mathfrak{F}} \alpha(|\underline{\nabla} \hat{w}|) \left(-(z(t) - C_1(\mathcal{D}))^2 + (z(t) - C_2(\mathcal{D}))^2 \right), \quad (\underline{x}, t) \in \mathfrak{B} \times (0, T), \end{aligned} \quad (2.68)$$

and find that $\alpha(|\underline{\nabla} \hat{w}|) = \frac{1}{|\underline{\nabla} \hat{w}|}$ is a good scaling so that the feedback is intrinsic with respect to the single layer definition, since the use of 1D Dirac function gives $\delta(w(\underline{x})) = \frac{\delta_{\mathfrak{F}}(\underline{x})}{|\underline{\nabla} w|}$. In fact we have in this case that the correction is exactly given by

$$\underline{\nabla} \mathcal{J}_{\text{MS}} = \delta_{\mathfrak{F}} \frac{1}{|\underline{\nabla} \hat{w}|} \left(-(z(t) - C_1(\mathcal{D}))^2 + (z(t) - C_2(\mathcal{D}))^2 \right),$$

In order to give some first elements of analysis, the idea is again to understand the stabilization brought by the feedback. Since it is non-linear we limit ourselves to a formal analysis for small errors around the target trajectory. With this aim in mind we expect the following property

$$\langle \underline{\nabla}^2 \mathcal{J}_{\text{MS}}(\tilde{w}), \tilde{w} \rangle \geq 0. \quad (2.69)$$

Following a shape derivation strategy [Delfour and Zolésio, 2011, Hintermüller and Ring, 2004], we then obtain in [18] the following sensitivity.

PROPOSITION 2.4.1 (CHAPELLE-COLLIN-MOIREAU)

For regular enough data, the second derivative of the data fitting around the target trajectory term is given with $\alpha(|\nabla \hat{w}|) = \frac{1}{|\nabla \hat{w}|}$ by

$$\begin{aligned}
\langle \nabla_w^2 \mathcal{J}_{MS}(\delta w_2), \delta w_1 \rangle &= \int_{\mathfrak{F}_w} \kappa \alpha(|\nabla w|) \left((z - C_1(\mathfrak{D}_w))^2 - (z - C_2(\mathfrak{D}_w))^2 \right) \delta w_2 \frac{\delta w_1}{|\nabla w|} d\sigma \\
&\quad - \int_{\mathfrak{F}_w} \alpha'(|\nabla w|) \left((z - C_1(\mathfrak{D}_w))^2 - (z - C_2(\mathfrak{D}_w))^2 \right) \delta w_2 \partial_n \delta w_1 d\sigma \\
&\quad - \int_{\mathfrak{F}_w} \alpha'(|\nabla w|) \partial_n^2 w \left((z - C_1(\mathfrak{D}_w))^2 - (z - C_2(\mathfrak{D}_w))^2 \right) \delta w_2 \frac{\delta w_1}{|\nabla w|} d\sigma \\
&\quad + 2 \int_{\mathfrak{F}_w} \alpha(|\nabla w|) \partial_n z (C_2(\mathfrak{D}_w) - C_1(\mathfrak{D}_w)) \delta w_2 \frac{\delta w_1}{|\nabla w|} d\sigma \\
&\quad - 2 \frac{1}{|\mathfrak{D}_w|} \int_{\mathfrak{F}_w} (z - C_1(\mathfrak{D}_w)) \frac{\delta w_1}{|\nabla w|} d\sigma \times \int_{\mathfrak{F}_w} \alpha(|\nabla w|) (z - C_1(\mathfrak{D}_w)) \delta w_2 d\sigma \\
&\quad - 2 \frac{1}{|\mathfrak{B} \setminus \mathfrak{D}_w|} \int_{\mathfrak{F}_w} (z - C_2(\mathfrak{D}_w)) \frac{\delta w_1}{|\nabla w|} d\sigma \times \int_{\mathfrak{F}_w} \alpha(|\nabla w|) (z - C_2(\mathfrak{D}_w)) \delta w_2 d\sigma \\
&\quad + \int_{\mathfrak{F}_w} \alpha(|\nabla w|) \left((z - C_1(\mathfrak{D}_w))^2 - (z - C_2(\mathfrak{D}_w))^2 \right) \partial_n \delta w_2 \frac{\delta w_1}{|\nabla w|} d\sigma,
\end{aligned}$$

hence for small estimation errors we have

$$\begin{aligned}
\langle d_w \mathcal{J}_{MS}(\tilde{w}), \tilde{w} \rangle &= 2(C_2(\mathfrak{D}_w) - C_1(\mathfrak{D}_w)) \int_{\mathfrak{F}_w} \partial_n z \left(\frac{\tilde{w}}{|\nabla w|} \right)^2 d\sigma \\
&\quad - 2 \left(\frac{C_2(\mathfrak{D}_w) - C_1(\mathfrak{D}_w)}{2} \right)^2 \left(\frac{1}{|\mathfrak{D}_w|} + \frac{1}{|\mathfrak{B} \setminus \mathfrak{D}_w|} \right) \left(\int_{\mathfrak{F}_w} \frac{\tilde{w}}{|\nabla w|} d\sigma \right)^2,
\end{aligned}$$

This gives the following proposition.

PROPOSITION 2.4.2 (CHAPELLE-COLLIN-MOIREAU)

Let us define the characteristic length h_z , – the wavelength of the front width in the data – by

$$\frac{1}{h_z} = \min_{x \in \mathfrak{F}_w} \frac{|\partial_n z|}{|C_1(\mathfrak{D}_w) - C_2(\mathfrak{D}_w)|}.$$

Assuming

$$\frac{1}{h_z} \geq \frac{1}{4} \left(\frac{1}{|\mathfrak{D}_w|} + \frac{1}{|\mathfrak{B} \setminus \mathfrak{D}_w|} \right) |\mathfrak{F}_w|, \tag{2.70}$$

then the condition (2.69) is satisfied, hence the observer effect is energy-decreasing in the linearized error.

Condition (2.70) pertains to the sharpness of the front in the data – in other words to image contrast – a condition that is clearly also required in image processing, see e.g. [Hintermüller and Ring, 2004].

In [18] we finally show that, once the state observer is defined, it is then possible to complement it with a parameter estimation stage in the spirit of [23, 24]. The discrepancy used for the parameter estimation remains \mathcal{J}_{MS} , rewritten in the following least-square-like form

$$\mathcal{J}_{MS} = \int_{\mathfrak{B}} \left(H(\phi_{w|\zeta_w, \zeta_\theta})(z - C_1(\mathfrak{D})) + (1 - H(\phi_{w|\zeta_w, \zeta_\theta}))(z - C_2(\mathfrak{D})) \right)^2 dx = \int_{\mathfrak{B}} J(z, y_{|\zeta_y, \zeta_\theta})^2 dx.$$

We then rely on the ROUKF after time and space discretization, and show that it is possible to jointly estimate the state, some diffusion parameters and also some initial condition parameters. This initial condition estimation allows to restart the estimation on multiple cycles of propagation when the front tracking is not good enough during the first cycle.

Topological gradient-based extension – In the recent work [31], we remark that the previous observer is limited in the sense that it can only correct the front $\Gamma_{\hat{w}}$ that is already present in the simulation. This means that, if we do not have a propagation front to be associated with the data, we are not able to compute any observer correction. We want to circumvent this limitation in order to track complex types of propagation patterns in reaction-diffusion problem. In electrophysiology, this will be particularly helpful to monitor a fibrillation on a patient.

In order to improve the observer formulation, we follow a strategy of increasing importance in shape optimization [Burger et al., 2004] or “level-set”-based image segmentation [Hintermüller and Laurain, 2009, He et al., 2007], where the required shape derivatives, used to modify the shape contours is complemented by a topological derivative that represents the sensitivity of \mathcal{J}_{MS} when removing a small part of the domain. We thus introduce

$$d_{\text{topo}} \mathcal{J}_{\text{MS}}(\mathfrak{D})(\underline{x}) = \lim_{\rho \rightarrow 0} \frac{\mathcal{J}_{\text{MS}}(\mathfrak{D} \setminus B_{\rho, \underline{x}}) - \mathcal{J}_{\text{MS}}(\mathfrak{D})}{|B_{\rho, \underline{x}} \cap \mathfrak{D}|}, \quad \forall \underline{x} \in \mathfrak{D},$$

$B_{\rho, \underline{x}}$ denoting a ball of radius ρ and center \underline{x} . This gives in our case

$$d_{\text{topo}} \mathcal{J}_{\text{MS}}(\underline{x}) = (z(\underline{x}, t) - C_1(\mathfrak{D}))^2 - (z(\underline{x}, t) - C_2(\mathfrak{D}))^2, \quad \forall \underline{x} \in \mathfrak{B}$$

Then we see in [31] that in order to define a feedback of adequate sign we must consider

$$\nabla_{\text{topo}} \mathcal{J}_{\text{MS}} = \left(1 + \text{sign} \left(d \mathcal{J}_{\text{MS}} \times (w - c_{\text{th}}) \right) \right) d_{\text{topo}} \mathcal{J}_{\text{MS}},$$

where the first term selects the region where we want to act

$$\left(1 + \text{sign} \left(d \mathcal{J}_{\text{MS}} \times (w - c_{\text{th}}) \right) \right) = \begin{cases} 0 & \text{if } \underline{x} \in I \cup III \\ 2 & \text{if } \underline{x} \in II \end{cases}$$

while the topological derivative $d \mathcal{J}_{\text{MS}}$ provides the direction (creation or destruction, see Fig.3.1 left and right, respectively). Therefore, the observer (2.68) is complemented to read

$$\begin{aligned} \frac{\partial \hat{w}}{\partial t} - \underline{\nabla} \cdot \underline{D} \underline{\nabla} \hat{w} &= k f(\hat{w}) \\ + \gamma_{\text{topo}} \left(1 + \text{sign} \left(((z - C_1(\mathfrak{D}))^2 - (z - C_2(\mathfrak{D}))^2) (w - c_{\text{th}})) \right) \right) & (z - C_1(\mathfrak{D}))^2 - (z - C_2(\mathfrak{D}))^2 \\ w_m + \gamma_{\text{sh}} \delta_{\mathfrak{F}} \alpha(|\underline{\nabla} \hat{w}|) \left(-(z(t) - C_1(\mathfrak{D}))^2 + (z(t) - C_2(\mathfrak{D}))^2 \right). & \end{aligned}$$

Application to the bidomain model – The application of this observer to electrophysiology is very straightforward as we simply apply the correction to the bidomain equation. However, we should mention that in practice the ECGI data allows to reconstruct the data only on the epicardium. In [18] and [31], we consider a surface bidomain model proposed in [Chapelle et al.,

2013], particularly well-suited to the atria very thin walls. This model is posed on the midsurface of the wall and therefore can directly use the front data as for our reaction-diffusion model (2.65). We typically end up with

$$\begin{cases} A_m \int_{\Sigma} \left(C_m \frac{\partial \hat{w}_m}{\partial t} + I_{\text{ion}}(\hat{w}_m) \right) \phi \, d\Gamma + \int_{\Sigma} \left(\vec{\sigma}_i \cdot (\vec{\nabla} \hat{w}_m + \vec{\nabla} \hat{u}_e) \right) \cdot \vec{\nabla} \phi \, d\Gamma \\ \quad = - \int_{\Sigma} \left(\lambda \vec{\nabla}_{\text{sh}} \hat{\mathcal{J}}_{\text{MS}} + \mu \vec{\nabla}_{\text{topo}} \hat{\mathcal{J}}_{\text{MS}} \right) \phi \, dS + A_m \int_{\Sigma} I_{\text{app}} \phi \, d\Gamma, \\ \int_{\Sigma} \left((\vec{\sigma}_i + \vec{\sigma}_e) \cdot \vec{\nabla} \hat{u}_e \right) \cdot \vec{\nabla} \psi \, d\Gamma + \int_{\Sigma} \left(\vec{\sigma}_i \cdot \vec{\nabla} w_m \right) \cdot \vec{\nabla} \psi \, d\Gamma = 0, \end{cases}$$

where $\vec{\nabla}$ is the surfacic gradient.

Concerning the ventricles, it is still possible to formally apply a feedback supported by the observed front, but this front is a line on the epicardium which should introduce even more technicalities when trying to justify that we have enough regularity on the front to define the observer.

We mention eventually that other works consider the problem of estimating the cardiac electrical state from data, in particular from front data. [Moreau-Villeger et al., 2006, Konukoglu et al., 2010] use a variational strategy with simplified models. In these strategies, however, they do not differentiate the front with respect to the state and limit their minimization to gradient-free approaches.

Cardiac modeling and model-data interaction

Tous les modèles sont faux, certains sont utiles

— G. Box

Chapter contents

3.1	Introduction	118
3.2	Energy preserving models and coupling	118
3.2.1	An energy preserving micro-macro model of the heart contraction	118
3.2.2	An energy balanced coupling of porous flows and hyperelastic formulations	125
3.3	Reduced-order modeling	129
3.3.1	Dimensional reductions of a cardiac model for effective validation and calibration	129
3.3.2	Proper Orthogonal Decomposition for parameter-dependent problems – application to parameter estimation	133
3.4	Model-data interaction for the cardiovascular system	133
3.4.1	Estimation of tissue contractility from cardiac Cine-MRI – a pig experiment	133
3.4.2	Identification of boundary support parameters in a fluid-structure vascular model using patient image data	134
3.4.3	Estimation in electrophysiology	134
3.4.4	Applications within international collaborations	135

3.1 Introduction

This chapter first summarizes my modeling results on the cardiovascular system. Regarding the micro-macro model of the heart contraction, we develop (with D. Chapelle and P. Le Tallec) original non-linear rheology laws and time-discretization to obtain energy balance at the continuous and discrete level. The topic of the heart tissue perfusion by the blood was the opportunity to revisit poromechanics and propose thermodynamically compatible formulation for systems presenting large displacements and strong fluid inertia. The question of model reduction is of crucial importance for the cardiac system if we expect to reduced time computations, hence for instance propose efficient models for monitoring. We have contributed to two types of model reduction, the first one is based on asymptotic reduction. This work initiated with D. Chapelle during my Master Thesis was concluded with R. Chabiniok and M. Caruel by comparing simulation results with Y. Lecarpentier's experiments on mice papillary muscles. The second type of reduction is based on reduced-basis reduction since we investigate POD reduction for our heart model (with D. Chapelle, A. Gariah and J. Sainte-Marie).

The second part of the chapter gathers my results on complete estimation trials on real data or in a real data context. Indeed, we have (with R. Chabiniok, and D. Chapelle, in collaboration with the medical doctors P.-F. Lesault, A. Rahmouni, J.-F. Deux) the first data assimilation result on real data for a heart model. We also have (with Philippe C. Bertoglio, N. Xiao, C. A. Figueroa, C. A. Taylor, D. Chapelle, and J.-F. Gerbeau) the first data assimilation result on real data for a blood flow simulator. Our results on electrophysiology (with D. Chapelle, A. Collin, C. Corrado and J.-F. Gerbeau) using ECG or ECGI data are about to be tested on real data as they are very promising when evaluated in a synthetic but very realistic applicative context. Finally, our work on data assimilation for the heart has induced fruitful collaboration/transfer with other teams, as for instance with Inria Team Asclepios or with Kings College London.

3.2 Energy preserving models and coupling

3.2.1 An energy preserving micro-macro model of the heart contraction

As already mentioned in the introduction, the modeling of the active mechanical behavior of the myocardium has been the object of abundant researches in the literature with two levels of focus: on the one hand, the micro-scale bio-chemico-mechanical behavior of the fundamental agents of the contraction, *i.e.* the actin-myosin bridges [Huxley, 1957, Huxley and Simmons, 1971, Eisenberg and Hill, 1978, Panerai, 1980, Bestel et al., 2001, Rice et al., 2003, Marcucci and Truskinovsky, 2010, Guérin et al., 2011] and on the other hand, at the tissue level in order to simulate the heart contraction at the organ scale [Glass et al., 1991, Guccione and McCulloch, 1993, Nash and Hunter, 2000, Rice and de Tombe, 2004, Sainte-Marie et al., 2006, Pathmanathan et al., 2010]. However, relatively little attention has so far been devoted to carrying over the microscopic considerations to the macroscopic level in the muscle tissue models [Engelbrecht et al., 2000]. Therefore, at the macroscopic level, most of formulations lack energy considerations – balances and exchanges – that are of utmost value, whereas such mechanisms are well-described at the cellular level in the biophysics literature. As a consequence, the formulations are often phenomenological and may lack mathematical background since energy balances are strong

properties to carry out an existence analysis, but also a numerical analysis. To circumvent this difficulty, some mathematical teams have made the choice to favor the mathematical foundation of their tissue-level formulation, taking some distance with the original physiological description of the muscle contraction of Huxley. On the contrary, we have tried in our work to show how micro and macro descriptions are perfectly compatible by showing how, in a non-linear large deformation context, we can integrate some state-of-the-art microscopic model of the actin-myosin attachment up to the macroscopic level in order to formulate a complete, well-balanced macroscopic model of the heart. This model then contains the most characteristic bio-physical features, can be shown – at least after linearization – to be well posed, and can be discretized efficiently with energy-consistent time-scheme.

We restart our presentation from the general solid formulation (1.13) given in the introduction. We here specify the boundary conditions. In the spirit of our work on cardiovascular modeling [26] – see also Section 3.4.2 – we model the external organs by visco-elastic boundary conditions on a sub-part of the epicardium which, in reference configuration, gives

$$\underline{\underline{T}} \cdot \underline{n} = k_s \underline{u} + c_s \underline{v} \text{ on } \Gamma_n(t).$$

Regarding the intra-cavity pressure load, we consider a uniform following pressure on the left and right endocardium easily written in deformed configuration

$$\underline{\underline{\sigma}} \cdot \underline{n}_t = -p_{v,i} \underline{n}_t \text{ on } \Gamma_{n,i}(t), i = \{1, 2\}.$$

Obviously, these choices are simplified. The external tissue support could be more deeply modeled with contact conditions– see some preliminary extension in [Imperiale, 2013] – and the intra-cavity pressure load corresponds in fact to a complex fluid-structure interaction problem to be set up. However, a reasonable heart model can be described by

$$\begin{cases} \partial_t \underline{u} = \underline{v}, & \text{in } \Omega_0 \\ \rho \partial_t \underline{v} - \operatorname{div}(\underline{\underline{T}}) = 0, & \text{in } \Omega_0 \\ \underline{\underline{T}} \cdot \underline{n} = k_s \underline{u} + c_s \underline{v}, & \text{on } \Gamma_n \\ \underline{\underline{T}} \cdot \underline{n} = -J p_{v,i} \underline{\underline{F}}^{-\top} \cdot \underline{n}, & \text{on } \Gamma_{c,i} \\ \underline{\underline{T}} \cdot \underline{n} = 0, & \text{on } \partial\Omega_0 \setminus ((\cup_i \Gamma_{c,i}) \cap \Gamma_n) \end{cases} \quad (3.1)$$

where the constitutive law describing $\underline{\underline{T}}$ must be specified. Now, most cardiac models where the active behavior is taken into account in the stress law define the second Piola-Kirchhoff stress tensor $\underline{\underline{\Sigma}} = \underline{\underline{F}}^{-1} \cdot \underline{\underline{T}}$ as

$$\underline{\underline{\Sigma}} = \underline{\underline{\Sigma}}_p + \sigma_{1D}(e_{1D}, t) \underline{\tau} \otimes \underline{\tau}$$

where $e_{1D} = \underline{\tau} \cdot \underline{\underline{e}} \cdot \underline{\tau}$ is the strain in the fiber direction.

3.2.1.1 A microscopic model of contraction adapted to large scale problems

In the active law σ_{1D} , a fundamental objective is to integrate the state-of-the art microscopic models of the muscle contraction. Indeed, the subcellular scale is where biochemistry and mechanics are intimately coupled, with the attachment of so-called cross-bridges within sarcomeres, namely, the creation of chemical bonds between myosin heads and specific sites on actin filaments. A cross-bridge in itself can be seen as an elementary chemical entity having internal

mechanical variables – or degrees of freedom (dof)– characterizing its attached or unattached state. In the original model [Huxley, 1957], the cross-bridge is seen as a system with one mechanical dof associated with a linear spring that is under tension as soon as the myosin head attaches to the actin filament, which collectively induces muscle contraction. This model was later refined in the literature [Huxley and Simmons, 1971, Eisenberg and Hill, 1978] by including additional chemical states in the attached configuration. Nowadays, this research is still very active with for example the original alternative approach [Marcucci and Truskinovsky, 2010] by which a purely mechanical model was substituted for the chemical states of the attached cross-bridge, with two dofs corresponding to one bi-stable element in series with a linear spring. Once the cross-bridge behavior has been modeled, we must aggregate over the spatial scales the behavior of the many individual cross-bridges at work within the sarcomeres, cells and tissue. Given the large number of cross-bridges – at the sarcomere level and above – it is quite natural to adopt a statistical description, as already proposed in [Huxley, 1957], by which the total active force/stress is given by the mean of the individual cross-bridge forces with an appropriate scaling factor. Typically σ_{1D} is directly related to n , the probability density functions of cross-bridges, which follow a dynamics of the form

$$\frac{\partial n}{\partial t} + \dot{e}_c \frac{\partial n}{\partial s} = (n_0 - n)f - ng, \quad (3.2)$$

where s is a microscopic variable, e_c is the fiber deformation and $n_0(e_c)$ is the maximum number of bridges that can be created for a given fiber deformation. Then a macroscopic active stress can be computed with

$$\tau_c(t) = \int \frac{\partial W_m(t, s)}{\partial s} n(t, s) ds,$$

with W_m the mechanical potential associated with each cross-bridge, f and g are binding and unbinding rates.

Among these models, the model envisioned in [Sainte-Marie et al., 2006] and completed in our work [14] represents a good compromise between the microscopic description and the need for a tractable model at the macroscopic level. The idea is to mitigate the resulting computational costs in the simulation process by making some approximations on the bridges density function. For instance [Zahalac, 1981] proposes to replace (3.2) by the dynamics of a limited number of so-called moments

$$\mu_p = \int_{\mathbb{R}} s^p n(s, t) ds.$$

with a closure relation, a strategy quite typical in the kinetic formalism. In fact, under certain modeling assumptions the moments equations are exact, and directly provide the active stresses themselves as solutions of a dynamical equation. This is the spirit of [Bestel et al., 2001] and [14]. Indeed, by choosing $W_m(t, s) = \frac{k_0}{2}(s + s_0)^2$ and

$$\begin{aligned} f(s, t) &= |u(t)|_+ \mathbb{1}_{s \in [0,1]}, \\ g(s, t) &= |u(t)| + \alpha |\dot{e}_c| - f(s, t). \end{aligned}$$

$$u(t) = |u(t)|_+ - |u(t)|_- \quad \text{with} \quad \begin{cases} |u(t)|_+ = k_{ATP} \mathbb{1}_{[Ca^{2+}] > C} \\ |u(t)|_- = k_{RS} \mathbb{1}_{[Ca^{2+}] < C} \end{cases}$$

we show in [14] that the moments

1. 0th-order moment: with an appropriate rescaling, this represents the equivalent stiffness of the sarcomere in the current configuration of active bridges, which we denote by k_c

$$k_c = k_0 \int_{\mathbb{R}} n(s, t) ds.$$

2. 1st-order moment: let τ_c be the stress associated with the set of “springs” considered at equilibrium when $s = -s_0 \leq 0$ – meaning that for $s = 0$ the spring is under tension:

$$\tau_c = k_0 \int_{\mathbb{R}} (s + s_0)n(s, t) ds.$$

satisfy

$$\begin{cases} \dot{k}_c = -(|u| + \alpha |\dot{e}_c|)k_c + n_0 k_0 |u|_+ \\ \dot{\tau}_c = -(|u| + \alpha |\dot{e}_c|)\tau_c + \dot{e}_c k_c + n_0 \sigma_0 |u|_+ \end{cases}$$

a dynamics close to the original model derivation in [Bestel et al., 2001]. Such a formulation is reasonably simple to simulate at the macroscopic level, since it only involves two more internal variables in the constitutive relation, as can be encountered in numerous complex mechanical formulations [Maugin and Muschik, 1994, Engelbrecht et al., 2000]. Moreover it contains crucial microscopic characteristics, with for instance the chemical entry u or the so-called Frank-Starling effect [Tortora and Derrikson, 2009] in n_0 . Therefore, this model produces comparable results as experiments at the fiber level, see our validation in [7]. And finally it shows a very interesting energy balance with the following result

PROPOSITION 3.2.1 (CHAPELLE-LE TALLEC-MOIREAU-SORINE)

The energy averaged over the collection of bridges

$$U_c = \frac{k_0}{2} \int_{\mathbb{R}} (s + s_0)^2 n(s, t) ds.$$

satisfies the dynamics

$$\begin{aligned} \dot{U}_c &= \frac{k_0}{2} \int_{\mathbb{R}} (s + s_0)^2 \dot{f} ds - (|u| + \alpha |\dot{e}_c|)U_c + \dot{e}_c \tau_c \\ &= -(|u| + \alpha |\dot{e}_c|)U_c + \dot{e}_c \tau_c + n_0 U_0 |u|_+, \end{aligned}$$

with $U_0 = \frac{k_0}{2}(s_0^2 + s_0 + \frac{1}{3}) > 0$, so that it can control the macroscopic variable – i.e. depending uniquely from the variables τ_c and k_c – variation

$$\Psi_c = \frac{1}{2k_c} \tau_c^2,$$

by

$$\forall t, U_c \geq \Psi_c.$$

This energy balance integrated over the scales is the key element for a complete mathematical analysis. Indeed, it shows that the macroscopic variable that will be simulated is controlled by the microscopic energy exchange that enters the mechanical energy balance (3.5).

3.2.1.2 General non-linear rheology for the cardiac fiber

In order to integrate completely the active part with the rest of the mechanical components, typically the passive 3D behaviors in $\underline{\Sigma}_p$, we propose to follow [Sainte-Marie et al., 2006] and rely on rheological models – see among others [Le Tallec, 1994]. The main idea is to describe the global macroscopic behavior resulting from the combination of several constitutive elements by an analogy with a combination of spring and damping elements in series and parallel.

Under the small displacements assumption, the natural rules of series and parallel associations apply. However, when considering the general non-linear case, the combined laws are more intricate as envisioned in [Sainte-Marie et al., 2006] and fully presented in our work [14]. In fact, let us consider a 1D element corresponding to two elastic materials in series. We then have for the deformation maps

$$\phi = \phi_2 \circ \phi_1 \Rightarrow \nabla \phi = \nabla \phi_2 \cdot \nabla \phi_1,$$

so that

$$1 + 2e = (1 + 2e_1)(1 + 2e_2). \quad (3.3)$$

Considering the stresses, we sum the free energies $\mathcal{G}(e) = \mathcal{G}_1(e_1) + \mathcal{G}_2(e_2)$ under the kinematical constraint (3.3). Minimizing the energy allows then to characterize e_1 et e_2 at the equilibrium

$$(e_1, e_2) = \underset{1+2e=(1+2e_1)(1+2e_2)}{\operatorname{argmin}} \mathcal{G}(e),$$

so that we have

$$\begin{cases} \mathcal{G}'_1 de_1 + \mathcal{G}'_2 de_2 = 0 \\ (1 + 2e_2) de_1 + (1 + 2e_1) de_2 = 0 \end{cases}$$

with \mathcal{G}'_1 and \mathcal{G}'_2 the derivatives of \mathcal{G}_1 and \mathcal{G}_2 with respect to the scalar strains e_1 and e_2 , respectively. We then obtain

$$\frac{\mathcal{G}'_1}{1 + 2e_2} = \frac{\mathcal{G}'_2}{1 + 2e_1}.$$

Finally, the total stress in the element $\sigma = \frac{\partial \mathcal{G}}{\partial e}$ is thus given by

$$\begin{aligned} d\mathcal{G} &= \sigma de = \mathcal{G}'_1 de_1 + \mathcal{G}'_2 de_2 \\ &= \frac{\mathcal{G}'_1}{1 + 2e_2} ((1 + 2e_2) de_1 + (1 + 2e_1) de_2) \\ &= \frac{\mathcal{G}'_1}{1 + 2e_2} de, \end{aligned}$$

and equally when switching the index 1 and 2. Therefore, the rheological law is finally modified to give

$$\sigma = \frac{\sigma_1}{1 + 2e_2} = \frac{\sigma_2}{1 + 2e_1}.$$

With the rheological non-linear relations, we can consider a full rheological model such as that presented in Figure 3.1 and then integrate the energy balance considerations of each

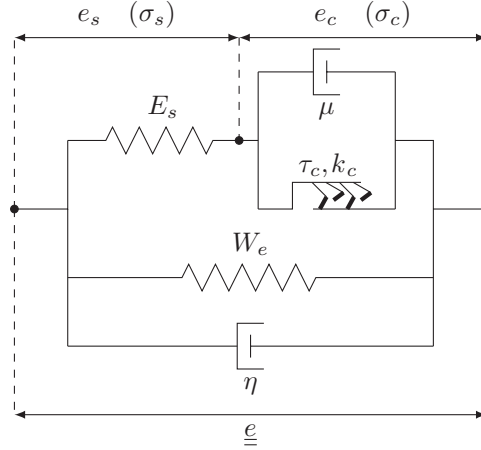


Figure 3.1: Hill-maxwell rheological model of the cardiac structure.

element. We end up in [14] with the formulation

$$\left\{ \begin{array}{l} \dot{\underline{u}} = \underline{v} \\ \int_{\Omega_0} \rho \dot{\underline{v}} \cdot \underline{v}^* \, d\Omega + \int_{\Omega_0} \underline{\underline{\Sigma}} : d_{\underline{u}} \underline{\underline{e}} \cdot \underline{v}^* \, d\Omega = \mathcal{P}_{\text{ext}}(\underline{v}^*), \quad \forall \underline{v}^* \in V \\ \underline{\underline{\Sigma}} = \frac{\partial W_e}{\partial \underline{\underline{e}}} + \frac{\partial W_v}{\partial \dot{\underline{\underline{e}}}} + \sigma_{1D} \underline{\underline{\tau}}_1 \otimes \underline{\underline{\tau}}_1 \\ (\tau_c + \mu \dot{e}_c)(1 + 2e_c)^3 = E_s(e_{1D} - e_c)(1 + 2e_{1D}) \\ \dot{k}_c = -(|u| + \alpha |\dot{e}_c|)k_c + n_0 k_0 |u|_+ \\ \dot{\tau}_c = -(|u| + \alpha |\dot{e}_c|)\tau_c + \dot{e}_c k_c + n_0 \sigma_0 |u|_+ \end{array} \right. \quad (3.4)$$

under the above definition of the fiber stress and strain

$$\sigma_{1D} = \left(\frac{1 + 2e_c}{1 + 2e_{1D}} \right) \sigma_c, \quad \sigma_c = \tau_c + \mu \dot{e}_c \quad \text{and} \quad e_{1D} = \underline{\underline{\tau}}_1 \cdot \underline{\underline{e}} \cdot \underline{\underline{\tau}}_1,$$

and where $\mathcal{P}_{\text{ext}}(\underline{v}^*)$ is the virtual work associated with the external forces. This model is proved to be thermodynamically compatible with the following energy balance.

PROPOSITION 3.2.2 (CHAPPELLE-LE TALLEC-MOIREAU-SORINE)

The model (3.4) satisfies the energy balance

$$\begin{aligned} & \frac{d}{dt} \left(\mathcal{K} + \mathcal{E}_e + \frac{1}{2} \int_{\Omega_0} E_s e_s^2 \, d\Omega + \int_{\Omega_0} U_c \, d\Omega \right) = \\ & \mathcal{P}_{\text{ext}}(\underline{v}) + \int_{\Omega_0} n_0 U_0 |u|_+ \, d\Omega - \int_{\Omega_0} (|u| + \alpha |\dot{e}_c|) U_c \, d\Omega - \int_{\Omega_0} \mu (\dot{e}_c)^2 \, d\Omega - \int_{\Omega_0} \frac{\partial W_v}{\partial \dot{\underline{\underline{e}}}} : \dot{\underline{\underline{e}}} \, d\Omega. \end{aligned} \quad (3.5)$$

where the various energy contributions are as follows:

- $\mathcal{K} = \frac{1}{2} \int_{\Omega_0} \rho |\underline{v}|^2 \, d\Omega$ is the kinetic energy;
- $\mathcal{E}_e = \int_{\Omega_0} W_e \, d\Omega$ is the hyperelastic energy of the 3D matrix;

- $\frac{1}{2} \int_{\Omega_0} E_s e_s^2 \, d\Omega$ is an additive passive elastic energy associated with the fiber;
- U_c is the microscopic elastic energy of the actin-myosin bridges.

For the source terms:

- \mathcal{P}_{ext} is the power of external forces;
- $\int_{\Omega_0} n_0 U_0 |u|_+ \, d\Omega$ is the positive power consumed by the actin-myosin engine.

As for the dissipative terms:

- $\int_{\Omega_0} (|u| + \alpha |\dot{e}_c|) U_c \, d\Omega$ is the energy dissipated during the binding-unbinding mechanisms;
- $\int_{\Omega_0} \mu (\dot{e}_c)^2 \, d\Omega$ is the (passive) viscous dissipation in the contractile element;
- $\int_{\Omega_0} \frac{\partial W_v}{\partial \underline{\underline{e}}} : \underline{\underline{e}} \, d\Omega$ is the dissipated energy due to the passive viscosity of the 3D matrix.

Proposition 3.2.2, combined with Proposition 3.2.1 then allows to produce a complete mathematical analysis of the model (3.4) at least for a linearized formulation but also with a mathematically grounded non-linear extension. This will be published in forthcoming works. Moreover it allows to propose the following energy-consistent discretizations

$$\left\{ \begin{array}{l}
 \frac{\underline{u}^{n+1} - \underline{u}^n}{\Delta t} = \frac{\underline{v}^{n+1} + \underline{v}^n}{2} \\
 \int_{\Omega_0} \rho \frac{\underline{v}^{n+1} - \underline{v}^n}{\Delta t} \cdot \underline{v}^* \, d\Omega + \int_{\Omega_0} \underline{\underline{\Sigma}}^{n+\frac{1}{2}\sharp} : \underline{\underline{d}} \underline{e}^{n+\frac{1}{2}\sharp} \cdot \underline{v}^* \, d\Omega = \mathcal{P}_{\text{ext}}^{n+\frac{1}{2}}(\underline{v}^*), \quad \forall \underline{v}^* \in V \\
 \underline{\underline{\Sigma}}^{n+\frac{1}{2}\sharp} = \frac{\partial W_e}{\partial \underline{\underline{e}}} \Big|^{n+\frac{1}{2}\sharp} + \frac{\partial W_v}{\partial \underline{\underline{e}}} \Big|^{n+\frac{1}{2}\sharp} + \sigma_{1D}^{n+\frac{1}{2}\sharp} \underline{\tau}_1 \otimes \underline{\tau}_1, \\
 \left(\sqrt{k_c^{n+1}} \left(\frac{\tau_c}{\sqrt{k_c}} \right)^{n+1} + \mu \frac{e_c^{n+1} - e_c^n}{\Delta t} \right) (1 + 2e_c^{n+\frac{1}{2}})^3 = E_s (e_{1D}^{n+\frac{1}{2}} - e_c^{n+\frac{1}{2}}) (1 + 2e_{1D}^{n+\frac{1}{2}}) \\
 \frac{k_c^{n+1} - k_c^n}{\Delta t} = - \left(|u^{n+1}| + \alpha \left| \frac{e_c^{n+1} - e_c^n}{\Delta t} \right| \right) k_c^{n+1} + n_0 k_0 |u^{n+1}|_+ \\
 \frac{1}{\Delta t} \left(\left(\frac{\tau_c}{\sqrt{k_c}} \right)^{n+1} - \left(\frac{\tau_c}{\sqrt{k_c}} \right)^n \right) = \sqrt{k_c^{n+1}} \frac{e_c^{n+1} - e_c^n}{\Delta t} \\
 \quad + \frac{n_0 \sigma_0 |u^{n+1}|_+}{\sqrt{k_c^{n+1}}} \left(1 - \frac{k_0}{2\sigma_0 \sqrt{k_c^{n+1}}} \left(\frac{\tau_c}{\sqrt{k_c}} \right)^{n+1} \right) \\
 \quad - \frac{1}{2} \left(|u^{n+\frac{1}{2}}| + \left| \frac{e_c^{n+1} - e_c^n}{\Delta t} \right| \right) \left(\frac{\tau_c}{\sqrt{k_c}} \right)^{n+1}
 \end{array} \right. \quad (3.6)$$

where we use the standard notation

$$g^{n+\frac{1}{2}} = \frac{g^n + g^{n+1}}{2},$$

except when specified otherwise for some variables that we denote by $g^{n+\frac{1}{2}\sharp}$, typically the strain values

$$\underline{\underline{e}}^{n+\frac{1}{2}\sharp} = \underline{\underline{e}}(\underline{u}^{n+\frac{1}{2}}),$$

$$\begin{aligned} d_{\underline{u}} \underline{e}^{n+\frac{1}{2}\sharp} \cdot \underline{v}^* &= \frac{1}{2} (\underline{F}(\underline{u}^{n+\frac{1}{2}}))^\top \cdot \underline{\nabla}_{\underline{x}} \underline{v}^* + \underline{\nabla}_{\underline{x}}^\top \underline{v}^* \cdot \underline{F}(\underline{u}^{n+\frac{1}{2}}), \\ \underline{\dot{e}}^{n+\frac{1}{2}\sharp} &= \frac{\underline{e}^{n+1} - \underline{e}^n}{\Delta t}. \end{aligned}$$

For the passive elastic stress

$$\begin{aligned} \left. \frac{\partial W_e}{\partial \underline{e}} \right|^{n+\frac{1}{2}\sharp} &= \frac{\partial W_e}{\partial \underline{e}}(\underline{e}^{n+\frac{1}{2}\sharp}) \\ &+ \left(\frac{W_e(\underline{e}^{n+1}) - W_e(\underline{e}^n)}{\Delta t} - \frac{\partial W_e}{\partial \underline{e}}(\underline{e}^{n+\frac{1}{2}\sharp}) : \underline{\dot{e}}^{n+\frac{1}{2}\sharp} \right) \frac{\underline{\dot{e}}^{n+\frac{1}{2}\sharp}}{\underline{\dot{e}}^{n+\frac{1}{2}\sharp} : \underline{\dot{e}}^{n+\frac{1}{2}\sharp}}, \end{aligned}$$

while viscous stresses are given by

$$\left. \frac{\partial W_v}{\partial \underline{\dot{e}}} \right|^{n+\frac{1}{2}\sharp} = \frac{\partial W_v}{\partial \underline{\dot{e}}}(\underline{\dot{e}}^{n+\frac{1}{2}\sharp}).$$

The series fiber stress is given by the combined formula

$$\sigma_{1D}^{n+\frac{1}{2}\sharp} = \frac{\sigma_s^{n+\frac{1}{2}\sharp}}{1 + 2e_c^{n+\frac{1}{2}}} = \frac{\sigma_c^{n+\frac{1}{2}\sharp}}{1 + 2e_s^{n+\frac{1}{2}}},$$

with

$$\sigma_s^{n+\frac{1}{2}\sharp} = E_s e_s^{n+\frac{1}{2}},$$

and

$$\sigma_c^{n+\frac{1}{2}\sharp} = \sqrt{k_c^{n+1}} \left(\frac{\tau_c}{\sqrt{k_c}} \right)^{n+1} + \mu \frac{e_c^{n+1} - e_c^n}{\Delta t}.$$

Indeed, we have the next theorem proved in [14].

THEOREM 3.2.3 (CHAPELLE-LE TALLEC-MOIREAU-SORINE)

By construction, the proposed time discretisation scheme (3.6) preserves the global energy dissipation properties of the original problem.

3.2.2 An energy balanced coupling of porous flows and hyperelastic formulations

Poromechanics has been a very active subject of research for decades, in particular in geosciences. There, in a context of small displacements mechanical theories have been developed to define the mechanical response of a two-phase system combining a solid skeleton with a fluid. We can classify the available approaches with the mixture theory [Biot, 1972, Coussy, 2004, de Boer, 2005, Loret and Simões, 2005] or with homogenization theory [Rohan and Cimmrman, 2010]. Recently, poromechanical models have found new application in life sciences since numerous organs are perfused with fluids, in particular blood. Considering the heart or the lungs for instance, these new systems face new regimes with large deformation and high fluid inertia imposing to revisit the field to circumvent various limitations of the existing theories. In the context of mixture theory we decide in [15] to propose a complete reformulation of a fluid perfusing a solid in large deformations without neglecting inertial effects. We believe that the mixture theory offers a very nice framework to devise adapted formulations at the organ scale

that are compatible with the thermodynamics principles. Therefore, they have energy balances allowing again to measure the physiological energetic exchange but also to propose formulations that are well-posed from a mathematical point of view and of stable discretizations even in non-linear configurations.

In the mixture theory we consider a material that contains at each point a volume fraction ϕ of fluid phase, and a remaining fraction $1 - \phi$ of solid phase. The mixture field will be denoted without subscript, whereas the solid phase fields are defined by a s subscript and the fluid phase fields by a f subscript.

Then by standard conservation laws we have the mass conservation on the deformed domain

$$\frac{d}{dt}(\rho_f \phi) + \nabla_{\underline{x}} \cdot (\rho_f \phi \underline{v}_s + \underline{w}) = \theta.$$

where θ represents a distributed mass source term, and $\underline{w} = \underline{w} = \rho_f \phi (\underline{v}_f - \underline{v}_s)$. Then we have the conservation of momentum leading to the principle of virtual work

$$\forall \underline{v}^* \in V(\Omega), \quad \mathcal{P}_i(\underline{v}^*) + \mathcal{P}_{\text{int}}(\underline{v}^*) = \mathcal{P}_{\text{ext}}(\underline{v}^*),$$

with

$$\begin{cases} \mathcal{P}_i(\underline{v}^*) &= \int_{\Omega_t} (\rho_s(1 - \phi)\underline{\gamma}_s + \rho_f\phi\underline{\gamma}_f) \cdot \underline{v}^* \, d\Omega = \int_{\Omega_0} (\rho_{s0}(1 - \phi_0)\underline{\gamma}_s + (\rho_{f0}\phi_0 + m)\underline{\gamma}_f) \cdot \underline{v}^* \, d\Omega \\ \mathcal{P}_{\text{int}}(\underline{v}^*) &= \int_{\Omega_t} \underline{\sigma} : \underline{\varepsilon}(\underline{v}^*) \, d\Omega = \int_{\Omega_0} \underline{\Sigma} : \underline{d}_u \underline{e} \cdot \underline{v}^* \, d\Omega \\ \mathcal{P}_{\text{ext}}(\underline{v}^*) &= \int_{\Omega_t} \rho \underline{f} \cdot \underline{v}^* \, d\Omega + \int_{\partial\Omega_t} \underline{t} \cdot \underline{v}^* \, d\Gamma = \int_{\Omega_0} (\rho_0 + m) \underline{f} \cdot \underline{v}^* \, d\Omega + \int_{\partial\Omega_0} \underline{t}_0 \cdot \underline{v}^* \, d\Gamma \end{cases}$$

where we adopt capitalize letters or a 0 subscript for variables on reference domain. The difficulty in [15] was then to derive in large deformation the Clausius-Duhem inequalities associated with the second principle of thermodynamics. This is summarized by the following results

THEOREM 3.2.4 (CHAPELLE-MOIREAU)

The second principle is verified with the following conditions:

- For the heat rate, we suppose that Fourier's law is satisfied, namely,

$$\underline{J}_Q = -\lambda_Q \nabla_{\underline{x}} T.$$

- For the stress tensor, we assume it is the sum of the three contributions

$$\underline{\Sigma} = \phi \underline{\Sigma}_{\text{vis}} + \frac{\partial \Psi}{\partial \underline{e}} + \frac{\partial \Psi_{\text{damp}}}{\partial \underline{\dot{e}}},$$

with $\Psi^{\text{damp}}(\underline{e}, \underline{\dot{e}})$ a viscous pseudo-potential convex in the variable $\underline{\dot{e}} = \frac{d\underline{e}}{dt} = \underline{d}_u \underline{e} \cdot \underline{v}_s$ and satisfying $\frac{\partial \Psi_{\text{damp}}}{\partial \underline{\dot{e}}}(\underline{e}, \underline{0}) = \underline{0}$, which entails

$$\frac{\partial \Psi_{\text{damp}}}{\partial \underline{\dot{e}}} : \underline{\dot{e}} \geq 0.$$

- For the fluid viscous term, we assume we always have the dissipation inequality

$$\underline{\sigma}_{\text{vis}} : \underline{\varepsilon}(\underline{v}_f) \geq 0.$$

- For the relative velocity of the fluid, there exists a positive definite second order tensor $\underline{\underline{K}}_f$ such that

$$\frac{1}{\rho_f} \underline{W} = \underline{\underline{K}}_f \cdot (-\nabla_{\underline{x}} p + \rho_f \underline{F}^\top \cdot (\underline{f} - \underline{\gamma}_f) + \frac{1}{\phi} \underline{F}^\top \cdot \nabla_{\underline{x}} \cdot (\phi \underline{\underline{\Pi}}_{vis})),$$

meaning in the Eulerian framework that

$$\frac{1}{\rho_f} \underline{w} = \underline{k}_f \cdot (-\nabla_{\underline{x}} p + \rho_f (\underline{f} - \underline{\gamma}_f) + \frac{1}{\phi} \nabla_{\underline{x}} \cdot (\phi \underline{\underline{\sigma}}_{vis})),$$

with $\underline{k}_f = \frac{1}{J} \underline{F} \cdot \underline{\underline{K}}_f \cdot \underline{F}^\top$.

We end up with the following strong formulation

$$\left\{ \begin{array}{l} \rho_{s0}(1 - \phi_0) \frac{d\underline{v}_s}{dt} - \nabla_{\underline{x}} \cdot (\underline{F} \cdot \underline{\underline{\Sigma}}) - J \phi^2 \underline{k}_f^{-1} \cdot (\underline{v}_f - \underline{v}_s) \\ \quad + p J \underline{F}^{-T} \cdot \nabla_{\underline{x}} \phi = \rho_{s0}(1 - \phi_0) \underline{f}, \quad \text{in } \Omega_0 \\ \frac{1}{J} \frac{d}{dt} (J \rho_f \phi \underline{v}_f) + \nabla_{\underline{x}} \cdot (\rho_f \phi \underline{v}_f \otimes (\underline{v}_f - \underline{v}_s)) - \theta \underline{v}_f + \phi^2 \underline{k}_f^{-1} \cdot (\underline{v}_f - \underline{v}_s) \\ \quad + \phi \nabla_{\underline{x}} p - \nabla_{\underline{x}} \cdot (\phi \underline{\underline{\sigma}}_{vis}) = \rho_f \phi \underline{f}, \quad \text{in } \Omega_t \\ \frac{1}{J} \frac{d}{dt} (J \rho_f \phi) + \nabla_{\underline{x}} \cdot (\rho_f \phi (\underline{v}_f - \underline{v}_s)) = \theta, \quad \text{in } \Omega_t \end{array} \right. \quad (3.7)$$

where we recognize in (3.7)₂ an equation very similar to the conservative form of the so-called Arbitrary Lagrangian Eulerian (ALE) formulation of the compressible Navier-Stokes equations [Vidrascu et al., 2005], where here the domain velocity is given by the skeleton *physical* velocity and the product $\rho_f \phi$ plays the role of a varying fluid mass density. However, compared with standard fluid-structure interaction problems, we have the additional distributed coupling term $\underline{k}_f^{-1} \cdot (\underline{v}_f - \underline{v}_s)$ representing the interaction between the two phases.

Moreover, the interest of satisfying the thermodynamical principles is that we can then prove an energy balance property useful both physically and mathematically.

THEOREM 3.2.5 (CHAPELLE-MOIREAU)

The solution of the general poromechanics problem written in (3.7) satisfies the following energy balance

$$\frac{d\mathcal{K}}{dt} + \frac{d\mathcal{W}}{dt} = - \int_{\Omega_0} \frac{\partial \Psi_{damp}}{\partial \underline{\dot{\epsilon}}} : \underline{\dot{\epsilon}} \, d\Omega - \int_{\Omega_t} \phi \underline{\underline{\sigma}}_{vis} : \underline{\underline{\epsilon}}(\underline{v}_f) \, d\Omega - \int_{\Omega_t} (\underline{v}_f - \underline{v}_s) \cdot \phi^2 \underline{k}_f^{-1} \cdot (\underline{v}_f - \underline{v}_s) \, d\Omega \\ + \mathcal{P}_{ext}^{total} + \mathcal{I}_{\mathcal{K}b} + \mathcal{I}_{\mathcal{K}\theta} + \mathcal{I}_{\mathcal{W}b} + \mathcal{I}_{\mathcal{G}\theta},$$

with

$$\mathcal{I}_{\mathcal{K}b} = -\frac{1}{2} \int_{\partial\Omega_t} \rho_f \phi \underline{v}_f^2 (\underline{v}_f - \underline{v}_s) \cdot \underline{n} \, d\Gamma, \quad \mathcal{I}_{\mathcal{K}\theta} = \frac{1}{2} \int_{\Omega_t} \underline{v}_f^2 \theta \, d\Omega,$$

the incoming rates of fluid kinetic energy due to the boundary flow and source term, respectively, and

$$\mathcal{I}_{\mathcal{W}b} = - \int_{\partial\Omega_t} \rho_f \phi \psi_m (\underline{v}_f - \underline{v}_s) \cdot \underline{n} \, d\Gamma, \quad \mathcal{I}_{\mathcal{G}\theta} = \int_{\Omega_t} g_m \theta \, d\Omega,$$

similar incoming rates of Helmholtz and Gibbs free energies.

In particular this gives the opportunity to define stable discretizations. In [15], we propose the discretization

$$\left\{ \begin{aligned} & \int_{\Omega_0} \rho_{s0}(1 - \phi_0) \frac{v_s^{n+1} - v_s^n}{\Delta t} \cdot \underline{v}^* d\Omega + \mathcal{P}_i^{f,n+\frac{1}{2}\sharp}(\underline{v}^*) + \int_{\Omega_0} \underline{\underline{\Sigma}}^{n+\frac{1}{2}\sharp} : d\underline{\underline{e}}^{n+\frac{1}{2}\sharp} \cdot \underline{v}^* d\Omega \\ & \hspace{15em} = \int_{\Omega_0} \rho_0 \underline{f}^{n+\frac{1}{2}} \cdot \underline{v}^* d\Omega + \int_{\partial\Omega_0} \underline{t}_0^{n+\frac{1}{2}} \cdot \underline{v}^* d\Gamma, \\ & \mathcal{P}_i^{f,n+\frac{1}{2}\sharp}(\underline{v}^*) + \int_{\Omega_{n+\frac{1}{2}}} (\phi^{n+\frac{1}{2}\sharp})^2 (v_f^{n+\frac{1}{2}\sharp} - v_s^{n+\frac{1}{2}}) \cdot \underline{\underline{D}}_f \cdot \underline{v}^* d\Omega \\ & \hspace{15em} = \int_{\Omega_{n+\frac{1}{2}}} (-\phi^{n+\frac{1}{2}\sharp} \underline{\nabla}_{\underline{x}} p^{n+\frac{1}{2}} + \phi^{n+\frac{1}{2}\sharp} \underline{f}^{n+\frac{1}{2}}) \cdot \underline{v}^* d\Omega \\ & \int_{\Omega_0} q^* \frac{m_f^{n+1} - m_f^n}{\Delta t} d\Omega + \int_{\Omega_{n+\frac{1}{2}}} \underline{\nabla}_{\underline{x}} \cdot (\rho_f \phi^{n+\frac{1}{2}\sharp} (v_f^{n+\frac{1}{2}\sharp} - v_s^{n+\frac{1}{2}})) q^* d\Omega = \int_{\Omega_{n+\frac{1}{2}}} q^* \theta^{n+\frac{1}{2}} d\Omega \end{aligned} \right. \quad (3.8)$$

to which we add the boundary conditions

$$v_f^{n+\frac{1}{2}\sharp} = v_s^{n+\frac{1}{2}} \text{ on } \partial\Omega_{n+\frac{1}{2}},$$

and in System (3.8) we make use of the following discretization choices :

- For the fluid inertia

$$\begin{aligned} \mathcal{P}_i^{f,n+\frac{1}{2}\sharp}(\underline{v}^*) &= \int_{\Omega_0} \frac{\underline{k}_f^{n+1} - \underline{k}_f^n}{\Delta t} \cdot \sqrt{m_f}^{n+\frac{1}{2}} \underline{v}^* d\Omega - \frac{1}{2} \int_{\Omega_{n+\frac{1}{2}}} \underline{\nabla}_{\underline{x}} \cdot (\rho_f \phi^{n+\frac{1}{2}\sharp} (v_f^{n+\frac{1}{2}\sharp} - v_s^{n+\frac{1}{2}})) \underline{v}_f^{n+\frac{1}{2}\sharp} \cdot \underline{v}^* d\Omega \\ &+ \int_{\Omega_{n+\frac{1}{2}}} \underline{\nabla}_{\underline{x}} \cdot (\rho_f \phi^{n+\frac{1}{2}\sharp} \underline{v}_f^{n+\frac{1}{2}\sharp} \otimes (v_f^{n+\frac{1}{2}\sharp} - v_s^{n+\frac{1}{2}})) \cdot \underline{v}^* d\Omega - \frac{1}{2} \int_{\Omega_{n+\frac{1}{2}}} \theta \underline{v}_f^{n+\frac{1}{2}\sharp} \cdot \underline{v}^* d\Omega. \end{aligned}$$

with

$$\phi^{n+\frac{1}{2}\sharp} = \frac{m_f^{n+\frac{1}{2}}}{\rho_f J(\underline{u}_s^{n+\frac{1}{2}})}, \quad m^{n+\frac{1}{2}} = m_f^{n+\frac{1}{2}} - \rho_f \phi_0.$$

whereas $m_f = \rho_f J\phi$ and $\underline{k}_f = \sqrt{m_f} \underline{v}_f$ are discretized such that

$$\underline{k}_f^{n+\frac{1}{2}} = \frac{\underline{k}_f^{n+1} + \underline{k}_f^n}{2}, \quad m^{n+\frac{1}{2}} = m_f^{n+\frac{1}{2}} - \rho_f \phi_0,$$

and

$$\begin{aligned} \left. \frac{\partial \underline{k}_f}{\partial t} \right|_{\underline{x}}^{n+\frac{1}{2}\sharp} &= \frac{\underline{k}_f^{n+1} - \underline{k}_f^n}{\Delta t} \\ \underline{v}_f^{n+\frac{1}{2}\sharp} &= \frac{\underline{k}_f^{n+\frac{1}{2}}}{\sqrt{m_f}^{n+\frac{1}{2}}} \end{aligned}$$

- Regarding the second Piola-Kirchhoff stress tensor we draw our inspiration from [Le Tallec and Hauret, 2003, Gonzalez, 2000] and propose

$$\underline{\underline{\Sigma}}^{n+\frac{1}{2}\sharp} = \left. \frac{\partial \Psi}{\partial \underline{\underline{e}}} \right|^{n+\frac{1}{2}\sharp} + \left. \frac{\partial \Psi_{\text{damp}}}{\partial \underline{\underline{e}}} \right|^{n+\frac{1}{2}\sharp},$$

with the viscous contribution given by

$$\frac{\partial \Psi_{\text{damp}}}{\partial \dot{\underline{e}}} \Big|^{n+\frac{1}{2}\#} = \frac{\partial \Psi_{\text{damp}}}{\partial \dot{\underline{e}}} (\underline{e}^{n+\frac{1}{2}\#}, \dot{\underline{e}}^{n+\frac{1}{2}\#}),$$

and the hyperelastic part by

$$\begin{aligned} \frac{\partial \Psi}{\partial \underline{e}} \Big|^{n+\frac{1}{2}\#} &= \frac{\partial \Psi}{\partial \underline{e}} (\underline{e}^{n+\frac{1}{2}\#}, m^{n+\frac{1}{2}}) \\ &+ \left(\frac{\Psi(\underline{e}^{n+1}, m^{n+\frac{1}{2}}) - \Psi(\underline{e}^n, m^{n+\frac{1}{2}})}{\Delta t} - \frac{\partial \Psi}{\partial \underline{e}} (\underline{e}^{n+\frac{1}{2}\#}, m^{n+\frac{1}{2}}) : \dot{\underline{e}}^{n+\frac{1}{2}} \right) \frac{\dot{\underline{e}}^{n+\frac{1}{2}}}{\dot{\underline{e}}^{n+\frac{1}{2}} : \dot{\underline{e}}^{n+\frac{1}{2}}}, \end{aligned}$$

while the pressure is obtained by

$$\frac{p^{n+\frac{1}{2}}}{\rho_f} = \frac{\partial \Psi}{\partial m} \Big|^{n+\frac{1}{2}\#} = \frac{\Psi(\underline{e}^{n+1}, m^{n+1}) - \Psi(\underline{e}^{n+1}, m^{n+\frac{1}{2}}) + \Psi(\underline{e}^n, m^{n+\frac{1}{2}}) - \Psi(\underline{e}^n, m^n)}{m^{n+1} - m^n}.$$

Finally we prove

THEOREM 3.2.6 (CHAPELLE-MOIREAU)

The time scheme (3.8) is unconditionally stable, and of second-order accuracy.

3.3 Reduced-order modeling

With the title “reduced order modeling” we broach the subject of finding strategies to accelerate the simulations of our models. This question has become very popular with the emergence of complex systems and is also often referred as reduced modeling which can give the false impression that the model is simplified. In our case, we have studied two types of model reduction: (1) a dimension reduction operated by considering simplified geometrical configurations and (2) a reduced-basis projection in the Galerkin spatial discretization of a model.

3.3.1 Dimensional reductions of a cardiac model for effective validation and calibration

In [36] and then in [7] we demonstrate how, using geometrical arguments, a generic 3D model can be used to derive associated reduced-dimensional models both in “0D” (zero-dimensional) – typically, to represent a cardiac cavity – and in “1D” one-dimensional – to model a fiber or a myocyte. Such reduced models can then be *combined* with 3D models to provide dramatic effectiveness gains without compromising modeling accuracy at the local scale. Hence we envision different purposes such as:

- 1D-0D: to obtain fast translations of experimentally assessed properties – based on 1D samples – to the “organ” level approximately represented by the 0D model;
- 1D-3D: to infer much more accurate translations to the organ level, e.g. including spatial heterogeneities and detailed fiber distributions;

- 0D-3D: to easily calibrate the constitutive properties based on global indicators prior to running 3D simulations.

To proceed to the model reduction, we consider the formulation (3.1) where we decide to make geometrical, hence kinematics assumptions. These assumptions consists in the shape of the system to be considered – namely, a sphere or a fiber – and an hypothesis of small thickness to derive an asymptotic behavior within the thickness. Note that our geometrical assumptions are coupled with geometrical assumptions within the constitutive law about the orthotropic behavior, and with the boundary conditions.

3.3.1.1 0D-formulation

We consider a simplified problem in which the geometry and the physical behavior are endowed with spherical symmetry properties. The simplified geometry for a ventricle is given by a sphere of radius R_0 and thickness d_0 in the stress-free reference configuration Ω_0 , see Fig.3.2. We

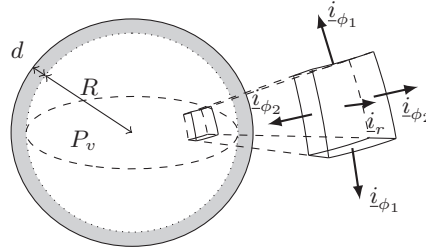


Figure 3.2: Spherical model of a ventricle

denote by $(\underline{i}_r, \underline{i}_{\phi_1}, \underline{i}_{\phi_2})$ an orthonormal basis and show that in this basis the displacement field with respect to the reference configuration is radial, namely, given by $\underline{u} = u \underline{i}_r = (R - R_0) \underline{i}_r$, and the right Cauchy-Green deformation tensor has the special form

$$\underline{\underline{C}} = \begin{pmatrix} C_{rr} & 0 & 0 \\ 0 & C & 0 \\ 0 & 0 & C \end{pmatrix},$$

where $\sqrt{C} = 1 + u/R_0$ is the ratio of circumferential lengths between the reference and deformed configurations. Moreover, assuming incompressible behavior, we have $\det \underline{\underline{C}} = 1$, hence $C_{rr} = C^{-2}$. Therefore, we have for example

$$(\underline{d}_{\underline{u}} \underline{e} \cdot \underline{y}^*)_{\phi\phi} = (1 + y/R_0)(y^*/R_0).$$

Then we proceed with classical arguments of shell theory that justify that the radial stress Σ_{rr} can be neglected compared to the orthoradial components [Chapelle and Bathe, 2011]. Therefore, in the incompressible limit of the second-Piola Kirchhoff definition

$$\underline{\underline{\Sigma}} = \underline{\underline{\Sigma}}_p (J_3 = 1) + \sigma_{1D}(e_{1D}, t) \underline{\underline{\tau}} \otimes \underline{\underline{\tau}} - p J \underline{\underline{C}}^{-1}$$

the Lagrange multiplier p can be explicitly inferred from $\Sigma_{rr} = 0$, *viz.*

$$p = C^{-2} (\underline{\underline{\Sigma}}_p)_{rr}.$$

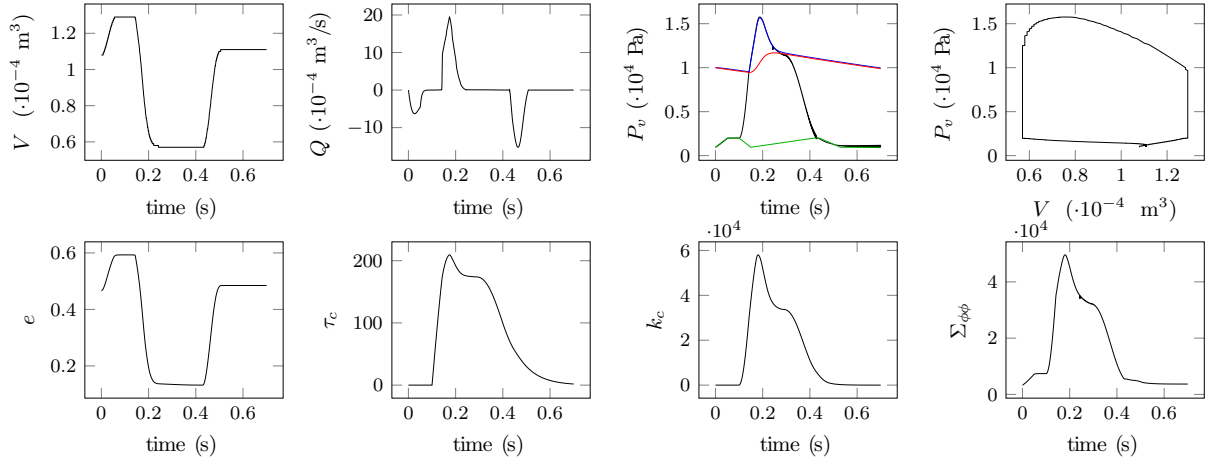


Figure 3.3: Cardiac cycle obtained with the 0D-model

Hence, we find

$$\begin{aligned} \underline{\underline{\Sigma}} : d_{\underline{u}} \underline{e} \cdot \underline{u}^* &= \left(1 + \frac{u}{R_0}\right) \frac{u^*}{R_0} (\Sigma_{\phi_1 \phi_1} + \Sigma_{\phi_2 \phi_2}) \\ &= \left(1 + \frac{u}{R_0}\right) \frac{u^*}{R_0} \Sigma_{\text{sph}}, \end{aligned}$$

with the combined stress quantity Σ_{sph} defined by

$$\Sigma_{\text{sph}} = (\underline{\underline{\Sigma}}_p)_{\phi_1 \phi_1} + (\underline{\underline{\Sigma}}_p)_{\phi_2 \phi_2} + \sigma_{1D} - 2C^{-3} (\underline{\underline{\Sigma}}_p)_{rr}.$$

hence the principle of virtual work leads – see [36] and [7] for details – to the ordinary differential equation

$$\rho d_0 \ddot{u} + \frac{d_0}{R_0} \left(1 + \frac{u}{R_0}\right) \Sigma_{\text{sph}} = P_v \left(1 + \frac{u}{R_0}\right)^2.$$

This model allows to compute in real-time complete cardiac cycles such as for example in Figure 3.3.

3.3.1.2 1D-formulation

For the isolated muscle fibers, we consider a 1D formulation – see Fig.3.4 – corresponding to a circular cylinder of radius R_0 and length L_0 in the reference configuration Ω_0 , with corresponding values R and L in the deformed configuration.

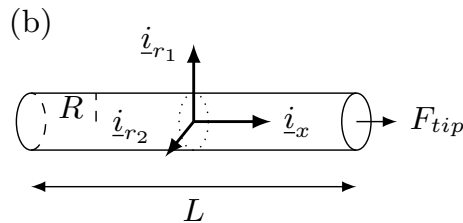


Figure 3.4: Cylindrical model of a cardiac muscle sample

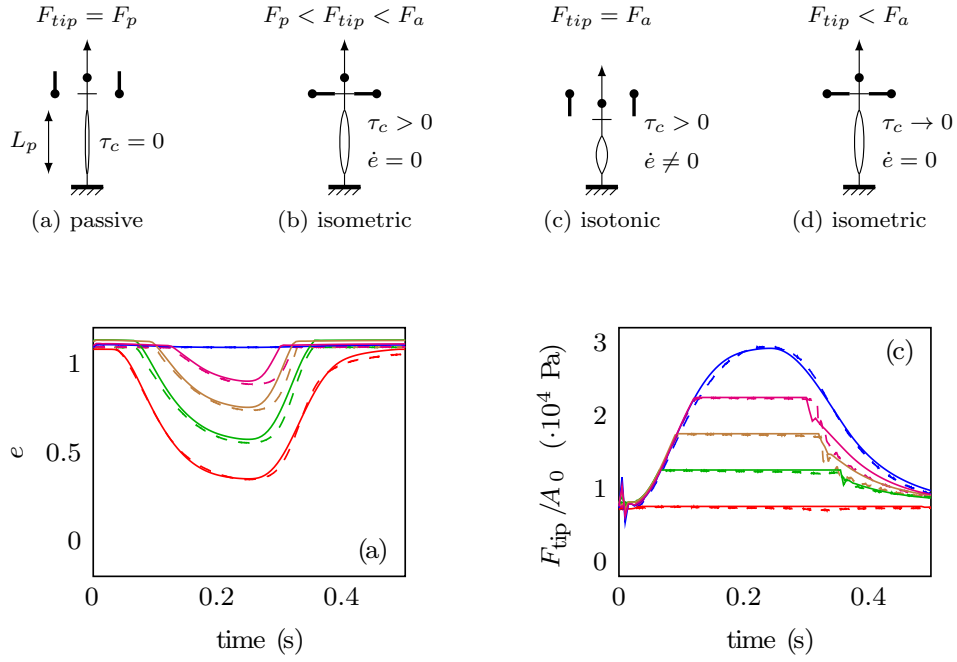


Figure 3.5: Strain (top) and stress (bottom) response of a single papillary muscle for a loading experiment (top). Dashed lines, experimental measurements; solid lines, simulations

As an orthonormal basis we use a first vector \underline{i}_x oriented along the fiber – i.e. $\underline{\tau} = \underline{i}_x$ – and we define two arbitrary equivalent directions ($\underline{i}_{r_1}, \underline{i}_{r_2}$) in the cross-section. An external force F_{tip} is applied at the end of the sample along the \underline{i}_x -direction, and we seek the resulting longitudinal displacement $u(x)$ at each point of the sample. Due to the incompressibility condition, the Cauchy-Green tensor takes the special form

$$\underline{\underline{C}} = \begin{pmatrix} C & 0 & 0 \\ 0 & C^{-\frac{1}{2}} & 0 \\ 0 & 0 & C^{-\frac{1}{2}} \end{pmatrix},$$

where $\sqrt{C} = 1 + u'(x)$ is now the length ratio in the \underline{i}_x -direction. Then we can compute quantities like

$$(\underline{d}_{\underline{u}} \underline{e} \cdot \underline{u}^*)_{xx} = (1 + u')(u^*)',$$

Following the same strategy as for the 0D formulation, we end up with the 1D principle of virtual work

$$\int_0^{L_0} [\rho \ddot{u} u^* + \Sigma_{xx} (1 + u')(u^*)'] dx = \frac{F_{tip}}{A_0} u^*(L_0), \quad \forall u^* \in \mathcal{V}$$

or in strong form

$$\begin{cases} \rho \ddot{u} - [\Sigma_{xx} (1 + u')] = 0 \\ \Sigma_{xx}(L_0)(1 + u'(L_0)) = \frac{F_{tip}}{A_0} \end{cases}$$

This type of model can then be used to simulate loading experiments on a fiber such as in Figure 3.5.

3.3.2 Proper Orthogonal Decomposition for parameter-dependent problems – application to parameter estimation

A second strategy in reduced-order modeling consists in the use of a projection of a Galerkin formulation over a reduced basis. In this respect, we already mentioned the use of the Proper Orthogonal Decomposition for such a reduction. This subject has led to intensive research and application in cardiac modeling. However, the electrophysiology problem has been more investigated [Boulakia et al., 2012, Chapelle et al., 2012] and also [13, 19] than the mechanical problem. In [13] however, we illustrate the use of such a POD formulation for our cardiac model, including some parameter estimation.

One key aspect of our investigation on POD, is the understanding of the robustness of the POD basis with respect to parameter variations in order to rely on the POD reduction in estimation. We prove in [13] a robustness estimate as soon as the POD basis has been constructed with trajectories computed with parameters surrounding the target value. The numerical investigation on the electrophysiological problem in [13, 19] justifies our theory. Moreover, our tests on the mechanical formulation, hence on a very different model formulation, are consistent with this estimate.

3.4 Model-data interaction for the cardiovascular system

In this last section, we want to present various cardiovascular applications of our sequential joint state and parameter estimation methodology. Indeed we have put a lot of effort in showing that our strategy is compatible with large systems and real data, so that it can be envisioned in the future to define through estimation patient-specific models, not only from a geometrical point of view but also from a biophysical point of view.

3.4.1 Estimation of tissue contractility from cardiac Cine-MRI – a pig experiment

In [8], we assess a joint state-parameter estimation procedure to identify some regional values of key biophysical parameters in a beating heart model, using actual Cine-MR images. We use a complete heart model of the type (3.4) estimated with a combination of a Luenberger observer for the state and a ROUKF filter for the parameters. The data at hand consist in a sequence of segmentations as described in Sections 2.4.1. In order to allow for a detailed assessment of the estimation results, we specifically devise and perform an animal experiment in which a controlled infarct was created. In this experiment, imaging and pressure data are acquired before and after infarction – at two subsequent stages. Therefore, we can quantitatively compare the estimation results pertaining to regional values for a major biophysical parameter of interest in this context – namely, the tissue contractility σ_0 in (3.4) characterizing the ability of the muscle fiber to generate active stresses under the effect of electrical activation – at the various stages. Moreover, we also acquire late enhancement images, a modality where a contrast agent is used to locate – but not quantify – an infarct region. This modality helps us to evaluate the accuracy of our estimation.

The results presented in [8] are very good in almost all the 17 AHA regions – the subdivision

used by cardiologists – allowing to localize but also relatively quantify the impact of the infarct. Not all the regions are in perfect accordance with the late enhancement modality but, in this case, we clearly see the impact of over-simplified boundary conditions that limit the model sensitivity.

Therefore we see that our method can be applied to very complex models with complex real (shape) data. Then, the use of the estimation completes the actual data with new information from the model but also allows to understand where the model should be improved to better adjusted to the patient data. Up to our knowledge, this result is the first result of full cardiac estimation using real data.

Note that this work was completed in [33] – see details in [Imperiale, 2013] – with synthetic data experiments where we combine cine-MRI data with tagged-MRI data in order to estimate a decreased contractility in the infarct regions but also an increased passive stiffness. Here, we show as expected that if we seek a richer estimation, we must rely on richer data.

3.4.2 Identification of boundary support parameters in a fluid-structure vascular model using patient image data

In [26], we propose some simplified visco-elastic boundary conditions in order to represent the tethering of the surrounding organs when modeling a vessel portion. Surprisingly, whereas fluid boundary condition is a subject of intensive research, there are few modeling papers on solid boundary conditions in cardiovascular modeling. This is particularly important for the ascending aorta which is connected to the moving heart and partially tied to the spine. In [26], we propose a calibration of the model, that allows to drastically reduce the motion error evaluated by comparing the computed deformation with a sequence of segmentations extracted from scan images. We then propose in [21] to automatize the boundary support parameter characterization with a sequential joint state and parameter estimation. The model is a full fluid-structure interaction problem and the data are again shape data defined by a sequence of boundary segmentations. The results presented in [21] show a substantial improvement of the simulation from the automatically identified parameters when compared to the manually calibrated ones of [26]. Moreover, certain parameter shows no convergence in the sequential estimation with persistent oscillations during the cardiac cycle. Again this is typical of modeling errors that are compensated by the estimation. In this case we find that this lack of identifiability was due to an undesignated region where the aorta is in reality sustained from below by the pulmonary trunk.

Again, the conclusion of this work is that it is now possible to couple complex models with state of the art estimation strategy. This type of FSI simulation take approximately one day of computational time for the direct simulation which limits the use of variational methods, hence the advantage of our hybrid sequential method. The model-data coupling allows to specify the model but also to evaluate it with natural systems that cannot be assessed otherwise.

3.4.3 Estimation in electrophysiology

As already mentioned, we have also proposed effective strategies for electrophysiology estimation.

In [18] and [31], we propose an original approach to complement the ECGI modalities. ECGI

consists in reconstructing the activation map from body surface potentials – a generalization of the classical ECGs. This method is now used in clinical applications as for instance with the cardioInsight technology¹. Our method shows how to reconstruct a bidomain state model and possibly jointly estimate some model parameters using the activation maps. Our method is adapted to complex electrical patterns such as fibrillation, etc. We believe that this approach can be of great potential with actual data.

Moreover, we proceed in [19] to a complete set up of a bidomain estimation using a weakly coupled electromechanical model with a combination of ECG and mechanical measurements (typically obtained from medical images and pressure measurements). We show in our synthetic examples that the associated inverse problem which consists in identifying the electrical parameters from all the available data – mechanical and electrical – is better defined than the pure electrophysiology inverse problem. This result is fundamental for helping the community to understand how the model should be chosen and the data be acquired to offer robust estimation.

3.4.4 Applications within international collaborations

We have also participated in large projects with the aim of delivering patient-specific models for cardiac applications. In [29] for instance, we participate to the set-up of a recursive quasi-static estimation based on the UKF filter in order to identify some parameters of the passive law. In [3], a nice experimental experiment is designed to evaluate the estimation accuracy for fluid-structure interaction problems with real data. In [20], a tentative of sequential estimation of contractility parameters is performed using only regional volumes data – a classical clinical indicator. In this last case, however, the resulting contractility is overestimated when compared to [8] due to simulation errors associated with the numerical locking of incompressible systems. However, the sensitivity remains accurate, validating again the efficiency of the ROUKF strategy.

¹www.cardioinsight.com




Personal References – Articles

- [1] A. Armiento, M. Doumic, P. Moireau, and H. Rezaei. Estimation from Moments Measurements for Amyloid Depolymerisation. *Journal of Theoretical Biology*, March 2016. [35](#)
- [2] G. Bal and P. Moireau. Fast numerical inversion of the attenuated Radon transform with full and partial measurements. *Inverse Problems*, 20(4):1137–1164, 2004. [34](#)
- [3] C. Bertoglio, D. Barber, N. Gaddum, I. Valverde, M. Rutten, P. Beerbaum, P. Moireau, R. Hose, and J.-F. Gerbeau. Identification of artery wall stiffness: In vitro validation and in vivo results of a data assimilation procedure applied to a 3D fluid-structure interaction model. *J Biomech*, 47(5):1027–1034, 2014. [32](#), [33](#), [98](#), [135](#)
- [4] C. Bertoglio, D. Chapelle, M. A. Fernández, J.-F. Gerbeau, and P. Moireau. State observers of a vascular fluid-structure interaction model through measurements in the solid. *Comput Method Appl M*, 256(C):149–168, April 2013. [28](#), [84](#), [85](#), [87](#)
- [5] C. Bertoglio, P. Moireau, and J.-F. Gerbeau. Sequential parameter estimation for fluid-structure problems: Application to hemodynamics. *Int. J. Numer. Meth. Biomed. Engng.*, 28(4):434–455, April 2012. [29](#), [32](#)
- [6] A.-C. Boulanger, P. Moireau, B. Perthame, and J. Sainte-Marie. Data Assimilation for hyperbolic conservation laws. A Luenberger observer approach based on a kinetic description. *Communications in Mathematical Sciences*, 13(3):587–622, 2015. [26](#), [28](#), [30](#), [32](#), [38](#), [87](#), [89](#), [91](#)
- [7] M. Caruel, R. Chabiniok, P. Moireau, Y. Lecarpentier, and D. Chapelle. Dimensional reductions of a cardiac model for effective validation and calibration. *Biomechanics and modeling in mechanobiology*, 13(4):897–914, December 2013. [33](#), [34](#), [38](#), [121](#), [129](#), [131](#)
- [8] R. Chabiniok, P. Moireau, P.-F. Lesault, A. Rahmouni, J.-F. Deux, and D. Chapelle. Estimation of tissue contractility from cardiac cine-MRI using a biomechanical heart model. *Biomechanics and modeling in mechanobiology*, 11(5):609–630, May 2012. [32](#), [68](#), [78](#), [101](#), [133](#), [135](#)
- [9] R. Chabiniok, V. Y. Wang, M. Hadjicharalambous, L. Asner, J. Lee, M. Sermesant, E. Kuhl, A. A. Young, P. Moireau, M. P. Nash, D. Chapelle, and D. A. Nordsletten. Multiphysics

- and multiscale modelling, data-model fusion and integration of organ physiology in the clinic: ventricular cardiac mechanics. *Interface Focus*, 6(20150083):24, February 2016. [33](#)
- [10] D. Chapelle, N. Cîndea, M. De Buhan, and P. Moireau. Exponential Convergence of an Observer Based on Partial Field Measurements for the Wave Equation. *Mathematical Problems in Engineering*, 2012:1–12, 2012. [28](#), [68](#), [69](#), [70](#), [73](#)
- [11] D. Chapelle, N. Cîndea, and P. Moireau. Improving convergence in numerical analysis using observers The wave-like equation case. *Mathematical Models and Methods in Applied Sciences (M3AS)*, pages 1–34, March 2012. [28](#), [31](#), [32](#), [68](#), [70](#), [76](#), [77](#), [78](#), [82](#)
- [12] D. Chapelle, M. Fragu, V. Mallet, and P. Moireau. Fundamental principles of data assimilation underlying the Verdandi library: applications to biophysical model personalization within euHeart. *Med Biol Eng Comput*, November 2012. [33](#), [38](#), [81](#)
- [13] D. Chapelle, A. Gariah, P. Moireau, and J. Sainte-Marie. A Galerkin Strategy with Proper Orthogonal Decomposition for Parameter-Dependent Problems - Analysis, Assessments and Applications to Parameter Estimation. *ESAIM: M2AN*, 47(6):1821–1843, November 2013. [24](#), [32](#), [64](#), [133](#)
- [14] D. Chapelle, P. Le Tallec, P. Moireau, and M. Sorine. An energy-preserving muscle tissue model: formulation and compatible discretizations. *Int J Multiscale Com*, 10(2):189–211, 2012. [20](#), [21](#), [33](#), [34](#), [120](#), [122](#), [123](#), [125](#)
- [15] D. Chapelle and P. Moireau. General coupling of porous flows and hyperelastic formulations—From thermodynamics principles to energy balance and compatible time schemes. *European Journal of Mechanics-B/Fluids*, 46:82–96, 2014. [33](#), [34](#), [125](#), [126](#), [128](#)
- [16] D. Chapelle, P. Moireau, and P. Le Tallec. Robust Filtering for Joint State-Parameter Estimation in Distributed Mechanical Systems. *Discrete Contin. Dyn. Syst.*, 23(1-2):65–84, 2009. [24](#), [29](#), [30](#), [95](#), [96](#)
- [17] N. Cîndea, A. Imperiale, and P. Moireau. Data assimilation of time under-sampled measurements using observers, the wave-like equation example. *ESAIM Control Optim. Calc. Var.*, 21(3):635–669, 2015. [31](#), [68](#), [78](#)
- [18] A. Collin, D. Chapelle, and P. Moireau. A Luenberger observer for reaction–diffusion models with front position data. *J Comput Phys*, 300(C):288–307, November 2015. [27](#), [28](#), [32](#), [34](#), [36](#), [94](#), [112](#), [113](#), [114](#), [115](#), [134](#)
- [19] C. Corrado, J.-F. Gerbeau, and P. Moireau. Identification of weakly coupled multiphysics problems. Application to the inverse problem of electrocardiography. *J Comput Phys*, 283(C):271–298, February 2015. [24](#), [29](#), [32](#), [38](#), [62](#), [63](#), [64](#), [98](#), [133](#), [135](#)
- [20] S. Marchesseau, H. Delingette, M. Sermesant, R. Cabrera-Lozoya, C. Tobon-Gomez, P. Moireau, R. M. F. i. Ventura, K. Lekadir, A. Hernandez, M. Garreau, E. Donal, C. Leclercq, S. G. Duckett, K. Rhode, C. A. Rinaldi, A. F. Frangi, R. Razavi, D. Chapelle, and N. Ayache. Personalization of a cardiac electromechanical model using reduced order unscented Kalman filtering from regional volumes. *Medical Image Analysis*, 17(7):816–829, October 2013. [32](#), [98](#), [135](#)

- [21] P. Moireau, C. Bertoglio, N. Xiao, C. A. Figueroa, C. A. Taylor, D. Chapelle, and J.-F. Gerbeau. Sequential identification of boundary support parameters in a fluid-structure vascular model using patient image data. *Biomechanics and modeling in mechanobiology*, 12(3):475–496, June 2013. [32](#), [78](#), [101](#), [134](#)
- [22] P. Moireau and D. Chapelle. Erratum of article “Reduced-order unscented Kalman filtering with application to parameter identification in large-dimensional systems” [MR2801324]. *ESAIM Control Optim. Calc. Var.*, 17(2):406–409, 2011. [24](#), [29](#), [66](#)
- [23] P. Moireau and D. Chapelle. Reduced-Order Unscented Kalman Filtering with Application to Parameter Identification in Large-Dimensional Systems. *ESAIM Control Optim. Calc. Var.*, 17(2):380–405, April 2011. [24](#), [29](#), [30](#), [53](#), [54](#), [65](#), [66](#), [96](#), [98](#), [114](#)
- [24] P. Moireau, D. Chapelle, and P. Le Tallec. Joint state and parameter estimation for distributed mechanical systems. *Comput Method Appl M*, 197(6-8):659–677, 2008. [24](#), [28](#), [29](#), [30](#), [37](#), [61](#), [62](#), [63](#), [68](#), [72](#), [77](#), [78](#), [82](#), [93](#), [94](#), [96](#), [114](#)
- [25] P. Moireau, D. Chapelle, and P. LeTallec. Filtering for distributed mechanical systems using position measurements: perspectives in medical imaging. *Inverse Problems*, 25(3):035010, March 2009. [25](#), [30](#), [32](#), [34](#), [68](#), [69](#), [70](#), [75](#), [78](#), [80](#), [82](#), [84](#), [85](#), [101](#), [102](#), [103](#), [108](#)
- [26] P. Moireau, N. Xiao, M. Astorino, C. A. Figueroa, D. Chapelle, C. A. Taylor, and J.-F. Gerbeau. External tissue support and fluid–structure simulation in blood flows. *Biomechanics and modeling in mechanobiology*, 11(1-2):1–18, 2012. [25](#), [33](#), [119](#), [134](#)
- [27] J.-M. Peyrat, C. A. Rinaldi, M. Sorine, M. Sermesant, R. Chabiniok, P. Chinchapatnam, T. Mansi, F. Billet, P. Moireau, K. Wong, J. Relan, K. Rhode, M. Ginks, P. Lambiase, H. Delingette, D. Chapelle, R. Razavi, and N. Ayache. Patient-specific electromechanical models of the heart for the prediction of pacing acute effects in CRT: a preliminary clinical validation. *Medical Image Analysis*, 16(1):201–215, January 2012. [33](#), [34](#)
- [28] M. Sermesant, P. Moireau, O. Camara, J. Sainte-Marie, R. Andriantsimiavona, R. Cimrman, D. L. G. Hill, D. Chapelle, and R. Razavi. Cardiac function estimation from MRI using a heart model and data assimilation: advances and difficulties. *Medical Image Analysis*, 10(4):642–656, August 2006. [7](#), [32](#)
- [29] J. Xi, P. Lamata, J. Lee, P. Moireau, D. Chapelle, and N. Smith. Myocardial transversely isotropic material parameter estimation from in-silico measurements based on a reduced-order unscented Kalman filter. *Journal of the Mechanical Behavior of Biomedical Materials*, 4(7):1090–1102, October 2011. [32](#), [135](#)



Personal References – Proceedings - Preprints - Thesis

- [30] D. Chapelle, M. A. Fernández, J.-F. Gerbeau, P. Moireau, J. Sainte-Marie, and N. Zemzemi. Numerical simulation of the electromechanical activity of the heart. In *Functional Imaging and Modeling of the Heart*, pages 357–365, 2009. [34](#)
- [31] A. Collin, D. Chapelle, and P. Moireau. Sequential State Estimation for Electrophysiology Models with Front Level-Set Data Using Topological Gradient Derivations. In *Proceedings of the 8th International Conference FIMH*, volume LNCS 9126, pages 402–411, 2015. [27](#), [34](#), [36](#), [115](#), [134](#)
- [32] Q. Duan, P. Moireau, E. D. Angelini, and D. Chapelle. Simulation of 3D ultrasound with a realistic electro-mechanical model of the heart. In *Functional Imaging and Modeling of the Heart*, pages 463–470, January 2007. [34](#)
- [33] A. Imperiale, R. Chabiniok, P. Moireau, and D. Chapelle. Constitutive Parameter Estimation Methodology Using Tagged-MRI Data. In *Functional Imaging and Modeling of the Heart*, pages 409–417. Springer Berlin Heidelberg, Berlin, Heidelberg, 2011. [26](#), [29](#), [30](#), [32](#), [34](#), [78](#), [103](#), [108](#), [134](#)
- [34] A. Imperiale, A. Routier, S. Durrleman, and P. Moireau. Improving efficiency of data assimilation procedure for a biomechanical heart model by representing surfaces as currents. In S. Ourselin, D. Rueckert, and N. Smith, editors, *Proceedings of the 7th International Conference FIMH*, volume LNCS 7945, pages 342–351, 2013. [26](#), [29](#), [30](#), [34](#), [103](#)
- [35] K. Mauffrey and P. Moireau. Optimal observers strategies for partial differential equations with applications to parabolic equations. *in preparation*, 2016. [56](#)
- [36] P. Moireau. Assimilation de données en modélisation cardiaque. Master’s thesis, Université Pierre et Marie Curie - Paris VI, 2005. [129](#), [131](#)
- [37] P. Moireau. A time-discrete optimal filtering approach for non-linear systems as a stable discretization of the mortensen observer. *Submitted to COCV*, 2015. [30](#), [37](#), [44](#), [48](#), [51](#)
- [38] P. Moireau. *Filtering based data assimilation for second order hyperbolic PDEs - Applications in cardiac mechanics*. PhD thesis, Ecole Polytechnique X, December 2008. [62](#), [63](#), [85](#)

- [39] P. Moireau and D. Chapelle. Effective estimation in cardiac modelling. In *Functional Imaging and Modeling of the Heart*, pages 361–372, January 2007. [32](#)
- [40] P. Moireau, D. Chapelle, and M. Yvinec. Cardiac Motion Extraction from Images by Filtering Estimation Based on a Biomechanical Model. In *Functional Imaging and Modeling of the Heart*, pages 220–228, January 2009. [32](#)
- [41] M. Sermesant, P. Moireau, R. Andriantsimiavona, J. Sainte-Marie, O. Camara, R. Cimrman, D. L. G. Hill, D. Chapelle, and R. Razavi. Progress toward using mri and a heart model to estimate patient-specific indices of cardiac function. In *ESAIM: Proceedings*, pages 224–234, January 2005. [32](#)



Bibliography

- [Aalto, 2014a] Aalto, A. (2014a). Convergence of discrete time Kalman filter estimate to continuous time estimate. *arXiv.org*. [13](#), [61](#), [43](#)
- [Aalto, 2014b] Aalto, A. (2014b). Spatial discretization error in Kalman filtering for discrete-time infinite dimensional systems. *arXiv.org*. [61](#), [43](#), [44](#)
- [Abdallah et al., 2012] Abdallah, F., Nicaise, S., and Valein, J. (2012). Uniformly exponentially or polynomially stable approximations for second order evolution equations and some applications. *ESAIM Control Optim. Calc. Var.* [76](#), [59](#)
- [Alves et al., 2009] Alves, C., Silvestre, A. L., Takahashi, T., and Tucsnak, M. (2009). Solving inverse source problems using observability. Applications to the Euler-Bernoulli plate equation. *SIAM J Control Optim.* [16](#), [92](#), [94](#), [74](#), [76](#)
- [Andrieu and Praly, 2006] Andrieu, V. and Praly, L. (2006). On the Existence of a Kazantzis-Kravaris/Luenberger Observer. *SIAM Journal on Control and Optimization*. [13](#), [14](#)
- [Auroux and Blum, 2008] Auroux, D. and Blum, J. (2008). A nudging-based data assimilation method: the Back and Forth Nudging (BFN) algorithm. *Nonlinear Processes In Geophysics*, [15](#)(2):305–319. [11](#), [81](#), [90](#), [12](#), [63](#), [72](#)
- [Auroux and Nodet, 2008] Auroux, D. and Nodet, M. (2008). The Back and Forth Nudging algorithm for data assimilation problems: theoretical results on transport equations. *ESAIM: COCV*, [1](#)(1). [90](#), [72](#)
- [Axel et al., 2005] Axel, L., Montillo, A., and Kim, D. (2005). Tagged magnetic resonance imaging of the heart: a survey. *Medical Image Analysis*, [9](#)(4):376–393. [108](#), [91](#)
- [Başar and Bernhard, 1995] Başar, T. and Bernhard, P. (1995). *H[∞]-Optimal Control and Related Minimax Design Problems - A Dynamic Game Approach*. Birkhäuser, 2nd edition. [96](#), [78](#)
- [Badra and Takahashi, 2014] Badra, M. and Takahashi, T. (2014). Feedback Stabilization of a Fluid-Rigid Body Interaction System. *Advances in Differential Equations*, [19](#)(11-12):1137–1184. [84](#), [66](#)

- [Banks and Fabiano, 1998] Banks, H. T. and Fabiano, R. H. (1998). Approximation issues for applications in optimal control and parameter estimation. *Numerical Mathematics and Scientific Computation*, pages 141–165. [14](#), [76](#), [59](#)
- [Banks and Ito, 1991] Banks, H. T. and Ito, K. (1991). A numerical algorithm for optimal feedback gains in high dimensional linear quadratic regulator problems. *SIAM Journal on Control and Optimization*. [14](#)
- [Banks et al., 1991] Banks, H. T., Ito, K., and Wang, C. (1991). Exponentially stable approximations of weakly damped wave equations. In *Estimation and control of distributed parameter systems (Vorau, 1990)*, pages 1–33. Birkhäuser, Basel, Basel. [76](#), [59](#)
- [Banks and Kunisch, 1989] Banks, H. T. and Kunisch, K. (1989). *Estimation Techniques for Distributed Parameter Systems*. Birkhauser Boston. [16](#)
- [Baras and Bensoussan, 1987] Baras, J. S. and Bensoussan, A. (1987). On observer problems for systems governed by partial differential equations. Technical Report SCR TR 86-47, DTIC. [10](#), [56](#), [11](#), [38](#), [39](#)
- [Baras et al., 1988] Baras, J. S., Bensoussan, A., and James, M. R. (1988). Dynamic observers as asymptotic limits of recursive filters: special cases. *Siam J Appl Math*, 48(5):1147–1158. [13](#), [44](#), [26](#)
- [Barbu and Da Prato, 1985] Barbu, V. and Da Prato, G. (1985). Hamilton-Jacobi equations in Hilbert spaces; variational and semigroup approach. *Annali di Matematica Pura ed Applicata*, 142(1):303–349. [47](#), [29](#)
- [Bardos et al., 1988] Bardos, C., Lebeau, G., and Rauch, J. (1988). Un exemple d’utilisation des notions de propagation pour le contrôle et la stabilisation des problèmes hyperboliques. *Rendiconti del Seminario Matematico del Universita Politecnico Torino*, Fascicolo speciale(Hyperbolic Equations (1987)):12–31. [73](#), [55](#), [56](#)
- [Bardos and Pironneau, 2005] Bardos, C. and Pironneau, O. (2005). Data assimilation for conservation laws. *Methods and Applications of Analysis*, 12(2):103–134. [87](#), [70](#)
- [Baudouin et al., 2013] Baudouin, L., De Buhan, M., and Ervedoza, S. (2013). Global Carleman estimates for waves and applications. *Communications in Partial Differential Equations*, 38(5):823–859. [72](#), [55](#)
- [Baumeister and Scondo, 1987a] Baumeister, J. and Scondo, W. (1987a). Adaptive methods for parameter identification. In *Optimization in mathematical physics (Oberwolfach, 1985)*, pages 87–116. Lang, Frankfurt am Main. [15](#), [16](#)
- [Baumeister and Scondo, 1987b] Baumeister, J. and Scondo, W. (1987b). Asymptotic embedding methods for parameter estimation. In *26th IEEE Conference on Decision and Control*, pages 170–174. IEEE. [92](#), [74](#)
- [Bellman, 1957] Bellman, R. (1957). *Dynamic Programming*. Princeton University Press. [11](#), [14](#), [46](#), [28](#)

- [Bensoussan, 1971] Bensoussan, A. (1971). *Filtrage optimal des systèmes linéaires*. Dunod. [9](#), [12](#), [14](#), [38](#), [58](#), [60](#), [77](#), [10](#), [41](#), [43](#), [98](#)
- [Bensoussan et al., 1993] Bensoussan, A., Da Prato, G., Delfour, M. C., and Mitter, S. K. (1993). *Representation and control of infinite-dimensional systems. Vol. II. Systems & Control: Foundations & Applications*. Birkhäuser Boston Inc., Boston, MA. [14](#)
- [Bestel et al., 2001] Bestel, J., Clément, F., and Sorine, M. (2001). A Biomechanical Model of Muscle Contraction. In *Medical Image Computing and Computer-Assisted Intervention – MICCAI 2001*, pages 1159–1161. Springer Berlin Heidelberg, Berlin, Heidelberg. [20](#), [118](#), [120](#), [121](#)
- [Biot, 1972] Biot, M. A. (1972). Theory of finite deformations of porous solids. *Indiana U Math J*, 21(7):597–620. [125](#)
- [Blum et al., 2009] Blum, J., Le Dimet, F.-X., and Navon, I. M. (2009). Data assimilation for geophysical fluids. *Computational Methods for the Atmosphere and the Oceans*, 14:385–441. [6](#)
- [Bokanowski et al., 2013] Bokanowski, O., Garcke, J., Griebel, M., and Klompaker, I. (2013). An adaptive sparse grid semi-Lagrangian scheme for first order Hamilton-Jacobi Bellman equations. *J Sci Comput*, 55(3):575–605. [51](#), [34](#)
- [Bonnabel et al., 2009] Bonnabel, S., Mirrahimi, M., and Rouchon, P. (2009). Observer-based Hamiltonian identification for quantum systems. *Automatica*, 45(5):1144–1155. [11](#), [12](#)
- [Bonnabel and Slotine, 2015] Bonnabel, S. and Slotine, J.-J. E. (2015). A Contraction Theory-Based Analysis of the Stability of the Deterministic Extended Kalman Filter. *IEEE Trans. Automat. Control*, 60(2):565–569. [54](#), [96](#), [37](#), [78](#)
- [Boulakia et al., 2012] Boulakia, M., Schenone, E., and Gerbeau, J.-F. (2012). Reduced-order modeling for cardiac electrophysiology. Application to parameter identification. *Int. J. Numer. Meth. Biomed. Engng.*, 28(6-7):727–744. [133](#)
- [Boutayeb et al., 1997] Boutayeb, M., Rafaralahy, H., and Darouach, M. (1997). Convergence analysis of the extended Kalman filter used as an observer for nonlinear deterministic discrete-time systems. *IEEE Transactions on Automatic Control*, 42(4):581–586. [12](#)
- [Breiten and Kunisch, 2015] Breiten, T. and Kunisch, K. (2015). Compensator Design for the Monodomain Equations . Technical Report SFB-Report No. 2014-017, SpezialForschungsbereich. [63](#), [45](#)
- [Bristeau et al., 2011] Bristeau, M.-O., Goutal, N., and Sainte-Marie, J. (2011). Numerical simulations of a non-hydrostatic shallow water model. *Computers and Fluids*, 47(1):51–64. [91](#), [73](#)
- [Bullo, 2005] Bullo, F. (2005). *Geometric control of mechanical systems*, volume 49. Springer Science & Business Media. [13](#), [14](#)
- [Burger et al., 2004] Burger, M., Hackl, B., and Ring, W. (2004). Incorporating topological derivatives into level set methods. *J Comput Phys*, 194(1):344–362. [115](#), [97](#)

- [Burq and Gérard, 1997] Burq, N. and Gérard, P. (1997). Condition nécessaire et suffisante pour la contrôlabilité exacte des ondes. *C. R. Acad. Sci. Paris Sér. I Math.*, 325(7):749–752. [73](#), [55](#)
- [Burq and Gérard, 2002] Burq, N. and Gérard, P. (2002). Contrôle optimal des equations aux derivees partielles. Cours de l’Ecole Polytechnique. [71](#), [53](#)
- [Burq and Lebeau, 2001] Burq, N. and Lebeau, G. (2001). Mesures de défaut de compacité, application au système de Lamé. *Ann. Sci. Ecole Norm. Sup. (4)*, 34(6):817–870. [83](#), [65](#)
- [Burq and Zworski, 2004] Burq, N. and Zworski, M. (2004). Geometric Control in the Presence of a Black Box. *Journal of the American Mathematical Society*, 17(2):443–471. [72](#), [54](#)
- [Carranza-Herrezuelo et al., 2010] Carranza-Herrezuelo, N., Bajo, A., Sroubek, F., Santamarta, C., Cristobal, G., Santos, A., and Ledesma-Carbayo, M. J. (2010). Motion estimation of tagged cardiac magnetic resonance images using variational techniques. *Computerized Medical Imaging and Graphics*, 34(6):514–522. [100](#), [108](#), [82](#), [91](#)
- [Casella and Berger, 2002] Casella, G. and Berger, R. L. (2002). *Statistical Inference*. Duxbury Press, 2nd edition. [7](#)
- [Chabot et al., 2015] Chabot, V., Nodet, M., Papadakis, N., and Vidard, A. (2015). Accounting for observation errors in image data assimilation. *Tellus A*. [39](#)
- [Chan and Vese, 2001] Chan, T. F. and Vese, L. A. (2001). Active contours without edges. *IEEE Trans Image Process*, 10(2):266–277. [113](#), [94](#)
- [Chapelle and Bathe, 2011] Chapelle, D. and Bathe, K. (2011). *The Finite Element Analysis of Shells - Fundamentals - Second Edition*. Computational Fluid and Solid Mechanics. Springer. [105](#), [111](#), [130](#), [87](#)
- [Chapelle et al., 2013] Chapelle, D., Collin, A., and Gerbeau, J.-F. (2013). A surface-based electrophysiology model relying on asymptotic analysis and motivated by cardiac atria modeling. *Mathematical Models and* [115](#), [116](#), [97](#)
- [Chapelle et al., 2012] Chapelle, D., Gariah, A., and Sainte-Marie, J. (2012). Galerkin approximation with proper orthogonal decomposition : new error estimates and illustrative examples. *ESAIM: M2AN*, 46(4):731–757. [64](#), [133](#), [46](#)
- [Chapouly and Mirrahimi, 2010] Chapouly, M. and Mirrahimi, M. (2010). Distributed source identification for wave equations: an observer-based approach. *arXiv.org*. [15](#), [16](#)
- [Chavent, 2010] Chavent, G. (2010). *Non linear Least Squares for Inverse problems*. Scientific Computation. Springer Netherlands. [16](#), [94](#), [76](#)
- [Chen et al., 2010] Chen, T., Wang, X., Chung, S., Metaxas, D. N., and Axel, L. (2010). Automated 3D Motion Tracking Using Gabor Filter Bank, Robust Point Matching, and Deformable Models. *Ieee T Med Imaging*, 29(1):1–11. [108](#), [109](#)
- [Cîndea and Munch, 2015] Cîndea, N. and Munch, A. (2015). Inverse problems for linear hyperbolic equations via a mixed formulation. *Inverse Problems*, 31(7):1–39. [10](#), [68](#), [50](#)

- [Clarysse et al., 2000] Clarysse, P., Magnin, I. E., Basset, C., Khouas, L., Croisille, P., Friboulet, D., and Odet, C. (2000). Two-dimensional spatial and temporal displacement and deformation field fitting from cardiac magnetic resonance tagging. *Medical Image Analysis*, 4(3):253–268. [108](#), [91](#)
- [Colli Franzone et al., 2014] Colli Franzone, P., Pavarino, L., and Scacchi, S. (2014). *Mathematical Cardiac Electrophysiology*, volume XIV of *MS&A*. Springer. [18](#), [19](#)
- [Coron, 2007] Coron, J.-M. (2007). *Control and nonlinearity*, volume 136 of *Mathematical Surveys and Monographs*. American Mathematical Society, Providence, RI. [14](#)
- [Court, 2014] Court, S. (2014). Stabilization of a fluid-solid system, by the deformation of the self-propelled solid. Part I: The linearized system. *EECT*, 3(1):59–82. [84](#), [66](#)
- [Courtier, 1997] Courtier, P. (1997). Dual formulation of four-dimensional variational assimilation. *Quarterly Journal of the Royal Meteorological Society*, 123(544):2449–2461. [10](#)
- [Coussy, 2004] Coussy, O. (2004). *Poromechanics*. John Wiley and Sons. [125](#)
- [Cox and Zuazua, 1994] Cox, S. and Zuazua, E. (1994). The Rate at Which Energy Decays in a Damped String. *Communications in Partial Differential Equations*, 19(1-2):213–243. [72](#), [54](#)
- [Cristofol et al., 2014] Cristofol, M., Kaddouri, I., Nadin, G., and Roques, L. (2014). Coefficient determination via asymptotic spreading speeds. *Inverse Problems*, 30(3):035005. [37](#), [99](#)
- [Curtain, 1975] Curtain, R. F. (1975). A survey of infinite-dimensional filtering. *SIAM Rev.*, 17:395–411. [9](#), [10](#)
- [Curtain and Pritchard, 1978] Curtain, R. F. and Pritchard, A. J. (1978). *Infinite dimensional linear systems theory*, volume 8 of *Lecture Notes in Control and Information Sciences*. Springer-Verlag, Berlin. [14](#)
- [Curtain and Zwart, 1995] Curtain, R. F. and Zwart, H. J. (1995). *An introduction to infinite-dimensional linear systems theory*, volume 21 of *Texts in Applied Mathematics*. Springer-Verlag, New York. [14](#), [63](#), [72](#), [45](#)
- [Daum, 1986] Daum, F. E. (1986). Exact finite-dimensional nonlinear filters. *IEEE Trans. Automat. Control*, 31(7):616–622. [44](#), [26](#)
- [de Boer, 2005] de Boer, R. (2005). *Trends in Continuum Mechanics of Porous Media*. Springer. [125](#)
- [Delfour and Zolésio, 2011] Delfour, M. and Zolésio, J.-P. (2011). *Shapes and Geometries: Analysis, Differential Calculus, and Optimization (Advances in Design and Control)*. SIAM, second edition. [113](#), [95](#)
- [Demetriou and Rosen, 1994a] Demetriou, M. A. and Rosen, I. G. (1994a). Adaptive identification of second-order distributed parameter systems. *Inverse Problems*, 10(2):261–294. [15](#), [16](#), [92](#), [74](#)

- [Demetriou and Rosen, 1994b] Demetriou, M. A. and Rosen, I. G. (1994b). On the persistence of excitation in the adaptive estimation of distributed parameter systems. *Automatic Control, IEEE Transactions on DOI - 10.1109/9.989154*, 39(5):1117–1123. [16](#), [94](#), [76](#)
- [Denney and Prince, 1995] Denney, T. and Prince, J. (1995). Reconstruction of 3-D left ventricular motion from planar tagged cardiac MR images: An estimation theoretic approach. *Ieee T Med Imaging*, 14(4):625–635. [108](#), [91](#)
- [Desai et al., 2003] Desai, R., Lele, T., and Viens, F. (2003). A Monte-Carlo method for portfolio optimization under partially observed stochastic volatility. In *Computational Intelligence for Financial Engineering, 2003. Proceedings. 2003 IEEE International Conference on*, pages 257–263. [37](#), [98](#)
- [Dontchev, 1996] Dontchev, A. L. (1996). Discrete approximations in optimal control. In *Non-smooth analysis and geometric methods in deterministic optimal control (Minneapolis, MN, 1993)*, pages 59–80. Springer, New York, New York, NY. [12](#)
- [Durrleman et al., 2009] Durrleman, S., Pennec, X., Trouvé, A., and Ayache, N. (2009). Statistical models of sets of curves and surfaces based on currents. *Medical Image Analysis*, 13(5):793–808. [103](#), [104](#), [85](#), [86](#)
- [Duyckaerts, 2007] Duyckaerts, T. (2007). Optimal decay rates of the energy of a hyperbolic-parabolic system coupled by an interface. *Asymptotic Analysis*, 51(1):17–45. [84](#), [87](#), [66](#), [69](#)
- [Eisenberg and Hill, 1978] Eisenberg, E. and Hill, T. L. (1978). A cross-bridge model of muscle contraction. *Prog Biophys Mol Bio*, 33(1):55–82. [20](#), [118](#), [120](#)
- [Engelbrecht et al., 2000] Engelbrecht, J., Vendelin, M., and Maugin, G. A. (2000). Hierarchical internal variables reflecting microstructural properties: application to cardiac muscle contraction. *J Non-Equil Thermody*, 25(2):119–130. [118](#), [121](#)
- [Ervedoza, 2009] Ervedoza, S. (2009). Spectral conditions for admissibility and observability of wave systems: applications to finite element schemes. *Numer Math*, 113(3):377–415. [14](#), [76](#), [59](#)
- [Ervedoza et al., 2008] Ervedoza, S., Zheng, C., and Zuazua, E. (2008). On the observability of time-discrete conservative linear systems. *Journal of functional Analysis*, 254(12):3037–3078. [76](#), [59](#)
- [Ervedoza and Zuazua, 2009a] Ervedoza, S. and Zuazua, E. (2009a). Uniform exponential decay for viscous damped systems. *Progress in Nonlinear Differential Equations and their Applications*, 78:95–112. [78](#), [61](#)
- [Ervedoza and Zuazua, 2009b] Ervedoza, S. and Zuazua, E. (2009b). Uniformly exponentially stable approximations for a class of damped systems. *Journal de Mathématiques Pures et Appliqués*, 91(1):20–48. [76](#), [77](#), [59](#)
- [Evensen, 2007] Evensen, G. (2007). *Data Assimilation – The Ensemble Kalman Filter*. Springer Verlag. [54](#), [37](#)

- [Feng and Prohl, 2004] Feng, X. and Prohl, A. (2004). Analysis of gradient flow of a regularized Mumford-Shah functional for image segmentation and image inpainting. *ESAIM: M2AN*, 38(2):291–320. [36](#), [99](#)
- [Fleming and Rishel, 1975] Fleming, W. and Rishel, R. (1975). *Deterministic and stochastic optimal control*. Springer. [13](#), [46](#), [28](#)
- [Fleming, 1997] Fleming, W. H. (1997). Deterministic nonlinear filtering. *Ann. Scuola Norm. Sup. Pisa Cl. Sci. (4)*, 25(3-4):435–454 (1998). [44](#), [47](#), [26](#), [29](#)
- [Fleming and McEneaney, 2000] Fleming, W. H. and McEneaney, W. M. (2000). A max-plus-based algorithm for a Hamilton–Jacobi–Bellman equation of nonlinear filtering. *SIAM Journal on Control and Optimization*, 38(3):683–710. [37](#), [51](#), [34](#), [98](#)
- [Formaggia et al., 2009] Formaggia, L., Quarteroni, A., and Veneziani, A., editors (2009). *Cardiovascular Mathematics – Modeling and simulation of the circulatory system*. Springer-Verlag Milan. [21](#), [22](#), [23](#)
- [Fridman, 2013] Fridman, E. (2013). Observers and initial state recovering for a class of hyperbolic systems via Lyapunov method. *Automatica*, 49(7):2250–2260. [14](#)
- [Gask, 1960] Gask, H. (1960). A Proof of Schwartz’s Kernel Theorem. *Mathematica Scandinavica*, 8:327–332. [59](#), [41](#)
- [Gérard, 1991] Gérard, P. (1991). Microlocal defect measures. *Communications in Partial Differential Equations*, 16(11):1761–1794. [73](#), [55](#)
- [Gillet-Chaulet et al., 2012] Gillet-Chaulet, F., Gagliardini, O., Seddik, H., Nodet, M., Durand, G., Ritz, C., Zwinger, T., Greve, R., and Vaughan, D. G. (2012). Greenland Ice Sheet contribution to sea-level rise from a new-generation ice-sheet model. *The Cryosphere Discuss*, 6:2789–2826. [39](#)
- [Glass et al., 1991] Glass, L., Hunter, P., and A, M., editors (1991). *Theory of Heart – Biomechanics, Biophysics, and Nonlinear Dynamics of Cardiac Function*. Institute for Nonlinear Science. Springer New York. [20](#), [118](#)
- [Glowinski et al., 1989] Glowinski, R., Kinton, W., and Wheeler, M. F. (1989). A mixed finite element formulation for the boundary controllability of the wave equation. *International Journal for Numerical Methods in Engineering*, 27(3):623–635. [14](#), [76](#), [59](#)
- [Gobbino, 1998] Gobbino, M. (1998). Gradient flow for the one-dimensional Mumford-Shah functional. *Annali della Scuola Normale Superiore di Pisa- . . .* [36](#), [99](#)
- [Gonzalez, 2000] Gonzalez, O. (2000). Exact energy and momentum conserving algorithms for general models in nonlinear elasticity. *Comput Method Appl M*, 190(13-14):1763–1783. [128](#)
- [Guccione and McCulloch, 1993] Guccione, J. M. and McCulloch, A. D. (1993). Mechanics of active contraction in cardiac muscle: Part I—Constitutive relations for fiber stress that describe deactivation. *Journal of biomechanical engineering*, 115(1):72–81. [20](#), [118](#)
- [Guérin et al., 2011] Guérin, T., Prost, J., and Joanny, J.-F. (2011). Dynamical behavior of molecular motor assemblies in the rigid and crossbridge models. *Eur Phys J E*, 34(6). [20](#), [118](#)

- [Hager and Horowitz, 1976] Hager, W. W. and Horowitz, L. L. (1976). Convergence and stability properties of the discrete Riccati operator equation and the associated optimal control and filtering problems. *SIAM Journal on Control and Optimization*, 14(2):295–312. [12](#), [61](#), [43](#)
- [Haine, 2014a] Haine, G. (2014a). An observer-based approach for thermoacoustic tomography. In *The 21st International Symposium on Mathematical Theory of Networks and Systems*, pages 1–9. [81](#), [63](#)
- [Haine, 2014b] Haine, G. (2014b). Recovering the observable part of the initial data of an infinite-dimensional linear system with skew-adjoint generator. *Mathematics of Control Signals and Systems*, 26(3):435–462. [11](#), [81](#), [12](#), [63](#)
- [Haine and Ramdani, 2012] Haine, G. and Ramdani, K. (2012). Reconstructing initial data using observers: error analysis of the semi-discrete and fully discrete approximations. *Numer Math*, 120(2):307–343. [81](#), [63](#)
- [Haraux, 1989] Haraux, A. (1989). Une remarque sur la stabilisation de certains systèmes du deuxième ordre en temps. *Portugal. Math.*, 46(3):245–258. [11](#), [71](#), [54](#)
- [Hastie et al., 2001] Hastie, T., Tibshirani, R., and Friedman, J. (2001). *The Elements of Statistical Learning*. Springer Series in Statistics. Springer New York Inc., New York, NY, USA. [16](#), [7](#)
- [Hautus, 1970] Hautus, M. L. J. (1970). Stabilization controllability and observability of linear autonomous systems. *Indagationes Mathematicae (Proceedings)*, 73(Complete):448–455. [73](#)
- [He et al., 2007] He, L., Kao, C. Y., and Osher, S. (2007). Incorporating topological derivatives into shape derivatives based level set methods. *J Comput Phys*, 225(1):891–909. [115](#), [97](#)
- [Hijab, 1982] Hijab, O. (1982). Asymptotic nonlinear filtering and large deviations. *Advances in Filtering and Optimal Stochastic Control*, pages 170–176. [44](#), [26](#)
- [Hijab, 1984] Hijab, O. (1984). Asymptotic Bayesian estimation of a first order equation with small diffusion. *Ann. Probab.*, 12(3):890–902. [44](#), [26](#)
- [Hill, 2004] Hill, T. H. (2004). *Free Energy Transduction And Biochemical Cycle Kinetics*. Dover. [20](#)
- [Hintermüller and Laurain, 2009] Hintermüller, M. and Laurain, A. (2009). Multiphase Image Segmentation and Modulation Recovery Based on Shape and Topological Sensitivity. *J Math Imaging Vis*, 35(1):1–22. [115](#), [97](#)
- [Hintermüller and Ring, 2004] Hintermüller, M. and Ring, W. (2004). An Inexact Newton-CG-Type Active Contour Approach for the Minimization of the Mumford-Shah Functional. *J Math Imaging Vis*, 20(1-2):19–42. [113](#), [114](#), [95](#), [96](#)
- [Hoffmann and Sprekels, 1985] Hoffmann, K. H. and Sprekels, J. (1985). On the identification of coefficients of elliptic problems by asymptotic regularization. *Numerical functional analysis and optimization*, 7(2-3):157–177. [92](#), [74](#)

- [Holzapfel and Ogden, 2009] Holzapfel, G. A. and Ogden, R. (2009). Constitutive modelling of passive myocardium: a structurally based framework for material characterization. *Phil. Trans. R. Soc. A*, 367:3445–3475. [20](#)
- [Humphrey, 2003] Humphrey, J. (2003). Continuum biomechanics of soft biological tissues. *P R Soc A*, 459(2029):3–46. [20](#)
- [Huxley, 1957] Huxley, A. F. (1957). Muscle structure and theories of contraction. *Prog Biophys Biophys Chem*, 7:255–318. [20](#), [118](#), [120](#)
- [Huxley and Simmons, 1971] Huxley, A. F. and Simmons, R. M. (1971). Proposed mechanism of force generation in striated muscle. *Nature*. [20](#), [118](#), [120](#)
- [Imperiale, 2013] Imperiale, A. (2013). *Image-based data assimilation methods for the personalization of mechanical models - Application to cardiac mechanics and tagged-MRI*. PhD thesis, Université Pierre et Marie Curie - Paris VI. [28](#), [32](#), [80](#), [81](#), [83](#), [102](#), [103](#), [106](#), [107](#), [108](#), [111](#), [119](#), [134](#), [63](#), [65](#), [84](#), [85](#), [88](#), [89](#), [91](#)
- [Ito et al., 2011] Ito, K., Ramdani, K., and Tucsnak, M. (2011). A time reversal based algorithm for solving initial data inverse problems. *DCDS-S*, 4(3):641–652. [81](#), [63](#)
- [James and Baras, 1988] James, M. R. and Baras, J. S. (1988). Nonlinear filtering and large deviations: A PDE-control theoretic approach. *Stochastics: An International Journal of Probability and Stochastic Processes*, 23(3):391–412. [13](#), [37](#), [44](#), [47](#), [26](#), [29](#), [98](#)
- [Joly, 2006] Joly, R. (2006). Convergence of the wave equation damped on the interior to the one damped on the boundary. *J. Differential Equations*, 229(2):588–653. [14](#)
- [Julier et al., 1995] Julier, S. J., Uhlmann, J. K., and Durrant-Whyte, H. (1995). A new approach for filtering nonlinear systems. *American Control Conference, 1995. Proceedings of the DOI - UR -*, 3:1628–1632 vol.3. [53](#), [54](#), [35](#), [36](#), [37](#)
- [Julier et al., 2000] Julier, S. J., Uhlmann, J. K., and Durrant-Whyte, H. (2000). A new method for the nonlinear transformation of means and covariances in filters and estimators. *Automatic Control, IEEE Transactions on DOI - 10.1109/9.989154*, 45(3):477–482. [53](#), [55](#), [35](#), [38](#)
- [Kailath et al., 2000] Kailath, T., Sayed, A. H., and Hassibi, B. (2000). *Linear estimation*, volume 1. Prentice Hall Upper Saddle River, NJ. [12](#), [13](#), [45](#), [50](#), [61](#), [27](#), [32](#), [44](#)
- [Kalman, 1960a] Kalman, R. E. (1960a). A new approach to linear filtering and prediction problems. *Journal of basic Engineering*, 82(1):35–45. [12](#), [44](#), [49](#), [51](#), [26](#), [31](#), [33](#)
- [Kalman, 1960b] Kalman, R. E. (1960b). Contributions to the theory of optimal control. *Bol. Soc. Mat. Mexicana (2)*, 5:102–119. [13](#)
- [Kalman and Bucy, 1961] Kalman, R. E. and Bucy, R. (1961). New results in linear filtering and prediction theory. *Trans. ASME J. Basic. Eng.*, 83:95–108. [11](#), [13](#), [44](#), [47](#), [49](#), [26](#), [29](#), [31](#)
- [Keener and Sneyd, 2004] Keener, J. and Sneyd, J. (2004). *Mathematical Physiology*. Springer. [18](#), [112](#), [113](#), [94](#), [95](#)

- [Khenissi et al., 2010] Khenissi, M., Daoulatli, M., and Dehman, B. (2010). Local Energy Decay for the Elastic System with Nonlinear Damping in an Exterior Domain. *SIAM Journal on Control and Optimization*, 48(8):5254–5275. [83](#), [65](#)
- [Kolmogorov, 1939] Kolmogorov, A. N. (1939). Sur l’interpolation et extrapolation des suites stationnaires. *CR Acad. Sci*, 208:2043–2045. [13](#)
- [Komornik, 1994] Komornik, V. (1994). *Exact controllability and stabilization. The multiplier method*. RAM: Research in Applied Mathematics. Masson, Paris. [72](#), [55](#)
- [Konukoglu et al., 2010] Konukoglu, E., Clatz, O., Menze, B. H., Stieltjes, B., Weber, M. A., Mandonnet, E., Delingette, H., and Ayache, N. (2010). Image Guided Personalization of Reaction-Diffusion Type Tumor Growth Models Using Modified Anisotropic Eikonal Equations. *Ieee T Med Imaging*, 29(1):77–95. [116](#)
- [Krener, 2003a] Krener, A. J. (2003a). The convergence of the extended Kalman filter. In *Lecture Notes in Control and Inform. Sci.*, pages 173–182. Springer, Berlin. [13](#), [54](#), [63](#), [96](#), [46](#), [78](#)
- [Krener, 2003b] Krener, A. J. (2003b). The convergence of the minimum energy estimator. In *New trends in nonlinear dynamics and control, and their applications*, pages 187–208. Springer, Berlin. [13](#), [47](#), [29](#)
- [Krener and Duarte, 1996] Krener, A. J. and Duarte, A. (1996). A hybrid computational approach to nonlinear estimation. In *Decision and Control, 1996., Proceedings of the 35th IEEE*, pages 1815–1819. [11](#), [71](#), [12](#), [53](#)
- [Krener and Hermann, 1977] Krener, A. J. and Hermann, R. (1977). Nonlinear controllability and observability. *IEEE Trans. Automat. Control*, AC-22(5):728–740. [13](#)
- [Lasiecka and Triggiani, 2000] Lasiecka, I. and Triggiani, R. (2000). *Control theory for partial differential equations: Volume 1, Abstract parabolic systems: Continuous and approximation theories*, volume 1. Cambridge University Press. [14](#)
- [Lasiecka and Triggiani, 2003] Lasiecka, I. and Triggiani, R. (2003). $L_2(\Sigma)$ -regularity of the boundary to boundary operator B^*L for hyperbolic and Petrowski PDEs. *Abstract Applied Analysis*, 2003(19):1061–1139. [57](#), [39](#)
- [Lasiecka et al., 1999] Lasiecka, I., Triggiani, R., and Yao, P. F. (1999). Inverse/observability estimates for second-order hyperbolic equations with variable coefficients. *Journal of mathematical analysis and ...*, 235(1):13–57. [72](#), [55](#)
- [Le Bris and Rouchon, 2013] Le Bris, C. and Rouchon, P. (2013). Low-rank numerical approximations for high-dimensional Lindblad equations. *Physical Review A*, 87(2):022125. [61](#), [44](#)
- [Le Dimet and Talagrand, 1986] Le Dimet, F.-X. and Talagrand, O. (1986). Variational algorithms for analysis and assimilation of meteorological observations: Theoretical aspects. *Tellus A*, 38(2):97–110. [10](#), [11](#)
- [Le Guyader and Vese, 2011] Le Guyader, C. and Vese, L. A. (2011). A combined segmentation and registration framework with a nonlinear elasticity smoother. *Comput Vis Image Und.* [100](#), [82](#)

- [Le Tallec, 1994] Le Tallec, P. (1994). Numerical Methods for Nonlinear Three-dimensional Elasticity. In Ciarlet, P. G. and Lions, J.-L., editors, *Handbook of Numerical Analysis*, pages 465–622. Handbook of Numerical Analysis. 20, 122
- [Le Tallec and Hauret, 2003] Le Tallec, P. and Hauret, P. (2003). Energy conservation in fluid structure interactions. *International Center Numerical Methods Engineering (CIMNE), Barcelona, 2003*, pages 94–107. 128
- [Lebeau, 1996] Lebeau, G. (1996). Equation des ondes amorties. In *Algebraic and geometric methods in mathematical physics*, pages 73–109. Kluwer Academic. 73, 55
- [Lebeau et al., 1992] Lebeau, G., Bardos, C., and Rauch, J. (1992). Sharp Sufficient Conditions for the Observation, Control, and Stabilization of Waves from the Boundary. *SIAM Journal on Control and Optimization*, 30(5):1024–1065. 73, 55
- [Lefebvre et al., 2002] Lefebvre, T., Bruyninckx, H., and de Schuller, J. (2002). Comment on "A new method for the nonlinear transformation of means and covariances in filters and estimators" [and authors' reply]. *Automatic Control, IEEE Transactions on DOI - 10.1109/9.989154*, 47(8):1406–1409. 54, 36
- [Li and Xu, 2011] Li, X.-D. and Xu, C.-Z. (2011). Infinite-dimensional Luenberger-like observers for a rotating body-beam system. *Systems & Control Letters*, 60(2):138–145. 11, 70, 82, 52, 65
- [Lions, 1968] Lions, J.-L. (1968). *Contrôle optimal de systèmes gouvernés par des équations aux dérivées partielles*. Avant propos de P. Lelong. Dunod, Paris. 14, 58, 59, 69, 72, 41, 52, 55
- [Liu, 1997] Liu, K. (1997). Locally distributed control and damping for the conservative systems. *SIAM Journal on Control and Optimization*, 35(5):1574–1590. 11, 12
- [Lombardi, 2013] Lombardi, D. (2013). Inverse problems in 1D hemodynamics on systemic networks: A sequential approach. *Int. J. Numer. Meth. Biomed. Engng.*, 30(2):160–179. 98, 80
- [Loret and Simões, 2005] Loret, B. and Simões, F. (2005). A framework for deformation, generalized diffusion, mass transfer and growth in multi-species multi-phase biological tissues. *Eur J Mech A-Solid*, 24(5):757–781. 125
- [Luenberger, 1964] Luenberger, D. G. (1964). Observing the state of a linear system. *Military Electronics, IEEE Transactions on*, 8(2):74–80. 11, 13, 67, 14, 50
- [Luenberger, 1966] Luenberger, D. G. (1966). Observers for multivariable systems. *IEEE Trans. Automat. Control*, 11(2):190–197. 11
- [Luenberger, 1971] Luenberger, D. G. (1971). An introduction to observers. *IEEE Transactions on Automatic Control*, 16:596–602. 11, 13, 67, 14, 50
- [Marchesseau et al., 2012] Marchesseau, S., Delingette, H., Sermesant, M., and Ayache, N. (2012). Fast parameter calibration of a cardiac electromechanical model from medical images based on the unscented transform. *Biomechanics and modeling in mechanobiology*. 98, 80

- [Marcucci and Truskinovsky, 2010] Marcucci, L. and Truskinovsky, L. (2010). Muscle contraction: A mechanical perspective. *Eur Phys J E*, 32(4):411–418. [20](#), [118](#), [120](#)
- [Maugin and Muschik, 1994] Maugin, G. A. and Muschik, W. (1994). Thermodynamics with Internal Variables. Part I. General Concepts. *J Non-Equil Thermody*, 19(3):217–249. [20](#), [121](#)
- [Miller, 2005] Miller, L. (2005). Controllability cost of conservative systems: resolvent condition and transmutation. *Journal of functional Analysis*, 218(2):425–444. [72](#), [54](#)
- [Mordukhovich, 1996] Mordukhovich, B. S. (1996). Optimization and finite difference approximations of nonconvex differential inclusions with free time. In *Nonsmooth analysis and geometric methods in deterministic optimal control (Minneapolis, MN, 1993)*, pages 153–202. Springer, New York, New York, NY. [12](#)
- [Moreau-Villegier et al., 2006] Moreau-Villegier, V., Delingette, H., Sermesant, M., Ashikaga, H., McVeigh, E., and Ayache, N. (2006). Building maps of local apparent conductivity of the epicardium with a 2-D electrophysiological model of the heart. *Biomedical Engineering, IEEE Transactions on*, 53(8):1457–1466. [116](#), [98](#)
- [Mortensen, 1968] Mortensen, R. E. (1968). Maximum-likelihood recursive nonlinear filtering. *J. Optim. Theory Appl.*, 2(6):386–394. [44](#), [47](#), [26](#), [29](#)
- [Nash and Hunter, 2000] Nash, M. P. and Hunter, P. (2000). Computational mechanics of the heart - From tissue structure to ventricular function. *Journal of Elasticity*, 61(1-3):113–141. [16](#), [20](#), [118](#), [7](#)
- [Nassiopoulos and Bourquin, 2010] Nassiopoulos, A. and Bourquin, F. (2010). Fast three-dimensional temperature reconstruction. *Comput Method Appl M*, 199(49-52):3169–3178. [10](#)
- [Navon, 1998] Navon, I. M. (1998). Practical and theoretical aspects of adjoint parameter estimation and identifiability in meteorology and oceanography. *Dynamics of Atmospheres and Oceans*, 27(1-4):55–79. [15](#)
- [Nussbaum and Pereverzev, 1999] Nussbaum, M. and Pereverzev, S. V. (1999). The degree of ill-posedness in stochastic and deterministic noise models (Preprint No 509, WIAS-Berlin). www.wias-berlin.de. [38](#), [98](#)
- [Pan et al., 2005] Pan, L., Prince, J., Lima, J., and Osman, N. (2005). Fast tracking of cardiac motion using-3D-HARP. *IEEE Transactions on Biomedical Engineering*, 52(8):1425–1435. [108](#), [91](#)
- [Panerai, 1980] Panerai, R. B. (1980). A model of cardiac muscle mechanics and energetics. *J Biomech*, 13(11):929–940. [20](#), [118](#)
- [Pathmanathan et al., 2010] Pathmanathan, P., Chapman, S., Gavaghan, D., and Whiteley, J. (2010). Cardiac electromechanics: the effect of contraction model on the mathematical problem and accuracy of the numerical scheme. *The Quarterly Journal of Mechanics and Applied Mathematics*, 63(3):375–399. [20](#), [118](#)
- [Pazy, 1983] Pazy, A. (1983). *Semigroups of Linear Operators and Applications to Partial Differential Equations*, volume 44 of *Applied Mathematical Sciences*. Springer-Verlag, New York. [68](#), [51](#)

- [Peng et al., 2010] Peng, Y., Xiang, X., and Jiang, Y. (2010). Nonlinear dynamic systems and optimal control problems on time scales. *ESAIM: COCV*, 17(3):654–681. [44](#), [26](#)
- [Pernot et al., 2011] Pernot, M., Couade, M., Mateo, P., Crozatier, B., Fischmeister, R., and Tanter, M. (2011). Real-Time Assessment of Myocardial Contractility Using Shear Wave Imaging. *JAC*, 58(1):65–72. [17](#), [35](#), [39](#), [99](#)
- [Perthame, 2004] Perthame, B. (2004). Mathematical tools for kinetic equations. *Bulletin of the American Mathematical Society*, 41(2):205–244. [37](#), [87](#), [91](#), [73](#)
- [Pham, 2001] Pham, D. T. (2001). Stochastic methods for sequential data assimilation in strongly nonlinear systems. *Monthly weather review*, 129(5):1194–1207. [14](#), [66](#), [48](#)
- [Pham et al., 1998a] Pham, D. T., Verron, J., and Christine Roubaud, M. (1998a). A singular evolutive extended Kalman filter for data assimilation in oceanography. *Journal of Marine systems*, 16(3-4):323–340. [14](#), [61](#), [62](#), [63](#), [64](#), [93](#), [44](#), [46](#), [74](#)
- [Pham et al., 1998b] Pham, D. T., Verron, J., and Gourdeau, L. (1998b). Filtres de Kaiman singuliers évolutifs pour l’assimilation de données en océanographie. *Comptes Rendus de l’Académie des Sciences-Series IIA-Earth and Planetary Science*, 326(4):255–260. [14](#), [66](#), [48](#)
- [Preumont, 2002] Preumont, A. (2002). *Vibration Control of Active Structures, An Introduction*. Kluwer Academic Publishers, 2nd edition. [69](#), [85](#), [52](#), [67](#)
- [Puel, 2008] Puel, J.-P. (2008). A non standard approach to a data assimilation problem and Tychonov regularization revisited. *SIAM Journal on Control and Optimization*, 48(2):1089–1111. [10](#), [11](#)
- [Ramanathan et al., 2004] Ramanathan, C., Ghanem, R. N., Jia, P., Ryu, K., and Rudy, Y. (2004). Noninvasive electrocardiographic imaging for cardiac electrophysiology and arrhythmia. *Nat Med*, 10(4):422–428. [100](#), [112](#), [82](#), [94](#)
- [Ramdani et al., 2005] Ramdani, K., Takahashi, T., Tenenbaum, G., and Tucsnak, M. (2005). A spectral approach for the exact observability of infinite-dimensional systems with skew-adjoint generator. *Journal of functional Analysis*, 226(1):193–229. [71](#), [72](#), [54](#)
- [Ramdani et al., 2007] Ramdani, K., Takahashi, T., and Tucsnak, M. (2007). Uniformly exponentially stable approximations for a class of second order evolution equations—application to LQR problems. *ESAIM Control Optim. Calc. Var.*, 13(3):503–527. [14](#), [76](#), [59](#)
- [Ramdani et al., 2015] Ramdani, K., Tucsnak, M., and Valein, J. (2015). Detectability and state estimation for linear age-structured population diffusion models. *HAL INRIA*. [37](#), [63](#), [73](#)
- [Ramdani et al., 2010] Ramdani, K., Tucsnak, M., and Weiss, G. (2010). Recovering the initial state of an infinite-dimensional system using observers. *Automatica*, 46(10):1616–1625. [11](#), [81](#), [12](#), [63](#)
- [Raymond and Vanninathan, 2010] Raymond, J.-P. and Vanninathan, M. (2010). Null controllability in a fluid-solid structure model. *J. Differential Equations*, 248(7):1826–1865. [84](#), [66](#)

- [Reif and Unbehauen, 1999] Reif, K. and Unbehauen, R. (1999). The extended Kalman filter as an exponential observer for nonlinear systems. *IEEE Trans. Signal Process.*, 47(8):2324–2328. [54](#), [63](#), [96](#), [46](#), [78](#)
- [Rice and de Tombe, 2004] Rice, J. J. and de Tombe, P. P. (2004). Approaches to modeling crossbridges and calcium-dependent activation in cardiac muscle. *Prog Biophys Mol Bio*, 85(2-3):179–195. [20](#), [118](#)
- [Rice et al., 2003] Rice, J. J., Stolovitzky, G., Tu, Y., and de Tombe, P. P. (2003). Ising Model of Cardiac Thin Filament Activation with Nearest-Neighbor Cooperative Interactions. *Biophys. J.*, 84(2):897–909. [20](#), [118](#)
- [Rochoux et al., 2013] Rochoux, M. C., Cuenot, B., Ricci, S., Trouvé, A., Delmotte, B., Massart, S., Paoli, R., and Paugam, R. (2013). Data assimilation applied to combustion. *Comptes Rendus Mécanique*, 341(1):266–276. [39](#)
- [Rohan and Cimrman, 2010] Rohan, E. and Cimrman, R. (2010). Two-Scale Modeling of Tissue Perfusion Problem Using Homogenization of Dual Porous Media. *Int J Multiscale Com*, 8(1):81–102. [125](#)
- [Rosen, 1991] Rosen, I. G. (1991). Convergence of Galerkin approximations for operator Riccati equations—a nonlinear evolution equation approach. *Journal of Mathematical Analysis and Applications*, 155(1):226–248. [59](#), [41](#)
- [Rossi et al., 2014] Rossi, S., Lassila, T., Ruiz-Baier, R., Sequeira, A., and Quarteroni, A. (2014). Thermodynamically consistent orthotropic activation model capturing ventricular systolic wall thickening in cardiac electromechanics. *Eur J Mech A-Solid*, 48:129–142. [20](#)
- [Rudy, 2013] Rudy, Y. (2013). Noninvasive electrocardiographic imaging of arrhythmogenic substrates in humans. *Circ Res*. [100](#), [112](#), [82](#), [94](#)
- [Russell, 1978] Russell, D. L. (1978). Controllability and stabilizability theory for linear partial differential equations: recent progress and open questions. *SIAM Rev.*, 20(4):639–739. [14](#)
- [Sainte-Marie et al., 2006] Sainte-Marie, J., Chapelle, D., Cimrman, R., and Sorine, M. (2006). Modeling and estimation of the cardiac electromechanical activity. *Computers & Structures*, 84(28):1743–1759. [7](#), [20](#), [21](#), [33](#), [118](#), [120](#), [122](#)
- [Shubov, 1997] Shubov, M. A. (1997). Spectral operators generated by damped hyperbolic equations. *Integral Equations Operator Theory*, 28(3):358–372. [72](#), [54](#)
- [Simon, 2006] Simon, D. (2006). *Optimal State Estimation: Kalman, H^∞ , and Nonlinear Approaches*. Wiley-Interscience. [12](#), [50](#), [32](#)
- [Slotine and Lohmiller, 1998] Slotine, J.-J. E. and Lohmiller, W. (1998). On contraction analysis for non-linear systems. *Automatica*, 34(6):683–696. [13](#), [14](#)
- [Smith et al., 2011] Smith, N. P., de Vecchi, A., McCormick, M., Nordsletten, D. A., Camara, O., Frangi, A. F., Delingette, H., Sermesant, M., Relan, J., Ayache, N., Krueger, M. W., Schulze, W. H. W., Hose, R., Valverde, I., Beerbaum, P., Staicu, C., Siebes, M., Spaan, J.,

- Hunter, P. J., Weese, J., Lehmann, H., Chapelle, D., and Rezavi, R. (2011). euHeart: personalized and integrated cardiac care using patient-specific cardiovascular modelling. *Interface Focus*, 1(3):349–364. [18](#), [17](#)
- [Tanabe, 1979] Tanabe, H. (1979). *Equations of evolution*, volume 6 of *Monographs and Studies in Mathematics*. Pitman (Advanced Publishing Program), Boston, Mass.-London. Translated from the Japanese by N. Mugibayashi and H. Haneda. [56](#), [57](#), [39](#)
- [Tataru, 1995] Tataru, D. (1995). Unique continuation for solutions to PDE's; between Hörmander's theorem and Holmgren's theorem. *Communications in Partial Differential Equations*, 20(5-6):855–884. [71](#), [53](#), [54](#)
- [Tataru, 1996] Tataru, D. (1996). Carleman estimates and unique continuation for solutions to boundary value problems. *J Math Pure Appl*, 75(4):367–408. [73](#), [55](#)
- [Tebou and Zuazua, 2007] Tebou, L. T. and Zuazua, E. (2007). Uniform boundary stabilization of the finite difference space discretization of the 1d wave equation. *Adv Comput Math*, 26(1-3):337–365. [76](#), [59](#)
- [Temam, 1971] Temam, R. (1971). Sur l'équation de Riccati associée à des opérateurs non bornés, en dimension infinie. *Journal of functional Analysis*, 7:85–115. [59](#), [41](#)
- [Titaud et al., 2010] Titaud, O., Vidard, A., Souopgui, I., and Le Dimet, F.-X. (2010). Assimilation of image sequences in numerical models. *Tellus A*, 62(1):30–47. [100](#), [82](#)
- [Tortora and Derrickson, 2009] Tortora, G. J. and Derrickson, B. (2009). *Principles of Anatomy and Physiology*. John Wiley & Sons, Inc, 12 edition. [19](#), [121](#)
- [Tucsnak and Weiss, 2009] Tucsnak, M. and Weiss, G. (2009). *Observation and control for operator semigroups*. Birkhäuser Advanced Texts: Basler Lehrbücher. Birkhäuser Verlag, Basel. [57](#), [69](#), [39](#), [52](#)
- [Uhlmann and Julier, 2002] Uhlmann, J. K. and Julier, S. J. (2002). Reduced sigma point filters for the propagation of means and covariances through nonlinear transformations. *American Control Conference, 2002. Proceedings of the 2002*, 2:887–892 vol.2. [55](#), [38](#)
- [Vaillant and Glaunès, 2005] Vaillant, M. and Glaunès, J. (2005). Surface matching via currents. *Inf Process Med Imaging*, 19:381–392. [103](#), [104](#), [106](#), [85](#), [86](#), [88](#)
- [Vidrascu et al., 2005] Vidrascu, M., Le Tallec, P., Gerbeau, J.-F., and Hauret, P. (2005). Fluid structure interaction problems in large deformation. *Comptes Rendus Mecanique*, 333:910–922. [127](#)
- [Weiss, 1989] Weiss, G. (1989). Admissible observation operators for linear semigroups. *Israel Journal of Mathematics*. [57](#)
- [Wiener, 1949] Wiener, N. (1949). *Extrapolation, interpolation, and smoothing of stationary time series*, volume 2. MIT press Cambridge, MA. [13](#)
- [Xiao, 2013] Xiao, N. (2013). *Simulation of 3-D Blood Flow in the Full Systemic Arterial Tree and Computational Frameworks for Efficient Parameter Estimation*. PhD thesis, Stanford University. [98](#), [80](#)

- [Xiao et al., 2013] Xiao, N., Alastruey, J., and Figueroa, C. A. (2013). A systematic comparison between 1-D and 3-D hemodynamics in compliant arterial models. *Int. J. Numer. Meth. Biomed. Engng.*, 30(2):204–231. [21](#)
- [Younes, 1998] Younes, L. (1998). Computable elastic distances between shapes. *Siam J Appl Math*, 58(2):565–586. [103](#)
- [Younes, 2010] Younes, L. (2010). *Shapes and diffeomorphisms*. Springer. [103](#), [104](#), [86](#)
- [Young, 1999] Young, A. A. (1999). Model tags: direct three-dimensional tracking of heart wall motion from tagged magnetic resonance images. *Medical Image Analysis*, 3(4):361–372. [109](#), [91](#)
- [Zabczyk, 1992] Zabczyk, J. (1992). *Mathematical control theory: an introduction*. Systems & Control: Foundations & Applications. Birkhäuser Boston Inc., Boston, MA. [14](#)
- [Zahalac, 1981] Zahalac, G. I. (1981). A distribution-moment approximation for kinetic theories of muscular contraction. *Mathematical Biosciences*, 114:55–89. [120](#)
- [Zhang, 2002] Zhang, Q. (2002). Adaptive observer for multiple-input-multiple-output (MIMO) linear time-varying systems. *IEEE Trans. Automat. Control*, 47(3):525–529. [16](#), [62](#), [93](#), [94](#), [44](#), [74](#), [76](#)
- [Zhang and Xu, 2001] Zhang, Q. and Xu, A. (2001). Global adaptive observer for a class of nonlinear systems. *Decision and Control, 2001. Proceedings of the 40th IEEE Conference on DOI - 10.1109/.2001.980478*, 4:3360–3365 vol.4. [93](#)
- [Zhang, 2000] Zhang, X. (2000). Explicit observability estimate for the wave equation with potential and its application. *R. Soc. Lond. Proc. Ser. A Math. Phys. Eng. Sci.*, 456(1997):1101–1115. [74](#), [56](#)
- [Zhang and Zuazua, 2006] Zhang, X. and Zuazua, E. (2006). Long-Time Behavior of a Coupled Heat-Wave System Arising in Fluid-Structure Interaction. *Arch. Ration. Mech. Anal.*, 184(1):49–120. [84](#), [66](#)
- [Zuazua, 2005] Zuazua, E. (2005). Propagation, Observation, and Control of Waves Approximated by Finite Difference Methods. *SIAM Review*, 47(2):197. [14](#), [69](#), [72](#), [76](#), [52](#), [55](#), [59](#)